STATIC AND MODAL ANALYSIS OF IN-PLANE FUNCTIONALLY GRADED STRUCTURES USING EXTENDED KANTOROVICH METHOD

A Thesis Submitted in

Partial Fulfillment of the Requirements

for the Degree of

DOCTOR OF PHILOSOPHY

By

AGYAPAL SINGH

(Roll No.146103022)

DEPARTMENT OF MECHANICAL ENGINEERING
INDIAN INSTITUTE OF TECHNOLOGY GUWAHATI
GUWAHATI (ASSAM)-781039

JANUARY, 2020

Certificate

This is to certify that the thesis entitled "**Static and Modal Analysis of In-Plane Functionally Graded Structures using Extended Kantorovich Method**" being submitted by **Mr. Agyapal Singh** to the Indian Institute of Technology, Guwahati, for the award of the degree of Doctor of Philosophy in Mechanical Engineering is a record of original bonafide research work carried out by him under my supervision and guidance. The thesis work, in my opinion, has reached the requisite standard fulfilling the requirements for the degree of Doctor of Philosophy.

The results contained in this thesis have not been submitted in part or full to any other University or Institute for the award of any degree or diploma.

Dr. Poonam Kumari
Associate Professor
Department of Mechanical Engineering
Indian Institute of Technology Guwahati
Guwahati - 781039

Declaration

I, Agyapal Singh (Roll no: 146103022) declare that the present written submission is my thoughts in my own words. I have adequately cited and referenced the original sources, where other's ideas have been involved. I also declare that I have adhered to all principles of academic honesty and integrity and have neither fabricated nor falsified any idea/data/fact/source in my submission. I understand that any violation of the above will be cause for disciplinary action by the Institute and can also evoke penal action from the sources which have thus not been properly cited or from whom proper permission has not been taken when needed.

(Agyapal Singh)

Date: Roll No. 146103022

Acknowledgements

First and foremost, I want to express my sincere gratitude toward my Ph.D. supervisor, Dr. Poonam Kumari, for providing me an opportunity to work under her supervision. I am grateful to her for her consistent guidance, motivation, patience, kindness and family support as well, over these years. She has always made available herself for discussions besides her busy schedules. Her enthusiasm, sublime work ethics, analytical abilities, and never-say-die attitude toward research and life as well, has natured my scientific skills and also inspired me immensely to work hard. I am proud to have her as my Ph.D. supervisor. Thank you, Ma'am, for all your help, advice, and support.

I want to thank my doctoral committee member, Prof., K. S. R. Krishna Murthy, Dr. Atanu Banerjee, and Dr. Arunasis Chakraborty, for their encouragement, insightful comments, and suggestions which have helped me to refine and widen my research from various perspectives. My sincere gratitude also goes to the Head of Department of Mechanical Engineering, Prof. Santosha K. Dwivedy, for providing all the resources needed for my research. I also thankful to all faculty and staff members of the Mechanical Engineering department who help me whenever I needed. Without their help, it would not have been possible to conduct my research. It is an honor for me to thank the Indian Institute of Technology Guwahati for giving me such an excellent opportunity for undergoing my research.

I gratefully acknowledge the Science and Engineering Research Board (India) for providing financial support through grant SB/FTP/ETA-420/2013 to support this research work. I am also thankful to the Ministry of Human Resource and Development (MHRD), Government of India for providing me financial support during my Ph.D. at IIT Guwahati.

I want to thank my senior and labmates, Dr. Susanta Behera, Sharnish Kar, Abhishek Yadav, Rupam Hazirika, Viwek, Dhirendra, Mukesh for their timely help, suggestions, and encouragements. I am indebted to my colleagues, Shashi Ratnakar and Akash Anil with whom I had a very good time.

My special gratitude goes to my family for their role in my life. I offer my regards to my loving parents, Mr. Gurmeet Singh and Mrs. Charnjeet Kaur, whose love, teachings, sacrifices, and blessings brought me this far. Their unconditional love, support, and trust on me are the most precious gift that I have. I am thankful to my younger brother, Amanpal Singh for his eternal love and all kind of support. I am also grateful to my in-laws for their love, understanding and motivating me to pursue my career.

I extend my sincere thank to my friends Jimmy, Buttar, Parry, Dana, and especially Praveen Kishor, Harry Dhani and Varun Nayyar who helped me emotionally, financially, socially during the tough time of my life. Thanks for being what you are.

Last but not least, I am immensely grateful to my best friend and life partner, Kamalpreet Kaur who sacrifices a lot for me, even her career. Her inspiration, understating, and faith in me have been my greatest strength. I am truly thankful for having you in my life. My thesis acknowledgment would be incomplete without thanking my son, Adeeb, whose smiling face always made me happy and inspired me. He has made our life wonderful. My parents, wife, son, and inlaws are the backbone of my happiness, and I dedicate my thesis to them.

Finally, I thank God for always being with me.

Agyapal Singh

Abstract

The concept of functionally graded materials (FGMs) spurred great attention from engineers and researchers due to their unique properties such as thermal resistance, low density, and high toughness. For different applications, the desired mechanical properties along any spatial direction are achieved by appropriate selection of the volume fraction. The remarkable characteristics of these materials over the laminated composite is that the FGM eliminates the sharp interfaces existing in laminated composites with a gradient interface that result in a decrease of both residual stresses and concentration of stresses which increase the mechanical stresses bearing capacity of structures. FGM with longitudinally or multidirectional varying material properties are more effective high-temperature resistant because in-plane or multidirectional functionally graded materials enable more accurate monitoring of the material properties. Therefore, an appropriate method is required to investigate the static and dynamic behavior of such structures, which also serve as the benchmark for their optimal design and fabrications. Although numerical methods and commercial finite element packages are available for a variety of structural problems, there is always a need for analytical solutions. The analytical elasticity models can predict the behavior of FGM structures more accurately as compared to the one or two-dimensional theories or numerical solutions. The extended Kantorovich method is undoubtedly one of the best technique that offers an analytical solution for complicated problems.

Hence, this research proposed an accurate analytical elasticity solution for static and dynamic analysis of in-plane functionally graded structures such as beams, flat panels, and rectangular plates using multi-term extended Kantorovich method. However, developing the analytical elasticity solutions for in-plane functionally graded structures are much more challenging than the composite laminated structures because material properties of structures are the function of a spatial coordinate (x). Therefore, ordinary differential equations (ODEs) obtained along the longitudinal direction having variables coefficients which are more difficult to solve analytically. This mathematical complexity is tackled by employing the modified power series method to solve the complex system of variable coefficient ODEs along the in-plane (axial) direction.

At first, an analytical 2D elasticity solution for static and free vibration analysis of axially functionally graded beams subjected to arbitrary boundary conditions using the multi-term extended Kantorovich method (EKM). The material properties of the beam are considered to vary linearly along its axial (x) direction. Modified Hamilton's principle is applied to derive the weak form of coupled governing equations in which all the stresses and displacements act as primary variables. Further, the extended Kantorovich method is employed to reduce the governing equations into sets of ordinary differential equations (ODEs) along the axial (x) and thickness (z) directions. The system of ODEs along the z-direction has constant coefficients which is solved analytically. But, the system of ODEs along x-direction has variable coefficients which is solved using a modified power series method. Interface continuity and boundary conditions are satisfied in exact point-wise manner which ensures the same order of accuracy for all field variables (stresses and displacements). Efficacy and accuracy of the present methodology are verified thoroughly with existing literature and 2D finite element solution. Benchmark numerical results are presented for various cases of material property variations under different type of boundary conditions. Significant effect of axial gradation on the static and dynamic behavior of the beam is observed.

Then, this extended Kantorovich approach is extended to much more complex problems such as in-plane functionally graded angle-ply flat panels and Levy-type plates. Benchmark numerical results are presented for single layered and multi-layered in-plane functionally graded rectangular plate and angle-ply flat panels. The influence of property variation on the deflections and stresses are studied and discussed comprehensively for arbitrary sets of boundary conditions and configurations. The current research will also be beneficial to model real-life panel structures in which its material properties deteriorate due to some environmental effect.

Apart from the above analysis of in-plane functionally grades elastic structures, a piezoelectricity based analytical solution is also developed for free vibration analysis of the angle-ply elastic and piezoelectric flat laminated panels under arbitrary boundary conditions. The numerical results are reported for various configurations such as elastic panels, sandwich panels and piezoelectric panels under arbitrary sets of boundary conditions. The effect of ply-angle and thickness to span ratio (s) on the dynamic behavior of the panels are also investigated. The presented 3D analytical solution will be helpful in the assessment of various 1D theories and numerical methods. More over, a 2D analytical free vibration solution is also developed for axially functionally graded (AFG) beams integrated with piezoelectric layers and subjected to arbitrary support boundary conditions. New benchmark numerical results are presented for a laminated elastic and axially functionally graded beams integrated with piezoelectric layers. All above analysis are more severe cases than a homogeneous beam and plate for assessing 1D/2D theories and other numerical model.

Contents

List of Figures

List of Tables

Chapter 1

Introduction

1.1 PREFACE

The continuous growth of the commercial use of space facilities has led to the development of new and more efficient aerospace vehicles. Composite materials have been successfully used in aircraft, shipbuilding, automotive and various other engineering applications for many years because of their flexibility in design, excellent strength to weight ratio and capability to have desired strength and stiffness. In laminated composites, two dissimilar materials are bonded together, which result in an abrupt change in material properties across the interfaces between layers. As a result, undesirable effects like the stress concentration and stress singularities usually occurs at the interface. Thus, the laminates may tend to debond, or cracks are likely to initiate at interfaces and propagate into the weaker material section leading to damage in the form of matrix cracking, delamination, and adhesive bond separation.

Functionally graded materials (FGMs) were therefore born to overcome these issues which have spurred great attention from engineers and researchers due to their unique properties such as thermal resistance, low density, and high toughness. For different applications, the desired mechanical properties along any spatial direction are achieved by appropriate selection of the volume fraction. The remarkable characteristics of these materials over the laminated composite is that the FGMs eliminate the sharp interfaces existing in laminated composites with a gradient interface that result in a decrease of both residual stresses and concentration of stresses which increase the mechanical stresses bearing capacity of structures. Thus many mathematical models have been developed to predict the static and dynamic behavior of functionally graded structures. But in most of the studies, the material gradation is considered along the thickness direction. However, the studies related to in-plane or multidirectional gradation are very limited but there are practical occasions which require grading of macroscopic properties along in-plane or multi directions.

In 2003, Columbia space shuttle disintegrated as it re-entered the Earth's atmosphere and killed all seven crew members. The physical cause for the loss of Columbia and its crew was a breach in

the thermal protection system of the space shuttle. A suitcase-size piece of insulating foam broke off from the External Tank (ET) and struck Columbia's left-wing which was made up of reinforced carbon-carbon composite panel. This damage eventually created a hole at the leading edge of the left-wing. During re-entry, this hole in the thermal protection system allowed superheated air to enter which weaken the structure progressively by melting the aluminum panels of the left-wing. The large aerodynamic forces caused loss of control and break-up the Orbiter [1, 2]. Such damage in space shuttles during re-entry in the atmosphere can be prevented by using the FGMs as protective thermal tiles because the gradation of material properties in an FGM decreases the thermal stresses, stress concentrations and residual stresses which found in conventional composites thermal sheets [3]. However, conventional FGMs also might not able to withstand in severe variations of temperature along the multi-direction, as observed in the space shuttles. Therefore, the FGMs having longitudinally or multidirectional gradation of material properties are more effective high-temperature resistant because in-plane or multidirectional functionally graded materials enable more accurate monitoring of the material properties. To investigate the static and dynamic behavior of such structures, an appropriate method is required, which will also serve as a benchmark for their optimal design and fabrications.

The analytical elasticity models can predict the behavior of FGMs structures more accurately as compared to the one or two-dimensional theories. Hence, this research proposed the development of accurate analytical elasticity solution for static and dynamic analysis of in-plane functionally graded structures such as beams, flat panels and rectangular plates using the multi-term extended Kantorovich method (EKM). However, developing the analytical elasticity solutions for in-plane functionally graded structures are much more challenging than the composite laminated structures because material properties of structures are the function of a spatial coordinate along the length. Therefore, ordinary differential equations (ODEs) obtained along the longitudinal direction having variables coefficients which are more difficult to solve analytically. This mathematical complexity is tackled by employing the modified power series method to solve the complex system of variable coefficient ODEs along the in-plane (axial) direction. At first, analytical elasticity solutions are developed for the static and free vibration analysis of axially functionally graded (AFG) beams. Then, it is extended to much more complex problems such as in-plane functionally graded angle-ply flat panels and Levy-type plates. The presented elasticity analytical model can predict boundary layer effects or edge effects accurately.

1.2 AN OVERVIEW ON FUNCTIONALLY GRADED MATERIALS

Functionally graded material is a composite material in which the microstructure is locally varied in one or more directions in a specific manner to achieve the desired properties as required for the specific application. The spatial variations of the microstructure are not a new thing to us. The idea of functionally graded microstructure is already exploited by nature for millions of years to form optimum structures. Bamboo, wood, teeth and bones are the excellent example of naturally occurring FGMs. Nature designed these materials to meet their expected requirements perfectly. This idea of the functionally graded microstructure is used to fabricate the thermal barrier for a space shuttle which is capable of withstanding a surface temperature of 2000 K and a temperature gradient of 1000 K across a 10 mm section [4]. The conventional ceramic tiles laminate are prone to cracking and debonding. In traditional thermal protection panels, the stress concentration is occurred at the tile/superstructure interface because of abrupt change in mechanical or thermal properties, as shown in Fig. 1.1(a). The FGMs can alleviate those stress concentrations by gradually varying material properties along the thickness of the structural component, as shown in Fig. 1.1(b).

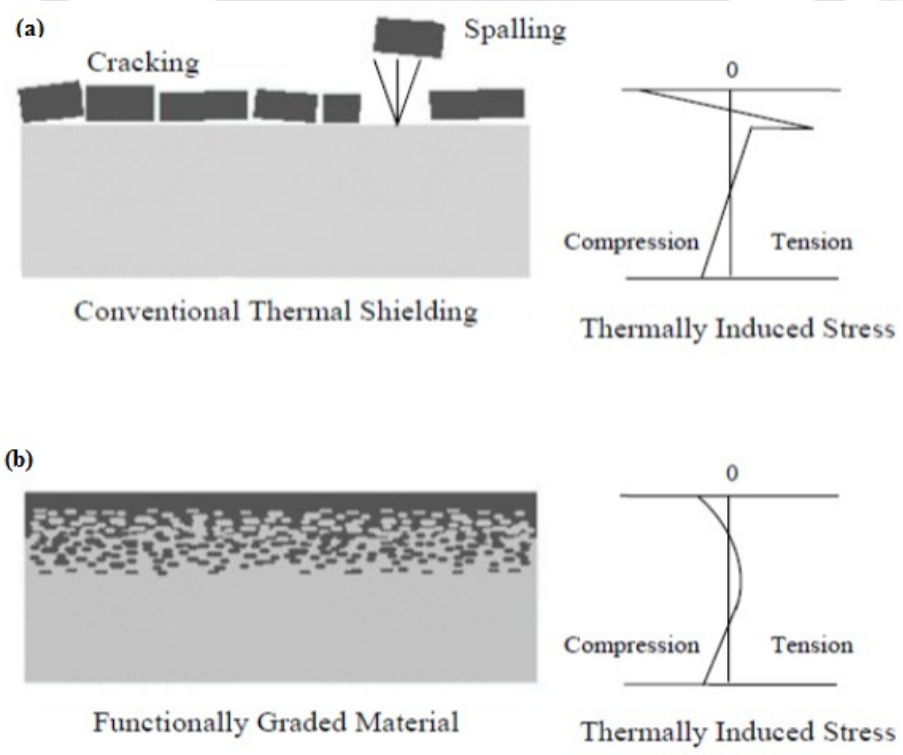

Fig. 1.1: Conventional Thermal Shield vs Functionally Graded Material Thermal Shield (Cooley [3])

1.2.1 Classification of FGMs

The overall properties of an FGM are unique and different from the constituting materials that form it. FGMs are classified according to (a) Gradation of FGM, (b) Properties variation across the coordinates, (c) Fabrication processes.

1.2.1.1 Based on Gradation of FGM

As per the gradient type, FGMs can be categorized as [5]

(a) Volume fraction gradient type - Gradation in a particular direction is achieved by controlling the volume fraction of the various constituent as shown in Fig. 1.2(a).

(b) Shape gradient type - The shape of microstructure changes across the dimension to achieve gradation of properties in a particular direction as shown in Fig. 1.2(b).

(c) Orientation gradient type - Gradation may also be obtained by changing the orientation of the microstructure in a specific direction as shown in Fig. 1.2(c).

(d) Size variation - This type of gradation is achieved by changing the size of microstructure as shown in Fig. 1.2(d).

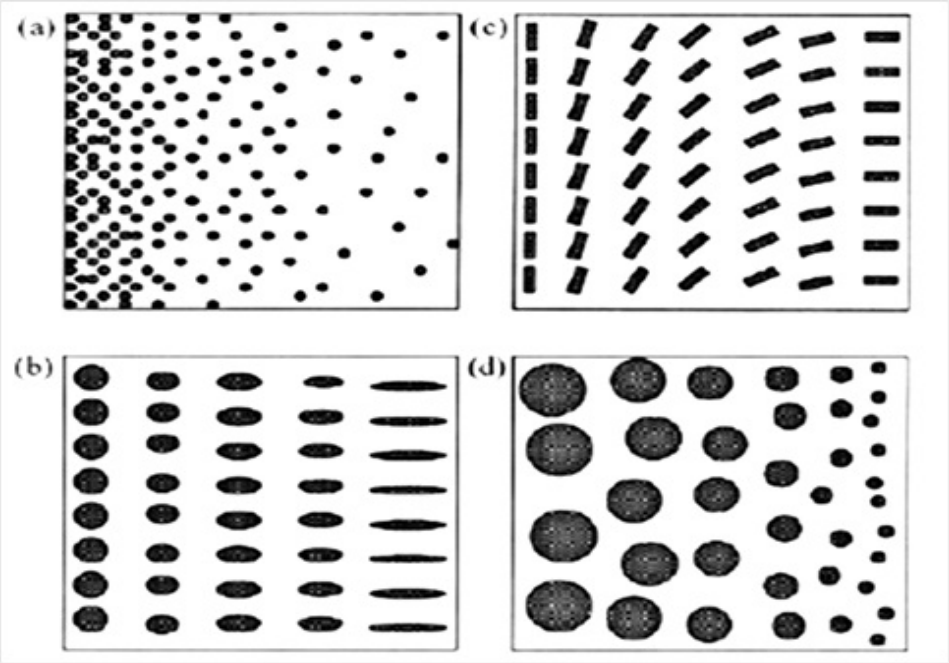

Fig. 1.2: FGMs based on gradation (El-Wazery and El-Desouky [5])

1.2.1.2 Based on Properties Variation Across the Coordinates

FGMs can also be categorized, on the basis of properties variation, in following way [6]

(a) Continuously graded materials - Material phases change in a continuous manner to achieve a continuous variation of the material as shown in Fig. 1.3(a). For example, human bone in which porosity and composition change continuously in its radial direction.

(b) Stepwise graded materials - Material phases change in a discontinuous manner such as stepwise manner as shown in Fig. 1.3(b). For example, in a spark plug, gradation is achieved by changing composition from a refractory ceramic to a metal in a stepwise manner.

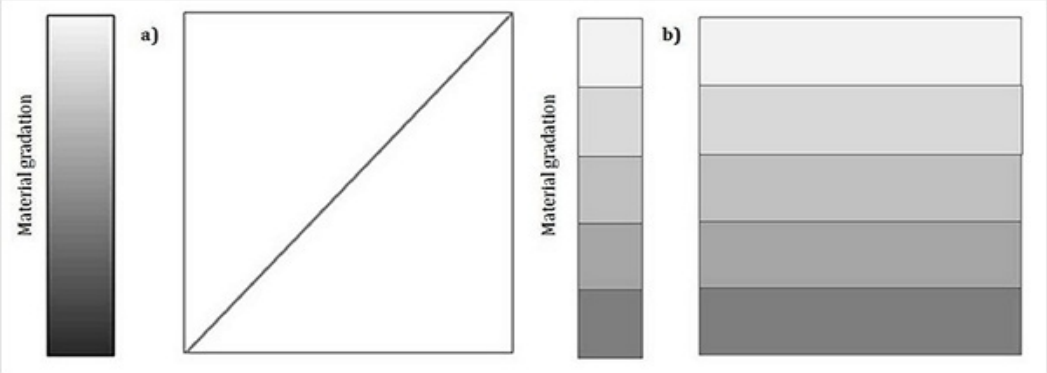

Fig. 1.3: FGMs based on properties variation (Udupa et al.[6])

1.2.1.3 Based on Fabrication Processes

The gradation of material property in components can be achieved by various fabrication methods. Based on processing techniques, FGMs are divided into following two categories [7].

(a) Thin FGM - Thin section or surface coating are used to obtain the gradation of properties. Thin FGM is produced by self-propagating high-temperature synthesis (SHS), physical or chemical vapour deposition (PVD, CVD), plasma spraying etc.

(b) Bulk FGM - While bulk FGM is a large volume of materials which require high labor fabrication processes. Bulk FGMs are manufactured by the method of centrifugal casting method, powder metallurgy technique and solid free form technique etc.

The detailed literature on FGM processing techniques can be found in recent review articles on FGM manufacturing, presented by Kieback et al. [8], and Suresh and Mortensen [9].

1.2.2 Potential Applications of Functionally Graded Materials

FGMs can be used widely in the different field of engineering. Here, some of their potential applications [5] are listed as,

(a) Production Engineering: In this field, the main application of FGM is to make thermal resistant cutting tools so that they can withstand to high mechanical load at elevated temperature. Usually, in a conventional lathe cutting tool, as shown in Fig. 1.4(a), crack occurs near the tip due to high temperature. But with the help of FGM, lathe cutting tool can be designed to improve its thermal and shock strength [5], as shown in Fig. 1.4(b).

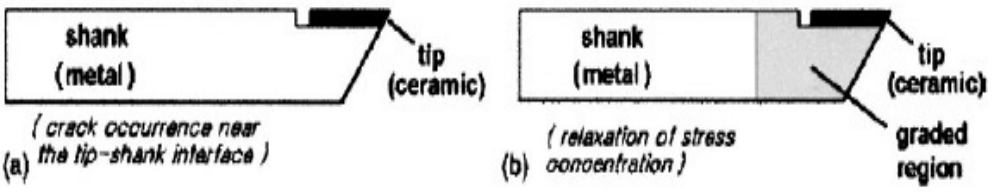

Fig. 1.4: Conventional vs. FGM Lathe Metal Cutting Tool (El-Wazery and El-Desouky [5])

(b) Power plant engineering: Oxidation resistant and thermal barrier FGM coating can be used to increase the life of a turbine blade.

(c) Aerospace: It is the ideal material to use for space plane body and rocket engine components because FGM can withstand very high-temperature gradient.

(d) Medicine: FGM is a perfect implant material to use for orthopedic and dental applications like bone replacement, knee joint replacement, and artificial teeth. As living tissues like bones and teeth are naturally characterized as functionally graded materials, thus to meet that kind of requirements artificial FGM biomaterial can be developed.

(e) Nuclear projects: Reliability is the key issue rather than cost in nuclear projects. Thus, FGMs can be used in fuel pallets and plasma wall of fusion reactor so that these structures are thermal resistant and leakproof to avoid industrial accidents.

(f) Communication field: FGM also finds its application in optoelectronics. For example, optical fiber wires require a good electrical resistance at the outer surface and a good refractive index material property at inner side. Hence, FGM is ideal for such requirements. FGM can also be used for audio video discs, high-speed transmission optical fibers, and computer circuit boards, etc.

(g) Defense: The ability to eliminate any crack propagation and debonding make the FGM useful for defense application. Thus, penetration resistant FGM can be used for bulletproof vests and armor plates.

(h) Automobile: FGMs can be successfully used for the car engine cylinders and many other components which require heat, wear, mechanical shock and corrosion resistant properties, simultaneously.

1.3 LITERATURE REVIEW

Theoretical analysis of functionally graded beams, panels, and plates are now an active area of research. Researcher used various type of methods to develop solutions for static and dynamic analysis of functionally graded beams, panels, and plates such as extended Pagano's approach asymptotic approach, Plevako method, Peano-Baker series method, power series method, and state space/Fourier series method. But in most of the studies, the material gradation is considered along the thickness direction. A comprehensive review of research related to static and dynamic analysis of functionally graded structures is presented by Birman and Byrd [10], Jha et al. [11], Thai at al. [12], Swaminathan et al. [13], Liew et al. [14], Wu el al. [15], and Wu and Liu [16]. Various analytical and numerical methods are used to investigate several types of structural problems, especially for composite and functionally graded beam and plates. The following Table 1.1 list some pioneered researcher and their important contribution to laminated and FGM structural research. In the succeeding subsections of this chapter, literature related to analysis of in-plane functionally graded beams, flat panels and rectangular plates are presented which are relevant to the scope of this work.

1.3.1 Static and Dynamic Analysis of Axially Functionally Graded Beams

Elishakoff and Candan [103] presented the first closed-form free vibration solution for axially graded Euler-Bernoulli beam using inverse solution techniques and the solution is based on beam theory. By employing Fredholm integral equations, Huang and Li [104] developed a free vibration solution for axially graded non-uniform Euler-Bernoulli beams subjected to arbitrary support conditions (simply-supported, clamped, and free ends). Giunta et al. [105] presented linear static analysis of simply-supported beams having axial or bi-directional material gradation based on refined theories. Wang and Wang [106] presented exact natural frequency analysis for an Euler-Bernoulli non-uniform beam subjected to arbitrary boundary conditions and having varying flexural rigidity and density along the axis of beam. Sarkar and Ganguli [107] presented an analytical model for free vibration analysis of non-uniform axially graded Euler-Bernoulli free-free beam and further extended their solution to axially graded Timoshenko beams [108]. Li et al. [109] presented exact

Table 1.1: Some pioneered researcher and their contribution to laminated and FGM structural research

Research Group	Contribution
Noor and Burden	Displacement-based theories for multilayered plates [17–19]
Saravanos and Heyliger	Static and free vibration analysis of laminated elastic and piezoelectric plates [20–26]
J. N. Reddy	Develop higher order theories for linear and nonlinear analysis of multilayered composite and FGM plates and shells [27–32]
Rakesh Kapania	Mechanics multilayered composite plates and shells using a layer-wise theory and nonlinear finite element [33–36]
R . C. Batra	Elasticity based analytical solution for static and dynamic analysis through-thickness FGM rectangular plates [37–40]
Tarun Kant	Analytical solutions for analysis of composite and FGM, plates and shells based on a higher-order refined theory [41–45].
Dumir et al.	Exact piezoelectric solution for piezoelectric composite beams, plates and shells [46–50]
Chih-Ping Wu	Three dimensional static and dynamic analysis of multilayered and functionally graded piezoelectric plates and shells [51–54]
Erasmo Carrera	Carrera unified formulation (CUF) for static, dynamic and buckling analysis of composite plates and shells [55–58]
Weiqiu Chen	Exact and Semi-analytical elasticity solution for composite and FG structures (Beam, plate and, shells) [59–67]
A. J. M. Ferreira	Static, free vibration and buckling analysis of composite and FGM plates using finite element and Meshless methods [68–71]
Ranjan Ganguli	Closed-form one-dimensional solutions for axially functionally graded beams and aeroelastic analysis of rotating blades [72–77].
Sridhar Idapalapati	Failure analysis of composite lap and scarf joints [78–81].
Yogesh Desai	Mixed theory-based analytical and FE solution for analysis of laminated beams and plates [82–85].
R. Lal	Vibrations and buckling analysis of non-homogenous circular and rectangular plates using classical plate theory [86–90]
B. P. Patel	Nonlinear analysis of composite/sandwich laminates using higher-order theories [91–94]
Kapuria et al.	3D analytical solutions for accurate prediction of interlaminar stresses in the composite and piezolaminated plate [95–98]
Amirtham Rajagopal	Nonlocal nonlinear analysis of functionally graded beams and plates using higher-order theories [99–102]

natural frequency analysis of simply-supported Euler-Bernoulli beam by considering exponential variation of density and stiffness along the axis of the beam. Tang and Wu [110] developed exact free vibration solutions for axially graded Timoshenko beams subjected to arbitrary boundary conditions. The density and stiffness of the beam are assumed to vary exponentially along the axis of the beam. Nguyen et al. [111] presented analytical solution for Euler-Bernoulli functionally graded beams (axially as well as through-the thickness) having tapered cross-section under static loading considering power-law variation of elastic modulus. Yuan et al. [67] presented exact solutions for the free vibration of arbitrarily supported Timoshenko beams having variable cross-section and material gradation along the axis of the beam. Rezaiee-Pajand and Hozhabrossadati [112] obtained closed-form free vibration solution for double-axially functionally graded Euler-Bernoulli beams subjected to arbitrary boundary conditions. Wang et al. [113] proposed an analytical solution for natural frequency analysis of two-directional functionally graded Euler-Bernoulli beams under clamped-free and hinged-hinged end supports. By using power series method, Huang and Rong [114] developed a free vibration solution for nonuniform axially graded Euler-Bernoulli beam by considering arbitrary gradation of material properties along the axis of beam. Using asymptotic development method (ADM) in conjunction with Euler-Bernoulli beam theory, Cao et al. [115] obtained an analytical solution for free vibration analysis of uniform axially functionally graded (AFG) beams subjected to arbitrary boundary conditions. Very recently, Cao et al. [116] extended this solution to free vibration analysis of non-uniform AFG beams under arbitrary boundary condition.

Static and dynamic analysis of AFG beams is much more challenging than the composite material beams because the material properties of the beam are function of a spatial coordinate (x) along length of the beam. Therefore, many researchers have developed the numerical solution for dynamic analysis of axially functionally graded beams, based on Euler-Bernoulli beam theory [117–129] and Timoshenko beam theory [130–138] and other one-dimensional beam theories [139–144]. Very recently, Chen et al. [145] presented an iso-geometric three-dimensional numerical solution for vibration analysis of AFG beams with variable thickness using the non-uniform rational B-splines(NURBS) basis functions. More extensive literature related to this category can be found in recent review articles presented by Sayyad and Ghugal [146, 147], and Zhang et al. [148].

The present review clearly indicates that most of the analytical and numerical solutions are based on one-dimensional beam theories. But, a two-dimensional elasticity solution is always needed for accurate prediction of static/dynamic behavior and edge effects of composite or functionally graded beams.

1.3.2 Analysis of piezoelectric beams and AFG beams integrated with piezoelectric layers

Piezoelectric material layers are used to regulate the static and dynamic behavior of the structures through actuation and sensing and also used to control the vibration generated during operation which increases safety, usability, and durability of structures [149]. It is very important to know the dynamic behavior of AFG beams integrated with piezoelectric layers under arbitrary boundary conditions. Bailey and Hubbard [150] employed distributed-parameter control theory to design and analyze the active vibration damper for a thin cantilever beam. Using Euler Bernoulli beam theory, Crawley and De Luis [151, 152] developed static and dynamic computational models for beams with highly distributed actuators and sensors which were either bonded on their top surface or embedded in between the elastic layers. Yang and Lee [153] presented an analytical model to obtain mode shapes and the fundamental frequencies of a stepped piezoelectric cantilever beam having surface bonded piezoelectric layers. By developing the constituent equations for piezoelectric bimorph beam, Low and Guo [154] presented a dynamic model with hysteresis for three-layered piezoelectric bimorph beam. Sunar [155] documented the application of piezoelectric materials in the field of sensing and active control of flexible structures in his review article. Saravanos and Heyliger [156], and Gopinathan et al. [157] presented a detailed review of several theories and analytical model for the analysis of smart piezoelectric structures. Kapuria et al. [50] developed a new efficient one-dimensional coupled model based on third-order zigzag approximation for the dynamic analysis of simply-supported piezoelectric composite beams. Further, Kapuria et al. [158] presented a new coupled consistent third-order theory (CTOT) to obtain an analytical solution for dynamic and static analysis of simply-supported hybrid piezoelectric beams. Using the pseudospectral method, Kekana [159] presented the free vibration solution for composite beams mounted with piezo patch acting as sensors and actuators. Based on the Euler-Bernoulli beam theory and Rayleigh-Ritz approximation, Della and Shu [160] developed a micromechanics technique to obtain the free vibration solution for beams embedded with piezoelectric material actuators and sensors. Further, Della and Shu [161] extended this approach to develop a dynamic solution for beams with piezoelectric inclusions. Using the transfer matrix, Wang [162] obtained fundamental frequencies and corresponding mode shapes of a beam with surface bonded pair of piezoelectric segments. Khdeir et al. [163] presented analytical solutions for the free vibration analysis of cross-ply piezolaminated beams embedded with piezoelectric actuators. The state-space approach is applied to obtain fundamental frequencies and corresponding mode shapes for arbitrary support conditions. Further, Khdeir and Aldraihem [164] presented a novel zig-zag theory for free vibration analysis of sandwich beams with softcore. Muthalif and Nordin [165] developed an approach to find an

optimum shape for cantilever-type energy harvester to improve its performance. Fu et al. [166] and Li et al. [167] presented free vibration analysis of functionally graded (FG) beams with piezoelectric sensors and actuators. Nilanjan Chattaraj and Ranjan Ganguli [168–170] presented Euler-Bernoulli based one-dimesional (1D) nonlinear analytical model to analyze the detailed electromechanical behavior of piezoelectric bimorph actuators at high magnitude electric field. Most of the above work on piezoelectric beam is based on one-dimensional theories.

Kapuria et al. [171] presented the exact 2D piezoelasticity solution for simply-supported beams with damping under harmonic electromechanical load. The more detailed literature on the free vibration analysis of elastic and piezoelectric beams can be found in the recent review articles presented by Gupta et al. [172], Hajianmaleki and Qatu [173], and Kumar [174]. An extensive literature survey has revealed that analytical 2D piezoelasticity free vibration solution for arbitrary supported beams is not available in the literature [146]. Very recently, using asymptotic development method (ADM) in conjunction with Euler-Bernoulli beam theory, Cao et al. [175] developed analytical solution solution for free vibration analysis of non-uniform and non-homogenous Euler-Bernoulli beam integrated with piezoelectric layers and subjected to arbitrary boundary conditions.

Due to the coupled constitutive relation between elastic and electric field, the behavior of these type of hybrid beam structures is very complicated. Hence, an efficient solution method is needful to predict the complex behavior of arbitrarily supported AFG beams integrated with piezoelectric layers which will also act as a benchmark for assessing other approximate or numerical method.

1.3.3 Static and Dynamic Analysis of In-plane Functionally Graded Plates

The literature related to static and dynamic analysis of functionally graded plates can be categorized into two broad categories as per the nature of gradation assumed in the FGM i.e. (i) through-thickness variation of material properties, and (ii) in-plane or multidirectional variation of material properties. Three-dimensional (3D) elasticity analytical model can predict the behavior of FGM structures more accurately as compared to the two-dimensional theories. However, developing the 3D solution is difficult because the material properties are varying along the spatial coordinate [176]. Most of the 3D solutions have been presented for the FGM structures with through-thickness variation of material properties, using different approaches such as asymptotic approach [177, 178], extended Pagano's approach [53, 179], Plevako method [180–183], power series method [37, 184], Peano-Baker series method [185], and state space/Fourier series method [186–192]. Recently, Lomtepatil et al. [193] presented semi-analytical three dimensional (3D) elasticity solution for simply-supported through-thickness functionally graded (FG) plate by using fourth-order Runge-Kutta algorithm. Very recently, Vafakhah and Neya [194] developed an exact three-dimensional solution for bending analysis of through-thickness functionally graded thick rectan-

gular plate subjected to simply-supported boundary conditions. The more extensive literature on through-thickness FGM structures can be found in recent review papers presented by Swaminathan et al. [13], Jha et al. [11], and Thai and Kim [12]. A brief review of literature related to analysis of in-plane functionally graded plates is given below.

- **3D elasticity solutions:** Aragh et al. [195] presented the three-dimensional free vibration solution for two-dimensional functionally graded fiber-reinforced (2D FGFR) curved panels considering a novel 2D six-parameter power-law distribution of material properties along its thickness and longitudinal directions. Two-dimensional generalized differential quadrature method (GDQM) is used to develop an accurate solution for free vibration and vibrational displacement field characteristics. The curved panel with two opposite edges simply-supported and other edges with arbitrary boundary conditions are analyzed. Asemi et al. [196] used the graded finite element for three-dimensional static analysis of two-dimensional functionally graded plates in which material properties vary along both the longitudinal and thickness directions continuously. Tahouneh and Naei [197] developed three-dimensional elasticity solution for 3D dynamic analysis of thick multi-directional functionally graded rectangular plates resting on a two-parameter elastic foundation. In the proposed solution, two opposite edges of rectangular plates have been simply-supported, and the other two edges have any possible combination of free, simply-supported and clamped boundary conditions. The material properties are assumed graded in thickness and in-plane directions following a novel 2D six-parameter power-law. The resulting governing equation is solved by two-dimensional differential quadrature method and the analysis illustrated that grading of material properties in two directions has higher capability of reducing the natural frequency than conventional 1D FGM. Using the scaled boundary finite element method, Xiang et al. [198] presented the three-dimensional elasticity solution for free vibration and the mechanical buckling of the plate with in-plane material inhomogeneity. The material properties are assumed graded only in the in-plane direction by a simple power law. In this paper, results are presented for isotropic plate subjected to all around simply-supported and all around clamped type support conditions.

  Lü et al. [199] employed the state-space formalism in conjunction with the differential quadrature method (DQM) to develop semi-analytical 3D elasticity solutions for bi-directional functionally graded orthotropic rectangular plates subjected to Levy-type support conditions. Material properties are assumed to vary exponentially along the longitudinal (x) and the thickness (z) directions of the plate. In this work, the author concluded that the deflection of plate is affected to a great extent by grading the material along in-plane direction. Recently,

Adineh and Kadkhodayan [200] presented thermo-elastic solution for a rectangular isotropic plate graded in all the three directions. A power law variation for material gradation is assumed and differential quadrature method is used to develop the numerical solution. Very recently, Ravindran and Bhaskar [201] presented three-dimensional elasticity analytical solution for static analysis of functionally graded orthotropic rectangular plates having in-plane uniaxial grading using a combination of Kantorovich and power series approaches. The fiber volume fraction is assumed to vary along with in-plane directions according to a specified grading law.

- **2D solutions:** Very first work in this direction is reported by Tomar et al. [202, 203] in which isotropic non-homogeneous circular plate and rectangular panel (plate with infinite length along an in-plane direction) were analyzed under free vibration case. For this study, Young's modulus and density are assumed to vary exponentially along x-axis of the panel whereas Poisson's ratio remains constant. The governing differential equation in deflection terms is developed by using the classical plate theory and differential equation with varying coefficients is solved using the Frobenius method. Aboudi et al. [204, 205] developed the generalized higher-order theory for the functionally graded orthotropic rectangular plate by considering the material properties varying in all the two orthogonal directions. They studied the influence of microstructure on the microscopic and macroscopic quantities which govern the response of composites. Fares and Zenkour [206] developed the buckling and free vibration of the nonhomogeneous orthotropic rectangular laminated plate by using higher-order plate theory (HPT), first-order plate theory (FPT), classical plate theory (CPT). They assumed the exponential variation of stiffness along x and y-axis of the plate. They concluded that the free vibration and state of stability are strongly affected by the degree of non-homogeneity. Liu et al. [207] obtained a Levy-type solution based on the classical plate theory (CPT) to analyze free vibration of a functionally graded rectangular plate. The Fourier series expansion technique and particular integration method are used to solve the fourth-order ordinary differential equation with variable coefficients. They considered material inhomogeneity along the in-plane direction rather than conventional thickness direction. Author observed that the in-plane grading of material properties significantly effect the natural frequencies of the plate. Further, the desired natural frequencies to meet any special requirements is also achieved by adjusting the in-plane grading parameters. Yu et al. [208] presented an analytical solution of a bending problem for a thin isotropic rectangular plate with in-plane variable stiffness under the distributed loads. In the rectangular plate, two-opposite-edges parallel to y-direction is assumed to be simply-supported. Flexural rigidity of the plate is assumed to vary in the plane

following the power law while Poisson's ratio remain constant. The fourth order governing equation with variable coefficient transformed into a Whittaker equation to obtain the analytical solution. Recently, Boreyri et al. [209] employed a truncated Taylor series expansion method to obtain the Levy-type solution for free vibration analysis of an in-plane exponentially graded rectangular plate. Very recently, Amirpour et al. [210, 211] presented analytical solutions for bending analysis of functionally graded isotropic rectangular plates with in-plane stiffness variation using higher-order shear deformation theory (HSDT). Power-law variation of material properties is considered along the in-plane direction.

Two-dimensional numerical solutions for rectangular plates are also developed by assuming in-plane or multidirectional variation of material properties based using the classical plate theory (CPT) for isotropic plates [212–222] and orthotropic plates [90, 223–232]. Similarly, some higher-order shear deformation theory (HSDT) based two-dimensional solutions are also available in literature for isotropic plate [233–236]. Very recently, Xue et al. [237] presented a numerical solution for free vibration analysis of in-plane functionally graded plates using a refined plate theory and isogeometric approach.

Based on the above literature survey, it is observed that,

(i) Three-dimensional analytical solution for static and dynamic analysis of in-plane functionally graded isotropic/orthotropic rectangular plate does not exist in the literature for arbitrary support conditions. Very recently, three-dimensional elasticity analytical solution is reported by Ravindran and Bhaskar [201] for static analysis of all around simply supported in-plane functionally graded plate

(ii) Mostly, numerical or semi-analytical techniques are used for three-dimensional analysis of in-plane or multidirectional functionally graded structures. These numerical techniques require more computational effort and large computer memory [13].

(iii) Most of the three-dimensional numerical solution is limited to functionally graded isotropic plates.

(iv) Most of the two-dimensional solution is based on classical plate theory. The analysis based on higher order shear deformation theory (HSDT) is very limited and only available for the isotropic plates.

However, the study related to the in-plane variation of material properties is very limited. There are practical occasions where grading of macroscopic properties in multi or in-plane directions is needed [238]. Boundary layer effects or edge effects in such FGM plates can be predicted accurately

by 3D elasticity analytical models [13]. Therefore, it is necessary to develop 3D elasticity analytical solutions to understand the behavior of arbitrarily supported longitudinally functionally graded plates.

1.3.4 3D piezoelectricity Solution for Dynamic analysis of Piezolaminated flat panels

A decade ago, the researchers introduced the concept of smart structures in which active material (piezoelectric) layers are integrated with host laminates. These structures are known as smart/adaptive or intelligent structures which can be used for health monitoring and vibration control purpose. Such hybrid (smart) structures are subjected to arbitrary loadings (static and dynamic loads) and boundary conditions. Due to electromechanical coupling in such piezoelectric laminates, the behavior of structure (like edge effect) is more complex and can lead to peeling of the piezoelectric actuators and sensors layers. Understanding their bending, buckling and free vibration behavior, with sufficient accuracy has gained research interest. Thus many mathematical models have been developed to predict the behavior of composite plates, sandwich plates, and piezoelectric laminated structures. Knowledge of fundamental frequencies and mode shapes are very much required for efficient design of smart structures. Three-dimensional (3D) semi-analytical/analytical solutions can accurately predict the natural frequencies and influence of electromechanical coupling. A brief review on 2D and 3D solution for free vibration analysis of flat panels is given below

Five decade ago, Jones [239] presented an exact free vibration solution for cross-ply simply-supported plate under plane strain condition (cylindrical bending). Further, [240] extended this approach to free vibration solution of angle-ply panels. After a long gap, Heyliger and Brooks [241] further extended this elastic solution to piezoelectric case where an exact solution was developed to acquire the natural frequencies and through-thickness modal distributions of simply-supported cross-ply piezoelectric plate in cylindrical bending. Further, Kumari et al. [242] presented 2D exact solutions for harmonic analysis of flat hybrid piezoelectric and magnetoelastic angle-ply panels under simply-supported boundary conditions. By employing Fourier series method, Yang et al. [243] obtained the forced vibration response of a composite elastic panel mounted with piezoelectric actuator layers at the top and bottom surfaces. By employing Stroh formalism, Vel et al. [244] presented an analytical technique to study the free vibration problem of a laminated elastic panel with either embedded or surface mounted piezoelectric patches of arbitrary thickness and width. Chen and Lee [245] presented the 3D free vibration solution of arbitrary supported cross-ply laminate in cylindrical bending using semi-analytical approach SSDQM (state space approach along the thickness and differential quadrature method (DQM) along in-plane direction). Using SSDQM, Zhou et al.[246] developed semi-analytical free vibration solution for arbitrarily supported orthotropic piezoelectric cross-ply flat panels. Further, Zhou et al. [247] extended this approach to investigate

the static and dynamic behaviour of cross-ply piezoelectric panels with interlaminar bonding imperfections. Very recently, Udayakumar and Gopal [248] employed a modified state space differential quadrature method to develop a dynamic solution for thick sandwich panel having soft core with general edge support conditions. Ebrahimi and Barati [249] investigated the thermal stability of magneto-electro-thermo-elastic functionally graded (METE-FG) nanoplates based on the nonlocal theory and a refined plate model. Ebrahimi and Barati [250] also developed a nonlocal strain gradient plate model for the damped vibration analysis of smart piezoelectric polymeric nanoplates resting on viscoelastic medium. Furthermore, Ebrahimi and Barati [251] presented an analytical model to study the effects of the magnetic field on the free vibration behavior of magneto-electro-elastic functionally graded smart nanoplates (MEE-FG) under arbitrary support conditions. Using the refined four-variable plate theory, Barati and Zenkour [252] developed an analytical solution for electro-thermo-mechanical vibrational analysis of a porous functionally graded piezoelectric (FGP) plate. Very recently, Abad and Rouzegar [253] presented exact wave propagation analysis for moderately thick Levy-type plate integrated with piezoelectric layers using spectral element method. The present literature survey is limited to the free vibration analysis of panels. The detailed literature about the mathematical models and solution techniques to analyze the static and the dynamic behavior of laminates can found in review articles [16, 254]. Very recently, Yan et al.[255] presented a 3D exact solution for the analysis of imperfect angle-ply smart plate in cylindrical bending and subjected to simply-supported boundary condition. KelvinVoigt viscoelastic model is implemented to describe the interfacial properties and state space method is applied to obtain the solution of simply-supported angle-ply panels with surface-bonded piezoelectric layers.

As 3D solutions of piezoelectric laminates involve complex mathematics, extracting the natural frequencies is furthermore challenging. Therefore, the two-dimensional solutions have also been proposed in this area. Using classical plate theory (CLT) and first-order shear deformation theory (FSDT), Khdeir [256] obtained the free and forced vibration solution of the anti-symmetric angle-ply flat panels under arbitrary boundary conditions. Messina [257] investigated the free vibration behavior of angle-ply composite multilayered panels using higher order plate theories. Further, Messina and Soldatos [258] extended it to dynamic case, where 2D parabolic shear deformable plate theory was used. This theory satisfy inter-laminar continuity of both shear stresses and displacements for the arbitrary stacking pattern. Based on equivalent single layer approximation, Shu [259] developed an accurate theory to obtain the free vibration response of cross-ply piezoelectric laminates subjected to arbitrary combination of boundary conditions. Further, Shu [260] extended this approach to study static and free vibration behaviors of cross-ply piezoelectric plate under cylindrical bending with interfacial shear slip. Kim [261] developed two enhanced theories

namely EFSDT (enhanced first-order shear deformation theory) and EHSDT (enhanced higher-order shear deformation theory) for composite and sandwich plates based on the mixed variational formulation and obtained analytical free vibration solutions for angle-ply simply-supported plates in cylindrical bending. Recently, Behera and Kumari [262] presented an exact analytical free vibration solution for Levy-type rectangular laminated plate based on efficient zig-zag theory (ZIGT) and third-order theory (TOT). But, two-dimensional solutions can not provide accurate free vibration response for thick laminates [254].

Based on literature survey, it is observed that no three-dimensional analytical solution exists for free vibration analysis of angle-ply laminated piezoelectric panel under arbitrary boundary conditions. Zhou et al. [246] also stated that usually for such cases the coupled piezo-elasticity analytical solutions is very difficult to drive. Apart from this, the following loopholes exist in the literature,

(i) In the majority of works (3D/2D), the first fundamental frequency is reported only. But, from practical designing of structures, at least three consecutive frequencies should be known.

(ii) Majority of results were presented for composite panels. Results for angle-ply sandwich panels are not available for arbitrary boundary conditions.

(iii) Mode shapes of piezolaminated panels under arbitrary supports condition are not available in literature

Hence, an efficient analytical solution is needed to predict the complex dynamic behavior of arbitrarily supported piezoelectric laminated panels which will also act as a benchmark for assessing other approximate or numerical method. Analytical techniques are preferred because of its simplicity and high accuracy. Moreover, the closed-form 3D piezoelasticity solution helps to understand the complex electro-mechanical behavior of hybrid panels and helps to make a suitable assumption for the kinematic and the kinetic field variables for developing 1D/2D plate theories.

1.4 EXTENDED KANTOROVICH METHOD

Initially, famous Russian mathematician/economist, Leonid Vitaliyevich Kantorovich, joint winner of the 1975 Nobel Prize in economic sciences [263], developed a method to eliminate the intrinsic limitation of the various numerical method (Ritz and Galerkin methods) related to satisfaction of natural and essential boundary conditions at initial step. He proposed a method, known as Kantorovich method [264] which gives closed-form (exact) solution along one direction by assuming the solution along other direction in the form initial functions. Later, Kerr [265, 266] extended the

Kantorovich method to obtain the analytical solution by reducing the bivariate partial differential equations (PDEs) to ordinary differential equations (ODEs) in two directions. In his approach, known as extended Kantorovich method (EKM), solution of the bivariate variable of PDEs is assumed as a series of products of two separable functions as,

$$w_m(x,y) = \sum_{i=1}^{n} f_i(x) g_i(y) \tag{1.1}$$

In the first step, $f_i(x)$ functions of x-direction are considered as unknown, and independent $g_i(y)$ functions of y-direction are assumed initially to start the solution process. By substituting the Eq. (1.1) in variational form of PDEs, a set of the ordinary differential equations (ODEs) is obtained for $f_i(x)$. These ODEs are solved in closed form manner to obtain the functions $f_i(x)$. In the second step, these $f_i(x)$ functions are considered as prior known functions and $g_i(y)$ function of y-direction considered as unknown. The similar approach of the first step is adopted to obtain the solution for $g_i(y)$ functions. These two iterative steps are repeated until the results converge to the desired degree of accuracy. This iterative process converges very fast (generally in two/three iterations), even when the initially assumed functions do not satisfy the boundary conditions of the problem, and moreover, the accuracy of the final obtained solution is independent of the initial guess. The selection of appropriate and inappropriate according to boundary conditions affects the solution at most to one or two more iteration steps. This independence from chosen the approximate initial function, according to the boundary condition of problems is the most crucial advantage of this method over other numerical or semi-analytical methods, *i.e.* Ritz and Galerkin methods.

Therefore, in the recent past, extended Kantorovich method becomes very popular to obtained analytical solutions for analyzing the statics, dynamics, and stability behavior of structures. This method has been applied successfully to get the accurate solution for several problems of elastic single layer [267, 268], multi-layer composite plates [269–274] and shells [275, 276] subjected to arbitrary boundary conditions. The detailed literature on extended Kantorovich method can be found in a recent review article presented by Singhatanadgid and Singhanart [277]. Recently, Kapuria and Kumari group presented three-dimensional (3D) analytical solution for various type of composite plates [278–280] and piezoelectric laminated plates [281, 282] subjected to arbitrary support condition using the extended Kantorovich method. Further, Kumari and Behera extended this approach to develop 3D free vibration solution for a rectangular composite plate [283] and piezo-laminated plate [284] under Levy-type support conditions. Recently, Moeenfard and Maleki [285] applied extended Kantorovich method to obtain the static response of micro-plates under electrostatic actuation. Very recently, Kumari and Kar [286] applied extended Kantorovich method to get analytical 3D elasticity solution for arbitrarily supported composite laminated cylindrical shell panels. Similarly, using three-dimensional multi-term extended Kantorovich method (3DMTEKM), An-

dakhshideh el al. [287] developed analytical 3D stress solution for generally laminated piezoelectric (PZT) plates to the interlaminar stresses.

It is apparent from the present literature review that all the problems which have been solved using extended Kantorovich method so far related to homogenous (constant property) plates and shells structures. The elasticity formulation of in-plane functionally graded structures also involves bivariate functions. But, till date, the EKM was not applied to develop elasticity solution for such arbitrary supported functionally graded structures because the final system of ODEs obtained after applying EKM has variable coefficients which are very difficult to solve in closed-form manner. It prevented a straight forward application of existing EKM to elasticity solutions of functionally graded structures.

1.5 OBJECTIVES OF THE PRESENT WORK

Based on literature survey, the following objectives were identified for present research work with the primary aim of (i) Developing two-dimensional elasticity analytical solution for static and modal analysis of axially functionally graded beam and (ii) Obtaining the 3D elasticity based analytical solution for in-plane functionally graded plate structures, and further (iii) Studying the effect of integrated piezoelectric layers on response of such structures. The specific objectives are:

1. To develop an analytical elasticity solution for static and free vibration analysis of axially functionally graded beams subjected to arbitrary boundary conditions using the mixed-field multi-term extended Kantorovich method (EKM).

2. To develop an accurate 3D elasticity solution for the in-plane functionally graded rectangular plate subjected to Levy-type boundary conditions, using the multi-term extended Kantorovich method (EKM).

3. To investigate the effect of boundary layer stresses for laminated rectangular plates bonded with a functionally graded adhesive inter-layer and study the effect of material properties gradation, aspect ratio and boundary condition on deformation and stresses.

4. To develop an analytical elasticity solution for the free vibration analysis of in-plane functionally graded rectangular plates subjected to Levy-type boundary conditions.

5. Further, this approach extended to develop an elasticity solution for static and free-vibration analysis of axially functionally graded angle-ply flat panels subjected to arbitrary boundary condition.

6. To present an accurate analytical solution based on coupled three-dimensional (3D) piezoelectricity equations for free vibration analysis of the angle-ply elastic and piezoelectric flat laminated panels under arbitrary boundary conditions.

7. To develop free vibration solution for arbitrary supported axially functionally graded beams integrated with piezoelectric layers.

1.6 ORGANISATION OF THE THESIS

The complete work presented in this thesis has been organized into seven chapters. Chapter 1 is devoted to the literature survey and the proposed objectives of the present work. An overview of the contents of the remaining six chapters is presented below.

Chapter 2 presents an analytical 2D elasticity solution for static and free vibration analysis of axially functionally graded beams subjected to arbitrary boundary conditions using the multi-term extended Kantorovich method (EKM). Further, the static and free vibration solution for the arbitrarily supported homogeneous beam are also obtained as a special case of the present study. The material properties of the beam are considered to vary linearly along its axial (x) direction. Modified Hamilton's principle is applied to derive the weak form of coupled governing equations in which all the stresses and displacements act as primary variables. Further, the extended Kantorovich method is employed to reduce the governing equations into sets of ordinary differential equations (ODEs) along the axial (x) and thickness (z) directions. The system of ODEs along the z-direction has constant coefficients which is solved analytically. But, the system of ODEs along x-direction has variable coefficients which is solved using a modified power series method. Interface continuity and boundary conditions are satisfied in exact point-wise manner which ensures the same order of accuracy for all field variables (stresses and displacements). Efficacy and accuracy of the present methodology are verified thoroughly with existing literature and 2D finite element solution. Benchmark numerical results are presented for various cases of material property variations under different type of boundary conditions. The influence of the axial gradation, aspect ratio and boundary conditions on the static and dynamic behavior of the beam are investigated. Significant effect of axial gradation on the static and dynamic behavior of the beam is observed.

Chapter 3, contains 3D elasticity based EKM solution for the static and free vibration analysis of in-plane functionally graded rectangular plate subjected to Levy-type boundary conditions. A linear variation of material compliances is assumed along its longitudinal (x) direction. Benchmark numerical results are presented for different sets of boundary conditions, aspect ratios and configurations by considering the various cases of material property gradation. For the first time, numerical results for a two-layered plate having different in-plane material gradation in each layer

are presented along with single layer plate results. The numerical study reveals that the EKM solution converges within just one/two terms for both single layer and two-layer FGM plates. It is observed that the static and dynamic response of plate is influenced greatly by the extent of material gradation along the in-plane direction. Effects of in-plane property gradation in the adhesive interlayer on deflections and stresses of the plate are also investigated under different boundary conditions. The present analytical solution can serve as a benchmark for assessing the accuracy of the 2D or 3D numerical solutions. The current research will also be beneficial to model rectangular plate structures and adhesive bonded rectangular plates in which material properties are degraded due to some environmental effect.

In Chapter 4, the generalized 3D EKM solution is presented for the static and free vibration analysis of longitudinally functionally graded angle-ply flat panels subjected to arbitrary boundary conditions. Benchmark numerical results are presented for single layered and multi-layered in-plane functionally graded angle-ply flat panels. Numerical results are validated thoroughly by comparing with 3D finite element (FE) results. The influence of property variation on the deflections and stresses are studied and discussed comprehensively for arbitrary sets of boundary conditions and configurations. The present method provided benchmark results to assess the validity and accuracy of different plate theories and computational models for the analysis of axially functionally graded angle-ply flat panels. The current research will also be beneficial to model real-life panel structures in which its material properties deteriorate due to some environmental effect.

In Chapter 5, a 3D piezoelectricity based analytical solution is developed for free vibration analysis of the angle-ply elastic and piezoelectric flat laminated panels under arbitrary boundary conditions. The present analytical solution is applicable to composite, sandwich and hybrid panels having arbitrary angle-ply lay-up, material properties and boundary conditions. The modified Hamilton's principle approach has been applied to derive the weak form of governing equations where stresses, displacements, electric potential, and electric displacement field variables are considered as primary variables. After that multi-term multi-field extended Kantorovich approach (MMEKM) is employed to transform the governing equation into two sets of algebraic-ordinary differential equations (ODEs), one along in-plane (x) and other along with the thickness (z) direction, respectively. These ODEs are solved in closed-form manner which ensures the same order of accuracy for all the variables (stresses, displacements, and electric variables) by satisfying the boundary and continuity equations in exact manner. A robust algorithm is developed for extracting the natural frequencies and mode shapes. The numerical results are reported for various configurations such as elastic panels, sandwich panels and piezoelectric panels under arbitrary sets of boundary conditions. The accuracy and efficacy of the present method have been established by

comparing the present numerical results with the results available in the literature and with the 3D FE results of ABAQUS. The effect of ply-angle and thickness to span ratio (s) on the dynamic behavior of the panels are also investigated. The presented 3D analytical solution will be helpful in the assessment of various 1D theories and numerical methods.

In Chapter 6, a novel 2D analytical free vibration solution is developed for axially functionally graded (AFG) beams integrated with piezoelectric layers and subjected to arbitrary support boundary conditions. The material properties of the elastic layers are considered to vary linearly along the axial (x) direction of the beam. Further, the free vibration solution for the arbitrarily supported piezo-laminated beams is also obtained as a special case of the present study. New benchmark numerical results are presented for a laminated piezoelectric beams and axially functionally graded beams integrated with piezoelectric layers. The influence of the axial gradation, aspect ratio and boundary conditions on the natural frequencies of the beam are also investigated. Moreover, the longitudinal variation of displacements and stresses (mode shapes) for various cases are also plotted for different support conditions. These numerical results can be used for assessing 1D beam theories and numerical techniques.

Finally, the major conclusions of this work and suggestions for future research are summarized in Chapter 7.

Chapter 2

Functionally Graded Beams- 2D Elasticity Analysis

An analytical two-dimensional (2D) elasticity solution for static and dynamic analysis of arbitrarily supported axially functionally graded (AFG) beams is presented first time in this chapter using the multi-term extended Kantorovich method (EKM). The material properties of the beam are considered to vary linearly along the axial (x) direction, as given in Sec. 2.1 . The modified Hamiltons principle is applied to derive the mixed form of governing equations in which stresses and displacements act as primary variables, as explained in Sec. 2.2. Further, the extended Kantorovich method is employed to reduce the governing equation into sets of ordinary differential equations (ODEs) along the axial (x) and thickness (z) directions, as explained in Sec. 2.3, 2.4 and 2.5. The ODEs along the z-direction have constant coefficients which are solved exactly in closed form manner for static and dynamic case in Sec. 2.4.1 and Sec. 2.4.1, respectively. Where the ODEs along x-direction have variable coefficients which are solved using the modified power series method, as explained in Sec. 2.5.1 and 2.5.2 for static and dynamic case, respectively. The boundary and continuity equations are satisfied in exact point-wise manners which ensures the same order of accuracy for all the variables. For free vibration case, the coefficient of final ODEs contains the frequency ω which is obtained by first bracketing the root and then using the bi-section method. It is found that the single-term solution is sufficient enough for obtaining the natural frequencies. Where the two-term solution is needed to predict the variation of stresses at very near to clamped and free edges. New benchmark numerical results are presented for a single-layered AFG beam and laminated AFG beams. Numerical results are presented for various variation cases to studied the effect of in-plane variation of material properties on the static and free vibration response of the beams in Sec. 2.8 and Sec. 2.9, respectively. The influence of the boundary conditions, configuration and aspect ratio on the static and free vibration response of the beam are also investigated. These numerical results can serve as a benchmark for assessing 1D beam theories and other semi-analytical or numerical techniques.

2.1 BASIC ASSUMPTION

Consider a cross-ply multilayered axially graded beam (Fig. 2.1) with span length a along x-direction and total thickness h along z-direction. It can have any arbitrary boundary conditions at $x = 0$ and a, and is subjected to uniformly distributed pressure loads of p_1 and p_2 applied on the bottom and top surfaces, respectively. The laminated AFG beam is made of L perfectly bonded layers of orthotropic materials with the principal material axis x_3 oriented along the z-direction. The mid-plane of the plate is chosen as the xy-plane. The principal material axis x_1 of the kth layer numbered from the bottom is at an angle θ_k to the x-axis. The thickness of the kth layer is $t^{(k)}$, and the z-coordinate of its bottom surface is denoted as z_{k-1}. The interface between the kth and the $(k+1)$th layer is named as the kth interface. The layer superscript is omitted unless needed for clarity.

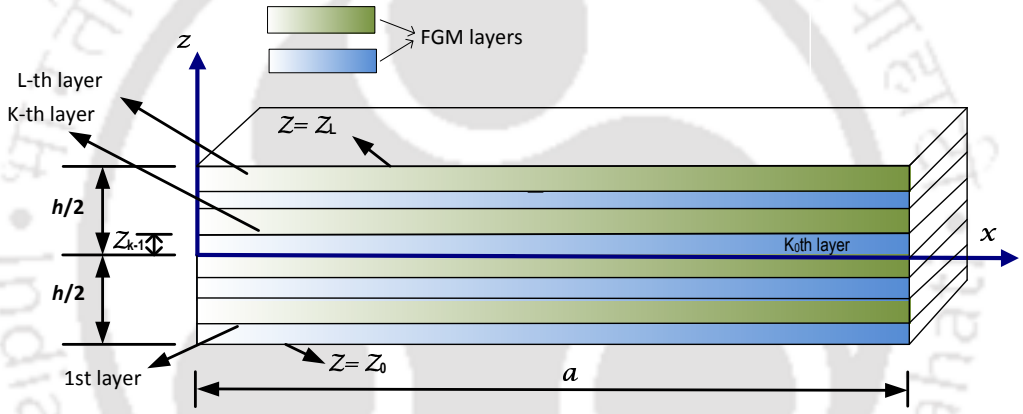

Fig. 2.1: Geometry of the AFG laminated beam.

The compliance and density of the elastic layers are assumed to vary linearly and continuously along the axis (x) of beam

$$\begin{aligned} \bar{s}^m_{1j}(\xi) &= \bar{s}_{1j}(1+\delta_1\,\xi) \Longrightarrow \bar{s}_{1j} + \hat{s}_{1j} \quad \text{for} \quad j = 1, 3 \\ \bar{s}^m_{55}(\xi) &= \bar{s}_{55}(1+\delta_2\,\xi) \Longrightarrow \bar{s}_{55} + \hat{s}_{55} \\ \rho^m(\xi) &= \rho(1+\delta_p\,\xi) \Longrightarrow \rho + \hat{\rho} \end{aligned} \tag{2.1}$$

where ξ non-dimensional parameter along x $(\xi = x/a)$. δ_1 and δ_2 are variation indexes which control the gradation in elastic properties, and δ_p is the variation index for density. These variation indexes can have any arbitrary value.

Various devices/equipment are subjected to various types of loading, boundary conditions and under chemical and gaseous environments such as hydrogen gas exposure, erosive and corrosive environment, under cryogenic conditions etc. Metals, composite materials, fibers, are adsorb hydrogen, moisture and other chemical. From the preliminary studies, it has been found that elastic

properties of composites change specifically along the span due to the diffusion of hydrogen atoms and other environmental effect [288–290]. Similarly, In biomedical sciences also, it has been found that stiffness of major bones in our body varies along the span of bone. To address the above issues, such type of variation is considered where the δ_1, δ_2 and δ_p may be positive or negative.

Comparison of present gradation model with other probabilistic gradation models, like Rule of Mixture, Mori-Tanaka scheme and Exponential function gradation, is presented in Appendix A. It is observed that the type of gradation profiles obtained from other probabilistic gradation models, can also be achieved in the present gradation model by selecting the proper gradation parameters (δ_1, δ_2 and δ_p).

2.2 GOVERNING EQUATIONS FOR FGM BEAMS

Since width is very small along y-direction, the displacement u and w considered along x-axis and z-axis, respectively are independent of y coordinate. Therefore, stresses $\sigma_y, \tau_{yz}, \tau_{xy}$ becomes zero. For such plane stress condition, constitutive equations of an orthotropic AFG lamina, when transformed from the material coordinate system (x_1, x_2, x_3) to the plate coordinate system (x, y, z) consider (2.1), can be written as,

$$\begin{bmatrix} \varepsilon_x \\ \varepsilon_z \\ \gamma_{zx} \end{bmatrix} = \begin{bmatrix} (\bar{s}_{11}+\hat{s}_{11}) & (\bar{s}_{13}+\hat{s}_{13}) & 0 \\ (\bar{s}_{13}+\hat{s}_{13}) & \bar{s}_{33} & 0 \\ 0 & 0 & (\bar{s}_{55}+\hat{s}_{55}) \end{bmatrix} \begin{bmatrix} \sigma_x \\ \sigma_z \\ \tau_{zx} \end{bmatrix} \tag{2.2}$$

where σ_i and τ_{ij} denote the normal and shear stress components, respectively and ε_i and γ_{ij} denote the normal and shear strains components, respectively. $\bar{s}_{ij}$ are the transformed elastic compliances, whose expressions in terms of the engineering properties, namely, Young's moduli Y_i, shear moduli G_{ij} and major Poisson's ratios ν_{ij}, are given as,

$$\bar{s}_{11} = 1/Y_1; \qquad \bar{s}_{13} = -\nu_{31}/Y_3 = -\nu_{13}/Y_1; \quad \bar{s}_{33} = 1/Y_3; \qquad \bar{s}_{55} = 1/G_{13} \tag{2.3}$$

Where $\hat{s}_{ij}$ are corresponding to variation of material properties. To ensure numerical stability in the solution process all entities are expressed in non-dimensional forms in such a way that, on substitution of dimensionless entities, the form of all of all governing equations remains unchanged.

$$\begin{array}{ll} s = h/a; & (\sigma_x^*, \sigma_y^*, \sigma_z^*, \tau_{yz}^*, \tau_{zx}^*, \tau_{xy}^*, p_\alpha^*) = (\sigma_x, \sigma_y, \sigma_z, \tau_{yz}, \tau_{zx}, \tau_{xy}, p_\alpha)/sY_0 \\ \bar{s}_{ij}^* = \bar{s}_{ij} Y_0; & (\varepsilon_x^*, \varepsilon_y^*, \varepsilon_z^*, \gamma_{yz}^*, \gamma_{zx}^*, \gamma_{xy}^*) = (\varepsilon_x, \varepsilon_y, \varepsilon_z, \gamma_{yz}, \gamma_{zx}, \gamma_{xy})/s \\ (u^*, v^*, w^*) = (u, v, w)/h; & (G_{ij}^*, Y_i^*) = (G_{ij}, Y_i)/Y_0 \\ [h^*, t^{*(k)}] = [h, t^{(k)}]/a & \end{array} \tag{2.4}$$

where Y_0 is the value of the Young's modulus used for non-dimensionalization. In subsequent mathematical equations the above dimensionless forms of the entities is used where the superscript

* is dropped for simplicity. The strain-displacement relations are,

$$\varepsilon_x = u_{,x}\,; \qquad \gamma_{zx} = w_{,x} + u_{,z}\,; \qquad \varepsilon_z = w_{,z} \tag{2.5}$$

where a subscript comma denotes differentiation. The extended Hamilton principle [283] in a mixed form for free vibration analysis of the AFG beam, without any body force source and unit width along y-direction, can be expressed as,

$$\begin{aligned}\int_t \int_V [&\delta u(\sigma_{x,x} + \tau_{xz,z} - \rho\ddot{u}) + \delta w(\tau_{zx,x} + \sigma_{z,z} - \rho\ddot{w}) + \delta\sigma_x(\varepsilon_x - u_{,x}) \\ &+\delta\sigma_z(\varepsilon_z - w_{,z}) + \delta\tau_{zx}(\gamma_{zx} - u_{,z} - w_{,x})]\,\mathrm{d}V\,\mathrm{d}t = 0, \quad \forall\ \delta u_i,\ \delta\sigma_i,\ \delta\tau_{ij}\end{aligned} \tag{2.6}$$

Where V denotes the volume of beam for per unit width along the y-direction. Equation (2.6) implies the following associated variationally consistent boundary conditions and which are satisfied exactly at boundary surfaces,

$$\sigma_{ij} n_j - \bar{T}_i^n = 0 \quad \text{on} \quad A_T \quad \text{and} \quad u_i - \bar{u}_i = 0 \quad \text{on} \quad A_u \tag{2.7}$$

where $\bar{T}_i^n$ are the components of the prescribed surface traction vector $\bar{T}^n$ on a surface with outward normal $\bar{n} = n_i\hat{e}_i$, $\hat{e}_i$ $(i = 1, 3)$ being the unit vectors along x, z directions. A_T and A_u are, respectively, the surface boundaries where surface traction's $\bar{T}_i^n$ and displacements $\bar{u}_i$ are prescribed. Substituting the expressions of strain components ε_x, ε_z and γ_{zx} from Eq. (2.2) into Eq. (2.6) yields

$$\begin{aligned}\int_t \int_a \int_h [&\delta u\{\sigma_{x,x} + \tau_{xz,z} - (\rho + \hat{\rho})\ddot{u}\} + \delta w\{\tau_{zx,x} + \sigma_{z,z} - (\rho + \hat{\rho})\ddot{w}\} \\ &+ \delta\sigma_x\{(\bar{s}_{11} + \hat{s}_{11})\,\sigma_x + (\bar{s}_{13} + \hat{s}_{13})\,\sigma_z - u_{,x}\} \\ &+ \delta\sigma_z\{(\bar{s}_{13} + \hat{s}_{13})\,\sigma_x + \bar{s}_{33}\,\sigma_z - w_{,z}\} \\ &+ \delta\tau_{zx}\{(\bar{s}_{55} + \hat{s}_{55})\,\tau_{zx} - u_{,z} - w_{,x}\}]\,\mathrm{d}z\,\mathrm{d}x\,\mathrm{d}t = 0\end{aligned} \tag{2.8}$$

Dimensionless in-plane coordinates ξ, and a local thickness coordinate $\zeta^{(k)}$ for the kth layer are introduced, which varies from 0 to 1.

$$\xi = x/a\,; \qquad \zeta^{(k)} = (z - z_{k-1})/t^{(k)} \tag{2.9}$$

The bottom and top surfaces of beam are subjected to uniform distributed pressure p_1 and p_2, respectively, and both the surface are also assumed shear traction free. Therefore support conditions at the top $(z = h/2)$ and bottom $(z = -h/2)$ surfaces of the beam expressed as,

$$\begin{aligned}&\text{at} \quad z = -h/2: \quad \sigma_z = -p_1; \quad \tau_{zx} = 0 \\ &\text{at} \quad z = h/2: \quad \sigma_z = -p_2; \quad \tau_{zx} = 0\end{aligned} \tag{2.10}$$

For perfect interlaminar bounding case, displacements (u ,w) and transverse stresses (σ_z, τ_{zx}) need to satisfy following condition at the kth interface,

$$[(u,\, w,\, \sigma_z,\, \tau_{zx})|_{\zeta=1}]^{(k)} = [(u,\, w,\, \sigma_z,\, \tau_{zx})|_{\zeta=0}]^{(k+1)} \tag{2.11}$$

Where, along x-axis (ξ=0 and 1), AFG beam can have any combination of following mechanical supports, such as,

$$\begin{aligned} &\text{Simply supported (S) :} && w = 0, && \sigma_x = 0 \\ &\text{Clamped (C) :} && u = 0, && w = 0 \\ &\text{Free (F) :} && \tau_{xz} = 0, && \sigma_x = 0 \end{aligned} \tag{2.12}$$

2.3 THE GENERALIZED MULTI-TERM EKM

The five field variables to be solved are $X_l = [\, u \quad w \quad \sigma_x \quad \sigma_z \quad \tau_{zx} \,]^{\mathrm{T}}$. Using the multi-term EKM [281], these field variables for the k^{th} lamina are expressed in n-term series consisting of the products of separable functions of ξ, ζ and time, as,

$$X_l = \sum_{i=1}^{n} f_l^i(\xi) g_l^i(\zeta) \cos\omega t + \delta_{l4}[p_a + z p_d], \qquad l = 1, 2, \ldots 5 \tag{2.13}$$

where $g_l^i(\zeta)$ and $f_l^i(\xi)$ are the unknown functions of ζ and ξ, respectively. Similarly, ω is unknown natural frequencies of the system. Here, n represents the number of terms in solution and the repeated index l does not mean summation here. To satisfy the nonhomogeneous boundary conditions for σ_z as given in Eq. (2.10), an additional term ($\delta_{l4}[p_a + z p_d]$) is superimposed to the above solution for σ_z. Where, δ_{l4} is Kroneckor's delta, $\delta_{l4} = 1$ for $l = 4$ and else $\delta_{l4} = 0$, $p_a = -(p_1 + p_2)/2$ and $p_d = -(p_2 - p_1)/h$. The functions $g_l^i(\zeta)$ are dependent on the k^{th} layer, while $f_l^i(\xi)$ functions are valid for all layers. These unknown functions (g and f) of ζ and ξ are to be solved in two iterative steps by satisfying all homogenous support conditions.

2.4 FIRST ITERATION STEP

In first step, x-direction functions $f_l^i(\xi)$ are assumed as known, while functions $g_l^i(\zeta)$ are solved. In the EKM, the initial trail functions are not required to satisfied the prescribed support conditions. Hence, to start the iterative process f_l^i are assumed as, $f_2^i(\xi)$=$f_3^i(\xi)$=$f_4^i(\xi)$=$\cos i\pi\xi$ and $f_1^i(\xi)$=$f_5^i(\xi)$=$f_l^i(\xi)$=$\sin i\pi\xi$. Hence, f_l^i are known, the variation δX_i is given as,

$$\delta X_l = \sum_{i=1}^{n} f_l^i(\xi) \delta g_l^i \cos\omega t, \qquad l = 1, 2, \ldots 8 \tag{2.14}$$

Functions $g_l^i(\zeta)$ are segregated into two column vectors $\bar{\mathbf{G}}$ and $\hat{\mathbf{G}}$. Where $\bar{\mathbf{G}}$ contains those particular $4n$ primary variables which are specified at the support and interface conditions along z-direction, in Eqs. (2.10)-(2.11). Where, $\hat{\mathbf{G}}$ contains the remaining $1n$ dependent variables:

$$\bar{\mathbf{G}} = [\, g_1^1 \dots g_1^n \quad g_2^1 \dots g_2^n \quad g_4^1 \dots g_4^n \quad g_5^1 \dots g_5^n \,]^{\mathrm{T}} \; ; \qquad \hat{\mathbf{G}} = [\, g_3^1 \dots g_3^n \,]^{\mathrm{T}} \tag{2.15}$$

Eqs. (2.13) and (2.14) are substituted into Eq. (2.8). Where the f_l^i are known functions integration along x-direction are evaluated. Since variations for δg_l^i are arbitrary, the coefficients of δg_l^i must vanish (equal to zero) which generates following set of $4n$ first order ODEs and $1n$ linear algebraic equations for each layer:

$$\mathbf{M}\bar{\mathbf{G}}_{,\zeta} = \bar{\mathbf{A}}(\omega)\bar{\mathbf{G}} + \hat{\mathbf{A}}\hat{\mathbf{G}} + \bar{\mathbf{Q}}_{\mathbf{p}}^{\mathbf{m}} \tag{2.16}$$

$$\mathbf{K}\hat{\mathbf{G}} = \tilde{\mathbf{A}}\bar{\mathbf{G}} + \tilde{\mathbf{Q}}_{\mathbf{p}}^{\mathbf{m}} \tag{2.17}$$

Where $\mathbf{M}_{4n\times 4n}$, $\bar{\mathbf{A}}_{4n\times 4n}$, $\hat{\mathbf{A}}_{4n\times 1n}$, $\mathbf{K}_{1n\times 1n}$ and $\tilde{\mathbf{A}}_{1n\times 4n}$ are known matrices. Non-zero elements of the matrices are given below:

$$\begin{aligned}
&M_{i_1j_1} = M_{j_4i_4} = \langle f_5^i f_1^j\rangle_a, && M_{i_2j_2} = M_{j_3i_3} = \langle f_4^i f_2^j\rangle_a \\
&\bar{A}_{i_1j_2} = \tfrac{-t}{a}\langle f_5^i f_{2,\xi}^j\rangle_a, && \bar{A}_{i_1j_4} = t\bar{s}_{55}\langle f_5^i f_5^j\rangle_a + \delta_2 t\bar{s}_{55}\langle \xi f_5^i f_5^j\rangle_a \\
&\bar{A}_{i_2j_3} = t\bar{s}_{33}\langle f_4^i f_4^j\rangle_a, && \hat{A}_{i_2j_1} = t\bar{s}_{13}\langle f_4^i f_3^j\rangle_a + \delta_1 t\bar{s}_{13}\langle \xi f_4^i f_3^j\rangle_a \\
&\hat{A}_{i_3j_4} = \tfrac{-t}{a}\langle f_2^i f_{5,\xi}^j\rangle_a, && \hat{A}_{i_4j_1} = \tfrac{-t}{a}\langle f_1^i f_{3,\xi}^j\rangle_a \\
&K_{i_1j_1} = \bar{s}_{11}\langle f_3^i f_3^j\rangle_a + \delta_1\bar{s}_{11}\langle \xi f_3^i f_3^j\rangle_a, && \tilde{A}_{i_1j_1} = \tfrac{1}{a}\langle f_3^i f_{1,\xi}^j\rangle_a \\
&\tilde{A}_{i_1j_3} = -\bar{s}_{13}\langle f_3^i f_4^j\rangle_a - \delta_1\bar{s}_{13}\langle \xi f_3^i f_4^j\rangle_a \\
&\bar{A}_{i_3j_2} = -\rho(1+\delta_p\,\xi)\omega^2 t\langle f_2^i f_2^j\rangle_a, && \bar{A}_{i_4j_1} = -\rho(1+\delta_p\,\xi)\omega^2 t\langle f_1^i f_1^j\rangle_a
\end{aligned} \tag{2.18}$$

where $i_p = (p-1)n + i$ and $j_q = (q-1)n + j$ for $p, q = 1, 2, \dots, 5$.

$\bar{\mathbf{Q}}_{\mathbf{p}}, \tilde{\mathbf{Q}}_{\mathbf{p}}$ are load vectors of size $4n$, and $1n$, respectively, whose non-zero terms are given by

$$\begin{aligned}
&\bar{Q}_{p_{i3}} = -t\langle f_2^i\rangle_a p_d, && \bar{Q}_{p_{i2}} = t\bar{s}_{33}\langle f_4^i\rangle_a\,(p_a^k + \zeta t p_d) \\
&\tilde{Q}_{p_{i1}} = -\bar{s}_{13}\langle f_3^i\rangle_a\,(p_a^k + \zeta t p_d) - (p_a^k + \zeta t p_d)\left\{\delta_1\bar{s}_{13}\langle \xi f_3^i\rangle_a\right\}
\end{aligned} \tag{2.19}$$

where the notation $\langle \dots\rangle_a = a\int_0^1(\dots)d\xi$ represent integration over the span length a and $p_a^k = p_a + p_d z_k$. Since the functions f_l^i are known functions, elements of the matrices defined in Eqs. (2.18)-(2.19) have been evaluated in close form. $\hat{\mathbf{G}}$ is obtained from Eq. (2.17) and put into Eq. (2.16) which yields a set of $5n$ first-order homogeneous ODEs as:

$$\bar{\mathbf{G}}_{,\zeta} = \mathbf{A}(\omega)\bar{\mathbf{G}} + \mathbf{Q}_{\mathbf{p}} \tag{2.20}$$

where $\mathbf{A} = \mathbf{M}^{-1}[\bar{\mathbf{A}} + \hat{\mathbf{A}}\mathbf{K}^{-1}\tilde{\mathbf{A}}]$ and $\mathbf{Q_p} = \mathbf{M}^{-1}[\bar{\mathbf{Q}}_\mathbf{p}^\mathbf{m} + \hat{\mathbf{A}}^\mathbf{m}\mathbf{K}^{\mathbf{m}-1}\tilde{\mathbf{Q}}_\mathbf{p}^\mathbf{m}]$. Above Eq. (2.20) represent a system of $4n$ non-homogeneous first order ODEs with constant coefficient (not function of coordinates) but coefficient A unknown natural frequencies (ω).

2.4.1 Solution for Static Case

For static case, those elements of matrices which is function of time (t) and natural frequencies (ω) becomes zero, $\bar{A}_{i_3 j_2}$=$\bar{A}_{i_4 j_1}$=0. Therefore, the coefficient of final system of first order ODEs Eq. (2.20) is no more function of unknown natural frequencies (ω). So, final system of ODEs Eq. (2.20) now expressed as,

$$\bar{\mathbf{G}}_{,\zeta} = \mathbf{A}\bar{\mathbf{G}} + \mathbf{Q_p} \tag{2.21}$$

The above solution of above equation is obtained by following the procedure described in Ref. [281]. The complementary solution of above equation is of the form $\bar{\mathbf{G}}_\mathbf{c}(\zeta) = e^{\lambda\zeta}\mathbf{Y}$, which on substitution in the homogeneous part of Eq. (2.21) yields an eigenvalue problem

$$\mathbf{AY} = \lambda\mathbf{Y} \tag{2.22}$$

Hence, the exponent λ and $\mathbf{Y}$ are the $4n$ eigenvalue and eigenvector pairs of matrix $\mathbf{A}$. The eigenvalues λ can be either real or occur in complex conjugate pairs. Thus, the complete complementary solution $\bar{\mathbf{G}}_\mathbf{c}(\zeta)$ can be expressed in terms of $4n$ real constants C_i as

$$\bar{\mathbf{G}}_\mathbf{c} = \sum_{i=1}^{4n} \mathbf{F}_i(\zeta) C_i \tag{2.23}$$

where $\mathbf{F}_i(\zeta)$ are column vector of functions corresponding to the eigenpair λ_i and Y_i. The particular solution $\bar{\mathbf{G}}_\mathbf{p}(\zeta)$ for this case,

$$\bar{\mathbf{G}}_\mathbf{p}(\zeta) = \mathbf{U_0} + \zeta\mathbf{U_1} \tag{2.24}$$

where

$$\mathbf{U_1} = -\mathbf{A}^{-1}\mathbf{Q}_{\mathbf{p}_1} \quad \text{and} \quad \mathbf{U_0} = -\mathbf{A}^{-1}[\mathbf{Q}_{\mathbf{p}_0} - \mathbf{U_1}] \tag{2.25}$$

Thus, the general solution of Eq. (2.21) is

$$\bar{\mathbf{G}}(\zeta) = \sum_{i=1}^{4n} \mathbf{F}_i(\zeta) C_i + \mathbf{U_0} + \zeta\mathbf{U_1} \tag{2.26}$$

The boundary and interface conditions in Eqs. (2.10)-(2.11) can also be written in terms of functions $g_l^i(\zeta)$ as

$$\text{for } k = 1, \quad \text{at } \zeta = 0: \quad g_4^i = 0, \quad g_5^i = 0$$

$$\text{for } k = L, \quad \text{at } \zeta = 1: \quad g_4^i = 0, \quad g_5^i = 0 \tag{2.27}$$

$$[(g_1^i,\, g_2^i,\, g_4^i,\, g_5^i)|_{\zeta=1}]^{(k)} = [(g_1^i,\, g_2^i,\, g_4^i,\, g_5^i)|_{\zeta=0}]^{(k+1)} \tag{2.28}$$

for $i = 1, 2, \ldots, n$. The $4n \times L$ constants $C_i^{(k)}$'s for L layers are obtained from the $4n$ boundary conditions and $4n \times (L-1)$ interface continuity conditions given by Eqs. (2.27) and (2.28). This completely determines $\bar{\mathbf{G}}(\zeta)$. Now, $\hat{\mathbf{G}}(\zeta)$ can be obtained by solving the algebraic equation (2.17). This completes the first iteration step for static case.

2.4.2 Solution for Free Vibration Case

For free vibration case, there is no external applied load so element corresponding to load vectors $\bar{\mathbf{Q}}_\mathbf{p}$, $\tilde{\mathbf{Q}}_\mathbf{p}$ is equals to zero ($\bar{Q}_{p_{i3}}$=$\bar{Q}_{p_{i2}}$=$\tilde{Q}_{p_{i1}}$=0). So, final system of ODE Eq. (2.20) now reduced to,

$$\bar{\mathbf{G}}_{,\zeta} = \mathbf{A}(\omega)\bar{\mathbf{G}} \tag{2.29}$$

The above equation is a system of homogeneous ODEs in which coefficient A contains the unknown natural frequencies (ω). The complimentary solution of Eq. (2.29) is obtained by applying the similar approach as discussed above. Where the terms corresponding to particular solution are equal to zero. Therefore, the final solution of Eq. (2.29) is,

$$\bar{\mathbf{G}}(\zeta) = \sum_{i=1}^{4n} \mathbf{F}_i(\zeta, \omega) C_i \tag{2.30}$$

After applying the traction free boundary condition at the top and bottom of the beam, Eqs. (2.27) and satisfying the interface continuity conditions (2.28), equation Eq. (2.30) yields

$$\sum_{i=1}^{4n} \mathbf{K}_{\mathbf{d}i}(\zeta, \omega) C_i = \mathbf{0} \tag{2.31}$$

where the coefficient matrix $\mathbf{K_d}$ depends on $\omega = \omega_n$. For non-trivial solution, it's determinant should be zero and ω can be obtained by finding roots of the equation $|det(\mathbf{K_d})|$=0 using bisection method. The undamped natural frequencies $\omega_{01} = \omega_n$ are determined by employing the approach of Kapuria and Achary [291]. Once the natural frequencies known then the mode shapes are obtained using the Eq. (2.30). In this way, first iteration step is completed for free vibration case.

2.5 SECOND ITERATION STEP

Now $g_l^i(\zeta)$ is known from the first step, whereas $f_l^i(\xi)$ are considered as unknown. So in this step, arbitrary variation is considered in f_l^i functions. Therefore, variation for this case is written from Eq. (2.13) as:

$$\delta X_l^i = \sum_{i=1}^{n} g_l^i(\zeta) \delta f_l^i \cos \omega t \quad \text{for} \quad l = 1, 2, \ldots, 5 \tag{2.32}$$

Similarly, like the first step, $f_l^i(\xi)$ are segregated into two column vectors $\bar{\mathbf{F}}$ and $\hat{\mathbf{F}}$. Where $\bar{\mathbf{F}}$ carries those particular $4n$ primary variables which come in the support conditions at edges $x = 0, 1$ and $\hat{\mathbf{F}}$ contains the remaining $1n$ variables,

$$\bar{\mathbf{F}} = [\, f_1^1 \dots f_1^n \quad f_2^1 \dots f_2^n \quad f_3^1 \dots f_3^n \quad f_4^1 \dots f_4^n \,]^{\mathrm{T}} \; ; \qquad \hat{\mathbf{F}} = [\, f_5^1 \dots f_5^n \,]^{\mathrm{T}} \tag{2.33}$$

Substituting Eq. (2.13) and Eq. (2.32) in Eq. (2.8), performing integration over ζ direction on the known functions of ζ, applying integration by parts wherever necessary, and equating the coefficient of δf_l^i to zero individually, yields the following system of differential-algebraic equations for f_l^i:

$$\mathbf{N}\bar{\mathbf{F}}_{,\xi} = \bar{\mathbf{B}}^{\mathbf{f}}(\xi,\omega)\bar{\mathbf{F}} + \hat{\mathbf{B}}^{\mathbf{f}}(\xi)\hat{\mathbf{F}} + \bar{\mathbf{P}}^{\mathbf{f}}_{\mathbf{m}}(\xi) \tag{2.34}$$

$$\mathbf{L}\hat{\mathbf{F}} = \tilde{\mathbf{B}}^{\mathbf{f}}(\xi)\bar{\mathbf{F}} + \tilde{\mathbf{P}}^{\mathbf{f}}_{\mathbf{m}} \tag{2.35}$$

where $\mathbf{N}_{4n\times 4n}$, $\bar{\mathbf{B}}^f_{4n\times 4n}$, $\hat{\mathbf{B}}^f_{4n\times 1n}$, $\mathbf{L}_{1n\times 1n}$ and $\tilde{\mathbf{B}}^f_{1n\times 4n}$ are known matrices. Similarly, $\bar{\mathbf{P}}^{\mathbf{f}}_{\mathbf{m}}$ and $\tilde{\mathbf{P}}^{\mathbf{f}}_{\mathbf{m}}$ are $4n \times 1$ and $1n \times 1$ column vectors comprising of the loading terms. Where $\bar{\mathbf{B}}^{\mathbf{f}} = \bar{\mathbf{B}} + \xi\bar{\mathbf{B}}^{\mathbf{v}}$, $\hat{\mathbf{B}}^{\mathbf{f}} = \hat{\mathbf{B}} + \xi\hat{\mathbf{B}}^{\mathbf{v}}$, $\tilde{\mathbf{B}}^{\mathbf{f}} = \tilde{\mathbf{B}} + \xi\tilde{\mathbf{B}}^{\mathbf{v}}$, $\bar{\mathbf{P}}^{\mathbf{f}}_{\mathbf{m}} = \bar{\mathbf{P}}_{\mathbf{m}} + \xi\bar{\mathbf{P}}^{\mathbf{v}}_{\mathbf{m}}$ and $\tilde{\mathbf{P}}^{\mathbf{f}}_{\mathbf{m}} = \tilde{\mathbf{P}}_{\mathbf{m}}$.

Non-zero elements of the matrices are given below,

$$\begin{aligned}
&N_{i_1j_1} = N_{j_3i_3} = \langle g_3^i g_1^j\rangle_h, && N_{i_2j_2} = N_{j_4i_4} = \langle g_5^i g_2^j\rangle_h \\
&\bar{B}_{i_1j_3} = \langle \bar{s}_{11} g_3^i g_3^j\rangle_h, && \bar{B}^v_{i_1j_3} = \delta_1\xi\langle \bar{s}_{11} g_3^i g_3^j\rangle_h \\
&\hat{B}_{i_1j_1} = \langle \bar{s}_{13} g_3^i g_4^j\rangle_h, && \hat{B}^v_{i_1j_1} = \delta_1\xi\langle \bar{s}_{13} g_3^i g_4^j\rangle_h \\
&\bar{B}_{i_2j_1} = -\langle g_5^i \tfrac{g_{1,\zeta}^j}{t}\rangle_h, && \bar{B}_{i_2j_4} = \langle \bar{s}_{55} g_5^i g_5^j\rangle_h \\
&\bar{B}^v_{i_2j_4} = \delta_2\xi\langle \bar{s}_{55} g_5^i g_5^j\rangle_h, && \bar{B}_{i_3j_4} = \langle \tfrac{g_{5,\zeta}^i}{t} g_1^i\rangle_h \\
&\hat{B}_{i_4j_1} = -\langle g_2^i \tfrac{g_{4,\zeta}^j}{t}\rangle_h, && L_{i_1j_1} = \langle \bar{s}_{33} g_4^i g_4^j\rangle_h \\
&\tilde{B}_{i_1j_3} = -\langle \bar{s}_{13} g_4^i g_3^j\rangle_h, && \tilde{B}^v_{i_1j_3} = -\delta_1\xi\langle \bar{s}_{13} g_4^i g_3^j\rangle_h \\
&\tilde{B}_{i_1j_2} = \langle g_4^i \tfrac{g_{2,\zeta}^j}{t}\rangle_h \\
&\bar{B}_{i_3j_1} = -a\rho\omega^2\langle g_1^i g_1^j\rangle_h, && \bar{B}^v_{i_3j_1} = -\delta_p\, a\rho\omega^2\xi\langle g_1^i g_1^j\rangle_h \\
&\bar{B}_{i_4j_2} = -a\rho\omega^2\langle g_2^i g_2^j\rangle_h, && \bar{B}^v_{i_4j_2} = -\delta_p\, a\rho\omega^2\xi\langle g_2^i g_2^j\rangle_h
\end{aligned} \tag{2.36}$$

Similarly, non-zero elements load vector are given as,

$$\begin{aligned}
&\bar{P}_{m_{i1}} = \langle \bar{s}_{13} g_3^i (p_a^k + p_d t\zeta)\rangle_h, && \bar{P}^v_{m_{i1}} = \delta_1\xi\langle \bar{s}_{13} g_3^i (p_a^k + p_d t\zeta)\rangle_h \\
&\bar{P}_{m_{i4}} = -p_d\langle g_2^i\rangle_h, && \tilde{P}_{m_{i1}} = -\langle \bar{s}_{33} g_4^i (p_a^k + p_d t\zeta)\rangle_h
\end{aligned} \tag{2.37}$$

where $\langle \dots \rangle_h = \sum_{k=1}^{L} t^{(k)} \int_0^1 (\dots)^{(k)}\, d\zeta$. Since $g^i(\zeta)$ are known in close form from previous step, so the above elements of matrices are obtained in closed form. The governing equations (2.34) and

(2.35) can be rewritten as,

$$\mathbf{N}\bar{\mathbf{F}}_{,\xi} = \{\bar{\mathbf{B}}(\omega) + \xi\bar{\mathbf{B}}^{\mathbf{v}}(\omega)\}\bar{\mathbf{F}} + (\hat{\mathbf{B}} + \xi\hat{\mathbf{B}}^{\mathbf{v}})\hat{\mathbf{F}} + (\bar{\mathbf{P}}_{\mathbf{m}} + \xi\bar{\mathbf{P}}^{\mathbf{v}}_{\mathbf{m}}) \tag{2.38}$$

$$\mathbf{L}\hat{\mathbf{F}} = (\tilde{\mathbf{B}} + \xi\tilde{\mathbf{B}}^{\mathbf{v}})\bar{\mathbf{F}} + \tilde{\mathbf{P}}_{\mathbf{m}} \tag{2.39}$$

Substituting algebraic equations (2.39) into Eq. (2.38) yields the following set of first order ODEs with varying coefficients for $\bar{\mathbf{F}}$,

$$\bar{\mathbf{F}}_{,\xi} = \{\mathbf{B_0}(\omega) + \xi\mathbf{B_1}(\omega) + \xi^2\mathbf{B_2}\}\bar{\mathbf{F}} + \mathbf{P_0} + \xi\mathbf{P_1} \tag{2.40}$$

where $\mathbf{B_0} = \mathbf{N^{-1}}(\bar{\mathbf{B}} + \hat{\mathbf{B}}\mathbf{L^{-1}}\tilde{\mathbf{B}})$, $\mathbf{B_1} = \mathbf{N^{-1}}(\bar{\mathbf{B}}^{\mathbf{v}} + \hat{\mathbf{B}}\mathbf{L^{-1}}\tilde{\mathbf{B}}^{\mathbf{v}} + \hat{\mathbf{B}}^{\mathbf{v}}\mathbf{L^{-1}}\tilde{\mathbf{B}})$, $\mathbf{B_2} = \mathbf{N^{-1}}(\hat{\mathbf{B}}^{\mathbf{v}}\mathbf{L^{-1}}\tilde{\mathbf{B}}^{\mathbf{v}})$ $\mathbf{P_0} = \mathbf{N^{-1}}(\bar{\mathbf{P}}_{\mathbf{m}} + \hat{\mathbf{B}}\mathbf{L^{-1}}\tilde{\mathbf{P}}_{\mathbf{m}})$, $\mathbf{P_1} = \mathbf{N^{-1}}(\bar{\mathbf{P}}^{\mathbf{v}}_{\mathbf{m}} + \hat{\mathbf{B}}^{\mathbf{v}}\mathbf{L^{-1}}\tilde{\mathbf{P}}_{\mathbf{m}})$

Equation (2.40) is set of simultaneous non-homogenous first order differential equations ($4n$) with variable coefficients in which coefficients are also function of the unknown natural frequencies (ω) of beam. These ODEs are solved using modified power series technique proposed by Kukla and Zamorska [292].

2.5.1 Solution for Static Case

Similarly along in-plane direction also, the elements of matrices which is function of time (t) and natural frequencies (ω) becomes zero, $\bar{B}_{i_3j_1}$=$\bar{B}_{i_4j_2}$=$\bar{B}^v_{i_3j_1}$=$\bar{B}^v_{i_4j_2}$=0 for static case. Therefore, the coefficient of final system of first order ODEs Eq. (2.40) is no more function of unknown natural frequencies (ω). So, final system of ODE Eq. (2.40) now expressed as,

$$\bar{\mathbf{F}}_{,\xi} = \{\mathbf{B_0} + \xi\mathbf{B_1} + \xi^2\mathbf{B_2}\}\bar{\mathbf{F}} + \mathbf{P_0} + \xi\mathbf{P_1} \tag{2.41}$$

Now, the final solution for present system of equations Eq. (2.41) is approximated in form of power series in the dimensionless axial coordinate ξ $(0 \leq \xi \leq 1)$ a as,

$$\bar{\mathbf{F}}(\xi) = \sum_{i=0}^{N_p} \frac{\mathbf{Y}_i\xi^i}{i!} \tag{2.42}$$

Substituting Eq. (2.42) into Eq. (2.41) gives

$$\sum_{i=1}^{N_p} \frac{\mathbf{Y}_i\xi^{i-1}}{(i-1)!} - \sum_{i=0}^{N_p}\left[\frac{\mathbf{B_0}\mathbf{Y}_i\xi^i}{i!} - \frac{\mathbf{B_1}\mathbf{Y}_i\xi^{i+1}}{i!} - \frac{\mathbf{B_2}\mathbf{Y}_i\xi^{i+2}}{i!}\right] - \mathbf{P_0} - \xi\mathbf{P_1} = 0$$

$$\implies \sum_{i=0}^{N_p} \frac{\mathbf{Y}_{i+1}\xi^i}{i!} - \mathbf{B_0}\sum_{i=0}^{N_p} \frac{\mathbf{Y}_i\xi^i}{i!} - \mathbf{B_1}\sum_{i=1}^{N_p} \frac{\mathbf{Y}_{i-1}\xi^i}{(i-1)!} - \mathbf{B_2}\sum_{i=2}^{N_p} \frac{\mathbf{Y}_{i-2}\xi^i}{(i-2)!} - \mathbf{P_0} - \xi\mathbf{P_1} = 0 \tag{2.43}$$

where a term $\mathbf{Y}_i$ is included only if $i \geq 0$. In Eq. (2.43), setting the coefficients of ξ^0, ξ^1 and of ξ^i as zero for $i \geq 2$ yields

$$\mathbf{Y}_1 = \mathbf{B_0}\mathbf{Y}_0 + \mathbf{P_0}; \quad \mathbf{Y}_2 = \mathbf{B_0}\mathbf{Y}_1 + \mathbf{B_1}\mathbf{Y}_0 + \mathbf{P_1} \tag{2.44}$$

and a recursive relation for $\mathbf{Y}_i$:

$$\mathbf{Y}_{i+1} = \mathbf{B_0}\mathbf{Y}_i + i\mathbf{B_1}\mathbf{Y}_{i-1} + i(i-1)\mathbf{B_2}\mathbf{Y}_{i-2} \qquad i \geq 2 \tag{2.45}$$

Then the coefficient $\mathbf{Y}_i$ is assumed to be of the form:

$$\mathbf{Y}_i = \hat{\mathbf{Z}}_i + \hat{\mathbf{H}}_i\mathbf{C}_0 \qquad i = 0, 1, 2, ... \tag{2.46}$$

Where $\hat{\mathbf{Z}}_i$ ($6n \times 1n$ column vectors), $\mathbf{C}_0$ ($6n \times 1n$ column vectors) and $\hat{\mathbf{H}}_i$ ($6n \times 6n$ matrices) are constants, and $\hat{\mathbf{Z}}_0 = 0$, $\hat{\mathbf{H}}_0$= I (unit matrix). By substituting Eq. (2.46) into Eqs. (2.44) and (2.45) the following recursive relations for $\hat{\mathbf{Z}}_i$ and $\hat{\mathbf{H}}_i$ are obtained

$$\hat{\mathbf{Z}}_0 = \mathbf{0}; \quad \hat{\mathbf{Z}}_1 = \mathbf{P_0}; \quad \hat{\mathbf{Z}}_2 = \mathbf{B_0}\hat{\mathbf{Z}}_1 + \mathbf{P_1}$$

$$\hat{\mathbf{Z}}_{i+1} = \mathbf{B_0}\hat{\mathbf{Z}}_1 + i\mathbf{B_1}\hat{\mathbf{Z}}_{i-1} + i(i-1)\mathbf{B_2}\hat{\mathbf{Z}}_{i-2} \quad \text{for} \quad i \geq 2 \tag{2.47}$$

$$\hat{\mathbf{H}}_0 = \mathbf{I}; \quad \hat{\mathbf{H}}_1 = \mathbf{B_0}; \quad \hat{\mathbf{H}}_2 = \mathbf{B_0}\hat{\mathbf{H}}_1 + \mathbf{B_1}$$

$$\hat{\mathbf{H}}_{i+1} = \mathbf{B_0}\hat{\mathbf{H}}_1 + i\mathbf{B_1}\hat{\mathbf{H}}_{i-1} + i(i-1)\mathbf{B_2}\hat{\mathbf{H}}_{i-2} \quad \text{for} \quad i \geq 2 \tag{2.48}$$

The general solution of Eq. (2.41) is

$$\bar{\mathbf{F}}^j(\xi) = \sum_{i=0}^{N_p} \frac{\hat{\mathbf{Z}}_i^j \xi^i}{i!} + \left(\sum_{i=0}^{N_p} \frac{\hat{\mathbf{H}}_i^j \xi^i}{i!} \right) \mathbf{C}_0 \tag{2.49}$$

By assuming

$$\mathbf{Z}_i = \frac{\hat{\mathbf{Z}}_i}{i!}; \quad \mathbf{H}_i = \frac{\hat{\mathbf{H}}_i}{i!}$$

Now, the final general solution of Eq. (2.41) can be written as,

$$\bar{\mathbf{F}}^j(\xi) = \sum_{i=0}^{N_p} \mathbf{Z}_i^j \xi^i + \left(\sum_{i=0}^{N_p} \mathbf{H}_i^j \xi^i \right) \mathbf{C}_0 \tag{2.50}$$

where $\mathbf{C}_0$ is evaluated by applying the boundary conditions of x-direction. The boundary conditions of x-direction from Eq. (2.12) can be written as,

$$\begin{aligned} &\text{Simply supported (S) :} && f_2^i = 0, \quad f_3^i = 0 \\ &\text{Clamped (C) :} && f_2^i = 0, \quad f_1^i = 0, \\ &\text{Free (F) :} && f_4^i = 0, \quad f_5^i = 0 \qquad (i = 1, 2, \ldots, n) \end{aligned} \tag{2.51}$$

The infinite power series in $\mathbf{Z}_i(\xi)$ and $\mathbf{H}_i(\xi)$ are truncated to a finite number of terms such that the contribution of two consecutive terms is less than a stipulated small number η ($= 10^{-10}$). Functions $\hat{\mathbf{F}}$ are obtained by substituting the solution of $\bar{\mathbf{F}}$ into Eq. (2.35).

2.5.2 Solution for Free Vibration Case

For the case of free vibration, all the elements in the load vectors ($\bar{\mathbf{P}}^{\mathbf{f}}_{\mathbf{m}}$ and $\tilde{\mathbf{P}}^{\mathbf{f}}_{\mathbf{m}}$) becomes zero due to absence of external applied load ($\bar{P}_{m_{i3}}$=$\bar{P}^{v}_{m_{i3}}$=$\bar{P}_{m_{i4}}$=$\tilde{P}_{m_{i1}}$=0). Therefore, load vectors $\mathbf{P_0}$ and $\mathbf{P_1}$ in Eq. (2.40) are now equals to zero. Therefore, the Eq. (2.40) reduced to,

$$\bar{\mathbf{F}}_{,\xi} = \{\mathbf{B_0}(\omega) + \xi\mathbf{B_1}(\omega) + \xi^2\mathbf{B_2}\}\bar{\mathbf{F}} \tag{2.52}$$

Now, Eq. (2.52) is a system of simultaneous homogeneous first order differential equations ($4n$), with variable coefficients which is function of ξ-coordinate and also contains natural frequencies (ω). Similarly, using above method, the final solution for present system of ODEs Eq. (2.52) is written in form of power series as,

$$\bar{\mathbf{F}}^j(\xi) = \sum_{i=0}^{N_p} \mathbf{Z}_i^j \xi^i + \left(\sum_{i=0}^{N_p} \mathbf{H}_i^j \xi^i \right) \mathbf{C}_0 \tag{2.53}$$

where constants $\mathbf{Z}_i$ and $\mathbf{H}_i$ are calculated from obtained recursive relations given in Eq. (2.47) and Eq. (2.48). But, $\mathbf{Z}_i$ is function of load vectors $\mathbf{P_0}$ and $\mathbf{P_1}$. For free vibration case, load vectors $\mathbf{P_0}$ and $\mathbf{P_1}$ is equal to zero due to which $\mathbf{Z}_i = 0$. Hence, above equation is reduced to,

$$\bar{\mathbf{F}}^j(\xi) = \left(\sum_{i=0}^{N_p} \mathbf{H}_i^j \xi^i \right) \mathbf{C}_0 \tag{2.54}$$

where unknown coefficient $\mathbf{C}_0$ depends on x-direction support conditions given in Eq. (2.51). Similarly, the number of terms (N_p) in power series is chosen large enough which ensure that the contribution of further succeeding terms is negligible and less than η ($= 10^{-10}$). After applying the boundary condition at ends $\xi = 0$ and $\xi = 1$ give in Eq. (2.51), Eq. (2.54) yields

$$\sum_{i=1}^{8n} \mathbf{K_d}_i(\xi) C_i = \mathbf{0} \tag{2.55}$$

where, the coefficient matrix $\mathbf{K_d}$ now depends on $\omega = \omega_m$. Similarly, ω can be obtained by finding roots of the equation $|det(\mathbf{K_d})|$=0 using bisection method. Now, the undamped natural frequencies $\omega_{11} = \omega_m$ are known and further, the mode shapes are determine using the Eq. (2.54).

Now $\bar{\mathbf{F}}$ is known functions and further substituted to Eq. (2.39) to obtained the $\hat{\mathbf{F}}$ functions. Now the second step is completed. These two step, one along z-direction (Sec. 2.4) and next along x-direction (Sec. 2.5) completed one iteration. These iteration steps has been continued till the desired level of accuracy achieved. The flow chart of iterative procedure of multi-term extended Kantorovich method is shown in Fig. 2.2

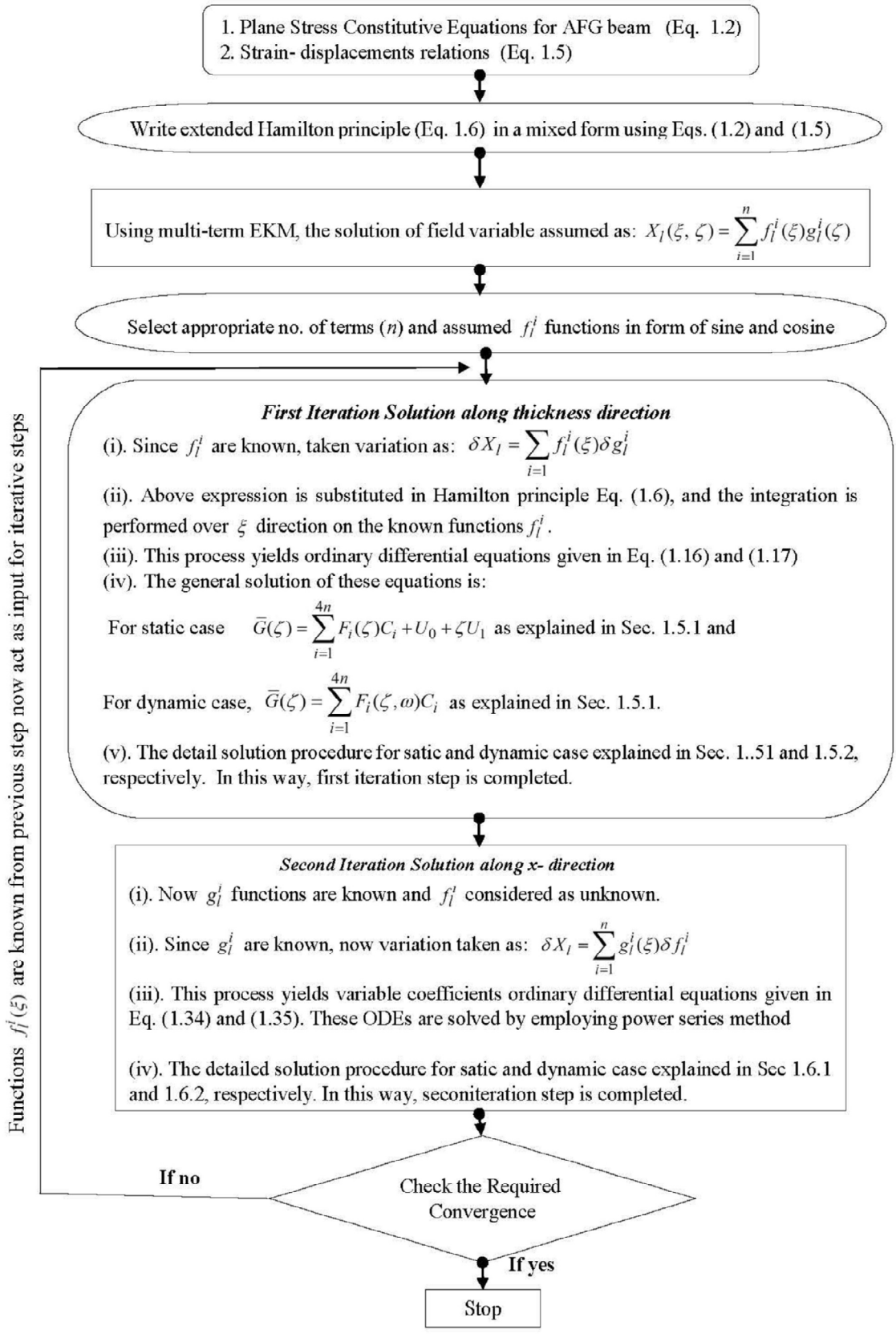

Fig. 2.2: Flow Chart of EKM approach

2.6 EVALUATION OF THE INTEGRALS

The integrals in Eqs. (2.18) and (2.19) are of the following types [293]:

$$\sum_{k=1}^{L} t^{(k)} \int_0^1 [g_p^i(\zeta) g_q^j(\zeta)]^{(k)}\, d\zeta; \qquad \sum_{k=1}^{L} t^{(k)} \int_0^1 [g_{p,\zeta}^i(\zeta) g_q^j(\zeta)]^{(k)}\, d\zeta; \qquad \sum_{k=1}^{L} t^{(k)} \int_0^1 [g_p^i(\zeta)]^{(k)}\, d\zeta$$
$$\sum_{k=1}^{L} t^{(k)} \int_0^1 [g_{p,\zeta}^i(\zeta)]^{(k)}\, d\zeta; \qquad \sum_{k=1}^{L} t^{(k)} \int_0^1 \zeta [g_p^i(\zeta)]^{(k)}\, d\zeta \tag{2.56}$$

The integrals in Eq. (2.56) can be further expressed in terms of the following basic integrals:

$$\int_0^1 F_r^p(\zeta) F_s^q(\zeta) d\zeta, \quad \int_0^1 F_{r,\zeta}^p(\zeta) F_s^q(\zeta) d\zeta, \quad \int_0^1 F_r^p(\zeta) d\zeta, \quad \int_0^1 F_{r,\zeta}^p(\zeta) d\zeta, \quad \int_0^1 \zeta F_r^p(\zeta) d\zeta \tag{2.57}$$

The evaluation of $\int_0^1 F_r^p(\zeta) F_s^q(\zeta) d\zeta$ will depend on the nature of the eigenvalues λ_r and λ_s. If both λ_r and λ_s are complex with $(\lambda_r = \alpha_r \pm \beta_r)$ and $(\lambda_s = \alpha_s \pm \beta_s)$, the product of $F_r^p(\zeta)$ and $F_s^q(\zeta)$ can be evaluated and summed over $(r, r+1)$ and $(s, s+1)$ as

$$\begin{aligned}
&[C_r e^{\alpha_r \zeta}(R_p \cos\beta_r\zeta - I_p \sin\beta_r\zeta) + C_{r+1} e^{\alpha_r\zeta}(R_p \sin\beta_r\zeta + I_p \cos\beta_r\zeta)] \times [C_s e^{\alpha_s\zeta}(R_q \cos\beta_s\zeta \\
&- I_q \sin\beta_s\zeta) + C_{s+1} e^{\alpha_s\zeta}(R_q \sin\beta_s\zeta + I_q \cos\beta_s\zeta)] \\
&= e^{(\alpha_r+\alpha_s)\zeta} \left\{ \frac{1}{2}[\cos(\beta_r - \beta_s)\zeta + \cos(\beta_r + \beta_s)\zeta]\, C_{rs}^1 + \frac{1}{2}[\sin(\beta_r + \beta_s)\zeta + \sin(\beta_r - \beta_s)\zeta]\, C_{rs}^2 \right. \\
&\left. + \frac{1}{2}[\sin(\beta_r + \beta_s)\zeta - \sin(\beta_r - \beta_s)\zeta]\, C_{rs}^3 + \frac{1}{2}[\cos(\beta_r - \beta_s)\zeta - \cos(\beta_r + \beta_s)\zeta]\, C_{rs}^4 \right\}
\end{aligned} \tag{2.58}$$

where

$$\begin{aligned}
C_{rs}^1 &= (C_r R_p + C_{r+1} I_p)(C_s R_q + C_{s+1} I_q); \quad C_{rs}^2 = (C_{r+1} R_p - C_r I_p)(C_s R_q + C_{s+1} I_q) \\
C_{rs}^3 &= (C_r R_p + C_{r+1} I_p)(C_{s+1} R_q - C_s I_q); \quad C_{rs}^4 = (-C_r I_p + C_{r+1} R_p)(-C_s I_q + C_{s+1} R_q)
\end{aligned} \tag{2.59}$$

For all other cases of λ_r and λ_s, the integrands can be expressed as a special case of Eq. (2.58) in terms of the products of trigonometric and exponential functions or only exponential functions (in case of both of the roots being real). For integrals involving $F_{r,\zeta}^p$, the derivative can be expressed as

$$F_{r,\zeta}^p = e^{\lambda_s\zeta}[R_p' \cos\beta_s\zeta - I_p' \sin\beta_s\zeta] \tag{2.60}$$

where $R_p' = (\alpha_r R_p - \beta_r I_p)$, $\quad I_p' = (\beta_r R_p + \alpha_r I_p)$. It is now evident that all integrals in Eq. (2.58) involve the evaluation of the following basic integrals which can be evaluated in closed form as follows:

$$I_1 = \int_0^1 e^{\alpha\zeta} \cos(\beta\zeta) d\zeta = \frac{e^\alpha(\alpha\cos\beta + \beta\sin\beta) - \alpha}{\alpha^2 + \beta^2} \tag{2.61}$$

$$I_2 = \int_0^1 e^{\alpha\zeta} \sin(\beta\zeta) d\zeta = \frac{e^\alpha(\alpha\sin\beta - \beta\cos\beta) + \beta}{\alpha^2 + \beta^2} \tag{2.62}$$

$$I_3 = \int_0^1 e^{\alpha\zeta} d\zeta = \left[\frac{e^{\alpha}-1}{\alpha}\right] \tag{2.63}$$

$$I_4 = \int_0^1 \zeta e^{\alpha\zeta}\cos(\beta\zeta)d\zeta = \frac{e^{\alpha}(\alpha\cos\beta+\beta\sin\beta)-\alpha I_1-\beta I_2}{\alpha^2+\beta^2} \tag{2.64}$$

$$I_5 = \int_0^1 \zeta e^{\alpha\zeta}\sin(\beta\zeta)d\zeta = \frac{e^{\alpha}(\alpha\sin\beta-\beta\cos\beta)-(\alpha I_2-\beta I_1)}{\alpha^2+\beta^2} \tag{2.65}$$

$$I_6 = \int_0^1 \zeta e^{\alpha\zeta} d\zeta = \left[\frac{1+(\alpha-1)e^{\alpha}}{\alpha^2}\right] \tag{2.66}$$

The special cases of the above integrals for $\alpha = 0$ and/or $\beta = 0$ are computed in closed form separately. Similarly, the integrals in Eqs. (2.36) and (2.37) have the following basic forms:

$$\int_0^1 \bar{f}_p^i(\xi)\bar{f}_q^j(\xi)d\xi; \quad \int_0^1 \bar{f}_p^i(\xi)\hat{f}_q^j(\xi)d\xi; \quad \int_0^1 \hat{f}_p^i(\xi)\hat{f}_q^j(\xi)d\xi;$$
$$\int_0^1 \bar{f}_{p,\xi}^i(\xi)\bar{f}_q^j(\xi)d\xi; \quad \int_0^1 \bar{f}_p^i(\xi)d\xi; \quad \int_0^1 \hat{f}_p^i(\xi)d\xi \tag{2.67}$$

where $\bar{f}$ and $\hat{f}$ represent the variable from $\bar{F}$ and $\hat{F}$ respectively. From Eq. (2.38), Eq. (2.39) and Eq. (2.50)

$$\bar{F}(\xi) = \sum_{i=0}^{N_p}\left(Z_i^j + H_i^j C_0\right)\xi^i$$

$$\hat{F}(\xi) = \sum_{i=0}^{N_p}\left(L^{-1}\tilde{B}Z_i^j + L^{-1}\tilde{B}H_i^j C_0\right)\xi^i + \sum_{i=0}^{N_p}\left(L^{-1}\tilde{B}^v Z_i^j + L^{-1}\tilde{B}^v H_i^j C_0\right)\xi^{i+1} + L^{-1}\tilde{P}_m$$

after putting $L^{-1}\tilde{B} = Lb$ and $L^{-1}\tilde{B}^v = Lbv$ and $L^{-1}\tilde{P}_m = Lp$ above equation is modified as:

$$\hat{F}(\xi) = \sum_{i=0}^{N_p}\left(LbZ_i^j + LbH_i^j C_0\right)\xi^i + \sum_{i=0}^{N_p}\left(LbvZ_i^j + LbvH_i^j C_0\right)\xi^{i+1} + Lp \tag{2.68}$$

For calculating the closed form integrating coefficient for Eq. (2.38) and Eq. (2.39), the following equation is used

$$\int_0^1 \bar{f}_p^i(\xi)\bar{f}_q^j(\xi)d\xi = \sum_{ip=0}^{N_p}\sum_{iq=0}^{N_p}\left\{\frac{(Z_{ip}^p + H_{ip}^p C_0)(Z_{iq}^q + H_{iq}^q C_0)}{ip+iq+1}\right\} \tag{2.69}$$

$$\int_0^1 \bar{f}_{p,\xi}^i(\xi)\bar{f}_q^j(\xi)d\xi = \sum_{ip=1}^{N_p}\sum_{iq=0}^{N_p}(ip)\left\{\frac{(Z_{ip}^p + H_{ip}^p C_0)(Z_{iq}^q + H_{iq}^q C_0)}{ip+iq}\right\} \tag{2.70}$$

$$\int_0^1 \bar{f}_p^i(\xi)d\xi = \sum_{ip=0}^{N_p}\left\{\frac{Z_{ip}^p + H_{ip}^p C_0}{ip+1}\right\} \tag{2.71}$$

$$\int_0^1 \bar{f}_p^i(\xi)\hat{f}_q^j(\xi)d\xi = J_1 + J_2 + J_3 \tag{2.72}$$

$$\int_0^1 \hat{f}_p^i(\xi)\hat{f}_q^j(\xi)d\xi = K_1 + K_2 + K_3 + K_4 + K_5 + K_6 + K_7 + K_8 + K_9 \tag{2.73}$$

$$\int_0^1 \hat{f}_p^i(\xi)d\xi = \sum_{ip=0}^{N_p}\left\{\frac{LbZ_{ip}^p + LbH_{ip}^p C_0}{ip+1} + \frac{LbvZ_{ip}^p + LbvH_{ip}^p C_0}{ip+2}\right\} + (Lp^p) \tag{2.74}$$

where

$$J_1 = \sum_{ip=0}^{N_p}\sum_{iq=0}^{N_p}\left\{\frac{(Z_{ip}^p + H_{ip}^p C_0)(LbZ_{iq}^q + LbH_{iq}^q C_0)}{ip+iq+1}\right\}$$

$$J_2 = \sum_{ip=0}^{N_p}\sum_{iq=0}^{N_p}\left\{\frac{(Z_{ip}^p + H_{ip}^p C_0)(LbvZ_{iq}^q + LbvH_{iq}^q C_0)}{ip+iq+2}\right\}$$

$$J_3 = \sum_{ip=0}^{N_p}\left\{\frac{(Z_{ip}^p + H_{ip}^p C_0)(Lp^q)}{ip+1}\right\}$$

$$K_1 = \sum_{ip=0}^{N_p}\sum_{iq=0}^{N_p}\left\{\frac{(LbZ_{ip}^p + LbH_{ip}^p C_0)(LbZ_{iq}^q + LbH_{iq}^q C_0)}{ip+iq+1}\right\}$$

$$K_2 = \sum_{ip=0}^{N_p}\sum_{iq=0}^{N_p}\left\{\frac{(LbZ_{ip}^p + LbH_{ip}^p C_0)(LbvZ_{iq}^q + LbvH_{iq}^q C_0)}{ip+iq+2}\right\}$$

$$K_3 = \sum_{ip=0}^{N_p}\left\{\frac{(LbZ_{ip}^p + LbH_{ip}^p C_0)(Lp^q)}{ip+1}\right\}$$

$$K_4 = \sum_{ip=0}^{N_p}\sum_{iq=0}^{N_p}\left\{\frac{(LbvZ_{ip}^p + LbvH_{ip}^p C_0)(LbZ_{iq}^q + LbH_{iq}^q C_0)}{ip+iq+2}\right\}$$

$$K_5 = \sum_{ip=0}^{N_p}\sum_{iq=0}^{N_p}\left\{\frac{(LbvZ_{ip}^p + LbvH_{ip}^p C_0)(LbvZ_{iq}^q + LbvH_{iq}^q C_0)}{ip+iq+3}\right\}$$

$$K_6 = \sum_{ip=0}^{N_p}\left\{\frac{(LbvZ_{ip}^p + LbvH_{ip}^p C_0)(Lp^q)}{ip+2}\right\}$$

$$K_7 = \sum_{iq=0}^{N_p}\left\{\frac{(Lp^p)(LbZ_{iq}^q + LbH_{iq}^q C_0)}{iq+1}\right\}$$

$$K_8 = \sum_{iq=0}^{N_p}\left\{\frac{(Lp^p)(LbvZ_{iq}^q + LbvH_{iq}^q C_0)}{iq+2}\right\}$$

$$K_9 = (Lp^p)(Lp^q)$$

where

$$n_p = ip + iq \qquad \text{for} \qquad (\bar{A}, \hat{A}, \tilde{A})$$

$$n_p = ip + iq + 1 \qquad \text{for} \qquad (\bar{A}^v, \hat{A}^v, \tilde{A}^v)$$

$$\cos(b+kt) = \cos(b)\cos(kt) - \sin(b)\sin(kt) \tag{2.75}$$

$$\cos(kt) = cos^k t - (k/2)\, cos^{k-2} t\, \sin^2 t + (k/4) cos^{k-4} t\, \sin^4 t - .....; \tag{2.76}$$

$$\sin(kt) = k\cos^{k-1} t \sin t + (k/3)\cos^{k-3} t \sin^3 t + (k/5)\cos^{k-5} t \sin^5 t + ...; \tag{2.77}$$

$$\cos t = \frac{a}{\sqrt{a^2+b^2}}; \qquad \sin t = \frac{-b}{\sqrt{a^2+b^2}} \tag{2.78}$$

2.7 MATERIAL PROPERTIES, CONFIGURATIONS AND ABAQUS MODELING

The numerical results are presented and discussed for a single layer and muti-layered beams, as shown in Fig. 2.3 under static and free vibration cases. Beam (a) is a single layered AFG beam. Where beam (b) is the two layered AFG beam with lay-up $[0/90^0]$ and Beam (c) is four layered AFG beam with symmetric lay-up $[0/90/90/0^0]$, respectively in which each ply has equal thickness. Numerical results are presented for constant property case (homogeneous beam) as well as axially

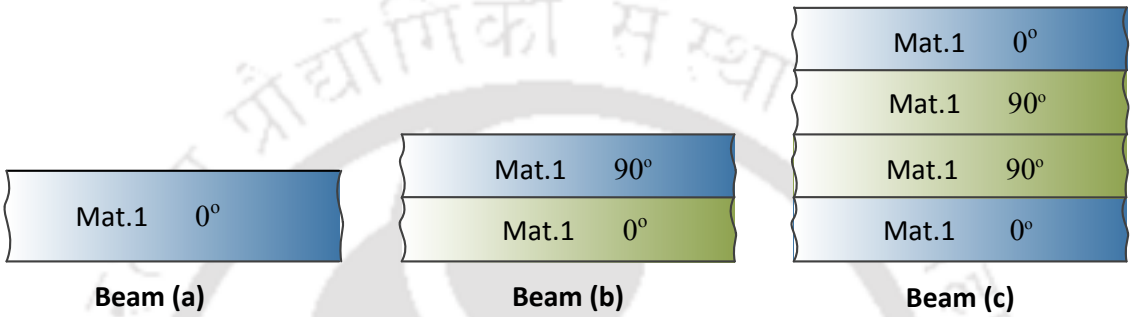

Fig. 2.3: Configuration of AFG beams

graded beams subjected to different support conditions. The material properties for isotropic beam and orthotropic beam are listed in Table 2.1

Table 2.1: Material constants

Material	Y_1	Y_2	Y_3	G_{23}	G_{13}	G_{12}	ν_{12}	ν_{13}	ν_{23}	ρ
Mat.0 (Isotropic)	66.2	66.2	66.2	24.887	24.887	24.887	0.33	0.33	0.33	1000
Mat.1 (Orthotropic)	181.0	10.3	10.3	2.87	7.17	7.17	0.28	0.28	0.33	1578

Units: Young's moduli Y_i and shear moduli G_{ij} in GPa; density (ρ) in Kg/m^3; Y_0= 10.3 GPa

For static case, it is assumed that beam subjected to a uniformly distributed pressure load $p_2 = p_0$ at the top of the beam. But for free vibration case, $p_2 = 0$ due to absence of any external applied load. The length of beam are assumed equal to unity ($a = 1$) for all cases and thickness of beams are taken according to thickness to span ratio ($s = h/a$). For $s = 0.2, 0.1, 0.05$ the value of h are 0.2, 0.1, 0.05, respectively. The beams are designated according to their support conditions at the edges $\xi = 0, 1$. For example, the beam which is clamped (C) at $\xi = 0$ and free (F) at $\xi = 1$, is called an C–F beam. For axially graded beam, there are no analytical results available in the literature. Therefore accuracy and efficiency of the present EKM method are verified thoroughly by comparing with 2D FE. Since it is a beam with a small width, plane stress element of ABAQUS [294] is used. Therefore, the 2D plane beam, with length a along x-direction and thickness h along z-

direction is modeled in ABAQUS using the element type CPS8R with a mesh size of 50 (length) ×16 (thickness), as shown in Fig. 2.4 and 2.5.

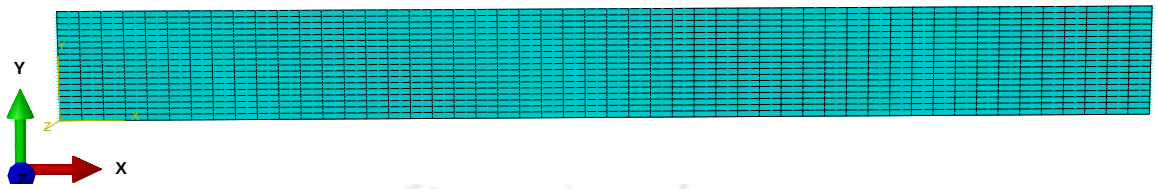

Fig. 2.4: Two-dimensional FE model of beam (s=0.1) with mesh discretization 50 (length) x 18 (thickness)

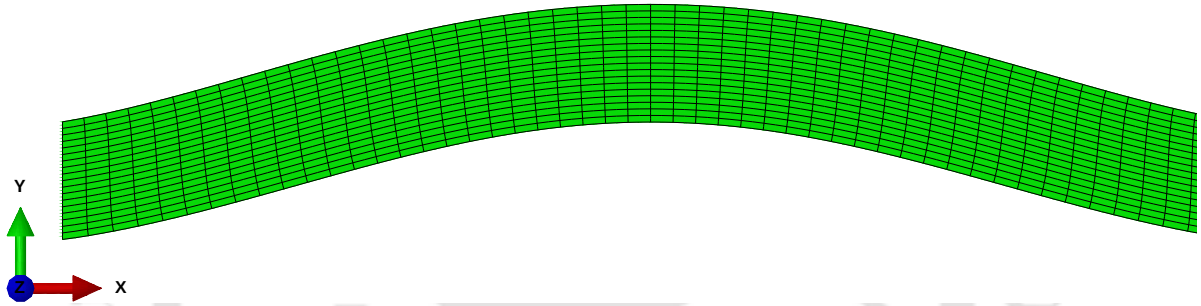

Fig. 2.5: Two-dimensional FE model of AFG beam (s=0.1) under C–C boundary conditions

For FG beams, the spatially graded property distribution (at different Gauss points) with the 20-node hexahedral solid element is implemented by employing user material subroutine (UMAT) in ABAQUS FE software [294]. For dynamic case, the variation of mass density is implemented by dividing the beam into 20 number of equal parts along the length and each part is assigned density value according to its center point. Converged results of EKM are presented for all the cases. The present results are in excellent agreement with 2D FE results for both cases (static and free vibration) under all the boundary conditions. In the succeeding subsections, all numerical results are thoroughly verified with 2D FE results and found an excellent agreement for all the cases.

2.8 NUMERICAL RESULTS FOR STATIC CASE

For static case, the present numerical results are non-dimensionalized with $s = h/a$, $Y_0 = 10.3$ GPa and $p_0 = 1$ as: $(\bar{u}, \bar{w}) = 100(u, s\ w)s^3 Y_0/p_0 h$; $(\bar{\sigma}_x, \bar{\tau}_{zx}) = (\sigma_x, \tau_{zx}/s)s^2/p_0$. Where, s $(= h/a)$ denote the thickness-to-span ratio. Results are plotted for different variation cases along with constant property case (homogeneous beam) to study the effect of axially varying material properties on bending behaviour of beam. Since there is no analytical elasticity solution exist for

a beam with longitudinal varying material properties. Therefore, the present method is validated with respect to 2D FE results. It is observed that present results are in excellent agreement with 2D FE results for all the cases.

2.8.1 Validation

A simply-supported composite beam consisting of four-ply of equal thickness $0.25h$ is considered for the validation. The accuracy of the present method has been investigated by comparing the result for beams of Mat. 1 with symmetric lay-up $[0^o/90^o/90^o/0^o]$ and unsymmetric lay-up $[0^o/90^o/0^o/90^o]$ as listed in Table 2.2. The present results are in excellent agreement with the results from the literature [295] for the simply-supported thick beam ($s = 0.2$), moderate beam ($s = 0.1$) and thin beam ($s = 0.05$). It is observed that for various span-to-thickness ratios s, the one-term solution (n = 1, iter = 1) gives an accurate prediction for simply supported support condition.

Table 2.2: Comparison of present EKM results with exact 2D elasticity results for homogeneous beam

		Lay-up $[0^o/90^o/90^o/0^o]$			Lay-up $[90^o/0^o/90^o/0^o]$		
Entity	s	2D Exact [295]	ZIGT [295]	Present	2D Exact [295]	ZIGT [295]	Present
	0.2	-2.6748	-2.6828	-2.6657	-3.7943	-3.7374	-3.7859
$\bar{w}(0.5a, 0)$	0.1	-1.4343	-1.4357	-1.4339	-2.4461	-2.4265	-2.4456
	0.05	-1.1152	-1.1152	-1.1152	-2.0958	-2.0895	-2.0959
	0.2	1.0711	1.0732	1.0995	0.15824	0.14273	0.16365
$\bar{\sigma}_x(0.5a, -0.5h)$	0.1	0.90587	0.90587	0.91728	0.12679	0.12273	0.12895
	0.05	0.86414	0.86414	0.86731	0.11878	0.11783	0.11939
	0.2	-1.0602	-1.0729	-1.1037	-1.4862	-1.5011	-1.5239
$\bar{\sigma}_x(0.5a, 0.5h)$	0.1	-0.9031	-0.90581	-0.91482	-1.3442	-1.3469	-1.3546
	0.05	-0.8635	-0.86436	-0.86646	-1.3081	-1.3094	-1.3108

2.8.2 Beam (a): Single Layered Beam

(i) Analysis of Isotropic Beam:

A thick single-layered isotropic AFG beam of Mat. 0, with $s = 0.2$, is considered for the numerical study, as shown in Fig. 2.3. Material properties of the isotropic beam is taken as:E=66.2 GPa, G=24.887 GPa, ν=0.33, as given in Table 2.1. Results are plotted for two material property variation cases, Case $(i)_a$: $\delta_1 = \delta_2 = 0.5$ and Case $(ii)_a$: $\delta_1 = \delta_2 = 1.0$. To study the effect of variation in material properties, the numerical results for constant

property case (homogenous beam) are also plotted along with the AFG cases. Since there is no analytical solution exist even for a isotropic beam with longitudinal varying material properties. Therefore, the present method is validated with respect to 2D FE results. The longitudinal variation of deflection and stresses (normal and shear) for different combination boundary conditions (eg. S–S, C–S, C–C, C–F) are presented in Figs. 2.6 to 2.9 for the thick beam ($s = 0.2$). Fig. 2.6 presents the longitudinal variation of deflections ($\bar{u}$, $\bar{w}$)

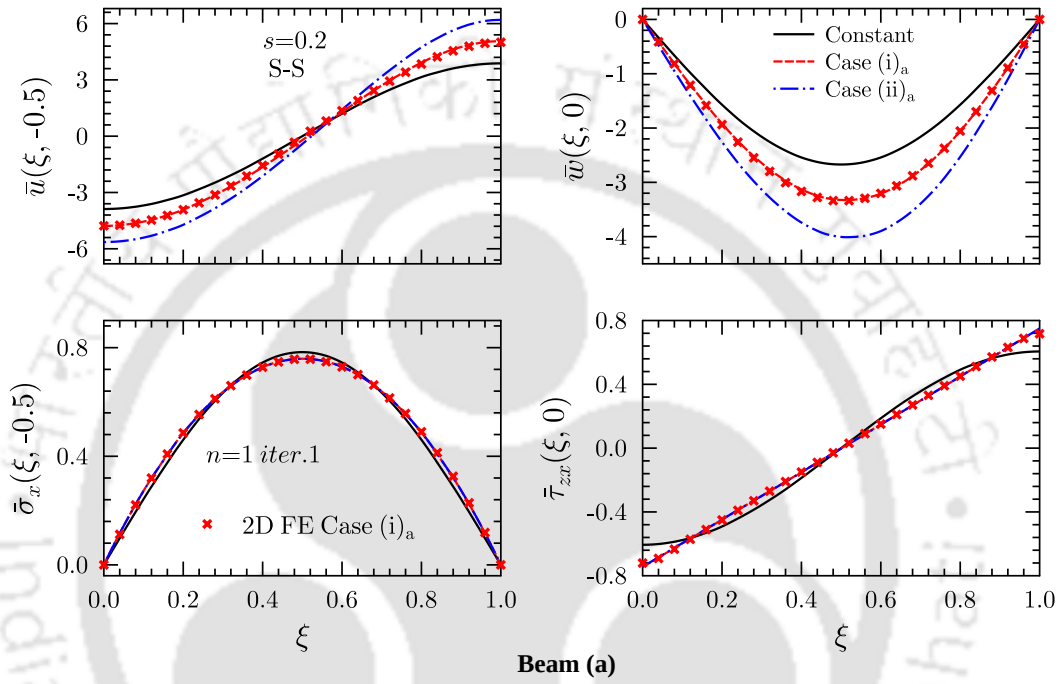

Fig. 2.6: Effect of variation in properties on longitudinal variations of deflections and stresses for AFG isotropic beam (a) subjected to S–S boundary condition

and stresses ($\bar{\sigma}_x$, $\bar{\tau}_{zx}$) for S–S (both edge simply supported) boundary conditions. It is observed that both in-plane and transverse deflections affected significantly by the gradation of material properties where stresses are not affected much. As the variation index increases, the magnitude of deflections ($\bar{u}$, $\bar{w}$) increases and the effect are nearly doubled as the variation index doubled. As variation index increases, the point of maximum deflection ($\bar{w}$) is also shifted toward edge ξ=1. In this figure, 2D FE results are also plotted for Case (i)$_a$. It is observed that present results are in excellent agreement with 2D FE results. For S–S, case one term solution gives an accurate prediction for all the entities.

In Figures 2.7 and 2.8, numerical results are plotted for C–S and C–C support conditions, respectively. For both C–S and C–C support conditions, it is also observed that the effect of gradation is significant on the deflections ($\bar{u}$, $\bar{w}$) as compared to the stresses ($\bar{\sigma}_x$, $\bar{\tau}_{zx}$). For these support conditions also, 2D FE matches excellently with the present solution. Here,

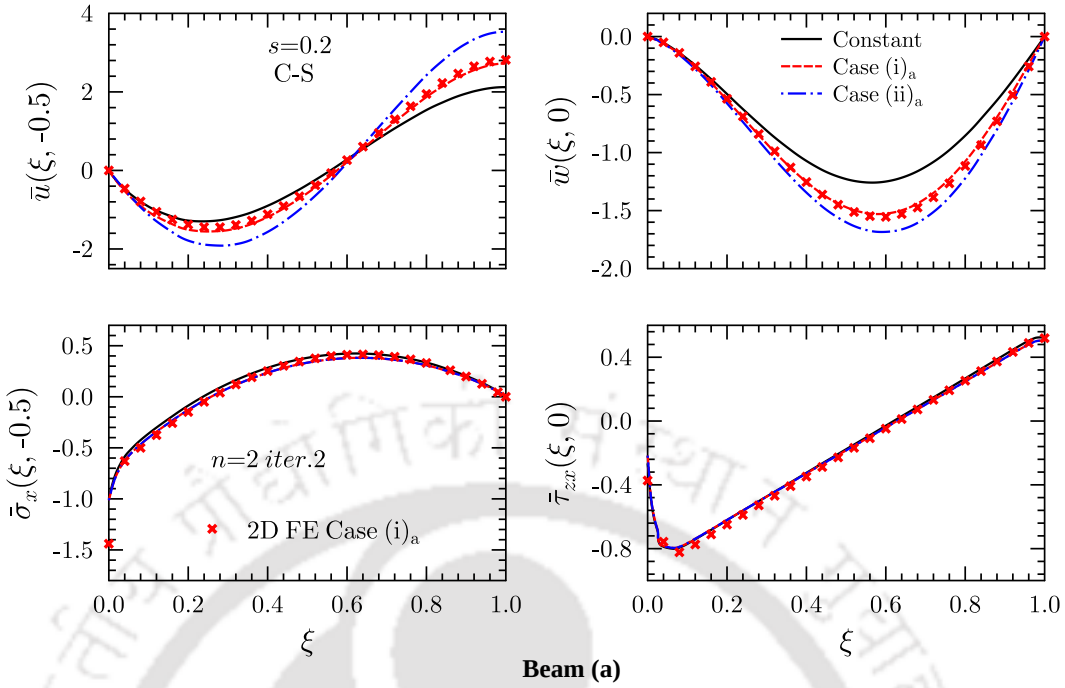

Fig. 2.7: Effect of variation in properties on longitudinal variations of deflections and stresses for AFG isotropic beam (a) subjected to C–S boundary condition

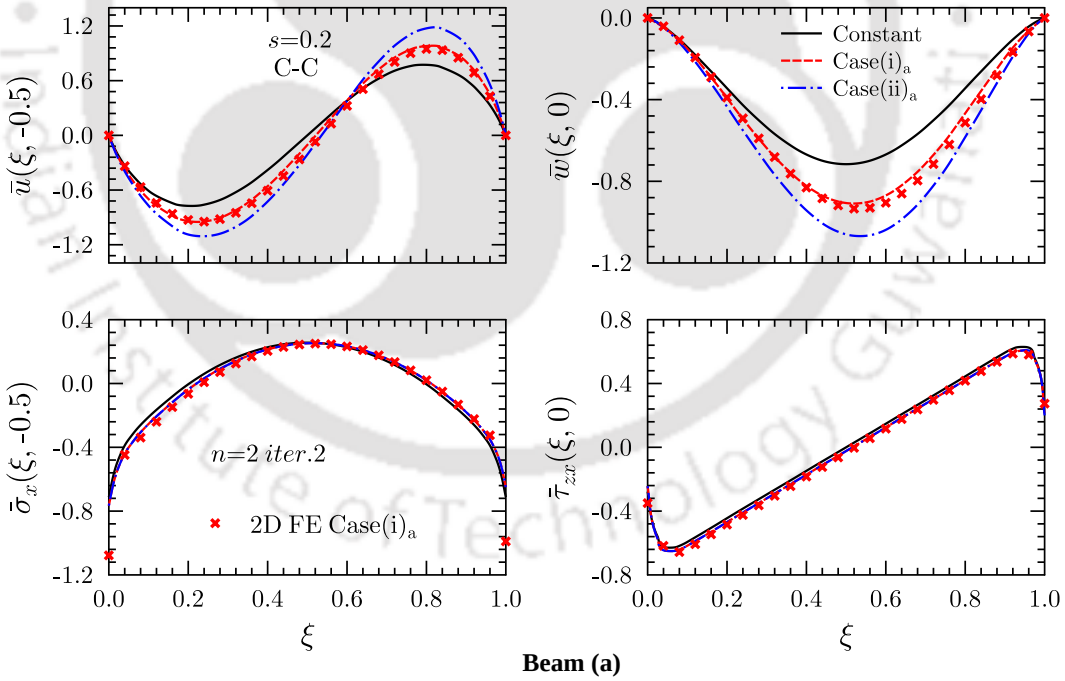

Fig. 2.8: Effect of variation in properties on longitudinal variations of deflections and stresses for AFG isotropic beam (a) subjected to C–C boundary condition

the two-term solution is needed for predicting accurate results near the clamped support. For C–C case, the effect of variation on deflections ($\bar{u}$, $\bar{w}$) are almost linear. The percentage increases in magnitude are almost doubled as the gradation index doubled. But for C–S case,

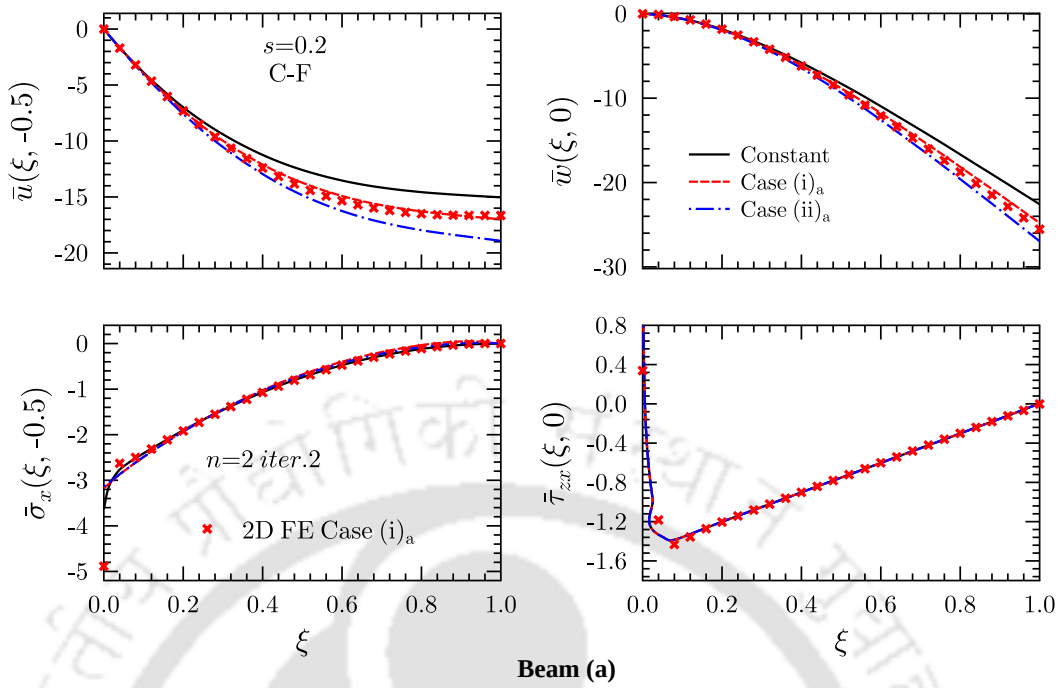

Fig. 2.9: Effect of variation in properties on longitudinal variations of deflections and stresses for AFG isotropic beam (a) subjected to C–F boundary condition

the percentage increases in deflections ($\bar{u}$, $\bar{w}$) for the first Case (i)$_a$ is more as compared to Case (ii)$_a$. As the variation index increases the location of maximum deflection shift toward the right for both C–S and C–C cases. In Fig 2.9, results are presented for C–F (clamped-free) boundary condition. For C–F case also, the effect of variation of material properties is more on deflections as compare to stresses . For C–F case, percentage increases in the magnitude of transverse deflection ($\bar{w}$) is less as compare to in-plane deflection ($\bar{u}$).

(ii) Analysis of Orthotropic Beam: A single-layer thick orthotropic beam (a) of Mat. 1, as shown in Fig. 2.3, having s=0.2 is considered for study in this section. Longitudinal variation of deflections ($\bar{u}$, $\bar{w}$) and stresses ($\bar{\sigma}_x$, $\bar{\tau}_{zx}$) for beam (a) have been presented in Figs. 2.10, 2.11 for simply-supported (S–S), clamped-simply supported (C–S), clamped-free supported (C–F) and clamped-clamped (C–C) boundary conditions, respectively. Results are plotted for different variation cases, Case (i)$_a$: $\delta_1 = \delta_2 = 0.5$, Case (ii)$_a$: $\delta_1 = \delta_2 = 1.0$, and Case(iii)$_a$: $\delta_1 = 2.0$, $\delta_2 = 1.0$ along with homogeneous case to study the effect of axially varying material properties on bending behaviour of beam. 2D FE results for case (ii)$_a$ is also plotted in these figures. It is observed that present EKM result are in excellent agreement with 2D FE results except for stresses at very clamped edges. This mismatch at very clamped edge is because the FE solution does not satisfy the conditions of applied normal at top and bottom surfaces for transverse stresses ($\bar{\sigma}_z$ and $\bar{\tau}_{zx}$) [279] and it can be verified from Fig. 2.13. It is observed that

for simply-supported boundary conditions single term (n=1, *iter*.1) gives accurate prediction for all the entities whereas two-term solution (n=2, *iter*.2) is required for the other boundary conditions. From Figs. 2.10 and 2.11, it is evident that for all the boundary conditions (S–S, C–S, C–F, C–C), deflections ($\bar{u}$, $\bar{w}$) is effected significantly with increase in variation indices whereas stresses ($\bar{\sigma}_x$, $\bar{\tau}_{zx}$) is least effected.

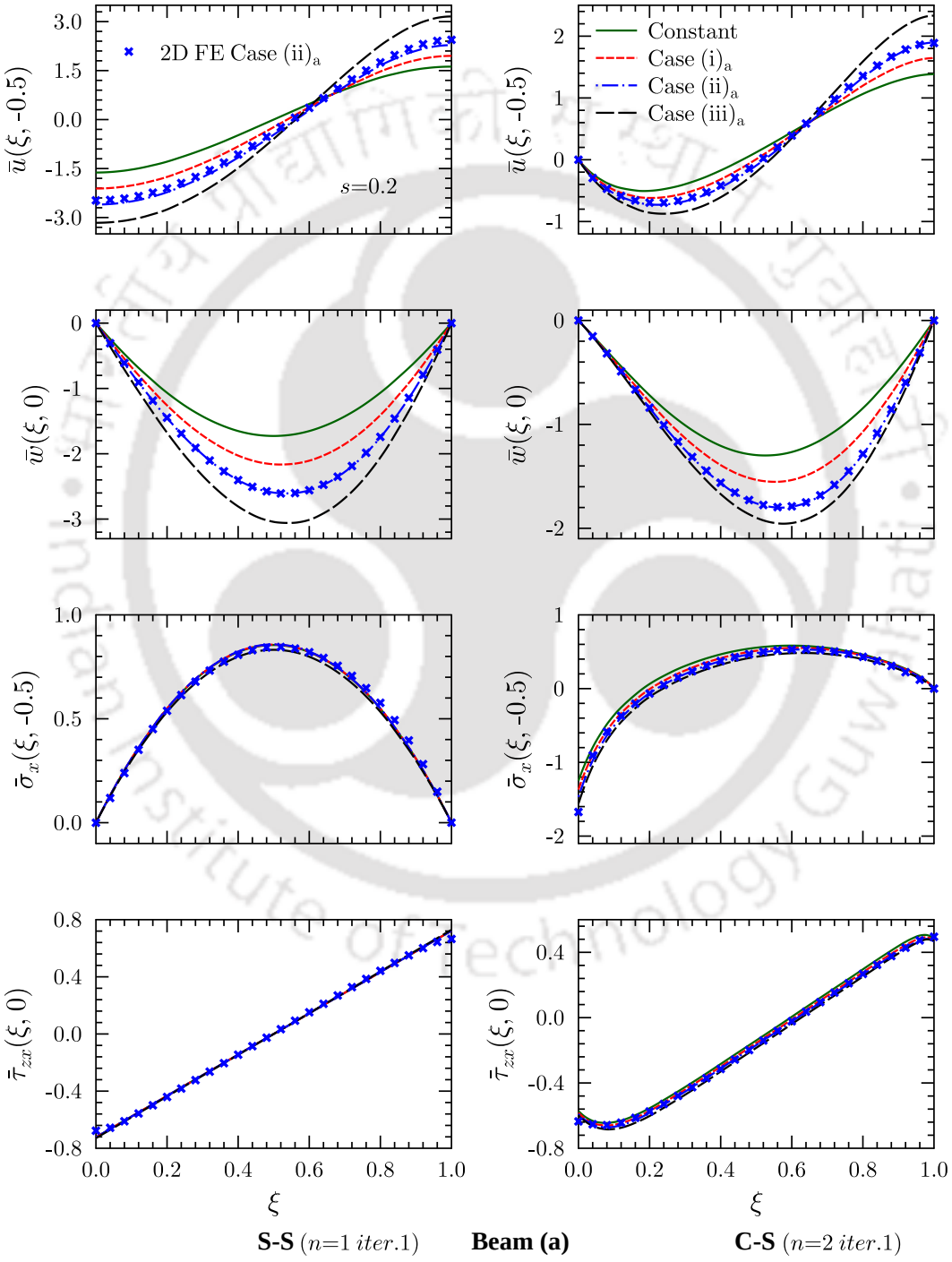

Fig. 2.10: Effect of variation in properties on longitudinal variations of deflection and stresses for beam (a) ($s = 0.2$) subjected to S–S and C–S boundary conditions

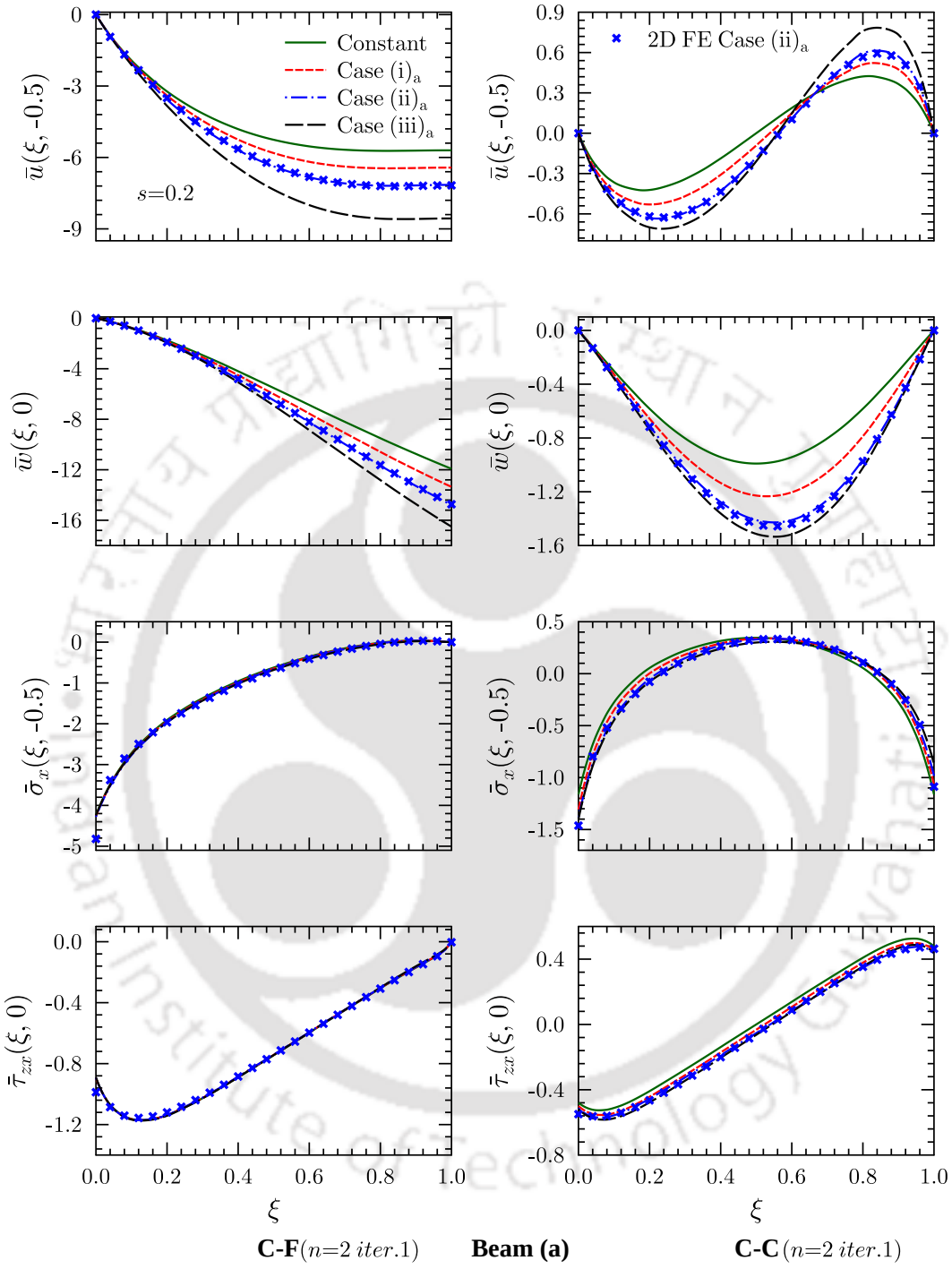

Fig. 2.11: Effect of variation in properties on longitudinal variations of deflection and stresses for beam (a) ($s = 0.2$) subjected to C–F and C–C boundary conditions

As variation indices increases, the point of maximum deflection ($\bar{w}$) for S–S, C–S and C–C boundary condition is shifted gradually toward $\xi = 1.0$. For S–S and C–F support conditions, percentage (%) increment in $\bar{w}$ is nearly equal for all the cases. But, for C–S and C–C support conditions, percentage increment in $\bar{w}$ for Case $(\text{iii})_\text{a}$ is very less as compared to Case $(\text{i})_\text{a}$ and

Case $(ii)_a$. For all the support conditions, axial displacement ($\bar{u}$) is influenced profoundly by an increase in variation index. It is observed that effect of varying material property on $\bar{u}$ is more pronounced near to simply-supported and free edges than the center of the beam. For S–S, C–S and C–C conditions, the effect of gradation on $\bar{u}$ are minimum, around $\xi = 0.6$, with respect to the constant case. All the lines cut the homogeneous case line at one point near to $\xi = 0.6$. For all the boundary conditions, the axial displacement ($\bar{u}$) increases abruptly for Case (iii_a) as compared to Case $(i)_a$ and Case $(ii)_a$. The longitudinal variation of in-plane displacement ($\bar{u}$) for S–S and C–C boundary condition become asymmetrical as the variation index increases. For both C–C and S–S conditions, asymmetry is the highest for Case $(iii)_a$ and a similar trend is observed for C–S case also. Figure 2.12 shows the longitudinal variation of stress $\bar{\sigma}_z$ for Case $(i)_a$ and homogeneous case of beam (a) under different boundary conditions. For C–C and C–S conditions, a longitudinal variation of $\bar{\sigma}_z$ become asymmetric for the axially graded beam as compared to the homogeneous beam. Figs. 2.10, 2.11 and 2.12 revealed that influence of axially graded material properties on the behavior of the beam depends significantly on boundary conditions of the beams.

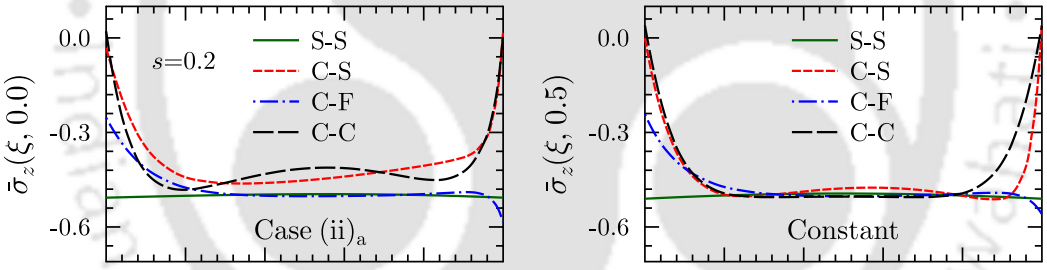

Fig. 2.12: Longitudinal variations of stress σ_z for homogeneous and AFG beam (b) ($s = 0.2$)

Through-thickness variations at different ξ location have been presented in Fig. 2.13 for Case $(ii)_a$ under C–S support conditions. 2D FE results for all ξ location are also plotted in the figure. It is revealed that the distribution of in-plane displacement $\bar{u}$ and stress $\bar{\sigma}_x$ match well with the 2D FE solution near to clamped support, but 2D FE fails in predicting the stresses $\bar{\sigma}_z$ and $\bar{\tau}_{zx}$ at the clamped edge. At the very clamped edge, 2D FE does not satisfy the boundary conditions for $\bar{\sigma}_z$ and τ_{zx} at the top and bottom surfaces of beams whereas present EKM solution satisfies these conditions exactly. As we move away from the clamped edge, 2D FE matches excellently with the present solution. It is observed that in-plane displacement ($\bar{u}$) and stress $\bar{\sigma}_x$ vary nonlinearly across the thickness near the edges. In most of the 1D theories, like Euler-Bernoulli and Timoshenko beam theory, in-plane displacement ($\bar{u}$) approximated linearly through the thickness. Therefore, these solution techniques can-

not predict the behavior accurately near the edges. Through-thickness variation of $\bar{\tau}_{zx}$ is parabolic and its magnitude decreases as we move from clamped edge to center of the beam. Similarly, through-thickness variations at different ξ location have been presented in Fig. 2.14 for homogeneous beam under C–S support conditions. A similar trend is observed for homogeneous case also. These benchmark results can be used to verify the accuracy of the 1D solution for homogeneous as well as axially FG beams.

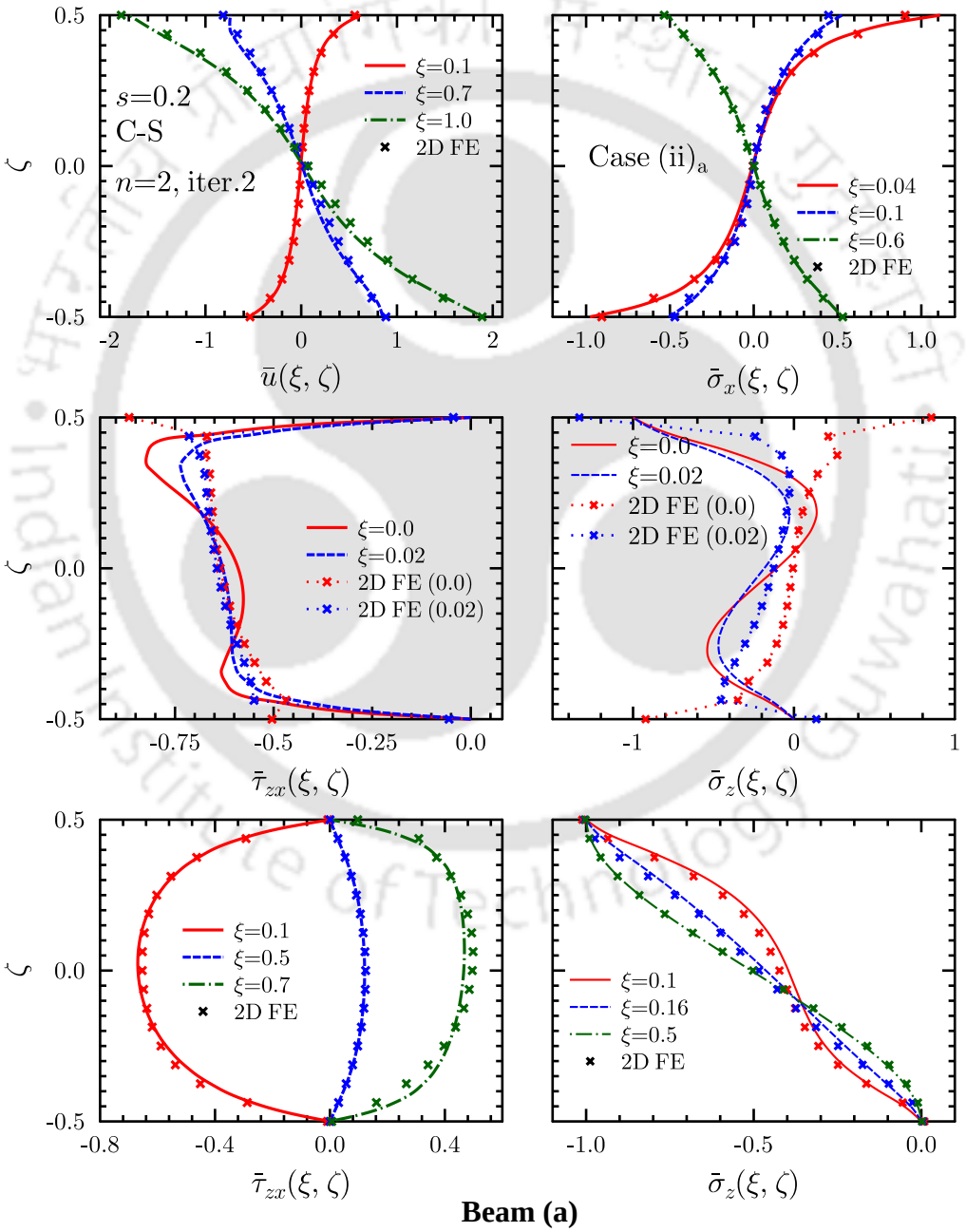

Fig. 2.13: Comparison of stresses distributions at different ξ-locations with 2D FE solution for beam (b) (Case(ii)$_a$, $s = 0.2$) under C–S boundary condition.

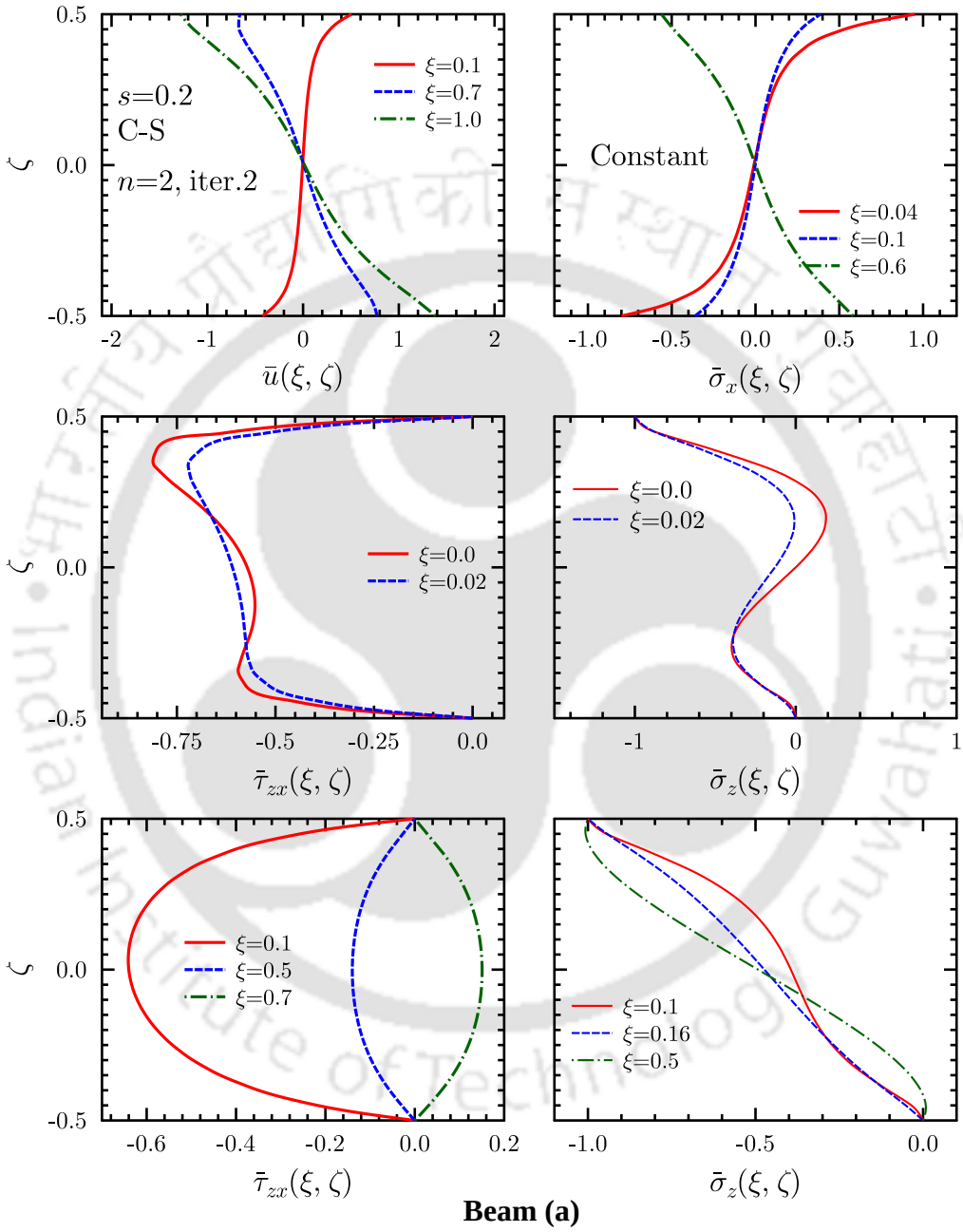

Fig. 2.14: Comparison of stresses distributions at different ξ-locations for homogeneous beam (a) ($s = 0.2$) under C–S boundary condition.

2.8.3 Beam (b): Two Layered Beam

A two layered beam (b) with the unsymmetrical lay-up schemes of $[0^o/90^o]$, as shown in Fig. 2.3, is considered for analysis in this section. Figures. 2.15, 2.16 and 2.17 depict the effect of variation index on longitudinal variation of deflections ($\bar{u}$, $\bar{w}$) and stresses ($\bar{\sigma}_x$, $\bar{\tau}_{zx}$) of beam (b) for C–S, C–F and C–C support conditions, respectively. Beam (b) is a two layered beam in which effect of longitudinal varying material property is investigated by taking different and same variation indices (δ_1, δ_2) for the top and bottom layer. Results are plotted for following variation cases of beam (b):

Case $(\text{i})_\text{b}$:- Bottom layer δ_1=δ_2=1.0, Top layer δ_1=δ_2=0.0; Case $(\text{ii})_\text{b}$:- Bottom layer δ_1=δ_2=1.0, Top layer δ_1=δ_2=1.0; Case $(\text{iii})_\text{b}$:- Bottom layer δ_1=δ_2=2.0, Top layer δ_1=δ_2=1.0 The layer-wise homogeneous case is also plotted in figures (2.15, 2.16 and 2.17) to investigate the effect of varying material property on the longitudinal variation of deflection and stresses. It is observed that deflections ($\bar{u}$, $\bar{w}$) are significantly affected for all boundary condition even by considering the axial variation of material property in one layer whereas stresses $\bar{\sigma}_x$, and $\bar{\tau}_{zx}$ are least affected for all cases. 2D FE results for case $(\text{ii})_\text{b}$ is also presented in Figs. 2.15, 2.16 and 2.17. The present results are in excellent agreement with 2D FE except for stress at very clamped edges.

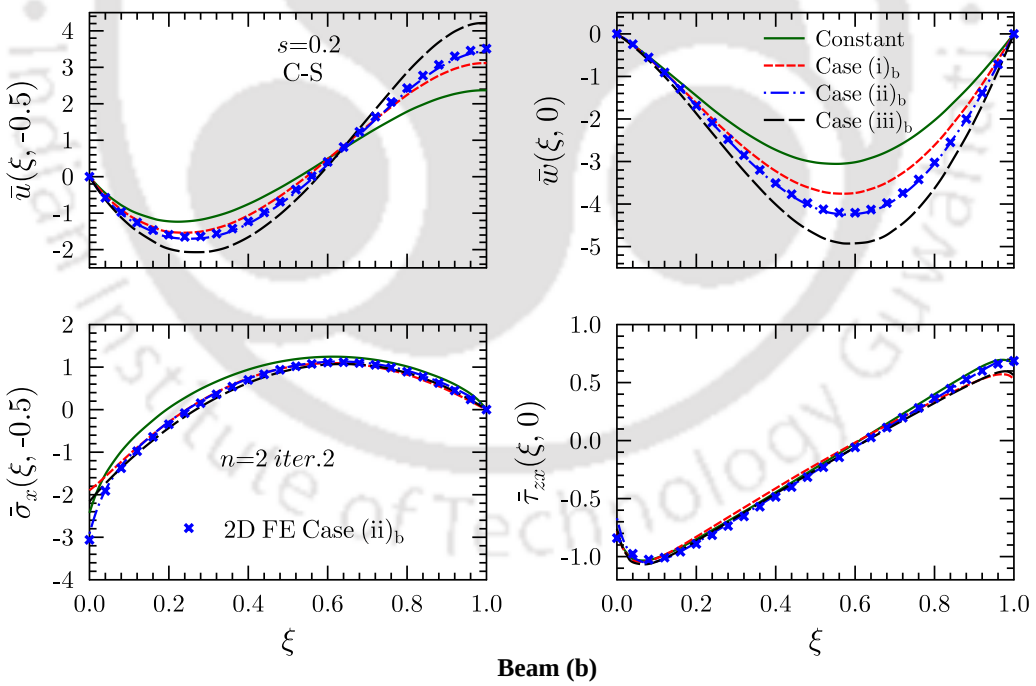

Fig. 2.15: Effect of variation in properties on longitudinal variations of deflection and stresses for beam (b) subjected to C–S boundary condition

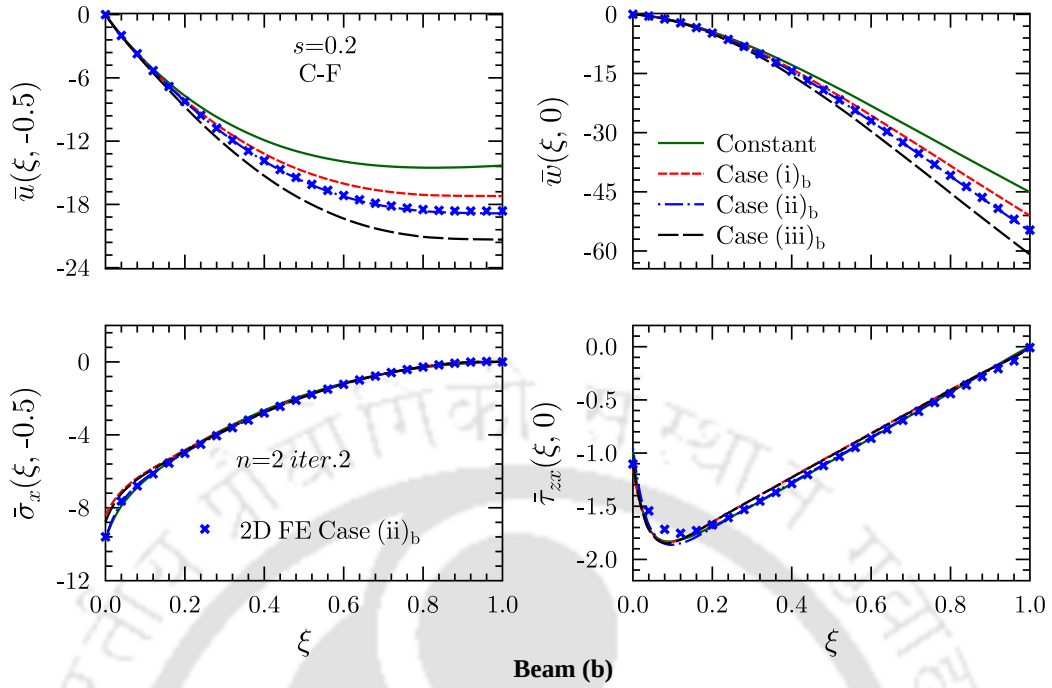

Fig. 2.16: Effect of variation in properties on longitudinal variations of deflection and stresses for beam (b) subjected to C–F boundary condition

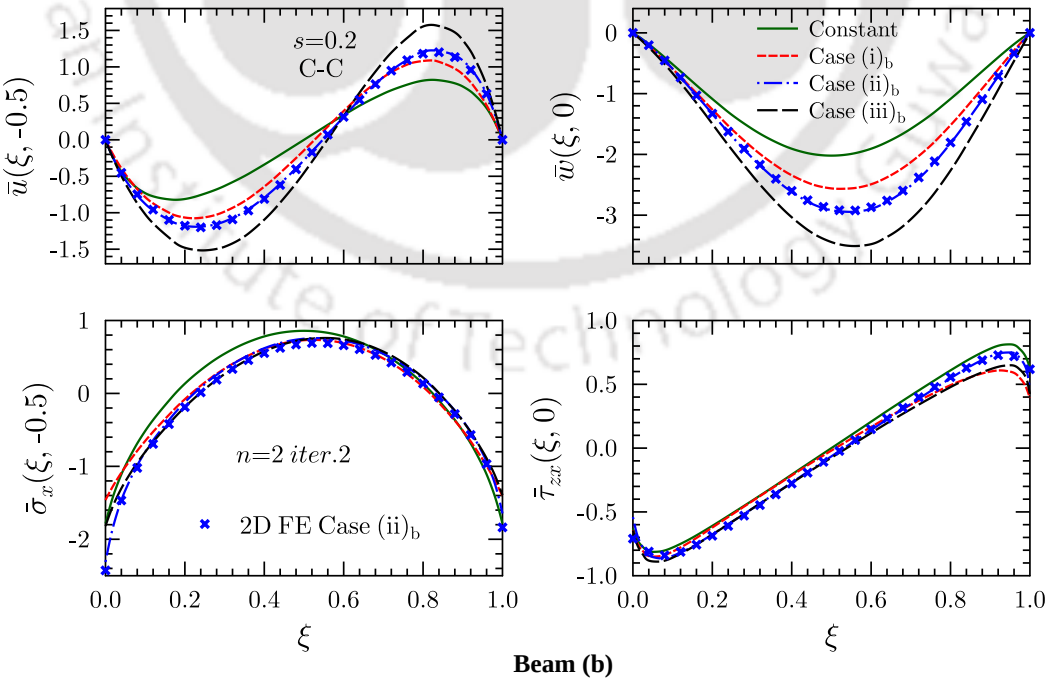

Fig. 2.17: Effect of variation in properties on longitudinal variations of deflection and stresses for beam (b) ($s = 0.2$) under C–C boundary condition

Fig. 2.18 shows through-thickness distribution of $\bar{u}$ and stresses $\bar{\sigma}_x$, $\bar{\sigma}_z$ and $\bar{\tau}_{zx}$ of beam (b) whose material properties varying according to Case (ii)$_\mathrm{b}$ and beam subjected to C–F boundary conditions. It is observed that stresses $\bar{\sigma}_z$ and $\bar{\tau}_{zx}$ are highly non-linear near to clamped support and 2D FE fail to predict it because finite element solution does not satisfy the boundary conditions and interface continuity conditions at very clamped edge.

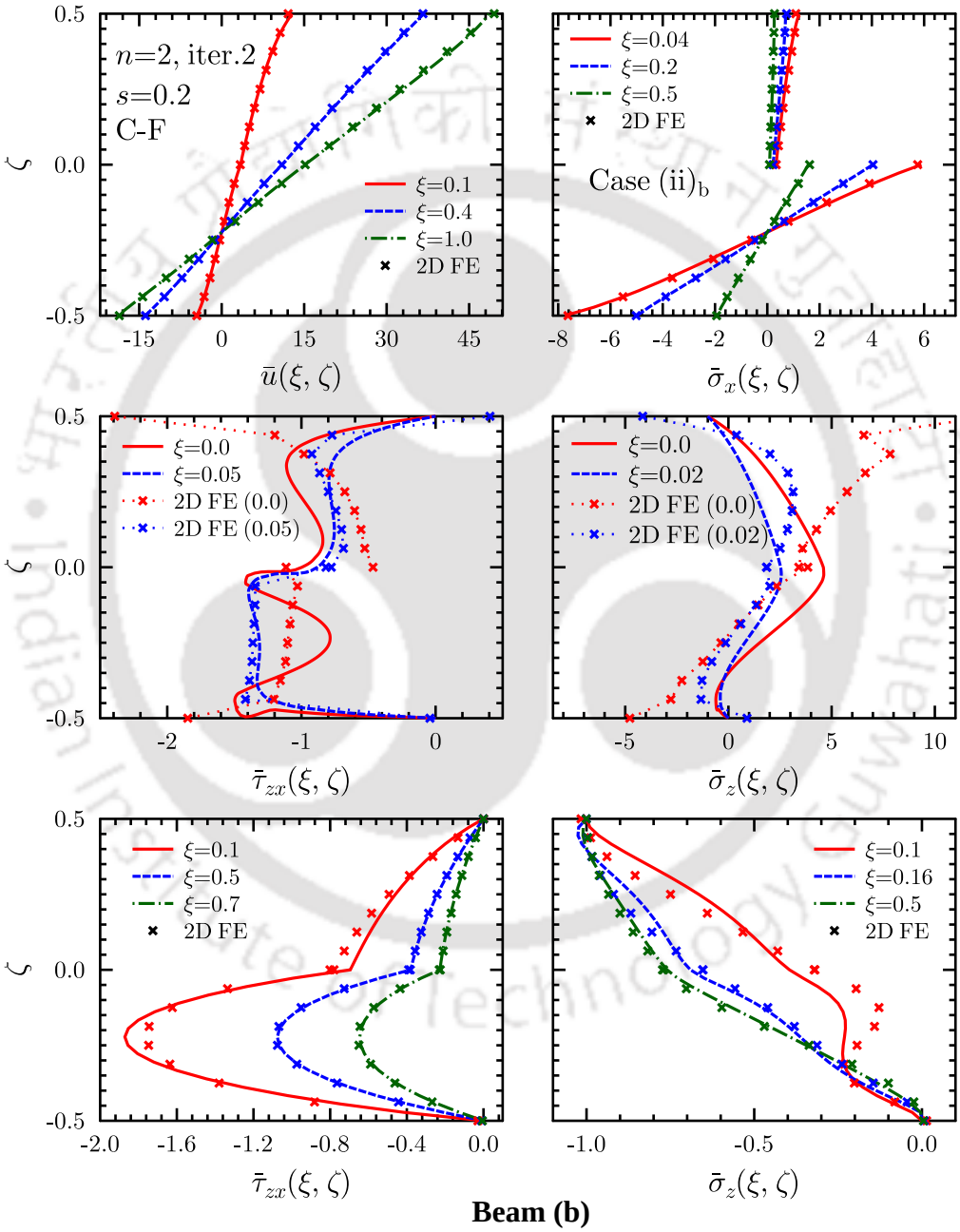

Fig. 2.18: Comparison of stresses distributions at different ξ-locations with 2D FE solution for AFG beam (b) (Case (ii)$_\mathrm{b}$, $s = 0.2$) under C–F boundary condition.

2.8.4 Beam (c): Four Layered Beam

A four-layer beam (c) with the symmetrical lay-up schemes of $[0^o/90^o/90^o/0^o]$, as shown in Fig. 2.3, is analyzed in this section. Results are presented for two cases of property variation, Case (i)$_c$ δ_1=δ_2=1.0 for all layer; Case (ii)$_c$ δ_1=δ_2=2.0 for all layer. Longitudinal variation of deflections ($\bar{u}$, $\bar{w}$) and stresses ($\bar{\sigma}_x$, $\bar{\tau}_{zx}$) for beam (c) have been plotted in Figs. 2.19, 2.20 and 2.21 for clamped-simply supported (C–S), clamped-free supported (C–F) and clamped-clamped (C–C) boundary conditions, respectively. Here, results for layer wise homogeneous beam (c) are also

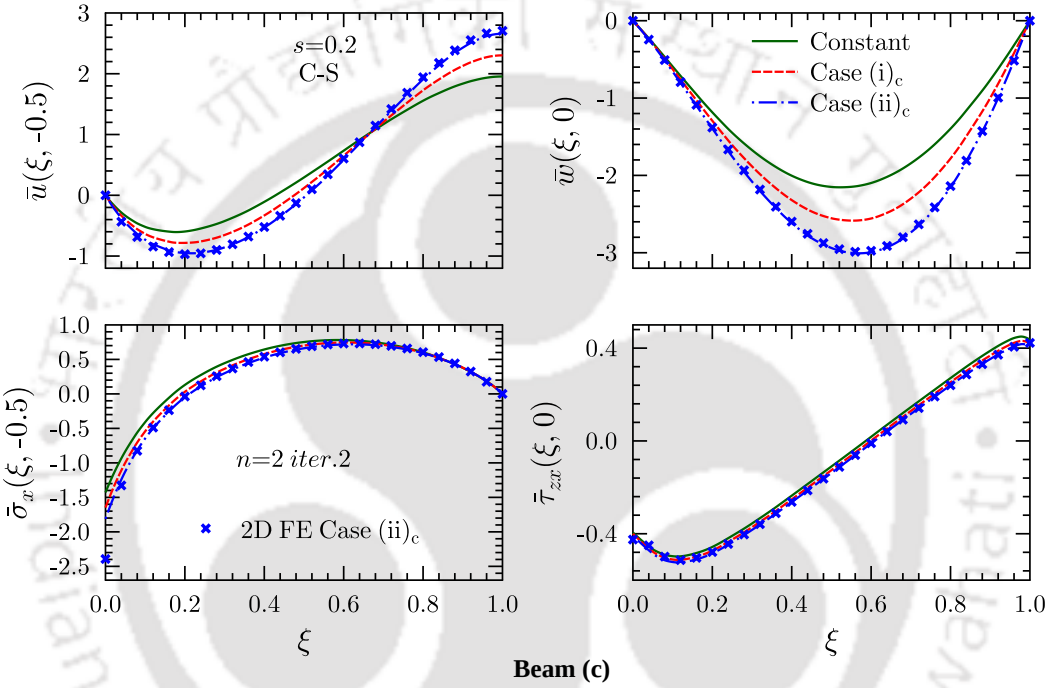

Fig. 2.19: Effect of variation in properties on longitudinal variations of deflection and stresses for beam (c) ($s = 0.2$) under C–S boundary condition

plotted to show the effect of axially graded material properties on deflections and stresses. 2D FE result for Case (ii)$_c$ is also plotted which is in good agreement with present results except for stresses at very clamped support. It is revealed that, the effect of axial gradation of property is more significant for deflections ($\bar{u}$, $\bar{w}$) as compared to stresses ($\bar{\sigma}_x$,$\bar{\tau}_{zx}$) for all three boundary condition (C–S, C–F, C–C). For beam (c) subjected to C–C boundary conditions, the longitudinal variation of deflections ($\bar{u}$, $\bar{w}$) become asymmetric as the variation index increases.

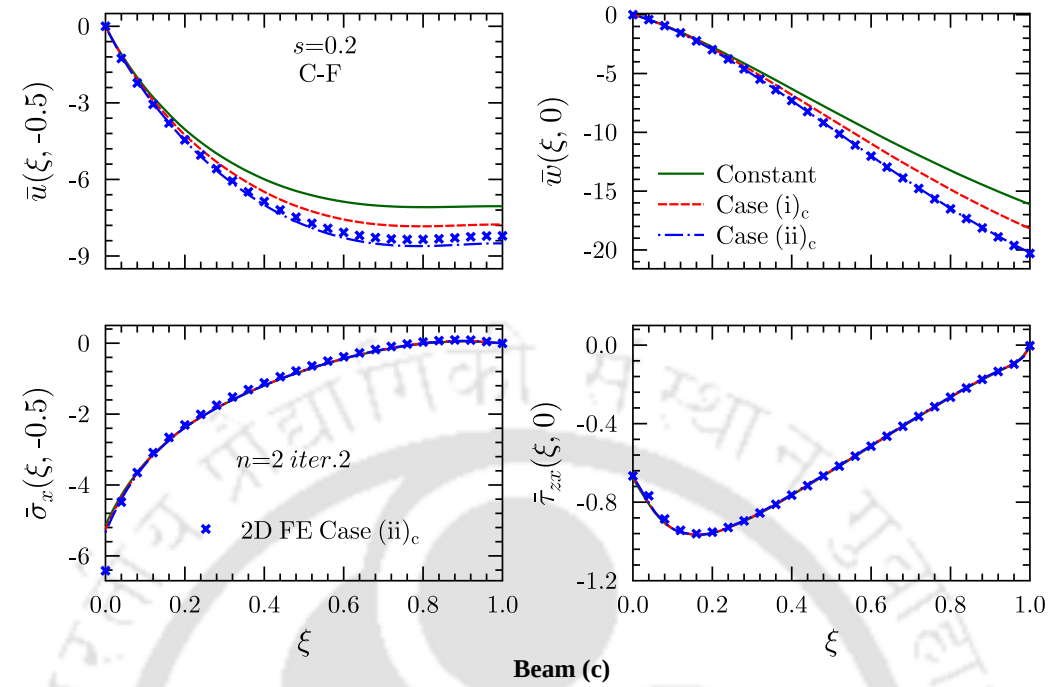

Fig. 2.20: Effect of variation in properties on longitudinal variations of deflection and stresses for beam (c) ($s = 0.2$) under C–F boundary condition

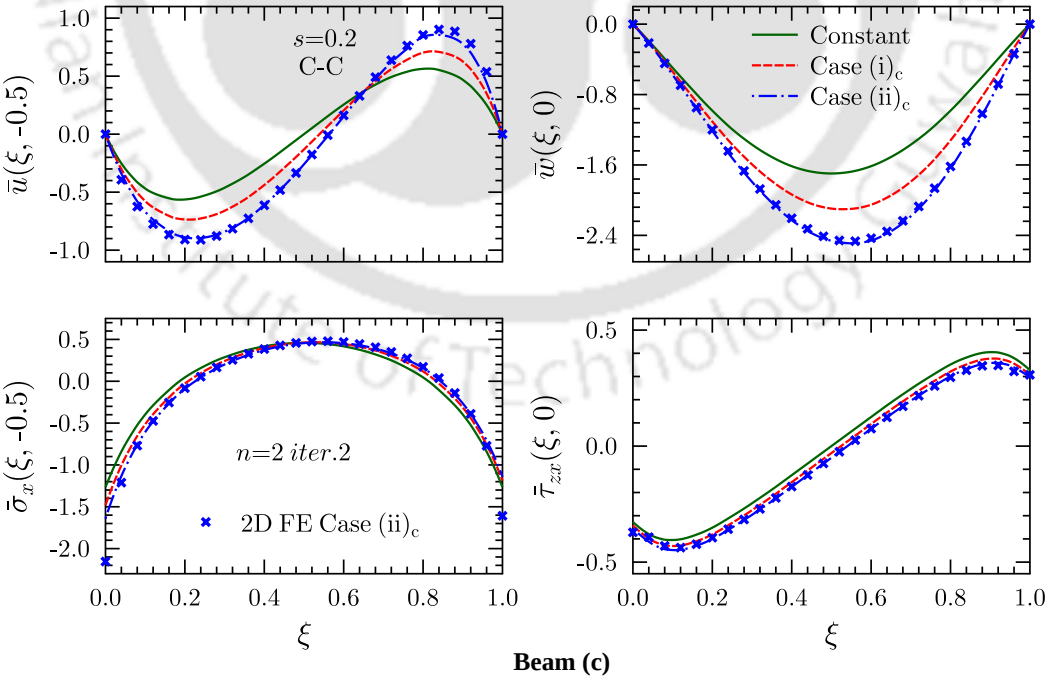

Fig. 2.21: Effect of variation in properties on longitudinal variations of deflection and stresses for beam (c) ($s = 0.2$) under C–C boundary condition

2.9 NUMERICAL RESULTS FOR DYNAMIC CASE

The natural frequencies ω are non-dimensionalized as $\omega^* = \omega h\sqrt{\rho/G_{12}}$. Where ρ= 1578 Kg/m^3 and G_{12}=7.17 GPa. The modal displacements and stresses are non-dimensionalized as: $(\bar{u},\, \bar{w}) = (u, w)/\max(u, w)$; $(\bar{\sigma}_x,\, \bar{\sigma}_z,\, \bar{\tau}_{zx}) = (\sigma_x,\, \sigma_z,\, \tau_{zx})\, h/(s\, Y_0 \max(u, w))$. Where $\max(u, w)$ denote the largest value of u and w along the thickness of beam for a particular vibration mode. Similarly, $s(= h/a)$ denote the thickness-to-span ratio. In the subsequent sections, results are obtained by taking n=1, iter.2 for S–S boundary condition and n=1, iter.3 for other boundary conditions.

2.9.1 Validation

In this section, present results are validated for constant property case with the available result from literature and also with 2D FE results. Numerical results are compared for a composite beam consisting of symmetric 4-ply laminate of Mat. 1 with lay-up [0/90/0/90^0] where each ply is of equal thickness 0.25h. The dimensionless natural frequencies of first five bending modes are compared in Table 2.3 for the S–S, C–C and C–F boundary conditions. For simply–supported boundary condition present results are compared with 2D exact results of Kapuria et al. [295]. To compare the numerical results, natural frequency parameters reported by Kapuria et al. [295] further non-dimensionalized as $\omega^* = \omega h\sqrt{\rho/G_{12}}$. Since no 2D exact or closed-form solution is available in literature for other type of support conditions. Therefore, present results are compared with 2D FE results for other combination of boundary conditions. Since it is a beam with a small width, plane stress element of ABAQUS [294] can be used. Therefore, the 2D plane beam with length a along x-direction and thickness h along z-direction is modeled in ABAQUS using the element type CPS8R with a mesh size of 50 (length) $\times$16 (thickness). It is observed that the presented results match excellently with Ref. [295] and 2D FE results.

2D elasticity based analytical solution is also not available in the literature for the axially graded beams. Therefore, the accuracy and efficiency of the present EKM solution for the axially graded beams are verified by comparing the present result with 2D FE. For AFG beams, the spatial gradation of elastic property (at different Gauss points) is implemented by employing user material subroutine (UMAT) [296]. The variation of mass density is implemented by dividing the beam into 20 number of equal parts along the length and each part is assigned density value according to its center point. Table 2.4 shows the comparison of the natural frequencies with 2D FE results for single layered beam (a) subjected to S–S, C–C and C–F boundary conditions. The results are compared for homogenous (constant property) case and property gradation Case (i)$_{\rm a}$: $\delta_1 = \delta_2 = \delta_p = 0.5$. The present results are in excellent agreement with 2D FE results for both cases and for all the boundary conditions. In the succeeding subsections, all the results are also thoroughly verified with

2D FE results and found an excellent agreement for all the cases.

Table 2.3: Comparison of first five lowest natural frequency parameters $\omega^* = \omega h\sqrt{\rho/G_{12}}$ for four layered composite beam $[(0^o/90^o/0^o/90^o)]$ subjected to different sets of boundary conditions $(s = 0.1)$

s	B.C.	n	1	2	3	4	5
0.05	S–S	Present	0.0318822	0.1119870	0.2149740	0.3262984	0.4405899
		2D exact	0.0318816	0.1119873	0.2149734	0.3262774	0.4405899
		2D FE	0.0318816	0.1119866	0.2149711	0.3263033	0.4405978
	C–S	Present	0.0459824	0.1273761	0.2268831	0.3347572	0.4467415
		2D FE	0.0460627	0.1279819	0.2281912	0.3367968	0.4493818
	C–C	Present	0.0602410	0.1415782	0.2376417	0.3430243	0.4529590
		2D FE	0.0614449	0.1427540	0.2406450	0.3468778	0.4579889
	C–F	Present	0.0116706	0.0611726	0.1546604	0.2592903	0.3707829
		2D FE	0.0116748	0.0643940	0.1555909	0.2611310	0.3735539
0.1	S–S	Present	0.1119870	0.3262990	0.5563598	0.7917446	1.0327890
		2D exact	0.1119861	0.3262954	0.5563586	0.7917434	1.0327854
		2D FE	0.1119866	0.3263033	0.5563662	0.7917644	1.0328220
	C–S	Present	0.1415773	0.3430237	0.5660394	0.7988317	1.0388345
		2D FE	0.1427481	0.3468483	0.5719003	0.8056772	1.0458801
	C–C	Present	0.1714813	0.3586193	0.5841088	0.8065768	1.0455009
		2D FE	0.1736364	0.3649762	0.5874638	0.8192953	1.0589970
	C–F	Present	0.0435130	0.1930565	0.4162172	0.6461126	0.8844087
		2D FE	0.0436191	0.1954047	0.4225730	0.6549351	0.8955506
0.2	S–S	Present	0.3262988	0.7950418	1.2794702	1.7860910	2.3029044
		2D exact	0.3262954	0.7917674	1.2794846	1.7860910	2.3029092
		2D FE	0.3262974	0.7917349	1.2795097	1.7861493	2.3029877
	C–S	Present	0.3586196	0.8065768	1.2908373	1.7953008	2.3099903
		2D FE	0.3649527	0.8192069	1.3036213	1.8059574	2.3181975
	C–C	Present	0.3975904	0.8227333	1.3051721	1.8050570	2.3176323
		2D FE	0.4131052	0.8442618	1.3286762	1.8252349	2.3346453
	C–F	Present	0.1408368	0.4887384	0.9830237	1.4712586	1.9854688
		2D FE	0.1425594	0.5044230	1.0077377	1.4909141	2.0017983

Table 2.4: Comparison of first five lowest natural frequency parameters $\omega^* = \omega h\sqrt{\rho/G_{12}}$ for single layered axially graded beams subjected to different sets of boundary conditions ($s = 0.1$)

Variation	B.C.	n	1	2	3	4	5
Constant	S–S	Present	0.1278214	0.4048405	0.7183917	1.0363056	1.3532438
		2D FE	0.1278213	0.4048283	0.7183977	1.0363002	1.3532595
	C–S	Present	0.1718361	0.4370542	0.7365858	1.0469044	1.3599797
		2D FE	0.1722569	0.4384903	0.7390017	1.0498594	1.3631341
	C–C	Present	0.2161815	0.4652442	0.7544107	1.0573630	1.3668714
		2D FE	0.2170197	0.4676719	0.7587804	1.0628584	1.3729497
	C–F	Present	0.0481663	0.2360164	0.5285832	0.8391847	1.1571825
		2D FE	0.0481879	0.2366745	0.5308692	0.8426406	1.1614863
Case $(\text{i})_\text{a}$ $\delta_1 = \delta_2 = \delta_p = 0.5$	S–S	Present	0.1020078	0.3237784	0.5745036	0.8287549	1.0823242
		2D FE	0.1020088	0.3237978	0.5745826	0.8289341	1.0826371
	C–S	Present	0.1388961	0.3538251	0.5938627	0.8413565	1.0910437
		2D FE	0.1391431	0.3546300	0.5952455	0.8431122	1.0930422
	C–C	Present	0.1728368	0.3725154	0.6044040	0.8469430	1.0945339
		2D FE	0.1735509	0.3744971	0.6079204	0.8513066	1.0993502
	C–F	Present	0.0387337	0.1922727	0.4302224	0.6792120	0.9329132
		2D FE	0.0387703	0.1928608	0.4317697	0.6815228	0.9358743

2.9.2 Beam (a): Single Layered Beam

An single-layer beam (a) of Mat. 1, as shown in Fig. 2.3, is considered for study in this section. First five lowest dimensionless natural frequencies $\omega^* = \omega h\sqrt{\rho/G_{12}}$ are tabulated for thin (s=0.05) AFG beam, moderately thick AFG beam (s=0.1) and thick AFG beam (s=0.2). Results are presented for different variation cases, Case(i)_a: $\delta_1 = \delta_2 = \delta_p = 0.5$; Case(ii)_a: $\delta_1 = \delta_2 = \delta_p = 1.0$; and $\text{Case(iii)}_\text{a}$: $\delta_1 = 2.0$, $\delta_2 = 1.0$, $\delta_p = 1.5$ along with constant properties (homogeneous) case (Constant: $\delta_1 = \delta_2 = \delta_p = 0.0$) to investigating the effect of axially varying material properties on natural frequencies of beam. In Tables 2.5, 2.6, 2.7 and 2.8 benchmark results are tabulated for S–S, C–S, C–C and C–F boundary conditions, respectively.

Significant effect of axial gradation is observed on the natural frequencies of the beam. As the variation indexes increases, the natural frequencies of the beam decreases significantly for all the boundary conditions. Percentage change in natural frequencies under different boundary conditions are plotted in Figs. 2.22, 2.23, 2.24 for s=0.05, s=0.1 and s=0.2, respectively. For all the support conditions and thickness to expect ratio (s), nearly 17 to 20% decrement is observed in first five natural frequencies for Case $(\text{i})_\text{a}$ as compared to constant property case. The percentage decrement

Table 2.5: Effect of axial gradation on first five lowest dimensionless natural frequencies $\omega^* = \omega h\sqrt{\rho/G_{12}}$ of single layer AFG beam (a) subjected to S–S boundary condition

s	n	Constant	Case (i)$_a$	Case (ii)$_a$	Case (iii)$_a$
0.05	1	0.0346950	0.0277025	0.0230070	0.0185024
	2	0.1278217	0.1023694	0.0854611	0.0705504
	3	0.2572639	0.2060162	0.1719718	0.1452568
	4	0.4048399	0.3240601	0.2703087	0.2326134
	5	0.5601880	0.4482517	0.3736654	0.3262804
0.1	1	0.1278214	0.1020078	0.0846418	0.0692965
	2	0.4048405	0.3237784	0.2696228	0.2314248
	3	0.7183917	0.5745036	0.4783397	0.4218492
	4	1.0363056	0.8287549	0.6899990	0.6176924
	5	1.3532438	1.0823242	0.9011909	0.8137298
0.2	1	0.4048408	0.3227079	0.2672228	0.2277016
	2	1.0363068	0.8280693	0.6883270	0.6149993
	3	1.6689200	1.3345080	1.1105119	1.0071818
	4	2.2979041	1.8381708	1.5305201	1.3968905
	5	2.9252245	2.3405200	1.9494209	1.7851514

Table 2.6: Effect of axial gradation on first five lowest dimensionless natural frequencies $\omega^* = \omega h\sqrt{\rho/G_{12}}$ of single layer AFG beam (a) subjected to C–S boundary condition

s	n	Constant	Case (i)$_a$	Case (ii)$_a$	Case (iii)$_a$
0.05	1	0.0515928	0.0414557	0.0346980	0.0286562
	2	0.1503237	0.1212638	0.1016836	0.0853232
	3	0.2781167	0.2244518	0.1882353	0.1605756
	4	0.4214070	0.3396743	0.2847402	0.2468409
	5	0.5725931	0.4607616	0.3857469	0.3385327
0.1	1	0.1718361	0.1388961	0.1165481	0.0989532
	2	0.4370542	0.3538251	0.2972184	0.2592109
	3	0.7365858	0.5938627	0.4976664	0.4420354
	4	1.0469044	0.8413565	0.7035823	0.6319684
	5	1.3599797	1.0910437	0.9111941	0.8241584
0.2	1	0.4652438	0.3785808	0.3184228	0.2803403
	2	1.0573630	0.8528651	0.7146713	0.6429448
	3	1.6782736	1.3477161	1.1263568	1.0235253
	4	2.3031633	1.8462682	1.5410051	1.4075193
	5	2.9285996	2.3461628	1.9571540	1.7928701

Table 2.7: Effect of axial gradation on first five lowest dimensionless natural frequencies $\omega^* = \omega h\sqrt{\rho/G_{12}}$ of single layer AFG beam (a) subjected to C–C boundary condition

s	n	Constant	Case (i)$_a$	Case (ii)$_a$	Case (iii)$_a$
0.05	1	0.0707979	0.0567053	0.0473592	0.0395629
	2	0.1718364	0.1376358	0.1149183	0.0979228
	3	0.2976472	0.2384165	0.1991194	0.1721932
	4	0.4370542	0.3501018	0.2923990	0.2557600
	5	0.5845337	0.4682137	0.3909936	0.3451098
0.1	1	0.2161815	0.1728368	0.1439336	0.1251151
	2	0.4652442	0.3725154	0.3108556	0.2753363
	3	0.7544107	0.6044040	0.5048326	0.4512559
	4	1.0573630	0.8469430	0.7071492	0.6368765
	5	1.3668714	1.0945339	0.9133659	0.8270961
0.2	1	0.5337514	0.4237473	0.3528818	0.3181117
	2	1.0748620	0.8613365	0.7195950	0.6506683
	3	1.6897318	1.3535650	1.1301059	1.0281662
	4	2.3079288	1.8480613	1.5418777	1.4088042
	5	2.9326076	2.3479079	1.9581848	1.7940255

Table 2.8: Effect of axial gradation on first five lowest dimensionless natural frequencies $\omega^* = \omega h\sqrt{\rho/G_{12}}$ of single layer AFG beam (a) subjected to C–F boundary condition

s	n	Constant	Case (i)$_a$	Case (ii)$_a$	Case (iii)$_a$
0.05	1	0.0125613	0.0101134	0.0084685	0.0071525
	2	0.0726125	0.0585600	0.0491412	0.0406566
	3	0.1830396	0.1480054	0.1245817	0.1044876
	4	0.3181782	0.2575950	0.2165860	0.1848773
	5	0.4666975	0.3772132	0.3167459	0.2744428
0.1	1	0.0481663	0.0387337	0.0326185	0.0275274
	2	0.2360164	0.1922727	0.1620990	0.1376544
	3	0.5285832	0.4302224	0.3627100	0.3154988
	4	0.8391847	0.6792120	0.5705052	0.5057231
	5	1.1571825	0.9329132	0.7814454	0.7003869
0.2	1	0.1672410	0.1341263	0.1125633	0.0966738
	2	0.6286820	0.5173935	0.4388937	0.3847385
	3	1.2855205	1.0436036	0.8777855	0.7859664
	4	1.9081666	1.5380711	1.2875724	1.1659284
	5	2.5444091	2.0456268	1.7095415	1.5546207

in natural frequencies is 30 to 33% for Case (ii)$_a$ and 38 to 46% for Case (iii)$_a$, respectively.

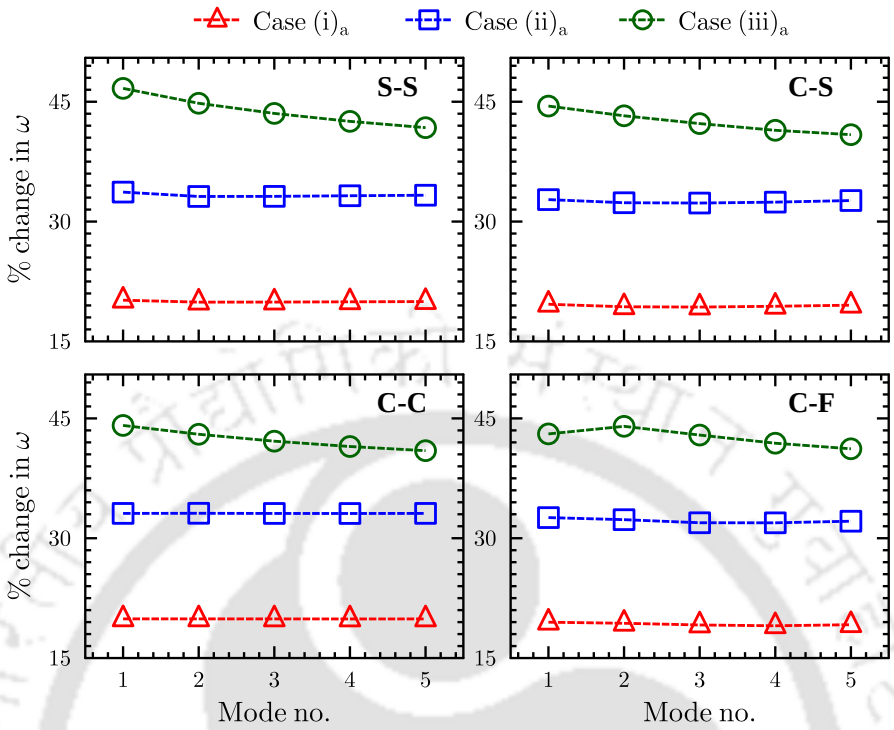

Fig. 2.22: Percentage change in first five lowest natural frequencies of beam (a) due to variation in material properties under S–S, C–S, C–C and C–F boundary conditions (s=0.05)

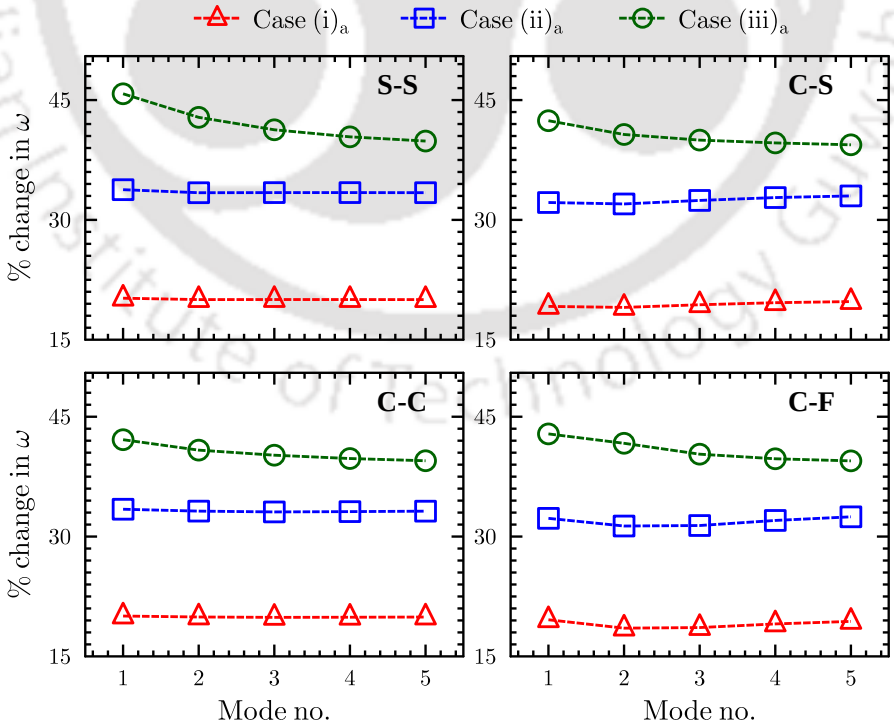

Fig. 2.23: Percentage change in first five lowest natural frequencies of beam (a) due to variation in material properties under S–S, C–S, C–C and C–F boundary conditions (s=0.1)

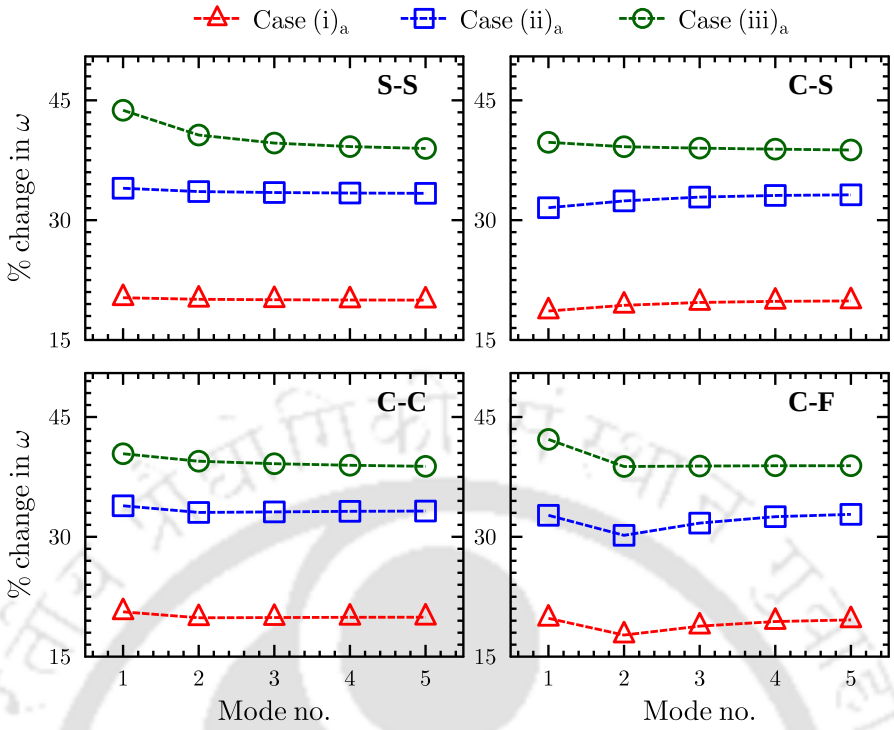

Fig. 2.24: Percentage change in first five lowest natural frequencies of beam (a) due to variation in material properties under S–S, C–S, C–C and C–F boundary conditions(s=0.2)

For all the variation cases, the effect of boundary conditions are significant on the lower mode natural frequencies and it is maximum for first vibration mode. But for higher mode frequencies the effect of boundary conditions is negligible. Similarly, for all the variation cases, a significant effect of thickness to expect ratio (s) is also observed on natural frequencies of the beams. As the thickness to expect ratio (s) increases the natural frequencies of all the vibration modes increases significantly. The effect of thickness to expect ratio (s) is more on lower mode frequencies as compared to higher mode frequencies.

Similarly, effect of axial gradation of density on natural frequencies of beams is studied in Table 2.9 under different boundary conditions. The elastic properties of beam kept constant by fix variation indexes δ_1 and δ_2 equal to zero ($\delta_1 = \delta_2$=0). The effect of density variation is studied by varying only the density variation index (δ_p) according to δ_p=0, 0.5, 1.0, 1.5. It is observed that as the density variation index (δ_p) increases the natural frequency of beam decreases. The percentage decrement in natural frequencies is 10% for δ_p=0.5 as compared to constant density case (δ_p=0) under all the support conditions. Where the percentage decrement in natural frequencies is 17 to 19% for δ_p=1.0 and 23 to 25% for δ_p=1.5, respectively. It is observed that effect is nearby double as the value of density variation index (δ_p) make double from δ_p=0.5 to δ_p=1.0.

Table 2.9: Effect of variation in density on first five lowest dimensionless natural frequencies $\omega^* = \omega h\sqrt{\rho/G_{12}}$ of single layer AFG beam (a) subjected to different boundary conditions

B.C.	δ_1=δ_2=0			
	δ_p=0	δ_p=0.5	δ_p=1	δ_p=1.5
S–S	0.1278214	0.1142941	0.1042823	0.0964963
	0.4048405	0.3626309	0.3318891	0.3080677
	0.7183917	0.6435106	0.5890205	0.5468361
	1.0363056	0.9282843	0.8496889	0.7888645
	1.3532438	1.2121975	1.1095974	1.0302133
C–S	0.1718361	0.1523307	0.1381865	0.1273432
	0.4370542	0.3923695	0.3594391	0.3337361
	0.7365858	0.6614518	0.6064116	0.5635835
	1.0469044	0.9393470	0.8608702	0.7999751
	1.3599797	1.2195447	1.1172729	1.0380423
C–C	0.2161815	0.1932459	0.1762276	0.1629847
	0.4652442	0.4164629	0.3807099	0.3529561
	0.7544107	0.6758177	0.6186393	0.5743550
	1.0573630	0.9473558	0.8674707	0.8056611
	1.3668714	1.2246745	1.1214403	1.0415984
C–F	0.0481663	0.0407228	0.0359192	0.0324924
	0.2360164	0.2092155	0.1900230	0.1753442
	0.5285832	0.4748746	0.4355488	0.4049064
	0.8391847	0.7541398	0.6918951	0.6434362
	1.1571825	1.0391222	0.9528775	0.8858817
F–C	0.0481663	0.0458946	0.0439092	0.0421559
	0.2360164	0.2135794	0.1969722	0.1840206
	0.5285832	0.4725087	0.4323294	0.4015864
	0.8391847	0.7497903	0.6855775	0.6363360
	1.1571825	1.0344598	0.9459583	0.8779089

Effect of longitudinal gradation of material property on the longitudinal variation on field variables (u, w, σ_x, τ_{zx}) are presented in Fig. 2.25 for the first vibration mode of AFG beam (a) (s=0.1) subjected to S–S boundary conditions boundary conditions. Similarly, the longitudinal variation of field variables (u, w, σ_x, τ_{zx}) for third vibration mode of AFG beam (a) (s=0.1) under S–S boundary condition are plotted in Fig. 2.26 for all the properties variation cases.

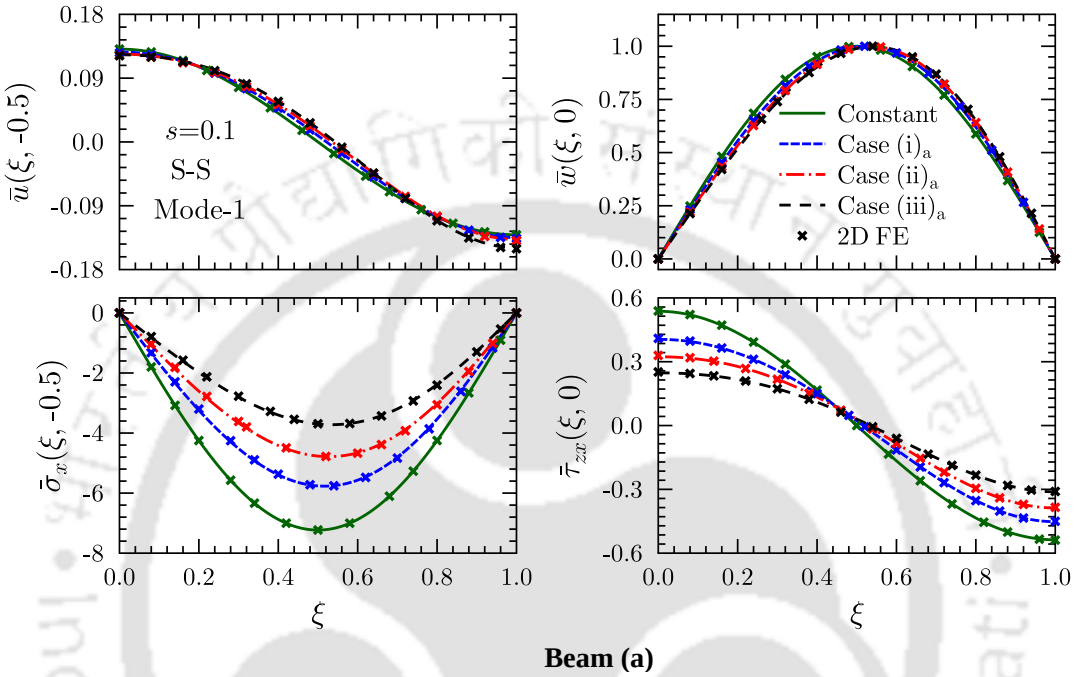

Fig. 2.25: Longitudinal variations of displacements and stresses for first vibration mode (Mode-1) of beam (a) under S–S boundary condition

Similarly, for C–S, C–C and C–F boundary conditions, the longitudinal variation of deflection and stresses for all the variation cases are plotted in Fig. 2.27 and 2.28 for first vibration mode of AFG beam (a) (s=0.1). Results for the constant properties case (homogeneous beam) are also potted in Figs. 2.25, 2.26, 2.27 and 2.28 to study the effect of gradation on longitudinal variation of entities. The 2D FE results for all the gradation cases are also plotted in these figures. The present results are in excellent agreement with 2D FE results for all the variation cases. For all the boundary conditions (S–S, C–C, C–F, C–S), the stresses ($\bar{\sigma}_x$, $\bar{\tau}_{zx}$) are affected significantly due to the gradation of material properties whereas deflections ($\bar{u}$, $\bar{w}$) are least affected. The stresses ($\bar{\sigma}_x$, $\bar{\tau}_{zx}$) are decreasing significantly as the variation index increases. It is observed that the influence of material gradient much more on the first mode shape as compared to higher vibration modes. It shows that the effect of material gradation on stresses become weaker as the mode number increasing.

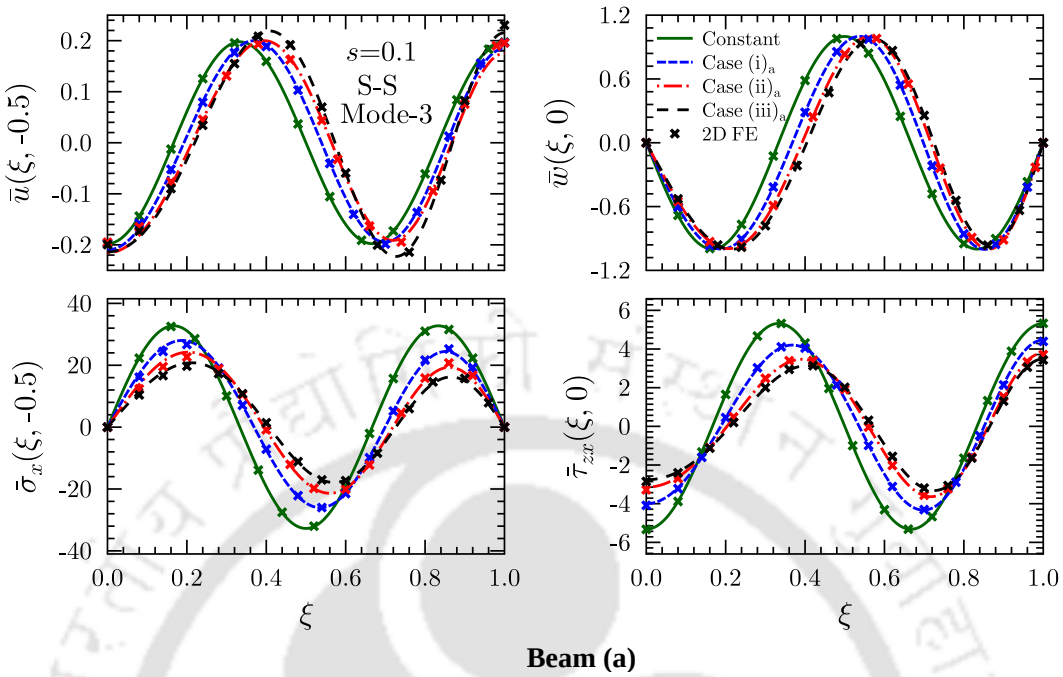

Fig. 2.26: Longitudinal variations of displacements and stresses for third vibration mode of beam (a) (Mode-3) under S–S boundary condition

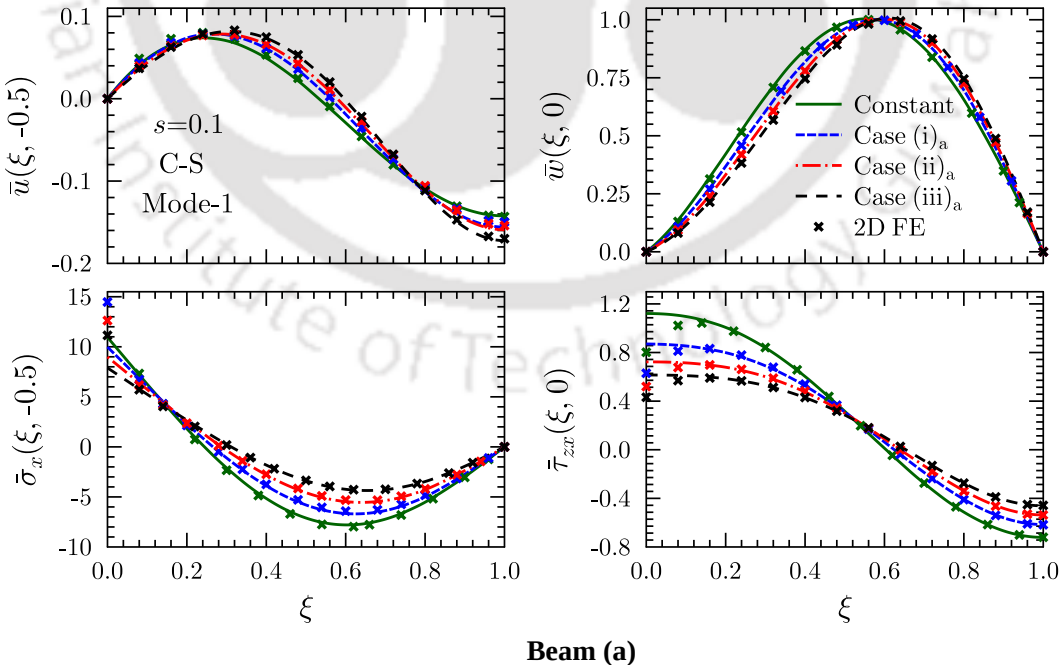

Fig. 2.27: Longitudinal variations of displacements and stresses for first vibration mode (Mode-1) of beam (a) under C–S boundary condition

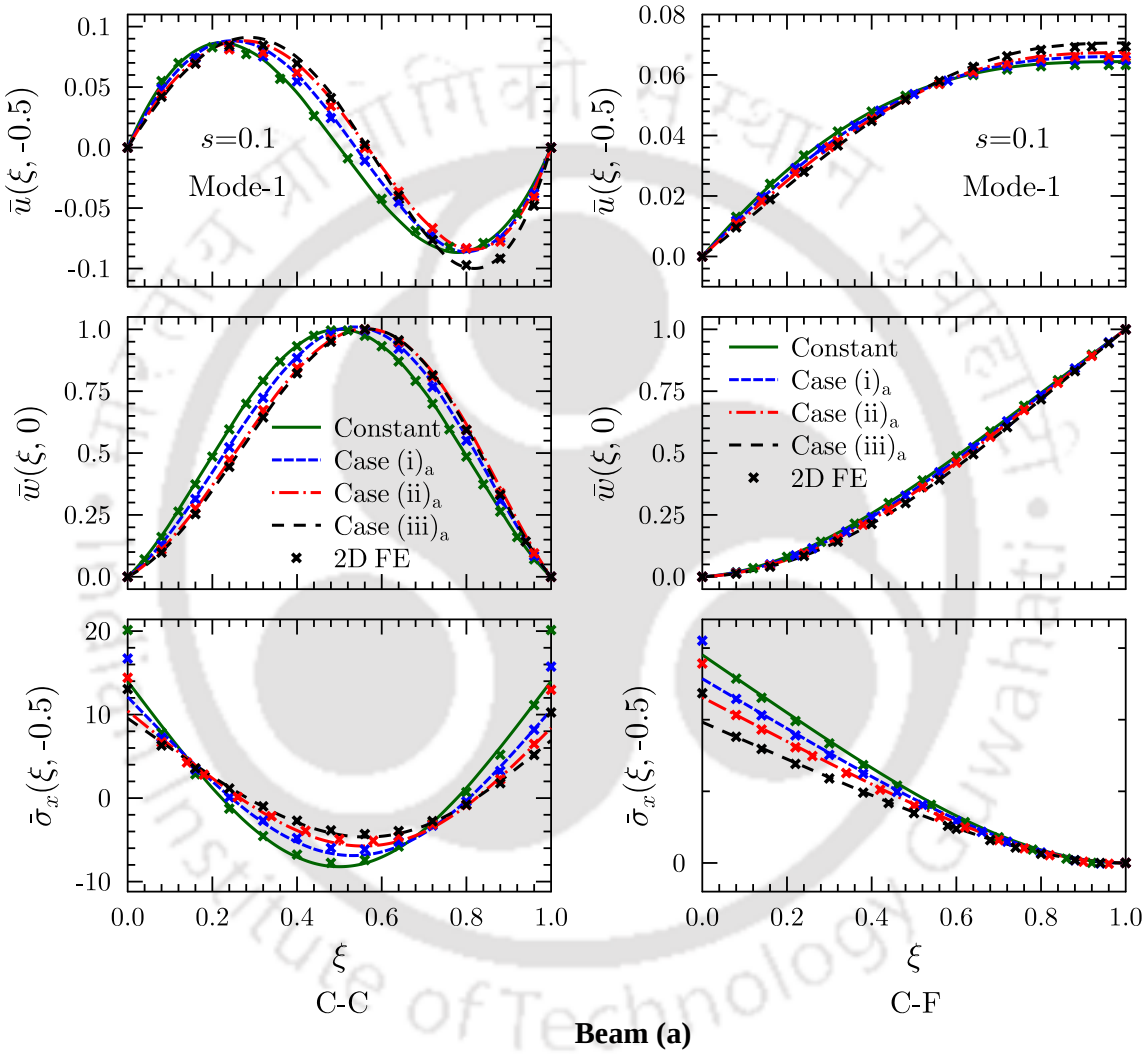

Fig. 2.28: Longitudinal variations of displacements and stresses for first vibration mode (Mode-1) of beam (a) under C–C and C–F boundary conditions

2.9.3 Beam (b): Two Layered Beam

An two layered axially functionally graded beam (b) with the unsymmetrical lay-up schemes of $[0^o/90^o]$, as shown in Fig. 2.3, is considered for study in this section. The material properties of layers are varying along the axial direction. Results are obtained for following variation cases of beam (b): Case $(i)_b$:- Bottom layer δ_1=δ_2=1.0, Top layer δ_1=δ_2=0.0; Case $(ii)_b$:- Bottom layer δ_1=δ_2=1.0, Top layer δ_1=δ_2=1.0; Case $(iii)_b$:- Bottom layer δ_1=δ_2=2.0, Top layer δ_1=δ_2=1.0

First five lowest dimensionless natural frequencies $\omega^* = \omega h\sqrt{\rho/G_{12}}$ are tabulated for two layered AFG beam (s=0.1) subjected to different boundary conditions. Results are presented for different variation cases, Case $(i)_b$, Case $(ii)_b$, and Case $(iii)_b$ along with constant properties case to study the effect of axially varying material properties on natural frequencies of two layered beam. In Table 2.10, benchmark results are tabulated for S–S, C–S, C–C and C–F boundary conditions, respectively. Significant effect of axial gradation is observed on the natural frequencies of the

Table 2.10: Effect of axial gradation on first five lowest dimensionless natural frequencies $\omega^* = \omega h\sqrt{\rho/G_{12}}$ of two-layered AFG beam (b) subjected different sets of boundary conditions (s=0.1)

B.C.	n	Constant	Case $(i)_b$	Case $(ii)_b$	Case $(iii)_b$
S–S	1	0.0634373	0.0504037	0.0420341	0.0356362
	2	0.2291463	0.1818752	0.1531865	0.1301802
	3	0.4525587	0.3579673	0.3026107	0.2564758
	4	0.7018743	0.5539555	0.4692666	0.3967874
	5	0.9605771	0.7578913	0.6425517	0.5426663
C–S	1	0.0935905	0.0737215	0.0628650	0.0535713
	2	0.2673312	0.2118343	0.1811608	0.1538217
	3	0.4863377	0.3883388	0.3297568	0.2807119
	4	0.7272262	0.5796490	0.4924048	0.4185029
	5	0.9780820	0.7783124	0.6611809	0.5613326
C–C	1	0.1279556	0.0996600	0.0856419	0.0721456
	2	0.3036654	0.2364383	0.2030333	0.1708736
	3	0.5177027	0.4044090	0.3467416	0.2913814
	4	0.7510200	0.5928751	0.5033907	0.4261509
	5	0.9948319	0.7868125	0.6675692	0.5656978
C–F	1	0.0230836	0.0184592	0.0156695	0.0135140
	2	0.1303072	0.1046773	0.0880789	0.0755343
	3	0.3222934	0.2589664	0.2192246	0.1873586
	4	0.5489311	0.4422151	0.3729061	0.3201660
	5	0.7932871	0.6390987	0.5376144	0.4591232

two layered beam (b). With the increment of the variation indexes, the natural frequencies of the beam (b) decreases significantly for all the boundary conditions. For simply supported boundary conditions, nearly 20 to 21% decrement is observed in the first five natural frequencies for Case $(i)_b$ as compared to constant property case under all the support conditions. Where the percentage decrement in natural frequencies is 33% for Case $(ii)_b$ and 43% for Case $(iii)_b$, respectively. Similarly, when the beam subjected to C–S boundary conditions, nearly 20% decrement is observed in the first five natural frequencies for Case $(i)_b$ as compared to constant property case under all the support conditions. Where the percentage decrement in natural frequencies is 32% for Case $(ii)_b$ and 42% for Case $(iii)_b$, respectively. Similarly, when the beam subjected to C–C boundary conditions, nearly 21 to 22% decrement is observed in the first five natural frequencies for Case $(i)_b$ as compared to constant property case under all the support conditions. Where the percentage decrement in natural frequencies is 33% for Case $(ii)_b$ and 43% for Case $(iii)_b$, respectively. Similarly, for C–F boundary conditions percentage decrement in natural frequencies are 19, 32 and 41% for Case $(i)_b$, Case $(ii)_b$ and Case $(iii)_b$, respectively. It is observed that the percentage effect due to gradation in material properties does not affect much with boundary conditions of beam.

For all the variation cases, the effect of boundary conditions are significant on the lower mode natural frequencies of the beam (b) and it is maximum for the first vibration mode. But for higher mode frequencies, the effect of boundary conditions are negligible. For all boundary conditions (S–S, C–S, C–C, C–F), the axial gradation of material property even in one layer significantly affected the natural frequencies of the beams .

2.9.4 Beam (c): Four Layered Beam

A four-layered beam (c) with the symmetrical lay-up schemes of $[0^o/90^o/90^o/0^o]$, as shown in Fig. 2.3 is considered for study in this section. The material properties of the layers are assumed to vary linearly along the axial direction of the beam. Results are presented for two cases of property variation, Case $(i)_c$ δ_1=δ_2=1.0 for all layer; Case $(ii)_c$ δ_1=δ_2=2.0 for all layer. In Table 2.11, first five lowest dimensionless natural frequencies $\omega^* = \omega h\sqrt{\rho/G_{12}}$ are tabulated for laminated AFG beam (c) for various type of boundary conditions i.e S–S, C–S, C–C and C–F, respectively. The numerical results of this sub-section are also thoroughly verified with 2D FE results. It is found that present results are in excellent agreement with 2D FE results for all type of support conditions. As the gradation indexes increases, the free vibration frequencies of the laminated beam (c) decreases significantly for all the boundary conditions. For all boundary conditions (S–S, C–S, C–C, C–F), nearly 31 to 33% decrement is observed in the first five natural frequencies for Case $(i)_c$ as compared to constant property case. The percentage decrement in natural frequencies is 47 to 50% for Case $(ii)_c$. For all the gradation cases, the effect of support conditions are very significant on the lower

Table 2.11: Effect of axial gradation on first five lowest dimensionless natural frequencies $\omega^* = \omega h\sqrt{\rho/G_{12}}$ of four-layered AFG beam (c) subjected different sets of boundary conditions (s=0.1)

B.C.	n	1	2	3	4	5
S–S	Constant	0.1119870	0.3262990	0.5563598	0.7917446	1.0327890
	Case (i)$_c$	0.0740734	0.2169678	0.3701399	0.5268909	0.6874461
	Case (ii)$_c$	0.0550271	0.1620978	0.2767338	0.3940655	0.5145194
C–S	Constant	0.1415773	0.3430237	0.5660394	0.7988317	1.0388345
	Case (i)$_c$	0.0964066	0.2330176	0.3817119	0.5365033	0.6961896
	Case (ii)$_c$	0.0730275	0.1744237	0.2881070	0.4042077	0.5239688
C–C	Constant	0.1714813	0.3586193	0.5767149	0.8047490	1.0455009
	Case (i)$_c$	0.1140508	0.2397260	0.3858625	0.5392708	0.6985208
	Case (ii)$_c$	0.0854071	0.1803063	0.2905173	0.4057814	0.5252800
C–F	Constant	0.0435130	0.1930565	0.4162172	0.6461210	0.8844219
	Case (i)$_c$	0.0294058	0.1330675	0.2852280	0.4384768	0.5992910
	Case (ii)$_c$	0.0224897	0.1022154	0.2155427	0.3317153	0.4504912

mode natural frequencies of the laminated beam (c) and it is maximum for the first vibration mode. But for higher mode frequencies the effect of support conditions is nominal. The percentage decrement in natural frequency due to gradation in material properties does not affect much with boundary conditions of beam.

2.10 SUMMARY

An accurate two-dimensional elasticity analytical solution is presented for static and free vibration analysis of axially functionally graded beam subjected to the arbitrary boundary condition using extended Kantorovich method. Further, static and free vibration results for the arbitrary supported homogeneous beam are obtained as a special case of present development. New benchmark results are presented for the axially functionally graded beams as well as a homogeneous beam subjected to arbitrary support conditions. For static case, single term (n=1, *iter*.1) gives accurate prediction for deflections and stresses for simply-supported case whereas two-term solution (n=2, *iter*.2) is required for the other boundary conditions. For free vibration case, the single term solution is sufficient enough to obtaining the accurate flexural frequencies for all the cases and boundary conditions. The influence of material properties variation on the static and dynamic response of axially FG beam, as compared to the homogeneous beam is investigated comprehensively by considering various material property variation cases. It is observed that the bending and free vibration behaviour of beam affected significantly by the axial gradation of material properties.

The percentage effect is almost increased by 1.5 times as the gradation indexes are increasing from 0.5 to 1. Further, the effects of axial gradation on the behavior of the beam depend significantly on boundary conditions of the beams. This development has shown that, by controlling the axial variation of material properties, the desired response of beam can be achieved for specific applications. The current research will also be beneficial to modeled real-life beam structures in which material properties of beam deteriorate due to some environmental effect. The present 2D elasticity analytical solution can be used for assessing the validity and accuracy of different beam theories and computational models for analysis of axially graded beams.

Chapter 3

Functionally Graded Rectangular Plates- 3D Elasticity Analysis

A three-dimensional analytical solution is developed for static [296] and free vibration analysis of longitudinally functionally graded plate subjected to Levy-type boundary conditions. A linear variation of material compliances and density are assumed along the x-direction, as given in Sec. 3.1.1. The Hamilton-type weak-form of governing equations, which has been developed in Chapter 2 for two-dimensional beams, is now extended to three-dimensional rectangular plates, as described in Sec. 3.1.2. The multi-term extended Kantorovich approach(EKM), as developed in Chapter 2, is applied to solve the governing equations in mixed form. By employing EKM, a set of ODEs with constant coefficient is obtained along the z-direction which is solved analytically in closed form, as explained in Sec. 3.3. Another set of ordinary differential equations (ODEs) with varying coefficients are obtained along the x-direction, which is solved by using the recently developed modified power series method in Sec. 3.4. Numerical results are presented for various configuration, aspect ratio, and boundary conditions under static bending in Sec. 3.6 and for free vibration case in Sec. 3.7. The present method is validated by comparing the results with those obtained using the 3D FE (ABAQUS). Effect of variation of the material property on the longitudinal variation of deflection, stresses, and natural frequencies is studied by considering various gradation cases in conjunction with the arbitrary support conditions at the ends of the plate. For the first time, numerical results for a two-layered plate having a different in-plane material variation in each layer are also presented along with single-layer plate results. Through-the-thickness variation of various entities for particular material indexes is also presented. Benchmark results for static and dynamic analysis are presented for various cases which can be used to validate approximate two-dimensional solutions and 3D numerical solutions.

The effects of longitudinally varying adhesive properties on the interfacial and inter-laminar stress distribution are also studied for the adhesively bonded rectangular plate in Sec. 3.6.3. The elastic properties of adhesive interlayer are assumed to vary linearly along the x-direction. A specific

predefined in-plane variation in adhesive mechanical property is assumed and their influence on bending response of bonded plate subjected to mechanical loading is investigated. The present method can be beneficial to modeled adhesive structure in which adhesive interlayer properties degraded due to some environmental effect.

3.1 THEORETICAL FORMULATION FOR FGM PLATES

3.1.1 In-plane Material Property Variation

The compliances of the layers are assumed to vary linearly along x-direction as:

$$\begin{aligned} &\bar{s}^m_{1j} = \bar{s}_{1j}(1+\delta_1\xi_1) \quad \text{for} \quad j = 1,2,3; \\ &\bar{s}^m_{55} = \bar{s}_{55}(1+\delta_2\xi_1); \quad \bar{s}^m_{66} = \bar{s}_{66}(1+\delta_2\xi_1) \\ &\rho^m(\xi) = \rho(1+\delta_p\,\xi) \end{aligned} \tag{3.1}$$

where δ_α is a parameter that governs the material properties variation, $\xi_1 = x/a$, $\xi_2 = y/b$ are non-dimensional quantities. For the present case, δ_1 is variation index for Young's modulus, δ_2 variation index for shear modulus or modulus of rigidity and δ_p is the variation index for density. The variation indexes (δ_1, δ_2 and δ_p) can be positive or negative. The property variation along the in-plane direction may be due to diffusion of chemicals such as hydrogen, corrosion or cyclic exposure to temperature, etc. Comparison of present gradation model with other probabilistic gradation models, like Rule of Mixture, Mori-Tanaka scheme and Exponential function gradation, is presented in Appendix A. The gradation profiles obtained from present gradation models and other probabilistic gradation models have a similar nature.

3.1.2 Basic Governing Equation for 3D Plate

The geometry of a multilayered FGM laminated plate as shown in Fig. 3.1 is considered for the analysis. The plate has length a, b and total thickness h along x, y and z-direction, respectively. Levy-type support conditions are assumed for the present case, i.e., simply-supported at $y = 0$ and b and arbitrary support end conditions at $x = 0$ and a. Perfect bonding is considered between the interface of two layers. The thickness of the kth layer and the z-coordinate of its upper surface is defined as $t^{(k)}$ and z_k. The layer superscript over the entities is omitted unless needed for clarity. The infinitesimal strain tensor is used

$$\varepsilon_{ij} = \frac{1}{2}(u_{i,j} + u_{j,i}) \qquad (i,j = x,y,z) \tag{3.2}$$

where $u_x = u$, $u_y = v$, $u_z = w$ and a subscript comma denotes differentiation.

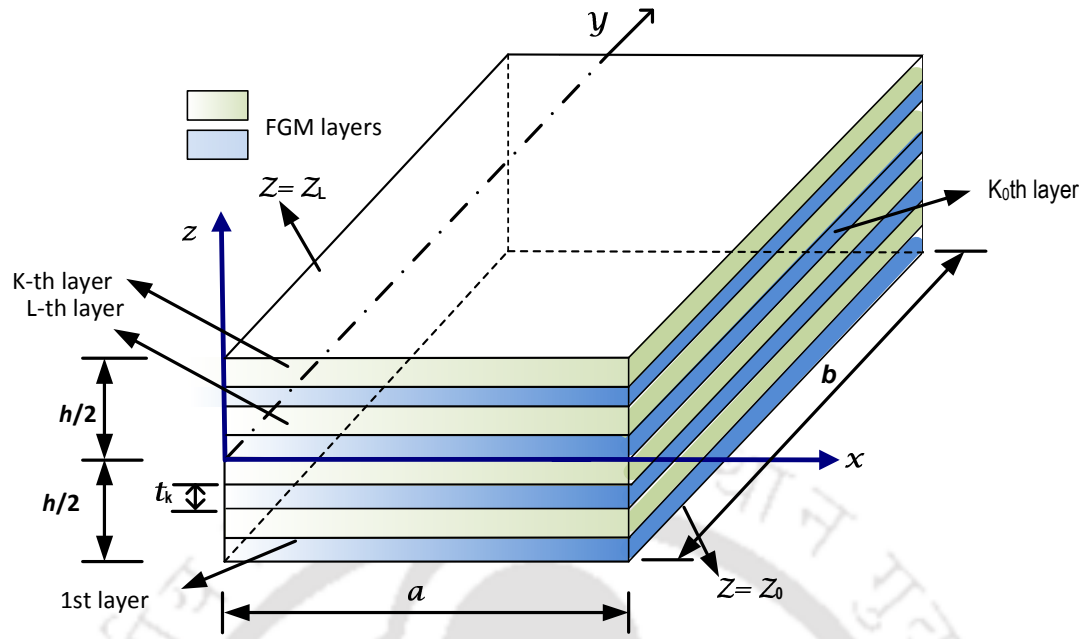

Fig. 3.1: Geometry of the FGM laminated plate.

The three-dimensional constitutive equations for a linear orthotropic lamina are given as

$$\varepsilon = \bar{S}^m \sigma \tag{3.3}$$

where $\varepsilon = [\varepsilon_x \quad \varepsilon_y \quad \varepsilon_z \quad \gamma_{yz} \quad \gamma_{xz} \quad \gamma_{xy}]^T, \qquad \sigma = [\sigma_x \quad \sigma_y \quad \sigma_z \quad \tau_{yz} \quad \tau_{xz} \quad \tau_{xy}]^T$

$$\bar{S}^m = \begin{bmatrix} \bar{S}_N^m & 0 \\ 0 & \bar{S}_S^m \end{bmatrix} \qquad \bar{S}_N^m = \begin{bmatrix} \bar{s}_{11}^m & \bar{s}_{12}^m & \bar{s}_{13}^m \\ \bar{s}_{12}^m & \bar{s}_{22} & \bar{s}_{23} \\ \bar{s}_{13}^m & \bar{s}_{23} & \bar{s}_{33} \end{bmatrix} \qquad \bar{S}_S^m = \begin{bmatrix} \bar{s}_{44} & 0 & 0 \\ 0 & \bar{s}_{55}^m & 0 \\ 0 & 0 & \bar{s}_{66}^m \end{bmatrix}$$

where σ and ε are the normal stress and strain components, respectively, τ and γ denote the shear stress and strain components, respectively. $\bar{S}^m$ is transformed elastic compliance.

The weak-form of governing equations using the Hamilton's-type mixed variational principle for a linear elastic medium without body force are expressed as,

$$\begin{aligned} \int_t \int_a \int_b \int_h \; & [\delta u(\tau_{xz,z} + \sigma_{x,x} + \tau_{xy,y} - \rho^m \ddot{u}) + \delta v(\tau_{yz,z} + \tau_{xy,x} + \sigma_{y,y} - \rho^m \ddot{v}) \\ & + \delta w(\sigma_{z,z} + \tau_{zx,x} + \tau_{yz,y} - \rho^m \ddot{w}) + \delta\sigma_x(\bar{s}_{11}^m \sigma_x + \bar{s}_{12}^m \sigma_y + \bar{s}_{13}^m \sigma_z - u_{,x}) \\ & + \delta\sigma_y(\bar{s}_{12}^m \sigma_x + \bar{s}_{22} \sigma_y + \bar{s}_{23} \sigma_z - v_{,y}) - \delta\sigma_z(w_{,z} - \bar{s}_{13}^m \sigma_x - \bar{s}_{23} \sigma_y - \bar{s}_{33} \sigma_z) \\ & - \delta\tau_{yz}(v_{,z} + w_{,y} - \bar{s}_{44} \tau_{yz}) - \delta\tau_{zx}(u_{,z} + w_{,x} - \bar{s}_{55}^m \tau_{zx}) \\ & + \delta\tau_{xy}(\bar{s}_{66}^m \tau_{xy} - v_{,x} - u_{,y})] \, \mathrm{d}z \, \mathrm{d}y \, \mathrm{d}x \, \mathrm{d}t = 0 \quad \forall \; \delta u_i, \; \delta\sigma_i, \; \delta\tau_{ij} \end{aligned} \tag{3.4}$$

The non-dimensional local thickness parameter $\zeta^{(k)}$ for the kth layer is defined as $\zeta^{(k)} = (z - z_{k-1})/t^{(k)}$ such that $0 \leq \zeta^k \leq 1$ for $z_{k-1} \leq z \leq z_k$. The top and bottom surfaces of FGM plate are

subjected to following boundary conditions,

$$z = (-h/2,\, h/2),: \qquad \sigma_z = -p_\alpha, \quad \tau_{yz} = 0, \quad \tau_{zx} = 0 \tag{3.5}$$

where p_α $(\alpha = 1, 2)$ is uniformly distributed pressure load. Following variables satisfy continuity conditions at the kth interface between kth and $(k+1)$th layers:

$$[(u,\, v,\, w,\, \sigma_z,\, \tau_{yz},\, \tau_{zx})|_{\zeta=1}]^{(k)} = [(u,\, v,\, w,\, \sigma_z,\, \tau_{yz},\, \tau_{zx})|_{\zeta=0}]^{(k+1)} \tag{3.6}$$

In the present solution methodology, the system of differential equations along the x and z-direction are solved analytically without dividing the plate into fictitious sub-layers. Therefore, displacements and equilibrium conditions for the fictitious interface are not required. Further, two ends of FGM plate ($\xi_1 = 0$ and 1) can be subjected to simply-supported (S), clamped (C) and free (F) support conditions, e.g.

$$\begin{aligned}
&\text{Simply-supported (S)}: && v = 0, && w = 0, && \sigma_x = 0 \\
&\text{Clamped (C)}: && u = 0, && v = 0, && w = 0 \\
&\text{Free (F)}: && \sigma_x = 0, && \tau_{xy} = 0, && \tau_{xz} = 0
\end{aligned} \tag{3.7}$$

The boundary conditions at the edges $\xi_2 = 0$ and 1 are assumed to be simply-supported:

$$u = 0, \qquad w = 0, \qquad \sigma_y = 0 \tag{3.8}$$

3.2 FOURIER SERIES-GENERALIZED EKM SOLUTION FOR PLATE

The field variables X_l^y are expressed in terms of Fourier series which satisfy the simply-supported boundary conditions at edges $y = 0, b$, given in Eq. (3.8) as

$$\begin{aligned}
(u,\, w,\, \sigma_x,\, \sigma_y,\, \sigma_z,\, \tau_{zx}) &= \sum_{m=1}^{\infty} (u,\, w,\, \sigma_x,\, \sigma_y,\, \sigma_z,\, \tau_{zx})_m \sin m\pi\xi_2 \\
(v,\, \tau_{yz},\, \tau_{xy}) &= \sum_{m=1}^{\infty} (v,\, \tau_{yz},\, \tau_{xy})_m \cos m\pi\xi_2
\end{aligned} \tag{3.9}$$

where $(\ )_m$ denotes the mth Fourier component which is a function of x and z. The solution of Eq. (3.4) for the field variables

$$\mathbf{X} = [\, u \quad v \quad w \quad \sigma_x \quad \sigma_y \quad \sigma_z \quad \tau_{xy} \quad \tau_{yz} \quad \tau_{zx} \,]^{\mathrm{T}} \tag{3.10}$$

is obtained using the mixed-field multiterm EKM proposed by Kapuria and Kumari [279]. Thus, the solution of the lth variable X_l of $\mathbf{X}$ for the kth layer takes the following form:

$$X_l(\xi_1, \xi_2, \zeta) = \sum_{m=1}^{\infty} [\, X_{lS}^y \mathrm{or} X_{lC}^y \,] \left\{ \sum_{i=1}^{n} f_{l_m}^i(\xi_1) g_{l_m}^i(\zeta) \cos\omega t + \delta_{l6}[p_a + z p_d] \right\} \tag{3.11}$$

$$X_l(\xi_1, \xi_2, \zeta) = \sum_{m=1}^{\infty} [\, X_{lS}^y \mathrm{or} X_{lC}^y \,]\, X_{l_m} \tag{3.12}$$

for $l = 1, 2, \ldots 9$. Wherein $X^y_{lS} = \sin m\pi\xi_2$, $X^y_{lC} = \cos m\pi\xi_2$ and $f^i_{l_m}(\xi_1)$, $g^i_{l_m}(\zeta)$ are unknown univariate functions of ξ_1 and ζ respectively, for the mth Fourier component and the ith term of the n-term series solution. These functions are to be determined iteratively, satisfying all homogeneous boundary conditions. Furthermore, $\delta_{l6} = 1$ for $l = 6$ and else $\delta_{l6} = 0$, $p_a = -(p_1 + p_2)/2$ and $p_d = -(p_2 - p_1)/h$. The repeated index l does not mean summation here. While functions $g^i_{l_m}(\zeta)$ are defined for the kth layer, functions $f^i_{l_m}(\xi_1)$ are valid for all layers. The subscript 'm' is dropped from the $f^i_{l_m}$ and $g^i_{l_m}$ for convenience.

3.3 STEP 1 - THICKNESS DIRECTION (z)

In this step, functions $f^i_l(\xi_1)$ along x-direction are initially assumed as,

$$\begin{aligned} f^i_1(\xi_1) = f^i_7(\xi_1) = f^i_9(\xi_1) &= \cos i\pi\xi_1 \\ f^i_2(\xi_1) = f^i_3(\xi_1) = f^i_4(\xi_1) = f^i_5(\xi_1) = f^i_6(\xi_1) = f^i_8(\xi_1) &= \sin i\pi\xi_1 \end{aligned} \tag{3.13}$$

which corresponds to the simply-supported edge condition at $\xi_1 = 0, 1$. In the MMEKM, the initial trial functions need not to satisfy the essential or natural boundary conditions. The functions $g^i_l(\xi_1)$ are to be solved in this step. For this purpose, first variation δX_l is obtained as,

$$\delta X_l(\xi_1, \xi_2, \zeta) = \sum_{m=1}^{\infty} [\, X^y_{lS} \text{or} X^y_{lC} \,]\, \delta X_{l_m}, \qquad l = 1, 2, \ldots 9 \tag{3.14}$$

where

$$\delta X_{l_m} = \sum_{i=1}^{n} f^i_l(\xi_1)\delta g^i_l \cos\omega t, \qquad l = 1, 2, \ldots 9 \tag{3.15}$$

As per equations (3.5) and (3.6), only six variable can be solved at a time. Therefore, functions g^i_l are divided into a column vector $\bar{\mathbf{G}}$ which contains variable appear in support and interface conditions, and a column vector $\hat{\mathbf{G}}$ contains rest of the variables.

$$\begin{aligned} \bar{\mathbf{G}} &= [\, g^1_1 \ldots g^n_1 \quad g^1_2 \ldots g^n_2 \quad g^1_3 \ldots g^n_3 \quad g^1_6 \ldots g^n_6 \quad g^1_8 \ldots g^n_8 \quad g^1_9 \ldots g^n_9 \,]^{\mathrm{T}} \\ \hat{\mathbf{G}} &= [\, g^1_4 \ldots g^n_4 \quad g^1_5 \ldots g^n_5 \quad g^1_7 \ldots g^n_7 \,]^{\mathrm{T}} \end{aligned} \tag{3.16}$$

By substituting Eqs. (3.11), (3.15) and (3.14) into Eq. (3.4), and integrating over ξ_1 direction, and using the fundamental lemma of variational principle, following set of ODEs ($6n$) and algebraic ($3n$) equations are obtained for δg^i_l for the kth layer,

$$\mathbf{M}\bar{\mathbf{G}}_{,\zeta} = \bar{\mathbf{A}}^{\mathbf{m}}(\omega)\bar{\mathbf{G}} + \hat{\mathbf{A}}^{\mathbf{m}}\hat{\mathbf{G}} + \bar{\mathbf{Q}}^{\mathbf{m}} \tag{3.17}$$

$$\mathbf{K}^{\mathbf{m}}\hat{\mathbf{G}} = \tilde{\mathbf{A}}^{\mathbf{m}}\bar{\mathbf{G}} + \tilde{\mathbf{Q}}^{\mathbf{m}} \tag{3.18}$$

where $\bar{\mathbf{A}}^{\mathbf{m}} = \bar{\mathbf{A}} + \bar{\mathbf{A}}^{\mathbf{v}}$; $\hat{\mathbf{A}}^{\mathbf{m}} = \hat{\mathbf{A}} + \hat{\mathbf{A}}^{\mathbf{v}}$; $\bar{\mathbf{Q}}^{\mathbf{m}} = \bar{\mathbf{Q}}_{\mathbf{p}} + \bar{\mathbf{Q}}_{\mathbf{p}}^{\mathbf{v}}$; $\mathbf{K}^{\mathbf{m}} = \mathbf{K} + \mathbf{K}^{\mathbf{v}}$; $\tilde{\mathbf{A}}^{\mathbf{m}} = \tilde{\mathbf{A}} + \tilde{\mathbf{A}}^{\mathbf{v}}$; $\tilde{\mathbf{Q}}^{\mathbf{m}} = \tilde{\mathbf{Q}}_{\mathbf{p}} + \tilde{\mathbf{Q}}_{\mathbf{p}}^{\mathbf{v}}$ and, $\mathbf{M}$, $\bar{\mathbf{A}}^{\mathbf{m}}$, $\hat{\mathbf{A}}^{\mathbf{m}}$, $\mathbf{K}^{\mathbf{m}}$ and $\tilde{\mathbf{A}}^{\mathbf{m}}$ are $6n \times 6n$, $6n \times 6n$, $6n \times 3n$, $3n \times 3n$ and $3n \times 6n$ matrices respectively and $\bar{\mathbf{Q}}_{\mathbf{p}}$, $\bar{\mathbf{Q}}_{\mathbf{p}}^{\mathbf{v}}$, $\tilde{\mathbf{Q}}_{\mathbf{p}}$ and $\tilde{\mathbf{Q}}_{\mathbf{p}}^{\mathbf{v}}$ are load vectors of size $6n \times 1n$, $6n \times 1n$, $3n \times 1n$ and $3n \times 1n$ respectively. The nonzero elements of $\mathbf{M}$, $\bar{\mathbf{A}}^{\mathbf{m}}$, $\hat{\mathbf{A}}^{\mathbf{m}}$, $\mathbf{K}^{\mathbf{m}}$, $\tilde{\mathbf{A}}^{\mathbf{m}}$, $\bar{\mathbf{Q}}_{\mathbf{p}}$, $\bar{\mathbf{Q}}_{\mathbf{p}}^{\mathbf{v}}$, $\tilde{\mathbf{Q}}_{\mathbf{p}}$ and $\tilde{\mathbf{Q}}_{\mathbf{p}}^{\mathbf{v}}$ matrices of Eqs. (3.17) and (3.18) are given below,

$$
\begin{aligned}
&M_{i_1j_1} = M_{j_6i_6} = \langle f_9^i f_1^j \rangle_a, \quad M_{i_2j_2} = M_{j_5i_5} = \langle f_8^i f_2^j \rangle_a, \quad M_{i_3j_3} = M_{j_4i_4} = \langle f_6^i f_3^j \rangle_a \\
&\bar{A}_{i_1j_3} = \tfrac{-t}{a} \langle f_9^i f_{3,\xi_1}^j \rangle_a, \quad \bar{A}_{i_1j_6} = t\bar{s}_{55} \langle f_9^i f_9^j \rangle_a, \quad \bar{A}^v_{i_1j_6} = \delta_2 t \langle \xi_1 \bar{s}_{55} f_9^i f_9^j \rangle_a \\
&\bar{A}_{i_2j_3} = -\bar{m}t \langle f_8^i f_3^j \rangle_a, \quad \bar{A}_{i_2j_5} = t\bar{s}_{44} \langle f_8^i f_8^j \rangle_a, \quad \bar{A}_{i_3j_4} = t\bar{s}_{33} \langle f_6^i f_6^j \rangle_a \\
&\hat{A}_{i_3j_1} = t\bar{s}_{13} \langle f_6^i f_4^j \rangle_a, \quad \hat{A}^v_{i_3j_1} = \delta_1 t \langle \xi_1 \bar{s}_{13} f_6^i f_4^j \rangle_a, \quad \hat{A}_{i_3j_2} = t\bar{s}_{23} \langle f_6^i f_5^j \rangle_a \\
&\bar{A}_{i_4j_5} = \bar{m}t \langle f_3^i f_8^j \rangle_a, \quad \bar{A}_{i_4j_6} = \tfrac{-t}{a} \langle f_3^i f_{9,\xi_1}^j \rangle_a, \quad \hat{A}_{i_5j_2} = -\bar{m}t \langle f_2^i f_5^j \rangle_a \\
&\hat{A}_{i_5j_3} = \tfrac{-t}{a} \langle f_2^i f_{7,\xi_1}^j \rangle_a, \quad \hat{A}_{i_6j_1} = \tfrac{-t}{a} \langle f_1^i f_{4,\xi_1}^j \rangle_a, \quad \hat{A}_{i_6j_3} = \bar{m}t \langle f_1^i f_7^j \rangle_a \\
&K_{i_1j_1} = \bar{s}_{11} \langle f_4^i f_4^j \rangle_a, \quad K_{i_1j_2} = \bar{s}_{12} \langle f_4^i f_5^j \rangle_a, \quad K^v_{i_1j_1} = \delta_1 \langle \xi_1 \bar{s}_{11} f_4^i f_4^j \rangle_a \\
&K^v_{i_1j_2} = \delta_1 \langle \xi_1 \bar{s}_{12} f_4^i f_5^j \rangle_a, \quad K_{i_2j_1} = K_{i_1j_2}, \quad K^v_{i_2j_1} = K^v_{i_1j_2} \\
&K_{i_2j_2} = \bar{s}_{22} \langle f_5^i f_5^j \rangle_a, \quad K_{i_3j_3} = \bar{s}_{66} \langle f_7^i f_7^j \rangle_a, \quad K^v_{i_3j_3} = \delta_2 \langle \xi_1 \bar{s}_{66} f_7^i f_7^j \rangle_a \\
&\tilde{A}_{i_1j_1} = \tfrac{1}{a} \langle f_4^i f_{1,\xi_1}^j \rangle_a, \quad \tilde{A}_{i_1j_4} = -\bar{s}_{13} \langle f_4^i f_6^j \rangle_a, \quad \tilde{A}^v_{i_1j_4} = -\delta_1 \langle \xi_1 \bar{s}_{13} f_4^i f_6^j \rangle_a \\
&\tilde{A}_{i_2j_2} = -\bar{m} \langle f_5^i f_2^j \rangle_a, \quad \tilde{A}_{i_2j_4} = -\bar{s}_{23} \langle f_5^i f_6^j \rangle_a, \quad \tilde{A}_{i_3j_1} = \bar{m} \langle f_7^i f_1^j \rangle_a \\
&\tilde{A}_{i_3j_2} = \tfrac{1}{a} \langle f_7^i f_{2,\xi_1}^j \rangle_a, \quad \bar{A}_{i_4j_3} = -\rho\omega^2 t \langle f_3^i f_3^j \rangle_a, \quad \bar{A}^v_{i_4j_3} = -\delta_p \omega^2 t \langle \rho\, \xi_1 f_3^i f_3^j \rangle_a \\
&\bar{A}_{i_5j_2} = -\rho\omega^2 t \langle f_2^i f_2^j \rangle_a, \quad \bar{A}^v_{i_5j_2} = -\delta_p \omega^2 t \langle \rho\, \xi_1 f_2^i f_2^j \rangle_a, \quad \bar{A}_{i_6j_1} = -\rho\omega^2 t \langle f_1^i f_1^j \rangle_a \\
&\bar{A}^v_{i_6j_1} = -\delta_p \omega^2 t \langle \rho\, \xi_1 f_1^i f_1^j \rangle_a
\end{aligned}
\tag{3.19}
$$

where $i_p = (p-1)n + i$ and $j_q = (q-1)n + j$ for $p, q = 1, 2, \ldots, 9$. Similarly non-zero terms of load vectors are given as

$$
\begin{aligned}
&\bar{Q}_{p_{i4}} = -t \langle f_3^i \rangle_a p_d, \quad \bar{Q}_{p_{i3}} = t\bar{s}_{33} \langle f_6^i \rangle_a \left(p_a^k + \zeta t p_d\right) \\
&\tilde{Q}_{p_{i1}} = -\bar{s}_{13} \langle f_4^i \rangle_a \left(p_a^k + \zeta t p_d\right) \quad \tilde{Q}_{p_{i2}} = -\bar{s}_{23} \langle f_5^i \rangle_a \left(p_a^k + \zeta t p_d\right) \\
&\tilde{Q}^v_{p_{i1}} = -\left(p_a^k + \zeta t p_d\right) \left\{ \delta_1 \langle \xi_1 \bar{s}_{13} f_4^i \rangle_a \right\}
\end{aligned}
\tag{3.20}
$$

where $p_a^k = p_a + p_d z_k$, $\bar{m} = m\pi$ and notation $\langle \ldots \rangle_a = a \int_0^1 (\ldots) d\xi_1$ represent integration over the span length (a). Since the functions f_l^i are known analytical functions, elements of the matrices defined in Eqs. (3.19) and (3.20) have been evaluated in close form. Solving the system of algebraic

equations (3.18) for $\hat{\mathbf{G}}$ and substituting back the solution into Eq. (3.17) yields

$$\bar{\mathbf{G}}_{,\zeta} = \mathbf{A}(\omega)\bar{\mathbf{G}} + \mathbf{Q_p} \tag{3.21}$$

with $\mathbf{A} = \mathbf{M}^{-1}[\bar{\mathbf{A}}^{\mathbf{m}} + \hat{\mathbf{A}}^{\mathbf{m}}\mathbf{K}^{\mathbf{m}-1}\tilde{\mathbf{A}}^{\mathbf{m}}]$ and $\mathbf{Q}_{\mathbf{p}}^{\mathbf{m}} = \mathbf{M}^{-1}[\bar{\mathbf{Q}}_{\mathbf{p}}^{\mathbf{m}} + \hat{\mathbf{A}}^{\mathbf{m}}\mathbf{K}^{\mathbf{m}-1}\tilde{\mathbf{Q}}_{\mathbf{p}}^{\mathbf{m}}]$. Equation (3.21) represents a system of $6n$ nonhomogeneous first order ODEs with constant coefficients.

3.3.1 Solution for Static Case

For static case, the elements of matrices which depend on natural frequencies (ω) and time (t) becomes zero, $\bar{A}_{i_4j_3}$=$\bar{A}_{i_5j_2}$=$\bar{A}_{i_6j_1}$=0 and $\bar{A}^v_{i_4j_3}$=$\bar{A}^v_{i_5j_2}$=$\bar{A}^v_{i_6j_1}$=0. Therefore, the coefficient of final system of first order ODEs, Eq. (3.21) is not function of unknown natural frequencies (ω). So, final system of ODEs along thickness direction, Eq. (3.21) now expressed as,

$$\bar{\mathbf{G}}_{,\zeta} = \mathbf{A}\bar{\mathbf{G}} + \mathbf{Q_p} \tag{3.22}$$

The above solution of above equation is obtained by employing same procedure as described in Chapter 2, Sec. 2.5.1. Thus, the general solution of Eq. (3.22) is

$$\bar{\mathbf{G}}(\zeta) = \sum_{i=1}^{6n} \mathbf{F}_i(\zeta)C_i + \mathbf{U_0} + \zeta\mathbf{U_1} \tag{3.23}$$

The $6n \times L$ constants $C_i^{(k)}$'s for L layers are obtained from the $6n$ boundary conditions and $6n \times (L-1)$ interface continuity conditions given by Eqs. (3.5) and (3.6). This completely determines $\bar{\mathbf{G}}(\zeta)$. Now, $\hat{\mathbf{G}}(\zeta)$ can be obtained by solving the algebraic equation (3.18). This completes the first iteration step for static case.

3.3.2 Solution for Dynamic Case

For free vibration case, the element corresponding to load vectors $\bar{\mathbf{Q}}_{\mathbf{p}}$, $\bar{\mathbf{Q}}_{\mathbf{p}}^{\mathbf{v}}$, $\tilde{\mathbf{Q}}_{\mathbf{p}}$ and $\tilde{\mathbf{Q}}_{\mathbf{p}}^{\mathbf{v}}$ is equals to zero due to absence of external applied load, ($\bar{Q}_{p_{i4}}$=$\bar{Q}_{p_{i3}}$=$\tilde{Q}_{p_{i1}}$=$\tilde{Q}_{p_{i2}}$=$\tilde{Q}^v_{p_{i1}}$=0). So, final system of ODE Eq. (3.21) now reduced to,

$$\bar{\mathbf{G}}_{,\zeta} = \mathbf{A}(\omega)\bar{\mathbf{G}} \tag{3.24}$$

The solution of Eq. (3.24) is obtained by applying the similar approach as discussed in Chapter 2, Sec. 2.5.2. The final solution of Eq. (3.24) can written as,

$$\bar{\mathbf{G}}(\zeta) = \sum_{i=1}^{6n} \mathbf{F}_i(\zeta, \omega)C_i \tag{3.25}$$

By applying the traction free boundary condition, Eq. (3.5) and the interface continuity conditions Eq. (3.6), Eq. (3.25) reduced to

$$\sum_{i=1}^{6n} \mathbf{K}_{\mathbf{d}i}(\zeta, \omega)C_i = \mathbf{0} \tag{3.26}$$

where the coefficient matrix $\mathbf{K_d}$ depends on $\omega = \omega_n$. For non-trivial solution, it's determinant is zero and ω can be obtained by finding roots of the equation $|det(\mathbf{K_d})|$=0 using bisection method. Similarly, $\hat{\mathbf{G}}(\zeta)$ can be obtained by solving the algebraic equation (3.18). In this way, first iteration step is completed for dynamic case.

3.4 STEP 2 - IN-PLANE DIRECTION (x)

The solution of $g_l^i(\zeta)$ from the previous step is now taken as known, whereas f_l^i are considered unknown. The variation $\delta\mathbf{X_l}$ for this case is given by,

$$\delta X_l(\xi_1, \xi_2, \zeta) = \sum_{m=1}^{\infty} [\, X_{lS}^y \text{or} X_{lC}^y \,]\, \delta X_{l_m}, \qquad l = 1, 2, \ldots 9 \tag{3.27}$$

where for in-plane direction,

$$\delta X_{l_m} = \sum_{i=1}^{n} g_l^i(\zeta) \delta f_l^i \cos\omega t, \qquad l{=}1{,}2{,}\ldots{,}9 \tag{3.28}$$

The functions $f_l^i(\xi_1)$ are partitioned into vector $\bar{\mathbf{F}}$ consisting of variables which appear in Eq. (3.7) and a vector $\hat{\mathbf{F}}$ contains the remaining variables.

$$\begin{aligned} \bar{\mathbf{F}} &= [\, f_1^1 \ldots f_1^n \quad f_2^1 \ldots f_2^n \quad f_3^1 \ldots f_3^n \quad f_4^1 \ldots f_4^n \quad f_7^1 \ldots f_7^n \quad f_9^1 \ldots f_9^n \,]^{\mathrm{T}} \\ \hat{\mathbf{F}} &= [\, f_5^1 \ldots f_5^n \quad f_6^1 \ldots f_6^n \quad f_8^1 \ldots f_8^n \,]^{\mathrm{T}} \end{aligned} \tag{3.29}$$

By substituting Eq. (3.11), Eq. (3.27) and Eq. (3.28) in Eq. (3.4), performing the integration over ζ direction on the known functions of ζ, and using the fundamental lemma of variational principle, yield the following ODEs ($6n$) and algebraic ($3n$) equations for f_l^i:

$$\mathbf{N}\bar{\mathbf{F}}_{,\xi_1} = \bar{\mathbf{B}}^{\mathbf{f}}(\xi_1, \omega)\bar{\mathbf{F}} + \hat{\mathbf{B}}^{\mathbf{f}}(\xi_1)\hat{\mathbf{F}} + \bar{\mathbf{P}}^{\mathbf{f}}_{\mathbf{m}}(\xi_1) \tag{3.30}$$

$$\mathbf{L}\hat{\mathbf{F}} = \tilde{\mathbf{B}}^{\mathbf{f}}(\xi_1)\bar{\mathbf{F}} + \tilde{\mathbf{P}}^{\mathbf{f}}_{\mathbf{m}} \tag{3.31}$$

where $\bar{\mathbf{B}}^{\mathbf{f}} = \bar{\mathbf{B}}(\omega) + \xi_1\bar{\mathbf{B}}^{\mathbf{v}}(\omega)$; $\hat{\mathbf{B}}^{\mathbf{f}} = \hat{\mathbf{B}} + \xi_1\hat{\mathbf{B}}^{\mathbf{v}}$; $\bar{\mathbf{P}}^{\mathbf{f}}_{\mathbf{m}} = \bar{\mathbf{P}} + \xi_1\bar{\mathbf{P}}^{\mathbf{v}}$; $\tilde{\mathbf{B}}^{\mathbf{f}} = \tilde{\mathbf{B}} + \xi_1\tilde{\mathbf{B}}^{\mathbf{v}}$; $\tilde{\mathbf{P}}^{\mathbf{f}}_{\mathbf{m}} = \tilde{\mathbf{P}}_{\mathbf{m}}$, and $\mathbf{N}$, $\bar{\mathbf{B}}^{\mathbf{f}}$, $\hat{\mathbf{B}}^{\mathbf{f}}$, $\mathbf{L}$ and $\tilde{\mathbf{B}}^{\mathbf{f}}$ are $6n \times 6n$, $6n \times 6n$, $6n \times 3n$, $3n \times 3n$ and $3n \times 6n$ matrices respectively, and $\bar{\mathbf{P}}^{\mathbf{f}}_{\mathbf{m}}$ and $\tilde{\mathbf{P}}^{\mathbf{f}}_{\mathbf{m}}$ are $6n \times 1$ and $3n \times 1$ column vectors comprising of the loading terms. The governing equations (3.30) and (3.31) can be rewritten as

$$\mathbf{N}\bar{\mathbf{F}}_{,\xi_1} = \{\bar{\mathbf{B}}(\omega) + \xi_1\bar{\mathbf{B}}^{\mathbf{v}}(\omega)\}\bar{\mathbf{F}} + (\hat{\mathbf{B}} + \xi_1\hat{\mathbf{B}}^{\mathbf{v}})\hat{\mathbf{F}} + (\bar{\mathbf{P}}_{\mathbf{m}} + \xi_1\bar{\mathbf{P}}^{\mathbf{v}}_{\mathbf{m}}) \tag{3.32}$$

$$\mathbf{L}\hat{\mathbf{F}} = (\tilde{\mathbf{B}} + \xi_1\tilde{\mathbf{B}}^{\mathbf{v}})\bar{\mathbf{F}} + \tilde{\mathbf{P}}_{\mathbf{m}} \tag{3.33}$$

The nonzero elements of $\mathbf{N}$, $\bar{\mathbf{B}}$, $\bar{\mathbf{B}}^{\mathbf{v}}$, $\hat{\mathbf{B}}$, $\hat{\mathbf{B}}^{\mathbf{v}}$, $\mathbf{L}$, $\tilde{\mathbf{B}}$, $\tilde{\mathbf{B}}^{\mathbf{v}}$, $\bar{\mathbf{P}}_{\mathbf{m}}$, $\bar{\mathbf{P}}^{\mathbf{v}}_{\mathbf{m}}$ and $\tilde{\mathbf{P}}^{\mathbf{f}}_{\mathbf{m}}$ matrices Eqs. (3.32) and (3.33) are given below

$$
\begin{aligned}
&N_{i_1j_1} = N_{j_4i_4} = \langle g_4^i g_1^j\rangle_h, \quad N_{i_2j_2} = N_{j_5i_5} = \langle g_7^i g_2^j\rangle_h, \quad N_{i_3j_3} = N_{j_6i_6} = \langle g_9^i g_3^j\rangle_h \\
&\bar{B}_{i_1j_4} = \langle \bar{s}_{11} g_4^i g_4^j\rangle_h, \quad \hat{B}_{i_1j_1} = \langle \bar{s}_{12} g_4^i g_5^j\rangle_h, \quad \bar{B}^v_{i_1j_4} = \delta_1\xi_1\langle \bar{s}_{11} g_4^i g_4^j\rangle_h \\
&\hat{B}_{i_1j_2} = \langle \bar{s}_{13} g_4^i g_6^j\rangle_h, \quad \hat{B}^v_{i_1j_1} = \delta_1\xi_1\langle \bar{s}_{12} g_4^i g_5^j\rangle_h, \quad \hat{B}^v_{i_1j_2} = \delta_1\xi_1\langle \bar{s}_{13} g_4^i g_6^j\rangle_h \\
&\bar{B}_{i_2j_1} = -\bar{m}\langle g_7^i g_1^j\rangle_h, \quad \bar{B}_{i_2j_5} = \langle \bar{s}_{66} g_7^i g_7^j\rangle_h, \quad \bar{B}^v_{i_2j_5} = \delta_2\xi_1\langle \bar{s}_{66} g_7^i g_7^j\rangle_h \\
&\bar{B}_{i_3j_1} = -\langle g_9^i \tfrac{g_{1,\zeta}^j}{t}\rangle_h, \quad \bar{B}_{i_3j_6} = \langle \bar{s}_{55} g_9^i g_9^j\rangle_h, \quad \bar{B}^v_{i_3j_6} = \delta_2\xi_1\langle \bar{s}_{55} g_9^i g_9^j\rangle_h \\
&\bar{B}_{i_4j_5} = \bar{m}\langle g_1^i g_7^j\rangle_h, \quad \bar{B}_{i_4j_6} = \langle \tfrac{g_{9,\zeta}^i}{t} g_1^j\rangle_h, \quad \hat{B}_{i_5j_1} = -\bar{m}\langle g_2^i g_5^j\rangle_h \\
&\hat{B}_{i_5j_3} = \langle \tfrac{g_{2,\zeta}^i}{t} g_8^j\rangle_h, \quad \hat{B}_{i_6j_2} = -\langle g_3^i \tfrac{g_{6,\zeta}^j}{t}\rangle_h, \quad \hat{B}_{i_6j_3} = \bar{m}\langle g_3^i g_8^j\rangle_h \\
&L_{i_1j_1} = \langle \bar{s}_{22} g_5^i g_5^j\rangle_h, \quad L_{i_1j_2} = \langle \bar{s}_{23} g_5^i g_6^j\rangle_h, \quad L_{i_2j_2} = \langle \bar{s}_{33} g_6^i g_6^j\rangle_h \\
&L_{i_2j_1} = L_{i_1j_2}, \quad L_{i_3j_3} = \langle \bar{s}_{44} g_8^i g_8^j\rangle_h, \quad \tilde{B}_{i_1j_2} = -\bar{m}\langle g_5^i g_2^j\rangle_h \\
&\tilde{B}_{i_1j_4} = -\langle \bar{s}_{12} g_5^i g_4^j\rangle_h, \quad \tilde{B}^v_{i_1j_4} = \delta_1\xi_1\langle \bar{s}_{12} g_5^i g_4^j\rangle_h, \quad \tilde{B}_{i_2j_3} = \langle g_6^i \tfrac{g_{3,\zeta}^j}{t}\rangle_h \\
&\tilde{B}_{i_2j_4} = -\langle \bar{s}_{13} g_6^i g_4^j\rangle_h, \quad \tilde{B}^v_{i_2j_4} = -\delta_1\xi_1\langle \bar{s}_{13} g_6^i g_4^j\rangle_h, \quad \tilde{B}_{i_3j_3} = \bar{m}\langle g_8^i g_3^j\rangle_h \\
&\tilde{B}_{i_3j_2} = \langle g_8^i \tfrac{g_{2,\zeta}^j}{t}\rangle_h, \quad \bar{B}_{i_4j_1} = -a\rho\omega^2\langle g_1^i g_1^j\rangle_h, \quad \bar{B}^v_{i_4j_1} = -\delta_p\, a\rho\omega^2\xi_1\langle g_1^i g_1^j\rangle_h \\
&\bar{B}_{i_5j_2} = -a\rho\omega^2\langle g_2^i g_2^j\rangle_h, \quad \bar{B}^v_{i_5j_2} = -\delta_p\, a\rho\omega^2\xi_1\langle g_2^i g_2^j\rangle_h, \; \bar{B}_{i_6j_3} = -\rho a\omega^2\langle g_3^i g_3^j\rangle_h \\
&\bar{B}^v_{i_6j_3} = -\delta_p\, a\rho\omega^2\xi_1\langle g_3^i g_3^j\rangle_h
\end{aligned}
\tag{3.34}
$$

Similarly, non-zero elements load vectors are given as,

$$
\begin{aligned}
&\bar{P}_{m_{i1}} = \langle \bar{s}_{13} g_4^i (p_a^k + p_d t\zeta)\rangle_h, \quad \bar{P}^v_{m_{i1}} = \delta_1\xi_1\langle \bar{s}_{13} g_4^i (p_a^k + p_d t\zeta)\rangle_h, \; \bar{P}_{m_{i6}} = -p_d\langle g_3^i\rangle_h \\
&\tilde{P}_{m_{i1}} = -\langle \bar{s}_{23} g_5^i (p_a^k + p_d t\zeta)\rangle_h, \; \tilde{P}_{m_{i2}} = -\langle \bar{s}_{33} g_6^i (p_a^k + p_d t\zeta)\rangle_h
\end{aligned}
\tag{3.35}
$$

where notation $\langle \ldots\rangle_h = \sum_{k=1}^{L} t^{(k)} \int_0^1 (\ldots)^{(k)}\, d\zeta$ represent integration across the thickness. Since $g_l^i(\zeta)$ are known in close form, all integrations in Eq. (3.34) and (3.35) are evaluated exactly in close form. Substituting $\hat{\mathbf{F}}$ from Eq. (3.33) into Eq. (3.32) yields the following set of first order ODEs with varying coefficients for $\bar{\mathbf{F}}$:

$$
\bar{\mathbf{F}}_{,\xi_1} = \{\mathbf{B_0}(\omega) + \xi_1\mathbf{B_1}(\omega) + \xi_1^2\mathbf{B_2}\}\bar{\mathbf{F}} + \mathbf{P_0} + \xi_1\mathbf{P_1} \tag{3.36}
$$

where $\mathbf{B_0} = \mathbf{N^{-1}}(\bar{\mathbf{B}} + \hat{\mathbf{B}}\mathbf{L^{-1}}\tilde{\mathbf{B}})$; $\mathbf{B_1} = \mathbf{N^{-1}}(\bar{\mathbf{B}}^{\mathbf{v}} + \hat{\mathbf{B}}\mathbf{L^{-1}}\tilde{\mathbf{B}}^{\mathbf{v}} + \hat{\mathbf{B}}^{\mathbf{v}}\mathbf{L^{-1}}\tilde{\mathbf{B}})$; $\mathbf{B_2} = \mathbf{N^{-1}}(\hat{\mathbf{B}}^{\mathbf{v}}\mathbf{L^{-1}}\tilde{\mathbf{B}}^{\mathbf{v}})$; $\mathbf{P_0} = \mathbf{N^{-1}}(\bar{\mathbf{P}}_{\mathbf{m}} + \hat{\mathbf{B}}\mathbf{L^{-1}}\tilde{\mathbf{P}}_{\mathbf{m}})$; $\mathbf{P_1} = \mathbf{N^{-1}}(\bar{\mathbf{P}}^{\mathbf{v}}_{\mathbf{m}} + \hat{\mathbf{B}}^{\mathbf{v}}\mathbf{L^{-1}}\tilde{\mathbf{P}}_{\mathbf{m}})$

Equation (3.36) is set of non-homogenous ODEs with variable coefficients.

3.4.1 Solution for Static Case

Similarly along in-plane direction also, the elements of matrices which depend on natural frequencies (ω) and time (t) becomes zero for static case, $\bar{B}_{i_4j_1}$=$\bar{B}_{i_5j_2}$=$\bar{B}_{i_6j_3}$=$\bar{B}^v_{i_4j_1}$=$\bar{B}^v_{i_5j_2}$=$\bar{B}^v_{i_6j_3}$=0. Therefore, the coefficients of final system of first order ODEs Eq. (3.36) is not now function of unknown natural frequencies (ω). So, final system of ODE Eq. (3.36) now expressed as,

$$\bar{\mathbf{F}}_{,\xi_1} = \{\mathbf{B_0} + \xi_1\mathbf{B_1} + \xi_1^2\mathbf{B_2}\}\bar{\mathbf{F}} + \mathbf{P_0} + \xi_1\mathbf{P_1} \tag{3.37}$$

Now, the final solution for present system of equations Eq. (3.37) is approximated in form of power series in the dimensionless axial coordinate ξ_1 $(0 \leq \xi_1 \leq 1)$ a as. Using the power series method as discussed in Chapter 2, Sec. 2.6.1, the final general solution of Eq. (3.37) can be written as,

$$\bar{\mathbf{F}}^j(\xi_1) = \sum_{i=0}^{N_p} \mathbf{Z}_i^j \xi_1^i + \left(\sum_{i=0}^{N_p} \mathbf{H}_i^j \xi_1^i\right) \mathbf{C}_0 \tag{3.38}$$

where $\mathbf{C}_0$ is evaluated by applying the boundary conditions of x-direction, given in Eq. (3.7). The infinite power series in $\mathbf{Z}_i(\xi_1)$ and $\mathbf{H}_i(\xi_1)$ are truncated to a finite number of terms such that the contribution of two consecutive terms is less than a stipulated small number η $(= 10^{-10})$.

3.4.2 Solution for Dynamic Case

For the dynamic case (free vibration), all the elements in the load vectors ($\bar{\mathbf{P}}^{\mathbf{f}}_{\mathbf{m}}$ and $\tilde{\mathbf{P}}^{\mathbf{f}}_{\mathbf{m}}$) becomes zero due to absence of external applied load ($\bar{P}_{m_{i1}}$=$\bar{P}^v_{m_{i1}}$=$\bar{P}_{m_{i6}}$=$\tilde{P}_{m_{i1}}$=$\tilde{P}_{m_{i2}}$=0). Therefore, load vectors $\mathbf{P_0}$ and $\mathbf{P_1}$ in Eq. (3.36) are now equals to zero. Therefore, the Eq. (3.36) reduced to,

$$\bar{\mathbf{F}}_{,\xi_1} = \{\mathbf{B_0}(\omega) + \xi_1\mathbf{B_1}(\omega) + \xi_1^2\mathbf{B_2}\}\bar{\mathbf{F}} \tag{3.39}$$

Now, Eq. (3.39) is a system of simultaneous homogeneous first order differential equations ($4n$), with variable coefficients which is function of ξ_1-coordinate and also contains natural frequencies (ω). Similarly, by employing power series method as discussed in Chapter 2, Sec. 2.6.2, the final solution for present system of ODEs Eq. (3.39) is written in form of power series as,

$$\bar{\mathbf{F}}^j(\xi_1) = \left(\sum_{i=0}^{N_p} \mathbf{H}_i^j \xi_1^i\right) \mathbf{C}_0 \tag{3.40}$$

where unknown coefficient $\mathbf{C}_0$ depends on x-direction support conditions given in Eq. (3.7). Similarly, the number of terms (N_p) in power series is chosen large enough which ensure that the contribution of further succeeding terms is negligible and less than η $(= 10^{-10})$. Now applying the boundary condition of ends $x = 0$ and $x = 1$ given in Eq. (3.7) which reduced Eq. (3.40) to

$$\sum_{i=1}^{8n} \mathbf{K}_{\mathbf{d}i}(\xi_1) C_i = \mathbf{0} \tag{3.41}$$

where, the coefficient matrix $\mathbf{K_d}$ now depends on $\omega = \omega_m$. Similarly, ω can be obtained by finding roots of the equation $|det(\mathbf{K_d})|$=0 using bisection method.

Functions $\hat{\mathbf{F}}$ are obtained by substituting the solution of $\bar{\mathbf{F}}$ into Eq. (3.33). Now the second step is completed and further, these two iteration steps of alternating directions are repeated to get the desired level of accuracy.

3.5 CONFIGURATIONS AND MATERIAL PROPERTIES

Numerical results are presented for a single layered and two-layered FGM plate, as shown in Fig. 3.2. The material properties for FGM plate and adhesive layer are listed in Table 3.1

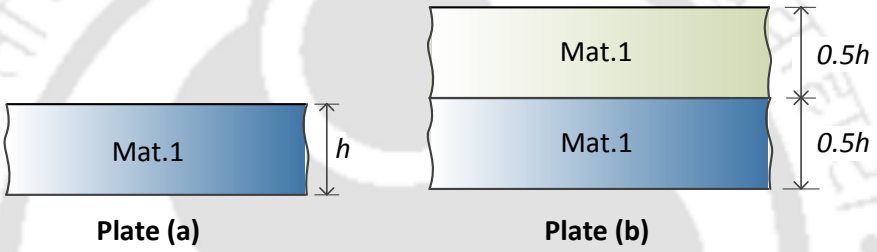

Fig. 3.2: Configuration of FGM plate.

Table 3.1: Material constants

Material	Y_1	Y_2	Y_3	G_{23}	G_{13}	G_{12}	ν_{12}	ν_{13}	ν_{23}	ρ
Mat. 1 (Gr/Ep)	181.0	10.3	10.3	2.87	7.17	7.17	0.28	0.28	0.33	1578
Mat. 2 (Adhesive)	4.2	4.2	4.2	1.59	1.59	1.59	0.32	0.32	0.32	

Units: Young's moduli Y_i and shear moduli G_{ij} in GPa; density (ρ) in Kg/m^3; Y_0= 10.3 GPa

The plates are designated according to their mechanical boundary conditions at the edges $\xi_1 = 0, 1$. For example, a plate which is simply-supported (S) at $\xi_1 = 0$ and free (F) at $\xi_1 = 1$, is called an S–F plate. To verify the accuracy and stability of the present solution various case of material properties variation along x-axis is considered for the plates. Since no other analytical solution exists, the present results are compared with the 3D FE solution. For 3D FE analysis, the spatially graded property distribution (at different Gauss points) with the 20-node hexahedral solid element is implemented by employing user material subroutine (UMAT) in ABAQUS FE software [294]. The converged FE results are obtained by discretizing the plate with a 50 (length) ×50 (width) ×18 (thickness) mesh.

3.6 NUMERICAL RESULTS FOR STATIC CASE

For static case, the numerical result are presented for square FGM plates ($a = b = 1$, $s = 0.2$) which are subjected to a pressure load $p_2 = p_0 \sin \pi\xi_2$ at the top of the plate. The results are presented in non-dimensionalized with $s = h/a$, $Y_0 = 10.3$ GPa and $p_0 = 1$ as:

$$(\bar{u}, \bar{v}, \bar{w}) = 100(u, v, ws)Y_0 s^3/p_0 h;$$
$$(\bar{\sigma}_x,\, \bar{\sigma}_y,\, \bar{\tau}_{xy},\, \bar{\tau}_{zx},\, \bar{\tau}_{yz}) = s^2(\sigma_x,\, \sigma_y,\, 10\tau_{xy},\, \tau_{zx}/s,\, \tau_{yz}/s)/p_0 \tag{3.42}$$

Where, s $(= h/a)$ denote the thickness-to-span ratio. To study the effect of in-plane gradation material properties on bending behaviour of plate, results are plotted for different variation cases along with constant property case (homogeneous plate). Since there is no analytical 3D elasticity based bending solution exist for the longitudinally functionally graded plates. Therefore, the present method is validated with respect to 3D FE results. It is observed that present results are in excellent agreement with 3D FE results for all the cases. Four type of variation of material properties are considered for plate (a) [Case (i) $_{\mathrm{a}}$: $\delta_1 = \delta_2 = 0.5$, Case (ii)$_{\mathrm{a}}$: $\delta_1 = \delta_2 = 1.0$, Case (iii)$_{\mathrm{a}}$: $\delta_1 = 2.0$, $\delta_2 = 1.0$ and Case (iv)$_{\mathrm{a}}$: $\delta_1 = 2.6$, $\delta_2 = 1.7$] while following two type of variation is considered for plate (b)

- Case (i)$_{\mathrm{b}}$: Bottom layer- $\delta_1 = 0.0$, $\delta_2 = 0.0$; Top layer- $\delta_1 = 0.5$, $\delta_2 = 0.5$
- Case (ii)$_{\mathrm{b}}$: Bottom layer- $\delta_1 = 0.3$, $\delta_2 = 0.2$; Top layer- $\delta_1 = 0.7$, $\delta_2 = 0.5$

3.6.1 Plate (a): Single Layered Plate

Effect of variation of material property on the longitudinal variation of deflection ($\bar{w}$), normal stresses ($\bar{\sigma}_x$, $\bar{\sigma}_y$,), and transverse shear stresses ($\bar{\tau}_{xz}$, $\bar{\tau}_{yz}$) are presented in Fig. 3.3 for the thick square plate ($s = 0.2$) under simply-supported (S–S) and simply supported-free (S–F) boundary conditions. The role of different boundary conditions in conjunction with material variation are also assessed in Fig. 3.4 for C–C and C–F cases and in Fig. 3.5 for C–S and F–F boundary conditions. Results for the constant property case (homogeneous plate) are also presented in Figs. 3.3, 3.4 and 3.5. The 3D FE results for the Case (i)$_{\mathrm{a}}$ and Case (iv)$_{\mathrm{a}}$ are also plotted to validate the present formulation. The present results are in excellent agreement with 3D FE results. The following distinctive observations are made:

(A) S–S Boundary Condition: (i) As the variation index increases, the magnitudes of deflection ($\bar{w}$) and stress ($\bar{\sigma}_y$) increase whereas in-plane stress ($\bar{\sigma}_x$) decreases. The rate of increment for $\bar{w}$, $\bar{\sigma}_y$ and $\bar{\tau}_{yz}$ is almost same whereas a decrease in $\bar{\sigma}_x$ is small. The percentage increment or decrement in entities with respect to constant properties case is presented in Table 3.2. As

the variation indexes are doubled (δ_1=δ_2=1.0), the deviation in $\bar{w}$, $\bar{\sigma}_y$, and $\bar{\tau}_{yz}$ at the center of the plate increase from 21.4%, 23.2% and 11.6% to 41.4%, 44.52%, and 22.63%, respectively with respect to constant properties case.

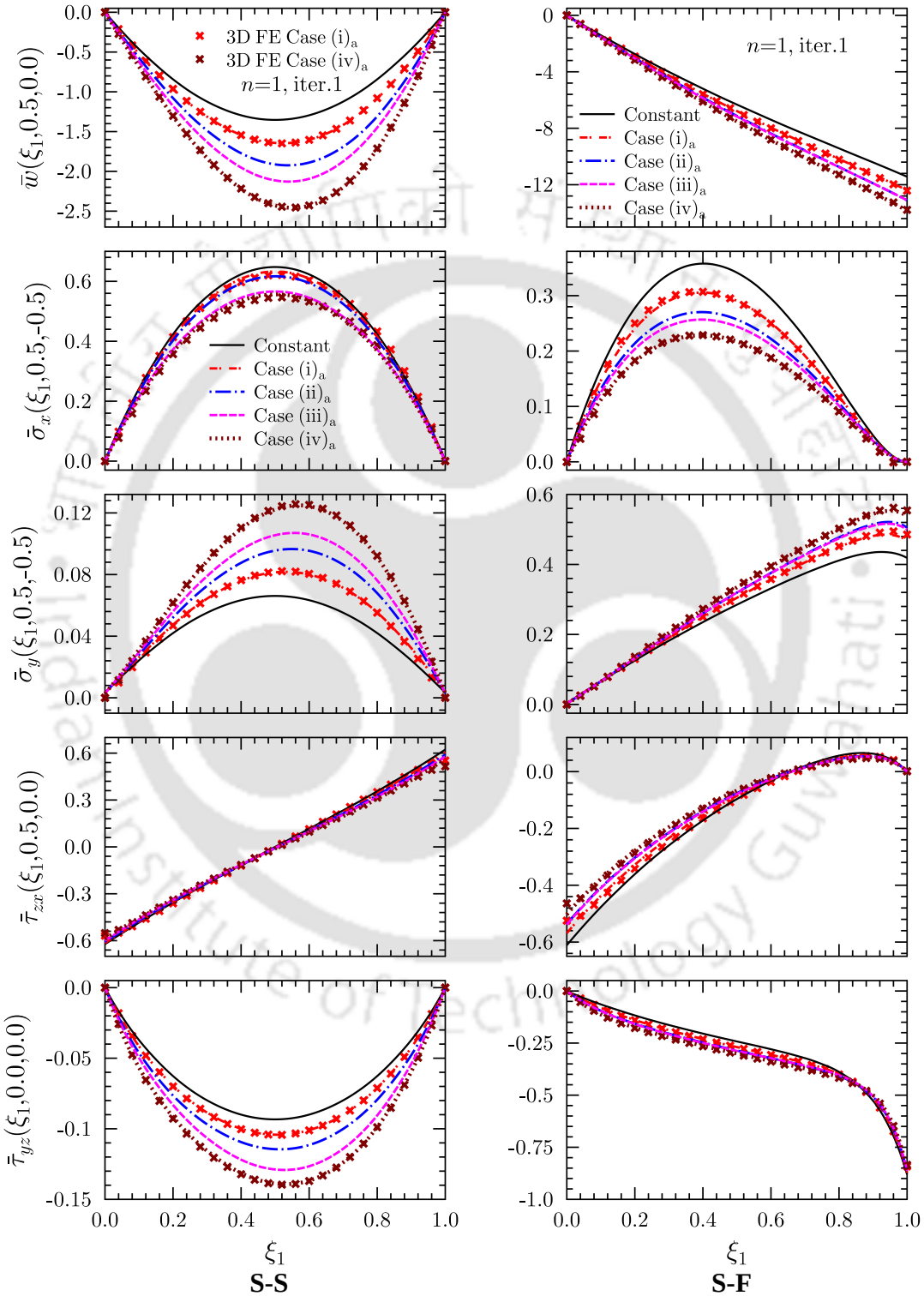

Fig. 3.3: Effect of variation in properties on longitudinal variations of deflection and stresses for single layer thick FGM plate ($s = 0.2$) subjected to S–S and S–F boundary conditions

Here, even the single term solution gives excellent accuracy., (ii) The position of maximum deflection ($\bar{w}$) and stresses ($\bar{\sigma}_y$, $\bar{\tau}_{yz}$) shifts toward the right side of the plate., (iii) $\bar{\tau}_{xz}$ is least affected by the variation in material properties.

(B) S–F Boundary Condition: (i) Deflection ($\bar{w}$) and stress ($\bar{\sigma}_y$) increase whereas $\bar{\sigma}_x$ decrease as the variation index increases but the rate of increment or decrement of deviation in magnitude is entirely different than S–S case. Result for Case $(ii)_a$ and Case $(iii)_a$ are very close to each other for all the entities. Thus support conditions significantly influence the behavior of the FGM plate., (ii) Similarly, for the S–F boundary condition, the deflection ($\bar{w}$) and stress ($\bar{\sigma}_y$) at $\xi_1 = 1$ is increased by 8.3% and 12.0%, respectively, for δ_1=δ_2=0.5. As the variation indexes are doubled (δ_1=δ_2=1.0), the deviation of $\bar{w}$ and $\bar{\sigma}_y$ increased to 14.6% and 20.7%, respectively. At the center of the plate, $\bar{\sigma}_x$ is decreased by 14.9%, and 11.2% increases $\bar{\tau}_{yz}$ for δ_1=δ_2=0.5. As the variation indexes are doubled, the maximum value of $\bar{\sigma}_x$ reduced by 24.8% and $\bar{\tau}_{yz}$ enhanced by 18.0%., (iii) For S–S case, longitudinal variations of $\bar{\sigma}_y$ and $\bar{\tau}_{yz}$ are significantly affected, and $\bar{\sigma}_x$ and $\bar{\tau}_{xz}$ are least affected. Whereas for S–F case, the reverse trend appears, the variation of material properties has a significant effect on $\bar{\sigma}_x$ and $\bar{\tau}_{xz}$ and has the least effect on $\bar{\tau}_{yz}$.

(C) C–C and C–F boundary conditions: The results for plates with C–C and C–F boundary conditions depicted in Fig. 3.4 for the different value of property variation indexes. It has observed in Ref. [280] that a two-term solution needed for accurate results near the clamped support, Therefore, for the present case, two-term converged EKM results are presented. For these cases also, present results are in excellent agreement with the 3D FE. For the plate subjected to C–C boundary condition and having δ_1=δ_2=0.5, the deflection ($\bar{w}$) and stresses $\bar{\sigma}_y$, $\bar{\tau}_{yz}$ at the center of the plate increased by 22.4%, 22.6%, and 12.2%, respectively, whereas $\bar{\sigma}_x$ decreased by 5.2%. As the variation index doubled (δ_1=δ_2=1.0), the deviation in $\bar{w}$ and stresses $\bar{\sigma}_y$, $\bar{\tau}_{yz}$ increased to 41.8%, 42.5%, and 22.9%, respectively, with respect to constant properties and $\bar{\sigma}_x$ decreased by 6.1%. Similarly, for the C–F plate, the deflection $\bar{w}$ and stress $\bar{\sigma}_y$ at $\xi_1 = 1$ increased by 10.5% and 12.2%, respectively, for δ_1=δ_2=0.5. As the variation indexes are doubled (δ_1=δ_2=1.0), the deviation of $\bar{w}$ and $\bar{\sigma}_y$ increase by 15.6% and 22.7%, respectively. $\bar{\tau}_{yz}$ at the center is increased by 15.5% for δ_1=δ_2=0.5. It is observed that the deflection ($\bar{w}$) and stresses ($\bar{\sigma}_y$, $\bar{\tau}_{yz}$) are significantly affected for both C–C and C–F boundary conditions whereas $\bar{\sigma}_x$ and $\bar{\tau}_{xz}$ are the least affected by the properties variation. The percentage change in entities due to property variation is presented in Table 3.2.

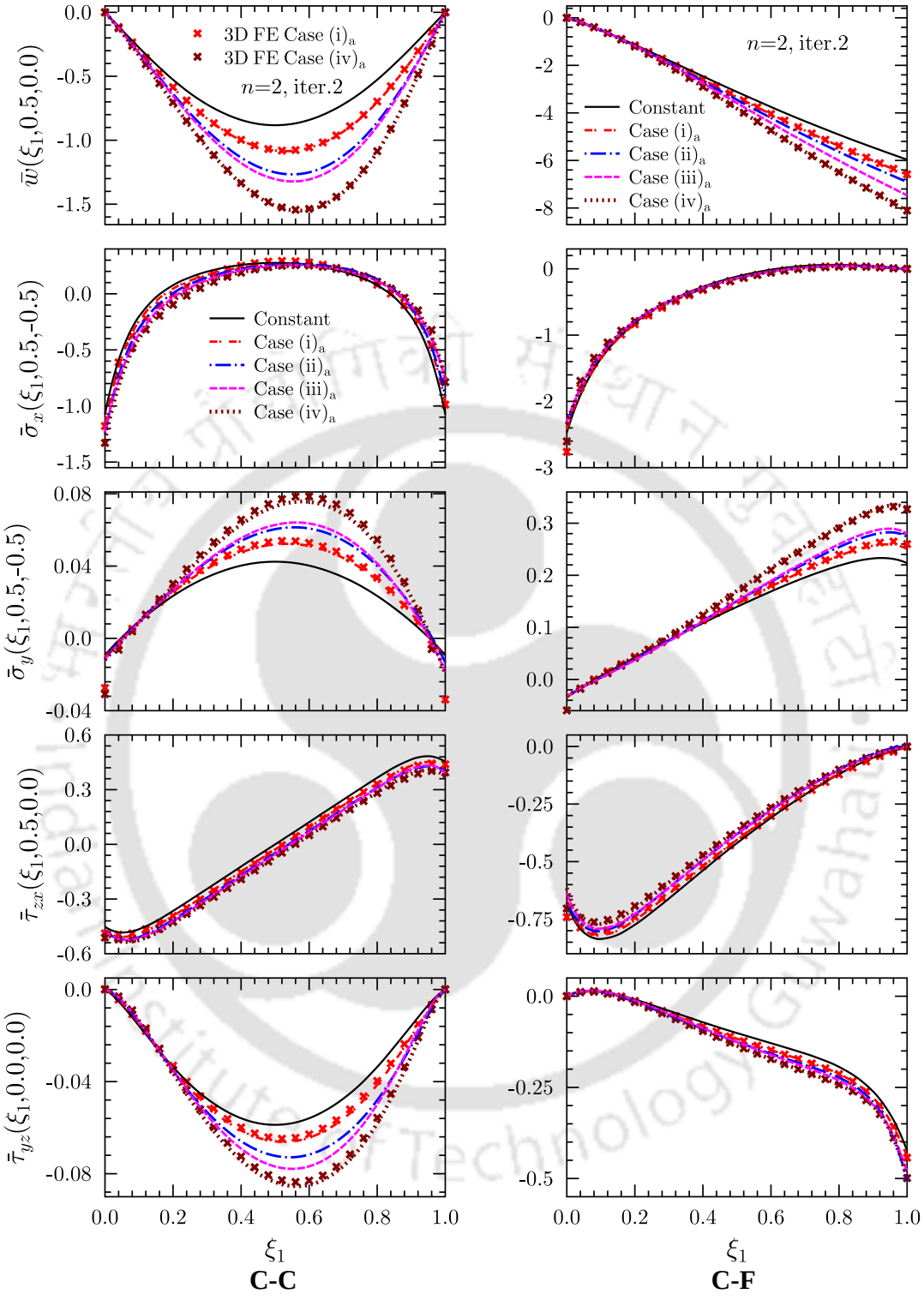

Fig. 3.4: Effect of variation in properties on longitudinal variations of deflection and stresses for single layer thick FGM plate ($s = 0.2$) subjected to C–C and C–F boundary conditions

(D) C–S and F–F boundary conditions: (i) Figure 3.5 depicts the effect of variation of material properties on the longitudinal variations of deflection and stresses for the plate subjected to C–S and F–F boundary conditions. For the C–S case, as the variation index increases,

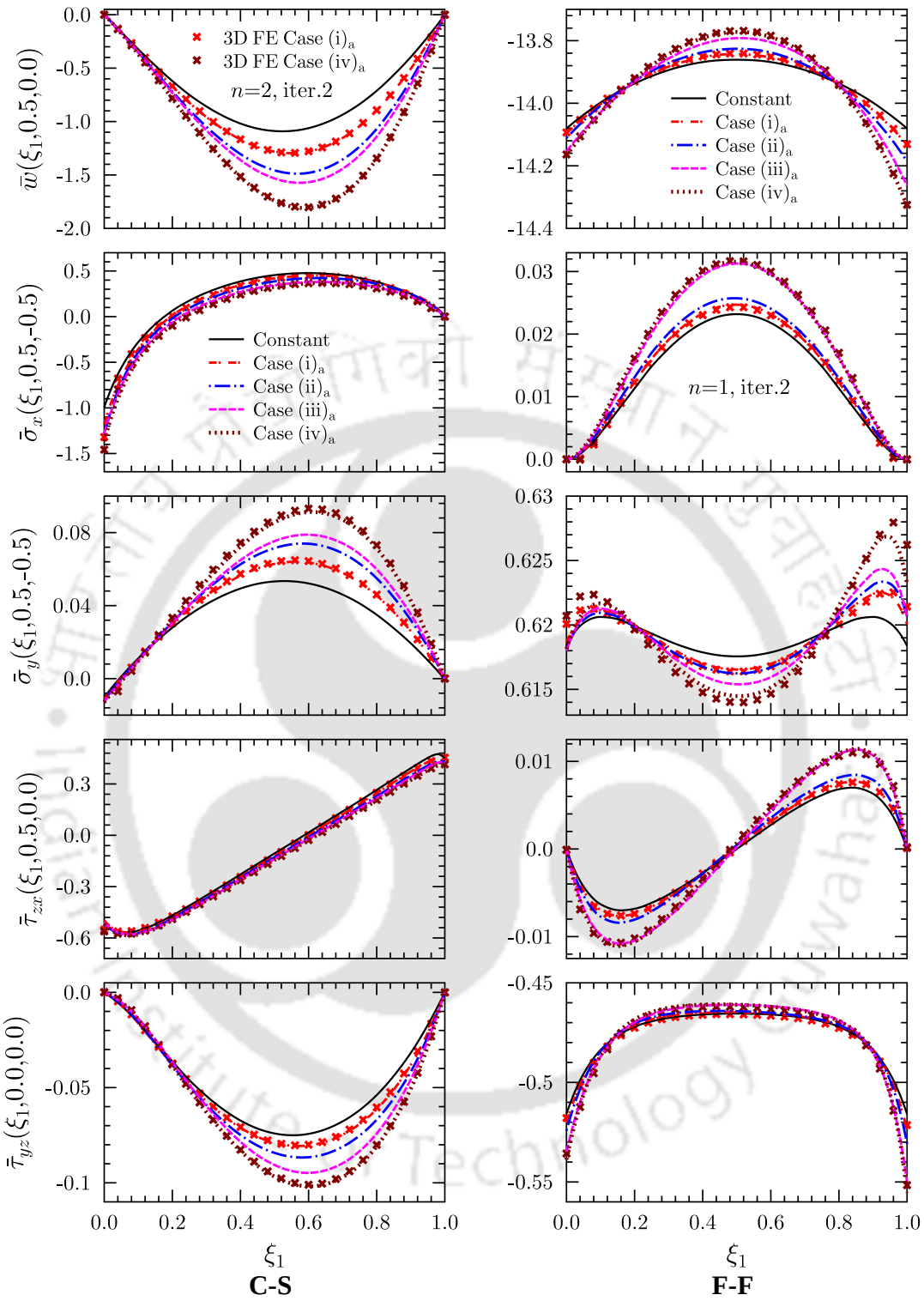

Fig. 3.5: Effect of variation in properties on longitudinal variations of deflection and stresses for single layer thick FGM plate ($s = 0.2$) subjected to C–S and F–F boundary conditions.

deflection ($\bar{w}$) and stresses ($\bar{\sigma}_y$, $\bar{\tau}_{yz}$) increased significantly whereas the increase in $\bar{\sigma}_x$ and $\bar{\tau}_{xz}$ is negligible., (ii) As the variation index increases, $\bar{w}$ and stress $\bar{\sigma}_y$ decrease in magnitude at the center of the plate but increase at free edges of the plate for F–F case. The boundary layer

Table 3.2: Percentage(%) change in deflection and stresses with respect to homogenous case (Constant), due to variation in material properties for plate (a)

B.C.	Entity(x, y, z)	Case (i)$_a$	Case (ii)$_a$	Case (iii)$_a$	Case (iv)$_a$
S–S	$\bar{w}$ (0.5,0.5,0.0)	21.42	41.36	56.23	79.57
	$\bar{\sigma}_x$ (0.5,0.5,-0.5)	-2.33	-4.78	-12.62	-14.09
	$\bar{\sigma}_y$ (0.5,0.5,-0.5)	23.16	44.52	59.60	84.91
	$\bar{\tau}_{zx}$ (1.0,0.5,0.0)	-2.73	-5.15	-7.06	-9.67
	$\bar{\tau}_{yz}$ (0.5,0.5,0.0)	11.64	22.63	38.04	48.75
S–F	$\bar{w}$ (1.0,0.5,0.0)	8.34	14.62	14.62	21.10
	$\bar{\sigma}_x$ (0.5,0.5,-0.5)	-14.91	-24.78	-28.52	-36.35
	$\bar{\sigma}_y$ (1.0,0.5,-0.5)	11.96	20.71	19.30	28.32
	$\bar{\tau}_{zx}$ (0.1,0.5,0.0)	-8.20	-14.44	-14.01	-20.77
	$\bar{\tau}_{yz}$ (0.5,0.5,0.0)	11.19	18.01	18.77	24.07
C–C	$\bar{w}$ (0.5,0.5,0.0)	22.42	41.80	47.81	72.01
	$\bar{\sigma}_x$ (0.5,0.5,-0.5)	-5.15	-6.07	-9.41	-13.81
	$\bar{\sigma}_y$ (0.5,0.5,-0.5)	22.55	42.46	47.99	72.17
	$\bar{\tau}_{zx}$ (1.0,0.5,0.0)	-5.80	-12.32	-13.53	-14.30
	$\bar{\tau}_{yz}$ (0.5,0.5,0.0)	12.23	22.91	30.82	42.31
C–F	$\bar{w}$ (1.0,0.5,0.0)	10.51	15.62	25.19	36.04
	$\bar{\sigma}_x$ (0.1,0.5,-0.5)	-0.12	-5.16	-4.61	-4.48
	$\bar{\sigma}_y$ (1.0,0.5,-0.5)	12.19	22.72	25.26	47.04
	$\bar{\tau}_{zx}$ (0.1,0.5,0.0)	-1.88	-4.11	-5.38	-7.85
	$\bar{\tau}_{yz}$ (0.5,0.5,0.0)	15.52	23.99	24.19	34.37
C–S	$\bar{w}$ (0.5,0.5,0.0)	17.73	33.81	40.77	59.92
	$\bar{\sigma}_x$ (0.5,0.5,-0.5)	-7.76	-15.02	-24.34	-28.29
	$\bar{\sigma}_y$ (0.5,0.5,-0.5)	18.08	34.29	41.46	60.86
	$\bar{\tau}_{zx}$ (0.1,0.5,0.0)	0.95	2.80	3.04	4.04
	$\bar{\tau}_{yz}$ (0.5,0.5,0.0)	6.66	13.78	22.35	30.60
F–F	$\bar{w}$ (1.0,0.5,0.0)	0.38	0.75	1.29	1.75
	$\bar{\sigma}_x$ (0.5,0.5,-0.5)	5.21	10.94	34.88	36.07
	$\bar{\sigma}_y$ (0.5,0.5,-0.5)	-0.17	-0.21	-0.35	-0.50
	$\bar{\tau}_{zx}$ (0.1,0.5,0.0)	13.23	22.42	55.69	61.99
	$\bar{\tau}_{yz}$ (0.5,0.5,0.0)	-0.14	-0.26	-0.95	-0.96

effects are observed in $\bar{\sigma}_y$ and $\bar{\tau}_{xz}$ near the free edge ($\xi_1 = 1$), which is highest for $\delta_1 = 2.6$, $\delta_2 = 1.7$., (iii) The longitudinal variation for F–F case is entirely different than behavior for S–S, S–F, C–C and C–S cases., (iv) Deflection for this case increases substantially toward the right side as the variation index increases. The results for Case (iii)$_a$ and Case (iv)$_a$ are very

close to each other which is not true for other different boundary conditions. For S–S, C–C, and F–F cases, the longitudinal variations of deflection and stresses become asymmetrical as the variation index for material properties increased, as expected.

Similarly, through-thickness variations of in-plane normal stresses ($\bar{\sigma}_x$, $\bar{\sigma}_y$), in-plane shear stress ($\bar{\tau}_{xy}$), transverse normal stress ($\bar{\sigma}_z$), and transverse shear stresses ($\bar{\tau}_{xz}$, $\bar{\tau}_{yz}$) are also presented Fig. 3.6 for Case (ii)$_a$ at different ξ_1 locations for C–F boundary condition. 3D FE results are also plotted for comparison, and it is observed that the two results match closely.

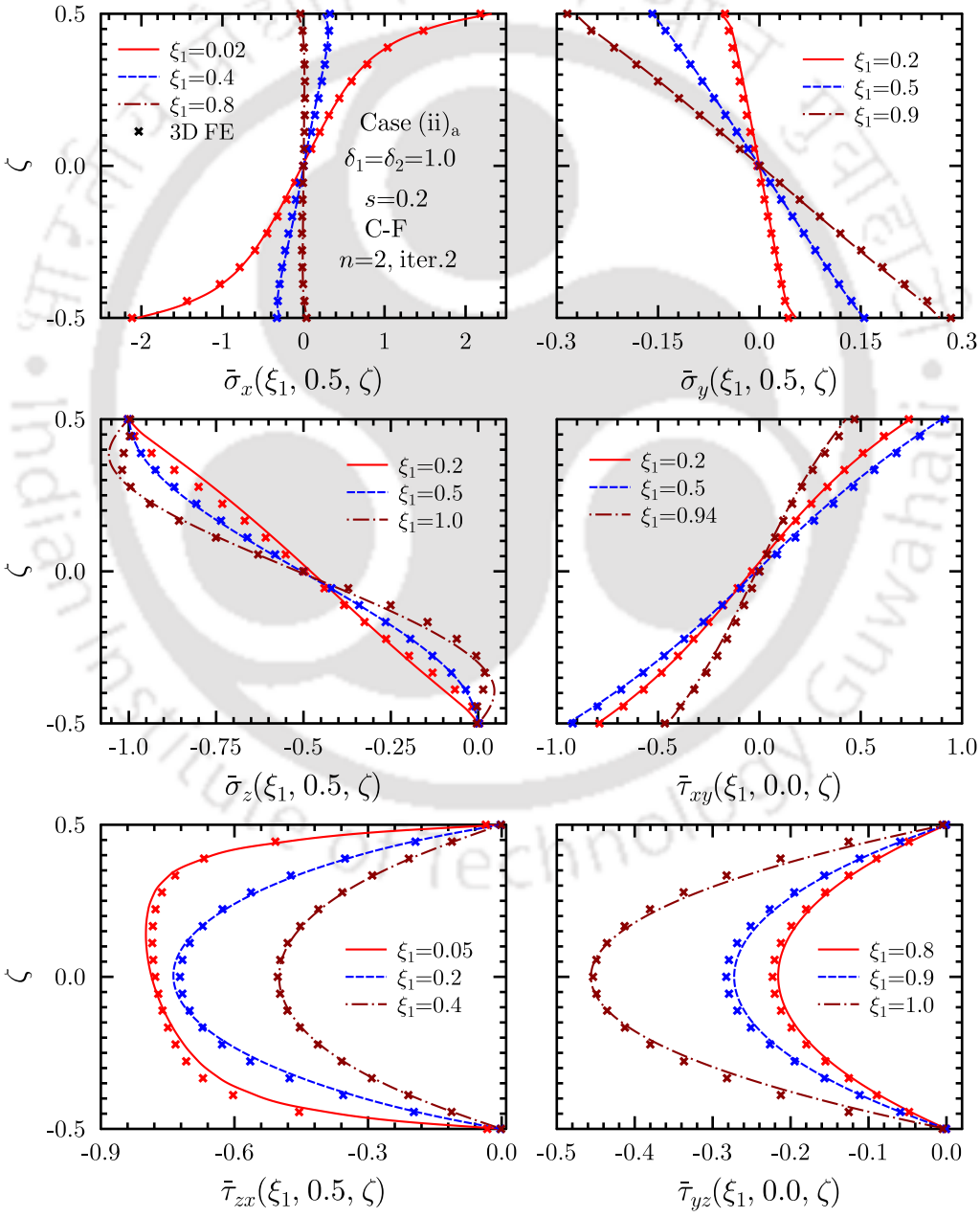

Fig. 3.6: Comparison of stresses distributions at different ξ_1-locations with 3D FE solution for single layer thick FGM plate ($s = 0.2$) under C–F boundary condition.

Effect of b/a ***ratio:***

For different values of b/a (1.5, 2, 4 and 10), through-thickness distribution of displacements $(\bar{v}, \bar{w})$ and stresses $(\bar{\sigma}_x,\ \bar{\sigma}_y,\ \bar{\tau}_{zx},\ \bar{\tau}_{yz})$ are plotted in Fig. 3.7 for thick FGM plate ($s = 0.2$) under gradation Case $(\text{ii})_\text{a}$ (δ_1=δ_2=1.0), and subjected to C-F boundary condition. It is observed that the magnitude of displacements and stresses are significantly affected by b/a ratio except $\bar{\sigma}_x$.

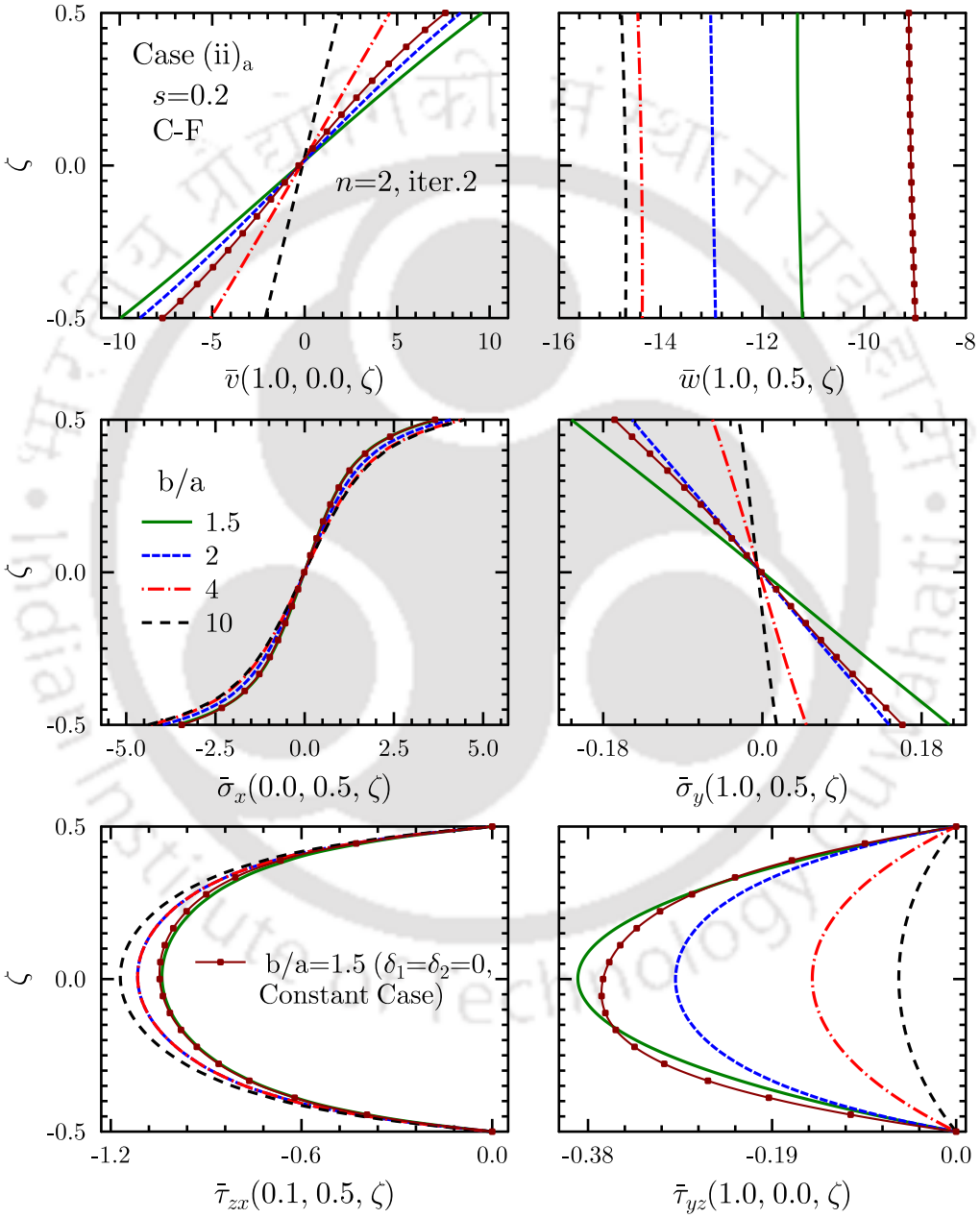

Fig. 3.7: Effect of b/a ratio on through-thickness distribution of deflections and stresses for single layer thick FGM plate ($s = 0.2$) subjected C-F boundary condition, and under gradation Case $(\text{ii})_\text{a}$.

Effect of thickness (s) ratio:

Figure 3.8 depicts the effect of thickness-to-span ratio ($s = h/a$) on through-thickness distribution of deflections ($\bar{u}$, $\bar{w}$) and stresses ($\bar{\sigma}_x$, $\bar{\tau}_{zx}$) for single-layer square FGM plate under gradation Case (ii)$_a$ (δ_1=δ_2=1.0), and subjected to S-F boundary condition. It is observed that the deflection ($\bar{w}$) and stresses ($\bar{\sigma}_x$, $\bar{\tau}_{zx}$) are significantly affected by thickness-to-span ratio (s) whereas $\bar{u}$ is comparatively less affected.

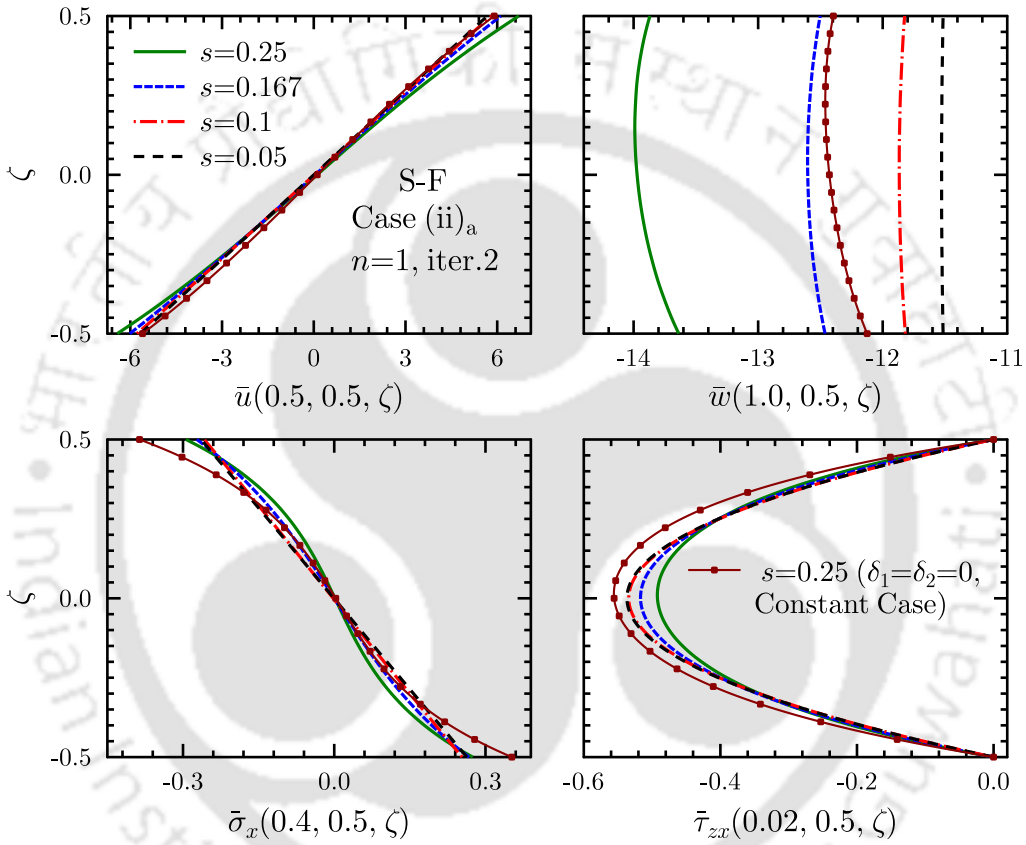

Fig. 3.8: Effect of thickness ratio (s) on through-thickness distribution of deflections and stresses for single-layered square FGM plate subjected to S-F boundary condition, and under gradation Case (ii)$_a$.

3.6.2 Plate (b): Two Layered Plate

For the first time, a two-layer plate having longitudinally graded properties with the different index for the top and the bottom layers is analysed analytically. The longitudinal variations of deflection ($\bar{w}$) and stresses ($\bar{\sigma}_x$, $\bar{\tau}_{xz}$) for the plate (b) under S–S and S–F boundary conditions are plotted in the Fig. 3.9. To verify the accuracy of the present solution for the multilayered plate, 3D FE results for case (2) are also plotted. Longitudinal variations of deflection and stresses for the layer-wise homogeneous case are also presented to study the effect of varying material properties. Figure 3.9 reveals that the in-plane variation of material properties even for one layer significantly affects the maximum deflection. The stresses $\bar{\sigma}_x$, $\bar{\tau}_{xz}$ are much less affected by the variation of properties for both S–S and S–F conditions.

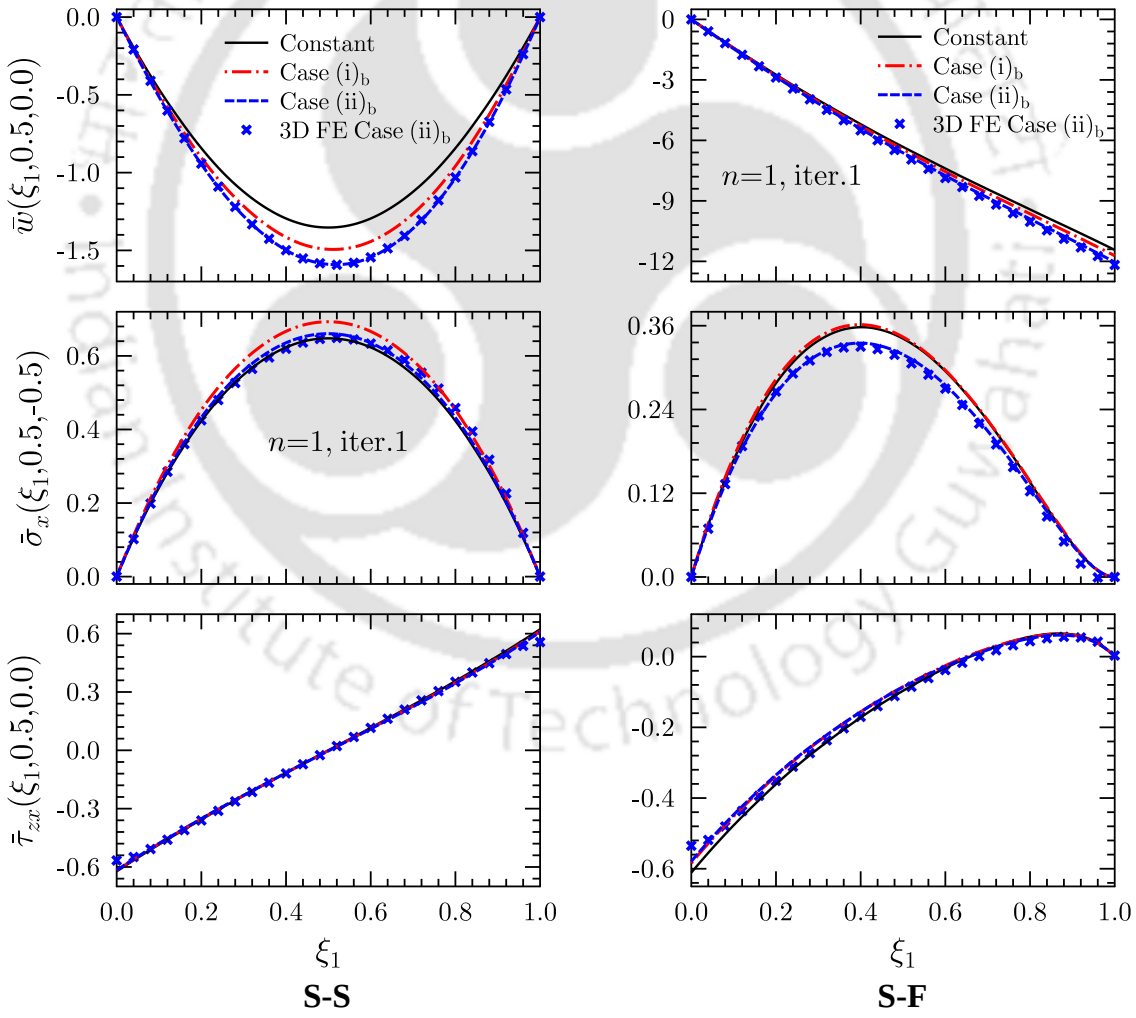

Fig. 3.9: Effect of variation in properties on longitudinal variations of deflection and stresses for two layered thick FGM plate ($s = 0.2$) subjected to S–S and S–F.

The deflection and stresses for the plate (b) under C–S and C–F boundary conditions are presented in Fig. 3.10. For both C–S and C–F case, the deflection ($\bar{w}$) is affected significantly by the gradation of properties along x-direction whereas $\bar{\sigma}_x$, $\bar{\tau}_{xz}$ are affected least.

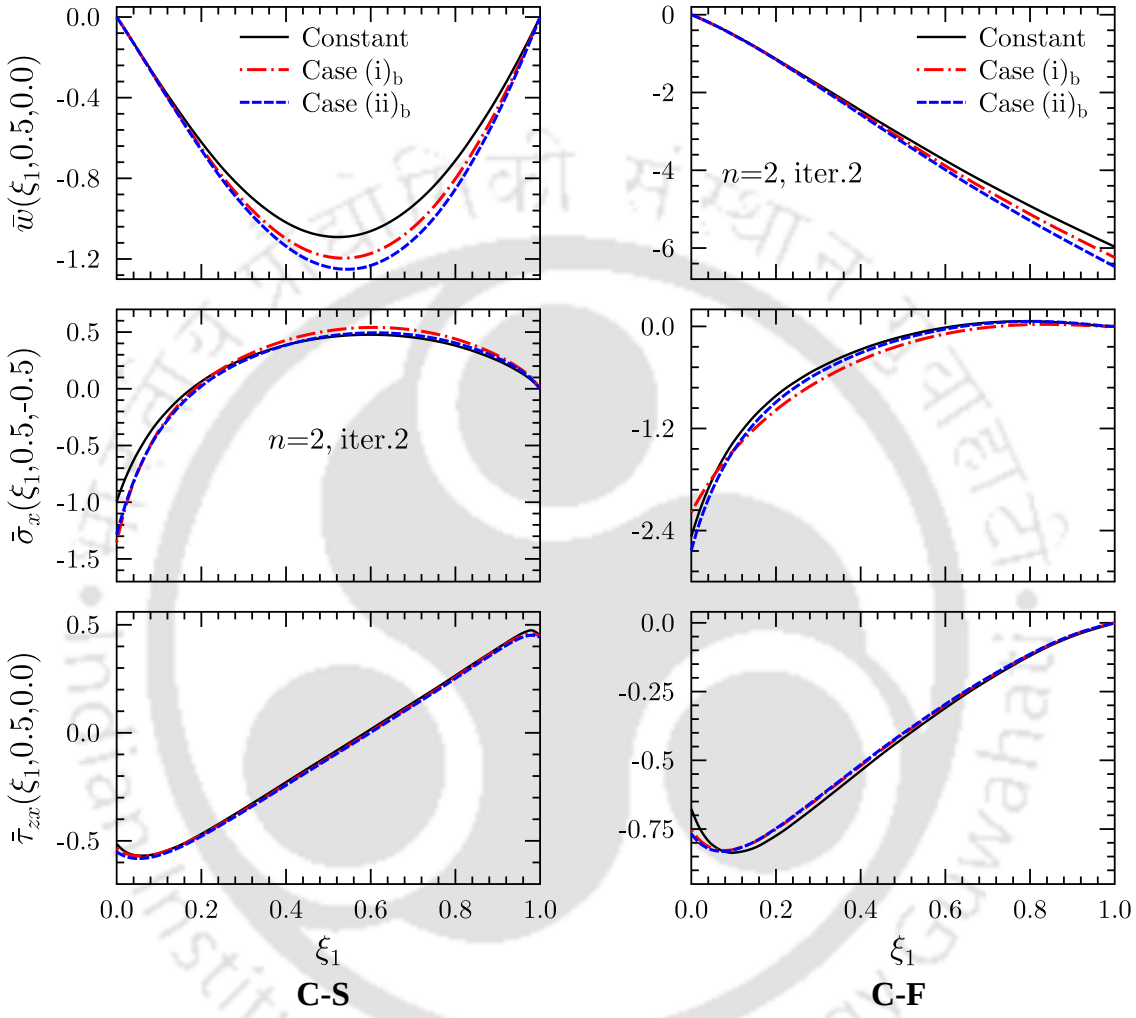

Fig. 3.10: Effect of variation in properties on longitudinal variations of deflection and stresses for two layered thick FGM plate ($s = 0.2$) subjected to C–S and C–F boundary conditions.

In Fig. 3.11, through-thickness variations of in-plane stresses ($\bar{\sigma}_x$, $\bar{\tau}_{xy}$) and transverse stresses ($\bar{\sigma}_z$, $\bar{\tau}_{xz}$) are plotted for Case (ii)$_\mathrm{b}$ at various ξ_1 locations under C–S boundary condition. The corresponding 3D FE results are also plotted for comparison, and it is observed that the MMEKM solution shows excellent agreement with the FE solution.

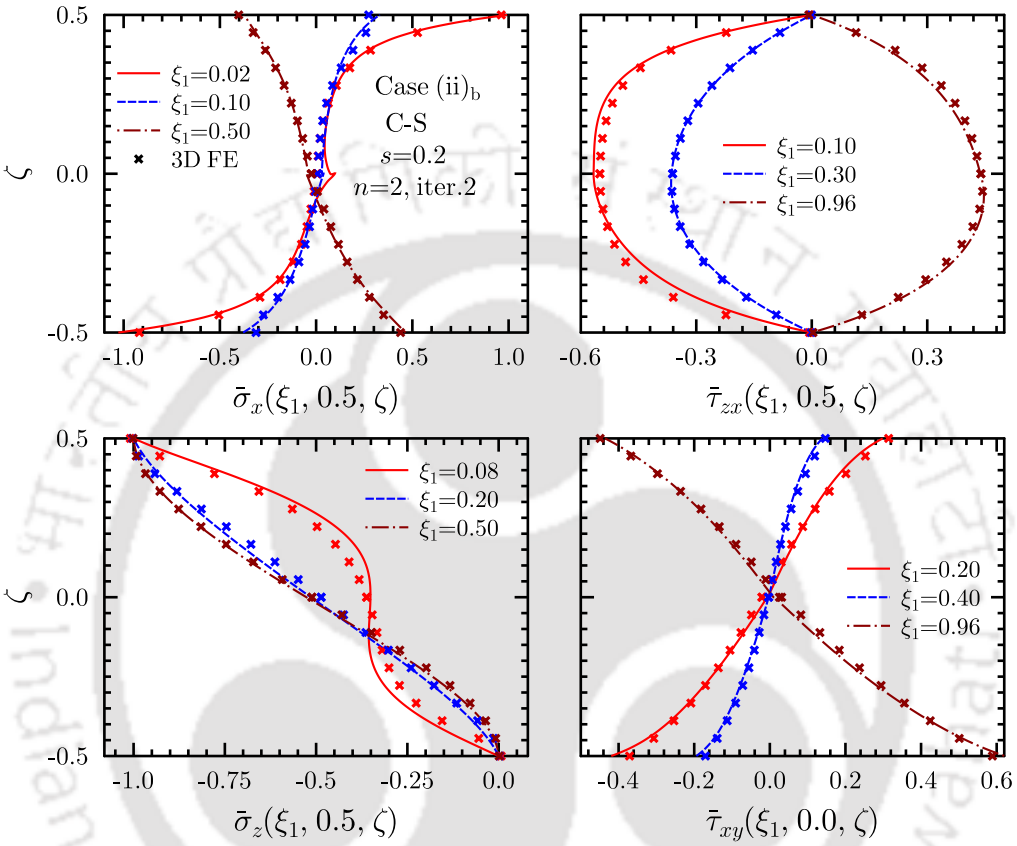

Fig. 3.11: Comparison of stresses distributions at different ξ_1-locations with 3D FE solution for two layered thick FGM plate ($s = 0.2$) under Case (ii)$_\mathrm{b}$ and subjected to C–S boundary condition

3.6.3 Accurate Estimation of Interlaminar Stresses for Laminated Rectangular Plates Bonded with Functionally Graded Adhesive Interlayer

Adhesively bonded joints are extensively used in aerospace, automotive and civil engineering due to higher fatigue resistance and the ability to join dissimilar materials [297]. Environmental factors, such as temperature and moisture degrading the mechanical properties and strength of adhesive joints [298]. On another hand, functionally grade adhesives have been developed to optimize the joint strength and to reduce the stress concentrations occurring in bonded joints [299]. For both cases, the elastic property of the adhesive varies along the particular coordinates. Hence, efficient three-dimensional analytical methods which can provide accurate stress solution for adhesive joints are required. Therefore to model these cases analytically and to provide benchmark results for such cases, an adhesively bonded rectangular plate is considered for the present study, as shown

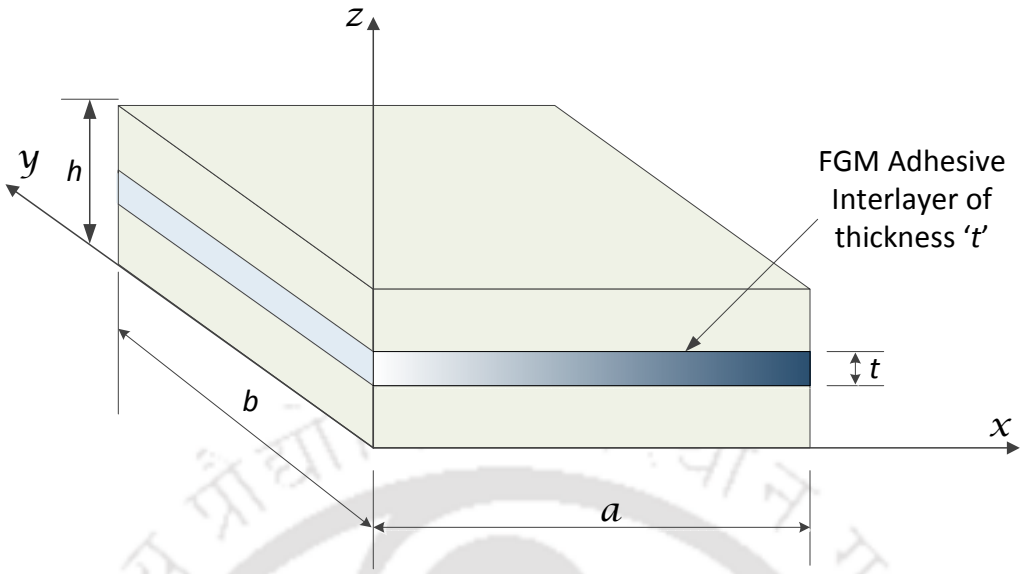

Fig. 3.12: Geometry of the adhesively bonded laminated plate.

in Fig. 3.12. The plates are made of orthotropic elastic material (Mat. 1) and bonded with a functionally graded adhesive interlayer (Mat. 2) of thickness t. The mechanical properties of adhesive layer are assumed to vary linearly along x-axis and their influence on bending response of bonded plate subjected to mechanical loading is investigated.

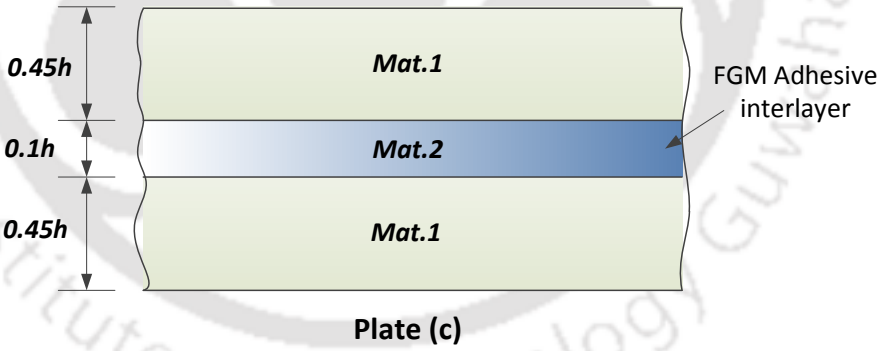

Fig. 3.13: Configuration of adhesively bonded laminated plate.

Numerical results are presented for two layered square plate (c) adhesively bonded by a functionally graded adhesive interlayer of thickness $t = 0.1h$ and $s = 0.2$, as shown in Fig. 3.12. Results are plotted for four cases, Case $(\text{i})_{\text{ad}}$: plate are assumed to be perfectly bonded i.e. no physical adhesive interlayer; Case $(\text{ii})_{\text{ad}}$: plate with adhesive interlayer ($t = 0.1h$) and the properties of adhesive interlayer are constant *i.e.* $\delta_1 = \delta_2 = 0$; Case $(\text{iii})_{\text{ad}}$: the properties of adhesive interlayer ($t = 0.1h$) are varying with index $\delta_1 = \delta_2 = 1.0$; Case $(\text{iv})_{\text{ad}}$: the properties of adhesive interlayer ($t = 0.1h$) are varying with index $\delta_1 = \delta_2 = 2.0$. The plate response is obtained for pressure load $p_2 = p_0 \sin \pi\xi_2$ at the top of the plate. Where, p_0 is the magnitude of applied pressure. The

material properties of the plate are taken as Mat. 1 and material properties of isotropic adhesive interlayer taken as Mat. 2. The results are non-dimensionalized with $Y_0 = 10.3$ GPa and $p_0 = 1$. using Eq. (3.42). The longitudinal variation of deflection ($\bar{w}$) and stresses (normal and shear) for functionally graded adhesive bonded plate are presented in Figs. 3.14, 3.15, 3.16 and 3.17 for S–S (Simply supported-Simply supported), C–S (Clamped–Simply supported), C–F (Clamped–Free), and S–F (Simply supported–Free) boundary conditions, respectively. In these figures, 3D FE results are also plotted for Case $(iii)_{ad}$. It is evident from the Figs. 3.14, 3.15, 3.16 and 3.17 that present results are in good agreement with 3D FE results for all the support conditions. For Simply supported boundary conditions (S–S and S–F) single term solution (n=1, iter.1) gives accurate results. Where for clamped supports (C–S and C–F), two terms solution (n=2, iter.2) is needed to predict the behaviour accurately.

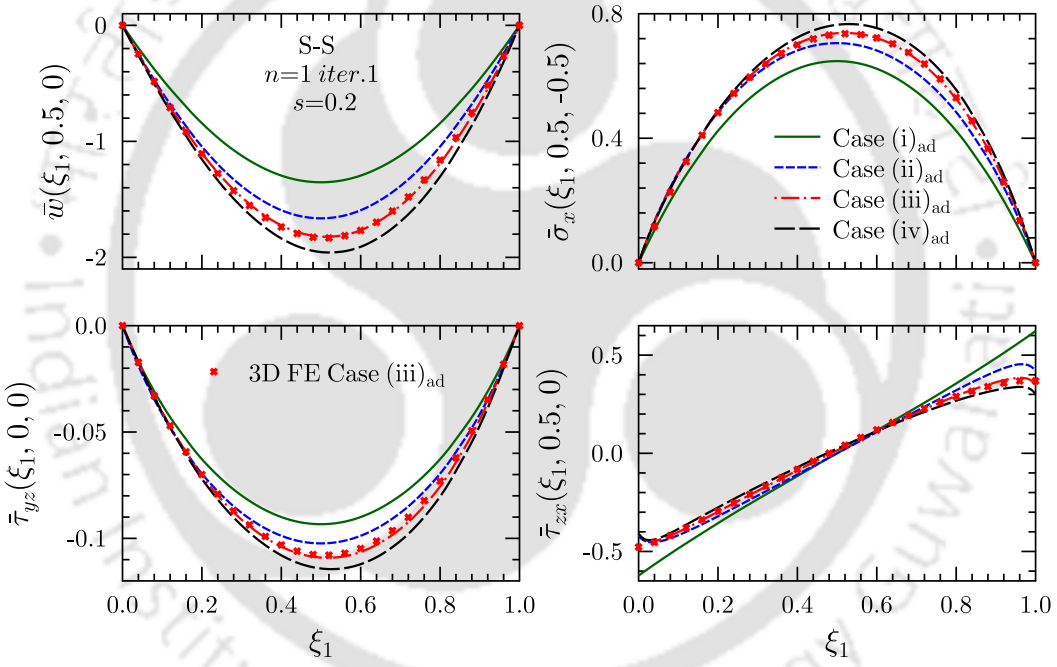

Fig. 3.14: Effect of variation in properties of adhesive layer on longitudinal variations of deflection and stresses for plate subjected to S–S boundary conditionn

From Fig. 3.14 and 3.15, it is observed that for S–S boundary condition the deflection ($\bar{w}$) and stresses ($\bar{\sigma}_x$, $\bar{\tau}_{yz}$ and $\bar{\tau}_{zx}$) are significantly affected with the in-plane gradation of adhesive interlayer properties. But for C–S case, only $\bar{w}$, $\bar{\tau}_{yz}$ and $\bar{\tau}_{zx}$ are affected more as compared to $\bar{\sigma}_x$. For both S–S and C–S support conditions, it is observed that the maximum deflection and stresses of plate increases and their point of maxima shifted toward the right side of the plate ($\xi = 1$) as the property variation index of adhesive interlayer increases. And for both cases, the magnitude of transverse shear stress $\bar{\tau}_{zx}$ decreases in adhesive layer as the variation index increases. For C–F boundary condition, $\bar{w}$ and $\bar{\tau}_{zx}$ are significantly affected by in-plae property gradation, while $\bar{\sigma}_x$ and $\bar{\tau}_{yz}$ are

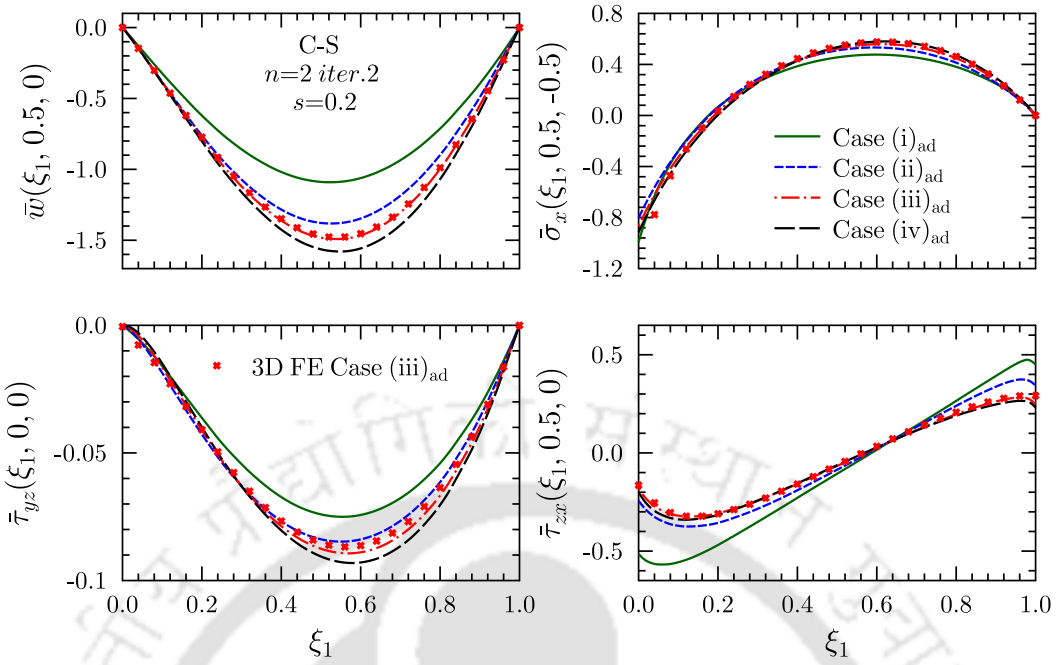

Fig. 3.15: Effect of variation in properties of adhesive layer on longitudinal variations of deflection and stresses for plate subjected to C–S boundary condition

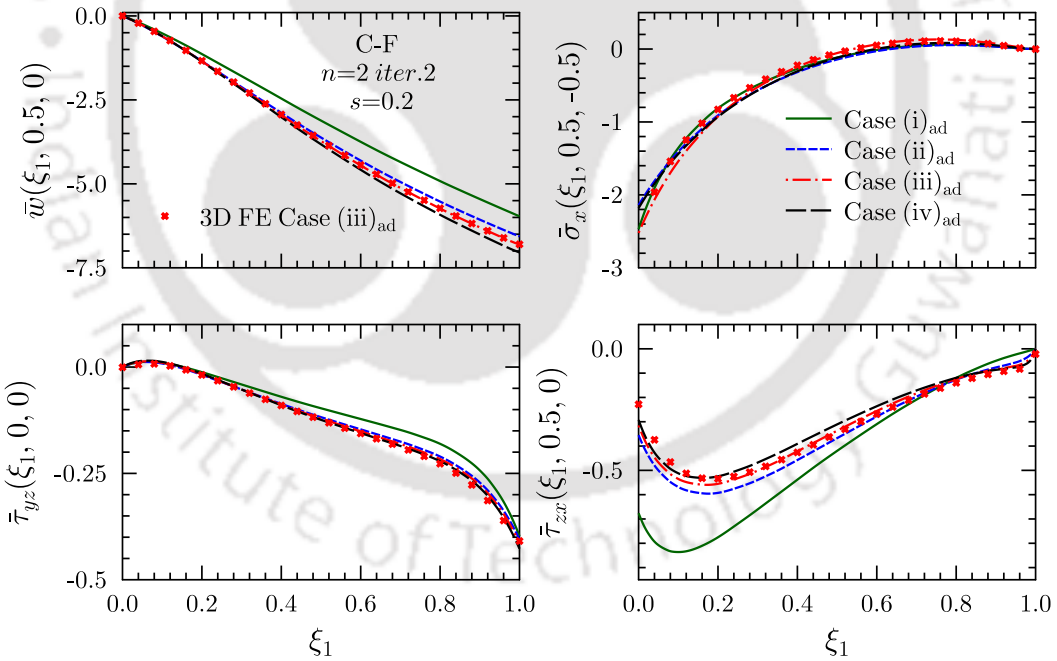

Fig. 3.16: Effect of variation in properties of adhesive layer on longitudinal variations of deflection and stresses for plate subjected to C–F boundary condition

least affected. For S–F condition, the effect of in-plane gradation of material properties of adhesive interlayer on deflection and stresses are comparatively less than other boundary conditions (S–S, C–F, C–S). For both C–F and S–F conditions, the magnitude of deflection $\bar{w}$ is increased whereas the shear stress $\bar{\tau}_{zx}$ in adhesive layer decreases as the variation index increases.

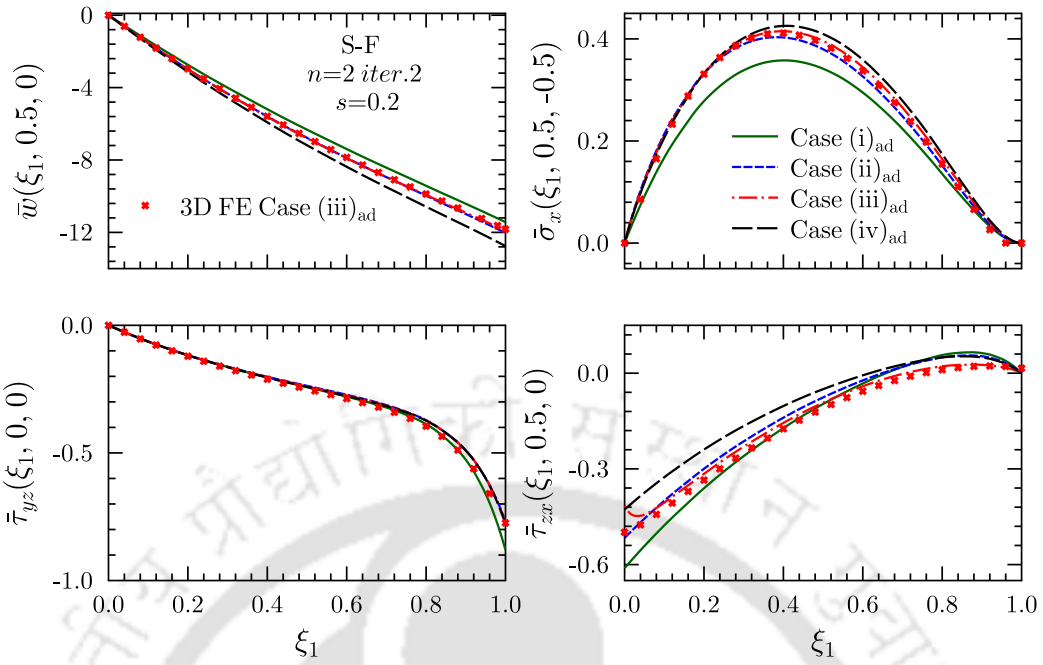

Fig. 3.17: Effect of variation in properties of adhesive layer on longitudinal variations of deflection and stresses for plate subjected to S–F boundary condition

3.7 NUMERICAL RESULTS FOR DYNAMIC CASE

For the present numerical study, two types of in-plane functionally graded plates, as shown in Fig. 3.2, are considered. Plate (a) is a single-layered in-plane FGM plate and Plate (b) is a two-layered FGM plate having different gradations in layers. To study the effect and benefits of in-plane gradation on the dynamic behaviour of plates, flexural frequencies and corresponding mode shapes are presented for various gradation cases, along with the constant (homogenous) property case, under different support conditions. The material properties for the present study are tabulated in Table 3.1. The natural frequencies ω are non-dimensionalized as $\omega^* = \omega h\sqrt{\rho/G_{12}}$. Where ρ and G_{12} are taken as 1578 Kg/m^3 and 7.17 GPa, respectively. The modal displacements and stresses are non-dimensionalized as:

$$(\bar{u},\, \bar{v},\, \bar{w}) = (u, v, w)/\max(u, v, w)$$

$$(\bar{\sigma}_x,\, \bar{\sigma}_y,\, \bar{\sigma}_z,\, \bar{\tau}_{zx},\, \bar{\tau}_{zy},\, \bar{\tau}_{xy}) = (\bar{\sigma}_x,\, \bar{\sigma}_y,\, \bar{\sigma}_z,\, \bar{\tau}_{zx},\, \bar{\tau}_{zy},\, \bar{\tau}_{xy})\, h/(s\, Y_0 \max(u, v, w))$$

Here $s(= h/a)$ represents the thickness-to-span ratio and max (w, v, u) denote the largest value of displacement w, v and u along the thickness of FGM plate in corresponding vibration mode. The length and width of the FGM rectangular plates is taken as unity $(a = b = 1)$ for all cases and further, the thickness of the rectangular plates is taken according to the thickness to span ratio $(s = h/a)$. For $s = 0.1, 0.2, 0.5$ the values of h are 0.1, 0.2, 0.5, respectively. The FGM plates are designated according to their support conditions at the edges $\xi_1 = 0, 1$. For example,

the functionally graded plate which is clamped (C) at $\xi_1 = 0$ and free (F) at $\xi_1 = 1$, is named as C–F plate. In the subsequential sections, converged numerical results are obtained by taking n=1, iter.2 for S–S boundary condition and n=1, iter.3 for other boundary conditions. To study the benefits and effects of in-plane gradation of material properties on the dynamic behaviour of the rectangular plates, three type of material property gradation cases are considered for plate (a), Case (i)$_a$: $\delta_1 = \delta_2 = \delta_p = 0.5$; Case (ii)$_a$: $\delta_1 = \delta_2 = \delta_p = 1.0$; and Case (iii)$_a$: $\delta_1 = 2.0$, $\delta_2 = 1.0$, $\delta_p = 1.5$ along with constant property (homogenous plate) case (Constant: $\delta_1 = \delta_2 = \delta_p = 0.0$). Similarly, two types of gradation cases are adopted for plate (b), along with constant property case

- Constant: Bottom layer- $\delta_1 = \delta_2 = \delta_p = 0.0$; Top layer- $\delta_1 = \delta_2 = \delta_p = 0.0$
- Case (i)$_b$: Bottom layer- $\delta_1 = \delta_2 = \delta_p = 0.0$; Top layer- $\delta_1 = \delta_2 = \delta_p = 0.5$
- Case (ii)$_b$: Bottom layer- $\delta_1 = \delta_2 = \delta_p = 0.5$; Top layer- $\delta_1 = \delta_2 = \delta_p = 1.0$

3.7.1 Validation

First of all, in Table 3.3, the accuracy of the present EKM solution is validated by comparing the present results for constant property case with the available results from literature reported by Kumari and Behera [283] for Levy-type composite plate. The numerical results is compared for a four-layered composite rectangular plate, made of graphite-epoxy (Mat.1) with symmetric layup $[0^o/90^o/90^o/0^o]$ and each ply has an equal thickness of $0.25h$ (a=b=1). The lowest five dimensionless flexural frequencies for m=1 and lowest four flexural frequencies for m=2 and 3 are compared in Table 3.3 for the S–S, C–C, C–F and F–F supports. To compare the numerical results, natural frequency parameters reported by Kumari and Behera [283] has been further non-dimensionalized as $\omega^* = \omega h\sqrt{\rho/G_{12}}$. It is observed that the presented results match excellently with Ref. [283] for all types of support conditions. Single-term EKM solution is sufficient to obtained the converged numerical results.

Because, no 3D elasticity based analytical solution is available in the literature for the in-plane FGM rectangular plates. Therefore, the accuracy and efficiency of the present solution for the in-plane FGM plates are verified by comparing the numerical results with 3D FE results. Commercial FE software ABAQUS [294] has been used to obtain the 3D FE results. For functionally graded rectangular plates, the spatial gradation in elastic property (at different Gauss points) has been implemented by employing user material subroutine (UMAT) [296]. The in-plane variation of mass density has been implemented by dividing the rectangular plate into 20 equal parts along the x-axis, and each part is assigned density value according to its center point. In Table 3.4, dimensionless flexural frequencies of single-layered plate (a) are compared with 3D FE results for S–S, C–C and

Table 3.3: Comparison of first five lowest natural frequency parameters $\omega^* = \omega h\sqrt{\rho/G_{12}}$ for four layered composite plate $[0^o/90^o/90^o/0^o]$ subjected to different sets of boundary conditions ($s = 0.2$)

(m)	S–S		C–C	
	Present	Ref. [283]	Present	Ref. [283]
1	0.1026096	0.1026096	0.1167292	0.1167276
	0.2098519	0.2098519	0.2162690	0.2162918
	0.3288927	0.3288927	0.3346613	0.3385567
	0.4541276	0.4541216	0.4585323	0.4584964
	0.5824980	0.5824980	0.5859834	0.5859750
2	0.1903298	0.1903298	0.1959211	0.1959163
	0.2664622	0.2664622	0.2704079	0.2702988
	0.3693200	0.3693200	0.3737919	0.3737823
	0.4855598	0.4855598	0.4892777	0.4892633
3	0.3070274	0.3070274	0.3092291	0.3092279
	0.3604963	0.3604963	0.3627004	0.3626836
	0.4430541	0.4430541	0.4463166	0.4463070
	0.5447686	0.5447686	0.5477733	0.5477650

(m)	C–F		F–F	
	Present	Ref. [283]	Present	Ref. [283]
1	0.0662324	0.0662323	0.0526757	0.0527126
	0.1410966	0.1411062	0.0720339	0.0720333
	0.2570523	0.2577978	0.1872843	0.1872747
	0.3766013	0.3781450	0.2969559	0.2919807
	0.5080375	0.5080088	0.4245017	0.4281728
2	0.1701329	0.1701233	0.1640790	0.1641066
	0.2172614	0.2172866	0.1805963	0.1805747
	0.3069279	0.3069267	0.2530791	0.2526920
	0.4134809	0.4028713	0.3438783	0.3442019
3	0.2932440	0.2932392	0.2894769	0.2894757
	0.3261264	0.3261875	0.3027629	0.3027557
	0.3923024	0.3924678	0.3523485	0.3523401
	0.4810292	0.4810892	0.4234002	0.4217126

C–F support conditions. The lowest three flexural frequencies are compared for m=1, 2 and 3. The numerical results are compared for constant property (homogenous) case along with gradation Case $(i)_a$. It is observed that the present numerical results are in excellent agreement with 3D

Table 3.4: Comparison of first five lowest natural frequency parameters $\omega^* = \omega h\sqrt{\rho/G_{12}}$ for single layered axially graded beams subjected to different sets of boundary conditions ($s = 0.1$)

	(m)	S–S		C–C		C–F	
		EKM	3D FE	EKM	3D FE	EKM	3D FE
Constant	1	0.1425721	0.1425712	0.2227041	0.2236401	0.0669087	0.0669467
		0.4148485	0.4148502	0.4720976	0.4746283	0.2500707	0.2508939
		0.7262878	0.7262974	0.7607679	0.7651472	0.5384486	0.5406553
	2	0.2054364	0.2054355	0.2539541	0.2627463	0.1472369	0.1472786
		0.4511420	0.4511356	0.5001534	0.5026013	0.3024082	0.3030464
		0.7518266	0.7518239	0.7826607	0.7869303	0.5716474	0.5738457
	3	0.3223617	0.3223534	0.3560484	0.3566639	0.2782057	0.2782656
		0.5263012	0.5263003	0.5642607	0.5665061	0.4015708	0.4022933
		0.8041029	0.8041150	0.8300865	0.8341219	0.6383723	0.6404033
Case(i)_a	1	0.1150735	0.1150757	0.1780050	0.1795169	0.0537628	0.0538150
		0.3325363	0.3325522	0.3785238	0.3805692	0.2034720	0.2042711
		0.5814061	0.5814801	0.6099282	0.6134324	0.4382743	0.4398167
	2	0.1725708	0.1725752	0.2154839	0.2163211	0.1222421	0.1223239
		0.3656333	0.3656542	0.4042664	0.4062726	0.2485905	0.2491990
		0.6045334	0.6046485	0.6297943	0.6332111	0.4668994	0.4684088
	3	0.2786048	0.2785958	0.3031225	0.3036065	0.2340916	0.2341690
		0.4358736	0.4358374	0.4648379	0.4664928	0.3375127	0.3381233
		0.6535053	0.6536087	0.6742895	0.6776025	0.5272912	0.5285405

FE results for both cases and for all the support conditions. From these comparisons of numerical results, It is established that the single-term EKM solution is adequate for obtaining accurate natural frequencies for all the gradation cases and boundary conditions.

In the subsequential subsections, 3D FE results are not tabulated along with present EKM results, but all numerical results have been thoroughly verified with 3D FE results. Furthermore, it is observed that present numerical results are in excellent agreement for all support conditions and gradation cases, and the difference between the present and the FE results are less than 2% for all the cases and support conditions. It shows that the present method is very accurate and efficient in predicting the natural frequencies and mode shape of FGM and composite plate. Further, the effect and benefits of in-plane gradation are assessed and discussed in subsequential subsections.

3.7.2 Plate (a): Single Layer FGM Plate

A single-layer plate (a), as shown in Fig. 3.2, is considered for study in this section. First five lowest dimensionless flexural frequencies, $\omega^* = \omega h\sqrt{\rho/G_{12}}$, are tabulated for m=1, 2 and 3. Results are presented for different variation cases, Case (i)$_a$: $\delta_1 = \delta_2 = \delta_p = 0.5$; Case (ii)$_a$: $\delta_1 = \delta_2 = \delta_p = 1.0$; and Case (iii)$_a$: $\delta_1 = 2.0$, $\delta_2 = 1.0$, $\delta_p = 1.5$ along with constant properties (homogeneous) case (Constant: $\delta_1 = \delta_2 = \delta_p = 0.0$) to investigating the effect and benefits of in-plane gradation of material properties on natural frequencies of plate.

(A): *Effect of in-plane gradation under different boundary conditions*

In Tables 3.5, 3.6, 3.7, 3.8, 3.9 and 3.10, benchmark numerical results are tabulated for S–S, C–S, C–C, C–F, S–F and F–F plates, respectively. The significant effect of in-plane gradation is observed on the flexural frequencies of the rectangular plates. As the variation indexes increases, the flexural frequencies of the rectangular plate decreases significantly under all the boundary conditions. But the quantitative effect largely depends upon the boundary conditions of the plate. Percentage change in natural frequencies are tabulated in Table 3.11 and 3.12, for all the support conditions (S–S, C–S, C–C, C–F, S–F and F–F). The percentage change in natural frequencies for S–S, C–S and C–C plate is tabulated in Table 3.11 and for C–F, S–F and F–F plate in table 3.12.

Table 3.5: Effect of in-plane gradation of material properties on natural frequencies $\omega^* = \omega h\sqrt{\rho/G_{12}}$ of single layer FGM plate (a) subjected to S–S boundary condition

(m)	Constant	Case (i)$_a$	Case (ii)$_a$	Case (iii)$_a$
1	0.1425721	0.1150735	0.0966053	0.0819778
	0.4148485	0.3325363	0.2775608	0.2402042
	0.7262878	0.5814061	0.4845722	0.4289112
	1.0430678	0.8346518	0.6953110	0.6237631
	1.3593445	1.0876254	0.9059480	0.8191832
2	0.2054364	0.1725708	0.1500175	0.1344698
	0.4511420	0.3656333	0.3085388	0.2719432
	0.7518266	0.6045334	0.5058334	0.4515771
	1.0630849	0.8527464	0.7120944	0.6414706
	1.3760404	1.1026733	0.9198956	0.8338811
3	0.3223617	0.2786048	0.2430172	0.2260948
	0.5263012	0.4358736	0.3725765	0.3398080
	0.8041029	0.6535053	0.5547957	0.4981686
	1.1031779	0.8903032	0.7476461	0.6778960
	1.4088210	1.1333276	0.9486382	0.8629330

For all the support conditions except F–F conditions, nearly 13 to 20% decrement is observed in first five flexural frequencies (m=1,2 and 3) for Case $(i)_a$, as compared to constant property case. The percentage decrement in natural frequencies is 24 to 33% for Case $(ii)_a$ and 34 to 43% for Case $(iii)_a$, respectively. Where for F–F support conditions, these decrements are 10-19 % for Case $(i)_a$, 20-33 % for Case $(ii)_a$ and 25-40 % for Case $(iii)_a$.

For all the variation cases, the effect of support conditions is significant on the lower mode natural frequencies (under m=1,2 and 3), and it is maximum for first vibration mode (m=1). But, the effect of boundary conditions is minimum on higher mode frequencies.

Table 3.6: Effect of in-plane gradation of material properties on natural frequencies $\omega^* = \omega h\sqrt{\rho/G_{12}}$ of single layer FGM plate (a) subjected to C–S boundary condition

(m)	Constant	Case $(i)_a$	Case $(ii)_a$	Case $(iii)_a$
1	0.1820873	0.1476743	0.1242689	0.1071697
	0.4452511	0.3608331	0.3034281	0.2649520
	0.7436884	0.5999118	0.5030228	0.4480569
	1.0532592	0.8467764	0.7083753	0.6374602
	1.3658407	1.0960417	0.9156072	0.8292331
2	0.2323129	0.1932914	0.1655077	0.1484402
	0.4767983	0.3891646	0.3296358	0.2927789
	0.7673456	0.6209753	0.5223555	0.4682790
	1.0724169	0.8638151	0.7239697	0.6538217
	1.3820931	1.1105023	0.9288321	0.8431244
3	0.3380868	0.2892516	0.2544694	0.2314260
	0.5458365	0.4532215	0.3898633	0.3523233
	0.8170570	0.6671905	0.5661305	0.5117914
	1.1113784	0.8999612	0.7581754	0.6882036
	1.4142624	1.1403428	0.9570545	0.8715674

Table 3.7: Effect of in-plane gradation of material properties on natural frequencies $\omega^* = \omega h\sqrt{\rho/G_{12}}$ of single layer FGM plate (a) subjected to C–C boundary condition

(m)	Constant	Case (i)$_a$	Case (ii)$_a$	Case (iii)$_a$
1	0.2227041	0.1780050	0.1493068	0.1308622
	0.4720976	0.3785238	0.3162815	0.2812500
	0.7607679	0.6099282	0.5097815	0.4567369
	1.0633306	0.8521088	0.7117493	0.6420879
	1.3724927	1.0993737	0.9176639	0.8319970
2	0.2616608	0.2154839	0.1842016	0.1650199
	0.5001534	0.4042664	0.3403797	0.3053003
	0.7826607	0.6297943	0.5280978	0.4758059
	1.0816806	0.8686429	0.7269769	0.6579280
	1.3882657	1.1135502	0.9306850	0.8455970
3	0.3560484	0.3031225	0.2658557	0.2419960
	0.5642607	0.4648379	0.3975473	0.3619082
	0.8300865	0.6742895	0.5715551	0.5190343
	1.1195610	0.9039932	0.7607151	0.6906642
	1.4198357	1.1430192	0.9584940	0.8736457

Table 3.8: Effect of in-plane gradation of material properties on natural frequencies $\omega^* = \omega h\sqrt{\rho/G_{12}}$ of single layer FGM plate (a) subjected to C–F boundary condition

(m)	Constant	Case (i)$_a$	Case (ii)$_a$	Case (iii)$_a$
1	0.0669087	0.0537628	0.0454504	0.0399131
	0.2500707	0.2034720	0.1725264	0.1477007
	0.5384486	0.4382743	0.3681862	0.3218164
	0.8474500	0.6861109	0.5765327	0.5123440
	1.1643415	0.9389467	0.7867490	0.7064540
2	0.1472369	0.1222421	0.1058995	0.0955152
	0.3024082	0.2485905	0.2122287	0.1886386
	0.5716474	0.4668994	0.3953527	0.3429290
	0.8727587	0.7079618	0.5961783	0.5330539
	1.1846583	0.9566027	0.8026838	0.7232003
3	0.2782057	0.2340916	0.2034468	0.1845911
	0.4015708	0.3375127	0.2938145	0.2629360
	0.6383723	0.5272912	0.4471520	0.3951861
	0.9224246	0.7528778	0.6391190	0.5760833
	1.2239314	0.9922358	0.8361943	0.7566077

Table 3.9: Effect of in-plane gradation of material properties on natural frequencies $\omega^* = \omega h\sqrt{\rho/G_{12}}$ of single layer FGM plate (a) subjected to S–F boundary condition

(m)	Constant	Case (i)$_a$	Case (ii)$_a$	Case (iii)$_a$
1	0.0447272	0.0367078	0.0316394	0.0287197
	0.2134392	0.1705476	0.1436556	0.1211490
	0.5113743	0.4120654	0.3445962	0.2971249
	0.8335024	0.6706028	0.5605919	0.4954323
	1.1557035	0.9283994	0.7751170	0.6942275
2	0.1379960	0.1162426	0.1018674	0.0923503
	0.2746891	0.2255231	0.1929558	0.1700130
	0.5489012	0.4449527	0.3750360	0.3296238
	0.8602997	0.6941305	0.5820497	0.5181702
	1.1767957	0.9470010	0.7921054	0.7121520
3	0.2718605	0.2318479	0.2034240	0.1836970
	0.3833444	0.3232067	0.2829903	0.2570355
	0.6207943	0.5103568	0.4363542	0.3910331
	0.9118809	0.7412158	0.6262765	0.5630094
	1.2170637	0.9838447	0.8267497	0.7473105

Table 3.10: Effect of in-plane gradation of material properties on natural frequencies $\omega^* = \omega h\sqrt{\rho/G_{12}}$ of single layer FGM plate (a) subjected to F–F boundary condition

(m)	Constant	Case (i)$_a$	Case (ii)$_a$	Case (iii)$_a$
1	0.0334670	0.0298129	0.0266799	0.0250349
	0.0667265	0.0556371	0.0487996	0.0448874
	0.2971237	0.2400280	0.2013481	0.1705164
	0.6137324	0.4916101	0.4092548	0.3562210
	0.9460649	0.7570368	0.6306249	0.5582979
2	0.1265390	0.1121850	0.0987733	0.0901766
	0.1660722	0.1377347	0.1251342	0.1235318
	0.3413613	0.2896543	0.2479217	0.2197796
	0.6521474	0.5261801	0.4391564	0.3882465
	0.9735730	0.7816312	0.6521426	0.5806018
3	0.2630859	0.2313337	0.1985303	0.1839427
	0.3004953	0.2617255	0.2491802	0.2321499
	0.4587361	0.3826996	0.3319370	0.3074037
	0.7214791	0.5903665	0.5029101	0.4466918
	1.0243607	0.8281448	0.6972155	0.6306201

Table 3.11: Percentage change in natural frequencies of plate (a) due to in-plane gradation of material properties under S–S, C–S and C–C boundary conditions

(m)	S–S			C–S			C–C		
	Case (i)$_a$	Case (ii)$_a$	Case (iii)$_a$	Case (i)$_a$	Case (ii)$_a$	Case (iii)$_a$	Case (i)$_a$	Case (ii)$_a$	Case (iii)$_a$
1	19.29	32.24	42.50	18.90	31.75	41.14	20.07	32.96	41.24
	19.84	33.09	42.10	18.96	31.85	40.49	19.82	33.01	40.43
	19.95	33.28	40.94	19.33	32.36	39.75	19.83	32.99	39.96
	19.98	33.34	40.20	19.60	32.74	39.48	19.86	33.06	39.62
	19.99	33.35	39.74	19.75	32.96	39.29	19.90	33.14	39.38
2	16.00	26.98	34.54	16.80	28.76	36.10	17.65	29.60	36.93
	18.95	31.61	39.72	18.38	30.86	38.59	19.17	31.94	38.96
	19.59	32.72	39.94	19.07	31.93	38.97	19.53	32.53	39.21
	19.79	33.02	39.66	19.45	32.49	39.03	19.70	32.79	39.18
	19.87	33.15	39.40	19.65	32.80	39.00	19.79	32.96	39.09
3	13.57	24.61	29.86	14.44	24.73	31.55	14.86	25.33	32.03
	17.18	29.21	35.43	16.97	28.58	35.45	17.62	29.55	35.86
	18.73	31.00	38.05	18.34	30.71	37.36	18.77	31.15	37.47
	19.30	32.23	38.55	19.02	31.78	38.08	19.25	32.05	38.31
	19.55	32.66	38.75	19.37	32.33	38.37	19.50	32.49	38.47

Table 3.12: Percentage change in natural frequencies of plate (a) due to in-plane gradation of material properties under C–F, S–F and F–F boundary conditions

(m)	C–F			S–F			F–F		
	Case $(i)_a$	Case $(ii)_a$	Case $(iii)_a$	Case $(i)_a$	Case $(ii)_a$	Case $(iii)_a$	Case $(i)_a$	Case $(ii)_a$	Case $(iii)_a$
1	19.65	32.07	40.35	17.93	29.26	35.79	10.92	20.28	25.20
	18.63	31.01	40.94	20.10	32.69	43.24	16.62	26.87	32.73
	18.60	31.62	40.23	19.42	32.61	41.90	19.22	32.23	42.61
	19.04	31.97	39.54	19.54	32.74	40.56	19.90	33.32	41.96
	19.36	32.43	39.33	19.67	32.93	39.93	19.98	33.34	40.99
2	16.98	28.08	35.13	15.76	26.18	33.08	11.34	21.94	28.74
	17.80	29.82	37.62	17.90	29.75	38.11	17.06	24.65	25.62
	18.32	30.84	40.01	18.94	31.68	39.95	15.15	27.37	35.62
	18.88	31.69	38.92	19.32	32.34	39.77	19.32	32.66	40.47
	19.25	32.24	38.95	19.53	32.69	39.48	19.72	33.02	40.36
3	15.86	26.87	33.65	14.72	25.17	32.43	12.07	24.54	30.08
	15.95	26.83	34.52	15.69	26.18	32.95	12.90	17.08	22.74
	17.40	29.95	38.09	17.79	29.71	37.01	16.58	27.64	32.99
	18.38	30.71	37.55	18.72	31.32	38.26	18.17	30.29	38.09
	18.93	31.68	38.18	19.16	32.07	38.60	19.15	31.94	38.44

(B): *Effect of in-plane gradation under different thickness (aspect) ratio (s)*

The effect of thickness ration (s) on natural frequencies of the plate (a) is assessed in Table 3.13 for different gradation cases. First five flexural frequencies of the plate (a) are tabulated in

Table 3.13: Effect of aspect ratio (s) on first five flexural frequencies of single layer FGM plate (a) subjected to C–F boundary condition

s	Mode	Constant	Case (i)$_a$	Case (ii)$_a$	Case (iii)$_a$
0.1	1	0.0669087	0.0537628	0.0454504	0.0399131
	2	0.1472369	0.1222421	0.1058995	0.0955152
	3	0.2500707	0.2034720	0.1725264	0.1477007
	4	0.2782057	0.2340916	0.2034468	0.1845911
	5	0.3024082	0.2485905	0.2122287	0.1886386
0.2	1	0.2293158	0.1858316	0.1577729	0.1398770
	2	0.4821463	0.4036489	0.3517734	0.3173398
	3	0.6749415	0.5547981	0.4711157	0.4148511
	4	0.8353930	0.6977093	0.6017672	0.5451425
	5	0.8372359	0.7055719	0.6178758	0.5577322
0.5	1	0.9063975	0.7465338	0.6405843	0.5768869
	2	1.7376933	1.4675503	1.2844077	1.1610341
	3	2.1162518	1.7358924	1.4741603	1.3368565
	4	2.6376425	2.2128526	1.9204224	1.7590696
	5	2.6847398	2.2764331	1.9954551	1.8015465

Table 3.13, under all gradation cases for different thickness ratios (s=0.1, 0.2, 0.5). It is observed that as the thickness ratio increases, the magnitude of flexural frequencies also increases because the plate becomes thicker. But effect of in-plane gradation almost same for the all thickness ratios. The percentage decrement in natural frequencies, due to gradation, are 15-19% for Case (i)$_a$, 25-32% for Case (ii)$_a$ and 33–40% for Case (iii)$_a$ under all the aspect ratio. This study shows that the effect of in-plane gradation is independent of the thickness of the plate. This fact is beneficial in the construction and design of components graded along the in-plane direction.

(B): *Effect of in-plane gradation of density*

Similarly, effect of in-plane gradation of density on the flexural frequencies of the plate (a) is studied in Table 3.14 under different boundary conditions such as S–S, C–S, C–F and F–F. The elastic properties of the plate kept constant by fix gradation indexes δ_1 and δ_2 equal to zero ($\delta_1 = \delta_2$=0). The effect of density variation is studied by varying only the density variation index (δ_p) according to δ_p=0, 0.5, 1.0, 1.5. First five flexural frequencies of the plate (a) are tabulated in

Table 3.14 for these density gradation cases. It is observed that as the density variation index (δ_p)

Table 3.14: Effect of variation in density on first five flexural frequencies $\omega^* = \omega h\sqrt{\rho/G_{12}}$ of single-layered FGM plate (a) subjected to different boundary conditions (s=0.1)

B.C.	Mode	δ_1=δ_2=0			
		δ_p=0	δ_p=0.5	δ_p=1	δ_p=1.5
S–S	1	0.1425721	0.1274750	0.1162967	0.1076021
	2	0.2054364	0.1836215	0.1674206	0.1548129
	3	0.3223617	0.2878792	0.2620851	0.2419757
	4	0.4148485	0.3716085	0.3400944	0.3156822
	5	0.4511420	0.4041418	0.3699325	0.3434192
C–S	1	0.1820873	0.1614841	0.1465213	0.1350415
	2	0.2323129	0.2061855	0.1871249	0.1724689
	3	0.3380868	0.3001908	0.2723100	0.2508150
	4	0.4452511	0.3996448	0.3660588	0.3398691
	5	0.4767983	0.4277893	0.3893587	0.3580320
C–F	1	0.0669087	0.0566491	0.0500037	0.0452537
	2	0.1472369	0.1249748	0.1104281	0.0999896
	3	0.2500707	0.2216122	0.2012618	0.1857058
	4	0.2782057	0.2364875	0.2089242	0.1890977
	5	0.3024082	0.2679640	0.2433948	0.2246158
F–F	1	0.0334670	0.0298558	0.0271495	0.0250425
	2	0.0667265	0.0602046	0.0558120	0.0525006
	3	0.1265390	0.1121890	0.1009767	0.0923069
	4	0.1660722	0.1506803	0.1408054	0.1333276
	5	0.2630859	0.2309417	0.2056881	0.1868528

increases, the natural frequency of the single-layered plate (a) decreases. The percentage decrement in natural frequencies 10–11% for δ_p=0.5 as compared to constant density case (δ_p=0) under S–S and C–S condition. Where the percentage decrement in natural frequencies is 17 to 19% for δ_p=1.0 and 23 to 25% for δ_p=1.5, respectively. It is observed that effect is nearby double as the value of density variation index (δ_p) make double from δ_p=0.5 to δ_p=1.0. The percentage decrement in natural frequencies under C–F condition are 11-15% for δ_p=0.5, 19-25% for δ_p=1.0 and 25-32% for δ_p=1.5. Similarly, the percentage decrement under F–F conditions are 9-12% for δ_p=0.5, 15-20% for δ_p=1.0 and 20-28% for δ_p=1.5. This study shows that the quantitative effect of density gradation also largely depends significantly upon boundary conditions of the plate.

The flexural mode shapes corresponding to the first four flexural frequencies of the plate (a) (s=0.1), under the constant case, are presented in Fig. 3.18 for S–S, C–S, C–C, C–F and F–F support conditions. The plate (a) vibrates in the symmetrical mode for S–S, C–C and F–F support condition, while asymmetrical mode for C–F, C–S case. Similarly, the first four flexural mode shapes of the plate (a) under Case $(ii)_a$ are also presented in Fig. 3.19 for S–S, C–S, C–C, C–F and F–F support conditions. It is observed that the shape of all flexural modes affected significantly by the gradation of material properties. The symmetrical flexural modes of S–S, C–C and F–F support conditions also become asymmetrical due to gradation of material properties.

Further, effect of in-plane gradation of properties on the longitudinal variation of displacements ($\bar{u}$, $\bar{v}$, $\bar{w}$)and stresses ($\bar{\sigma}_x$, $\bar{\sigma}_y$, $\bar{\tau}_{xy}$, $\bar{\tau}_{zx}$, $\bar{\tau}_{yz}$) are presented in Fig. 3.20 for the first vibration mode of FGM plate (a), (s=0.1), subjected to S–S support conditions. Similarly, the longitudinal variation of deflection and stresses, for first vibration mode of FGM plate (a)(s=0.1) and under all the gradation cases, are plotted in Fig. 3.21, 3.22, 3.23 and 3.24 under C–S, C–F, S–F and F–F boundary conditions, respectively. To evaluate the effects of gradation on deflections and stresses of the vibrating plate the numerical results for the constant properties case (homogeneous plate) are also potted in all the figures. The corresponding 3D FE results for gradation cases, Case $(i)_a$, are also plotted in these figures. The excellent agreement between present results and 3D FE results is observed for all support conditions. Further, significant effect of in-plane gradation on the stresses ($\bar{\sigma}_x$, $\bar{\tau}_{xy}$ and $\bar{\tau}_{zx}$) are observed for all the boundary conditions (S–S, S–F, F–F, C–F and C–S), whereas deflections ($\bar{u}$, $\bar{v}$, $\bar{w}$) are least affected under all the support conditions. The stresses $\bar{\sigma}_x$, $\bar{\tau}_{xy}$ and $\bar{\tau}_{zx}$ are decreasing significantly as the variation index increases. The variation of material properties along the x-direction significantly affects the x-dependent stresses ($\bar{\sigma}_x$, $\bar{\tau}_{xy}$ and $\bar{\tau}_{zx}$) for all the boundary conditions (S–S, C–S, C–C, C–F, S–F). However, the effect of gradation on other stresses (σ_y, τ_{xy}) is comparatively less for all the boundary conditions. The behavior of the plate under the F–F condition is quite different from the plate subjected to other boundary conditions. The plate becomes more sensitive under the F-F support condition. Therefore, all the entities are affected significantly by the in-plane gradation of material properties. Moreover, the effect of in-plane gradation of material properties is maximum for plate subjected to free support conditions, as compared to plate subjected to clamped support conditions. It shows that the effect of properties gradation on stresses and deflections becomes weaker as the plate subjected to clamped support conditions.

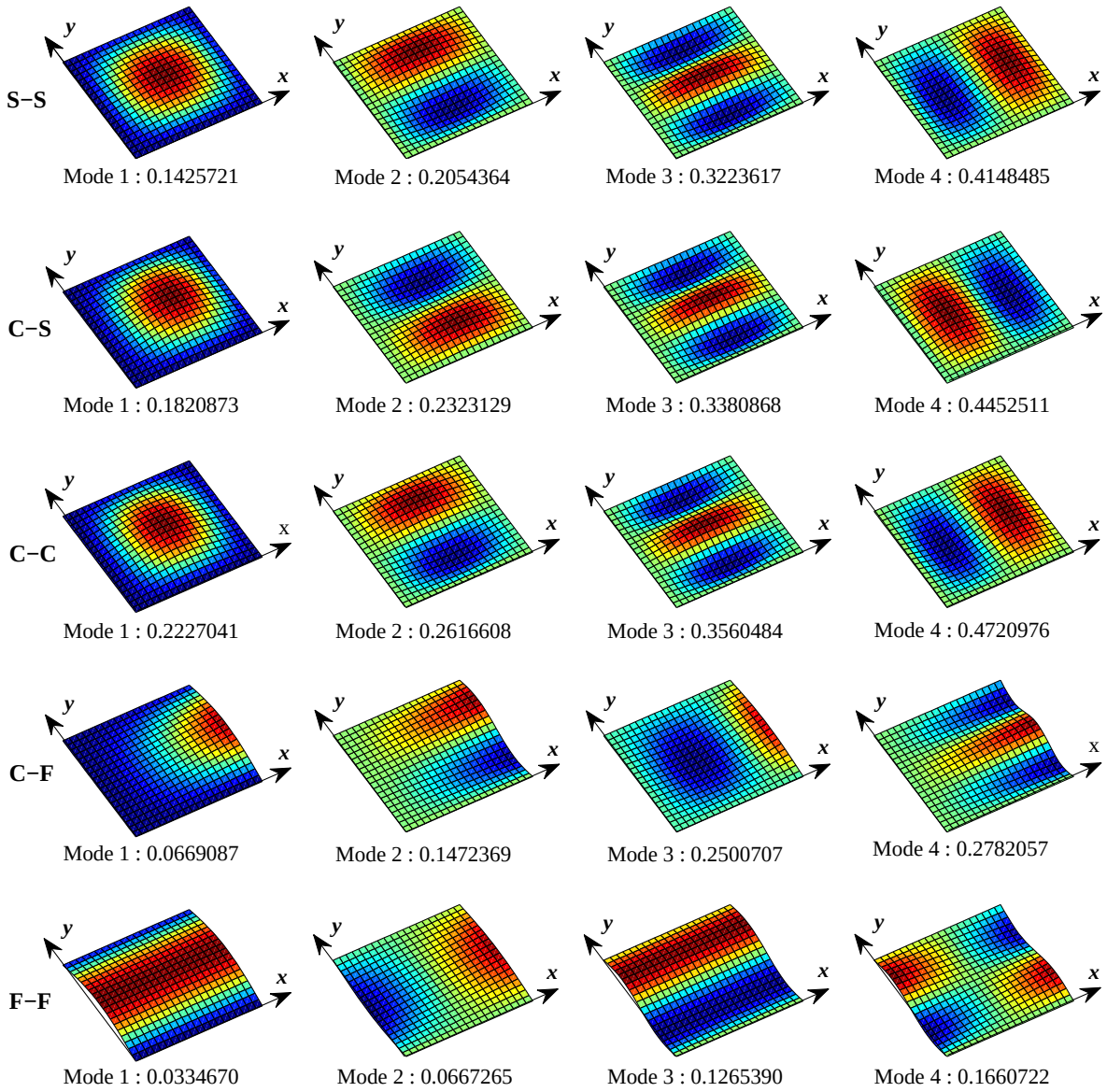

Fig. 3.18: First four flexural mode shapes with the frequencies for plate (a) (s=0.1) subjected to different boundary conditions (S–S, C–S, C–C, C–F and F–F), under constant properties case

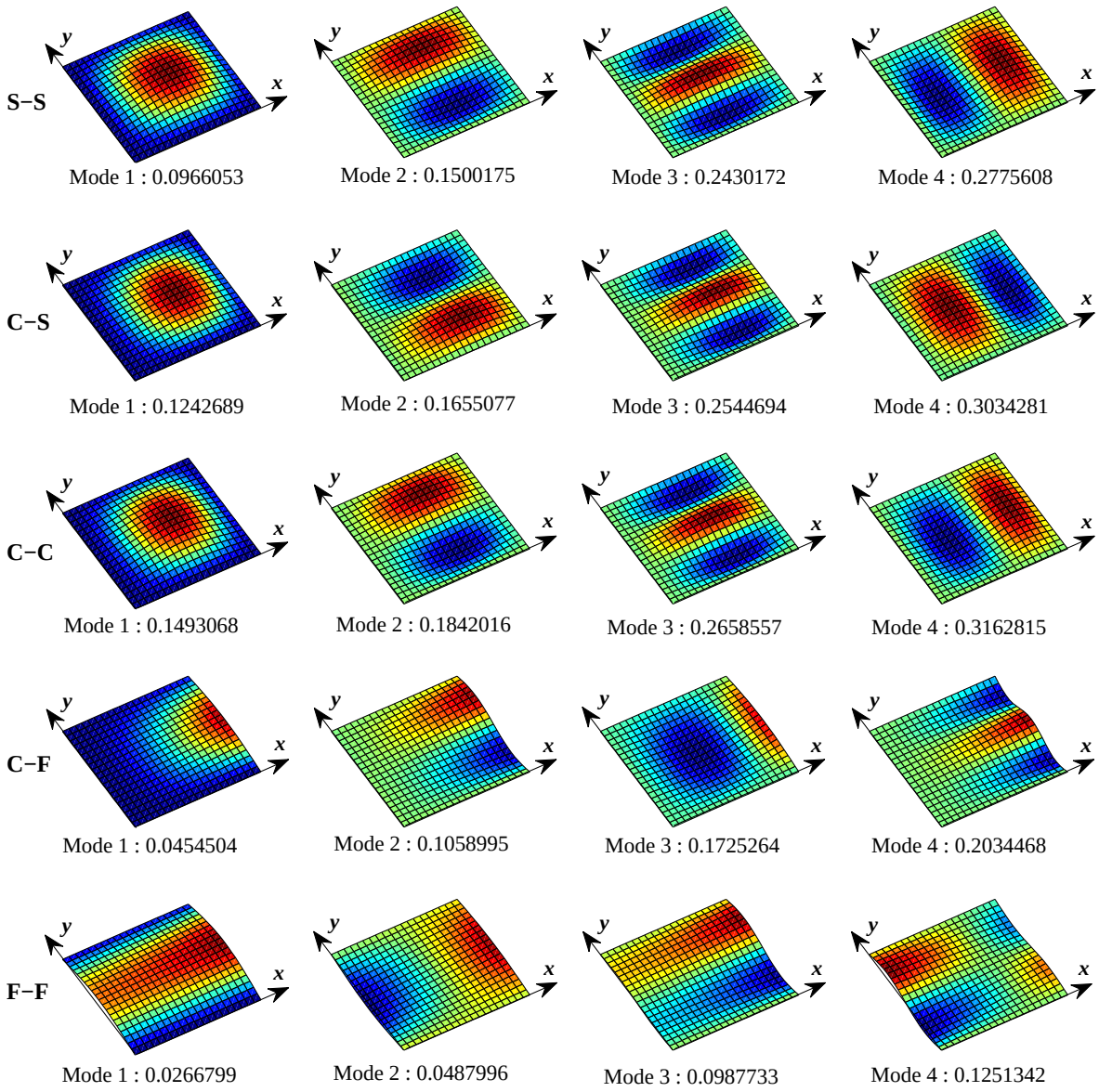

Fig. 3.19: First four flexural mode shapes with the frequencies for plate (a) (s=0.1) subjected to different boundary conditions (S–S, C–S, C–C, C–F and F–F), under Case(ii)$_{\mathrm{a}}$

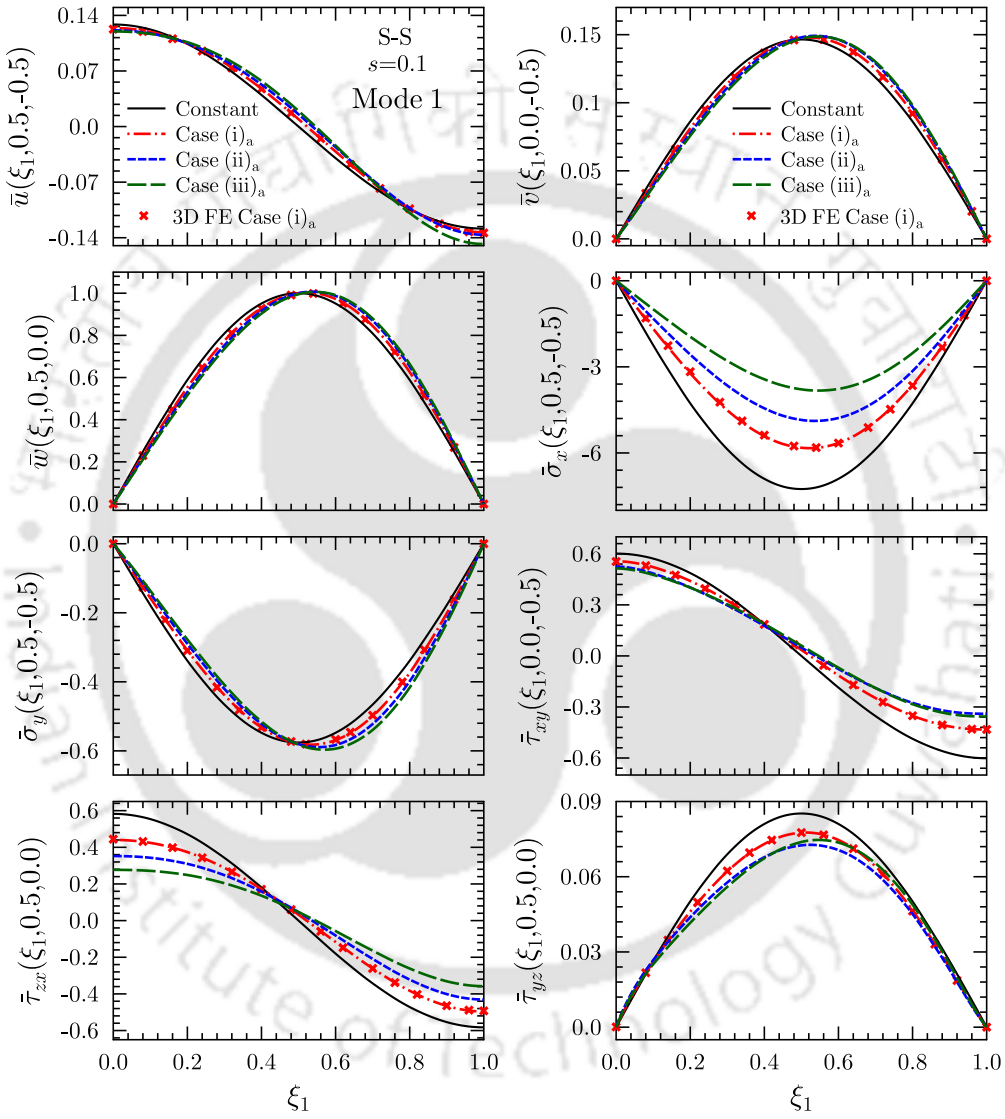

Fig. 3.20: Longitudinal variations of displacements and stresses for first vibration mode of plate (a) (Mode-1) under S–S boundary condition

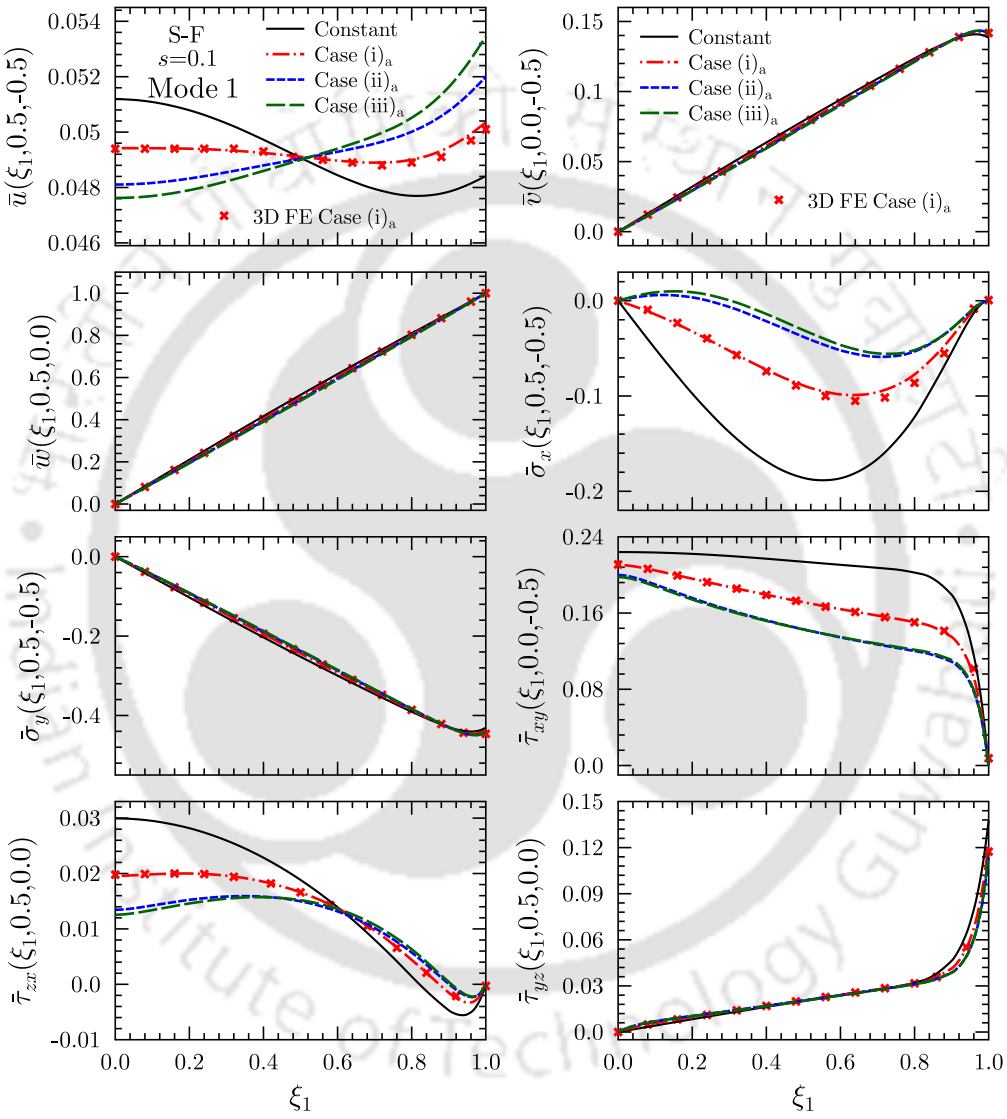

Fig. 3.21: Longitudinal variations of displacements and stresses for first vibration mode of plate (a) (Mode-1) under C–S boundary condition

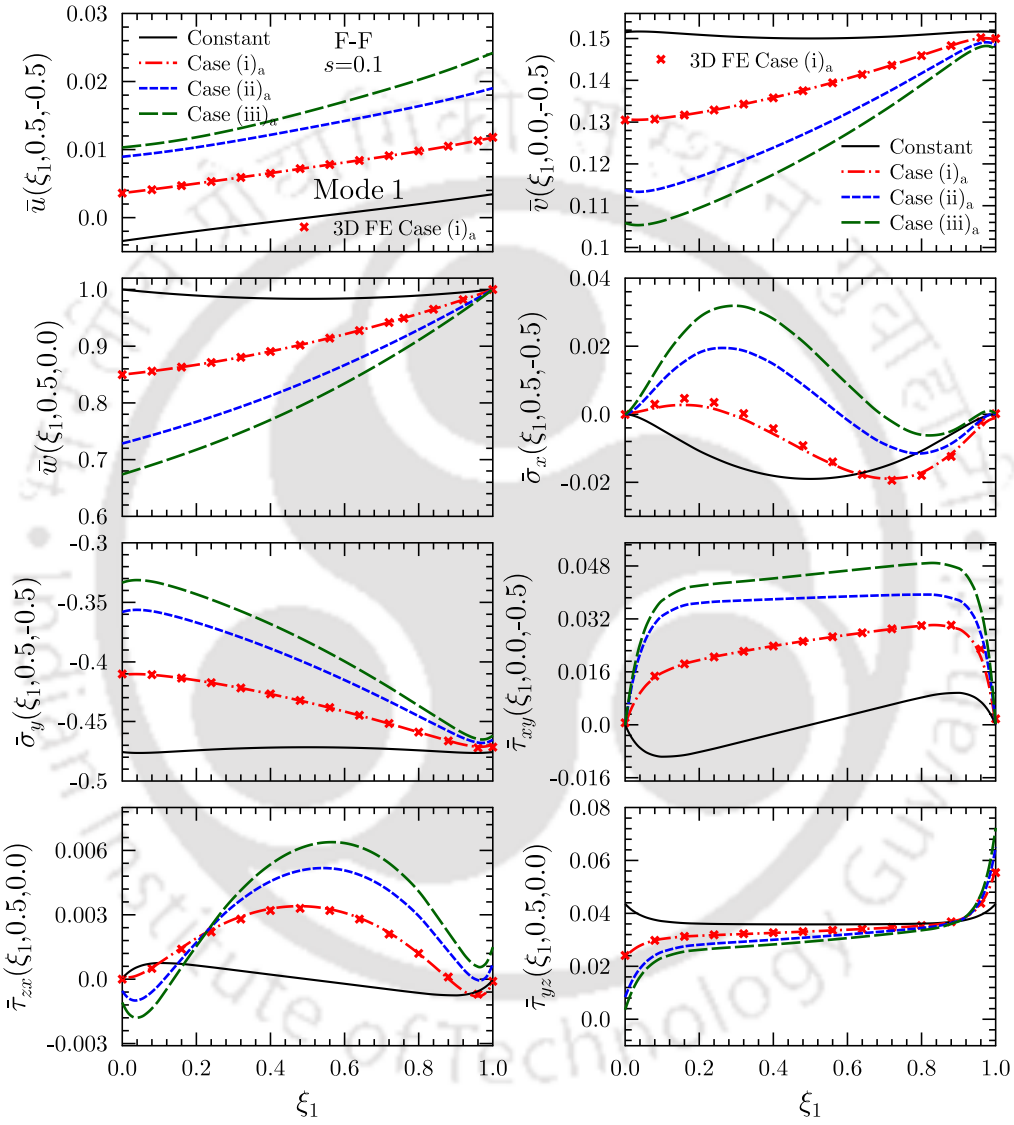

Fig. 3.22: Longitudinal variations of displacements and stresses for first vibration mode of plate (a) (Mode-1) under C–F boundary condition

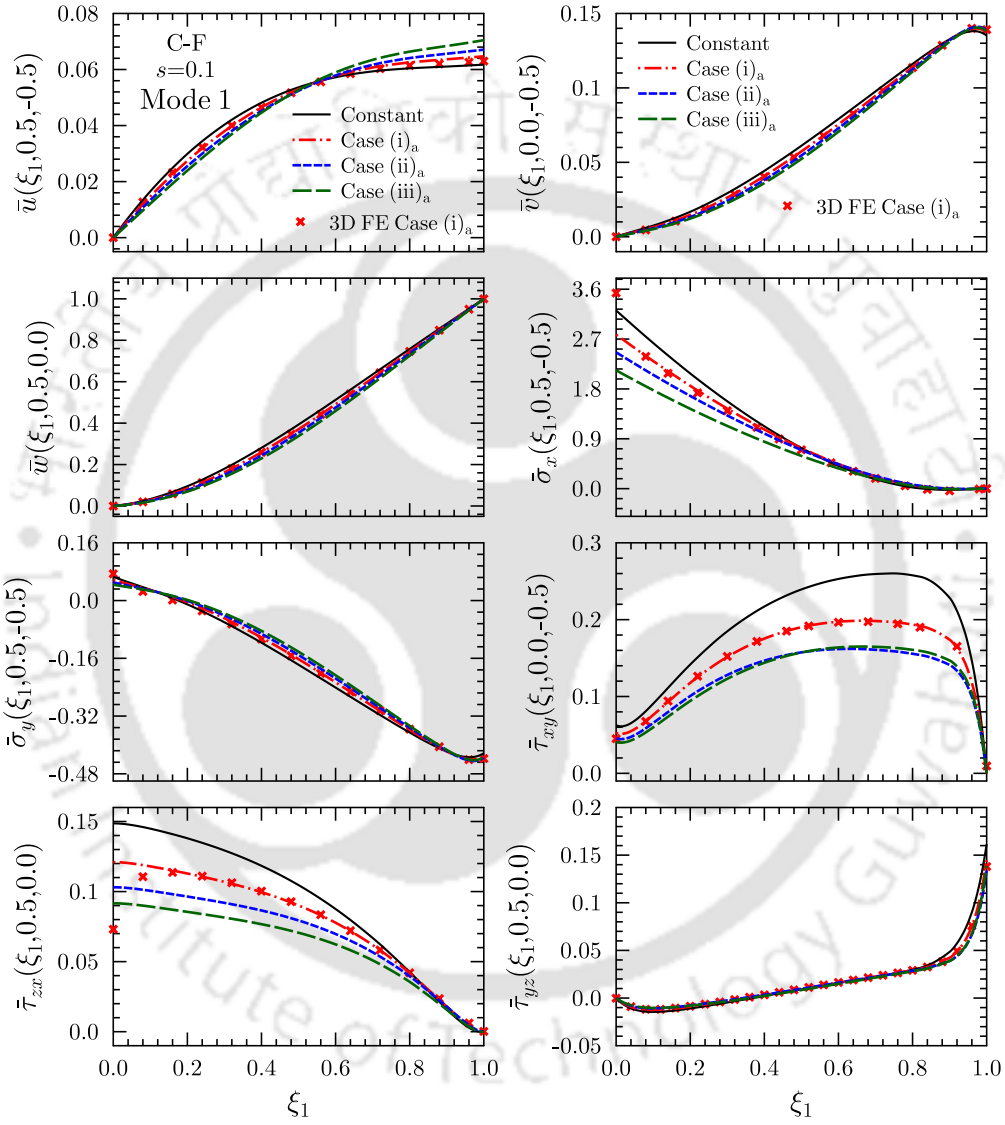

Fig. 3.23: Longitudinal variations of displacements and stresses for first vibration mode of plate(a) (Mode-1) under S–F boundary condition

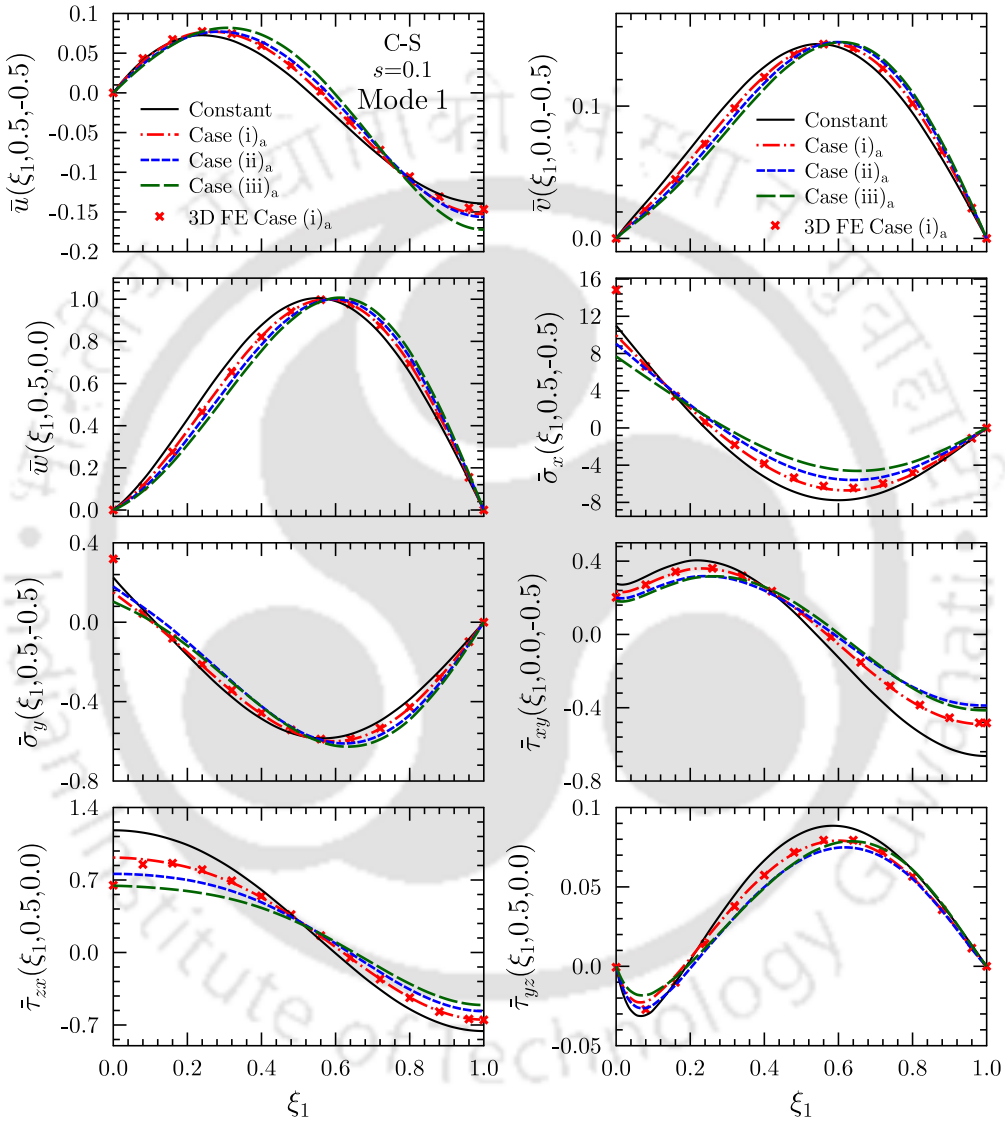

Fig. 3.24: Longitudinal variations of displacements and stresses for first vibration mode of plate (a) (Mode-1) under F–F boundary condition

Similarly, the through-thickness variation of deflections ($\bar{u}$, $\bar{v}$, $\bar{w}$) and stresses ($\bar{\sigma}_x$, $\bar{\tau}_{xy}$, $\bar{\tau}_{zx}$ and $\bar{\tau}_{yz}$) for the first mode under gradation Case (i)$_a$ is presented in Fig. 3.25 for C–F support conditions. The results are plotted for different ξ_1 locations and it is observed that the present results are in excellent agreement with 3D FE results. Maximum transverse stresses ($\bar{\tau}_{zx}$ and $\bar{\tau}_{yz}$) are observed at the mid of the plate (a) where in-plane stresses are maximum at the top and bottom surface of plate (a).

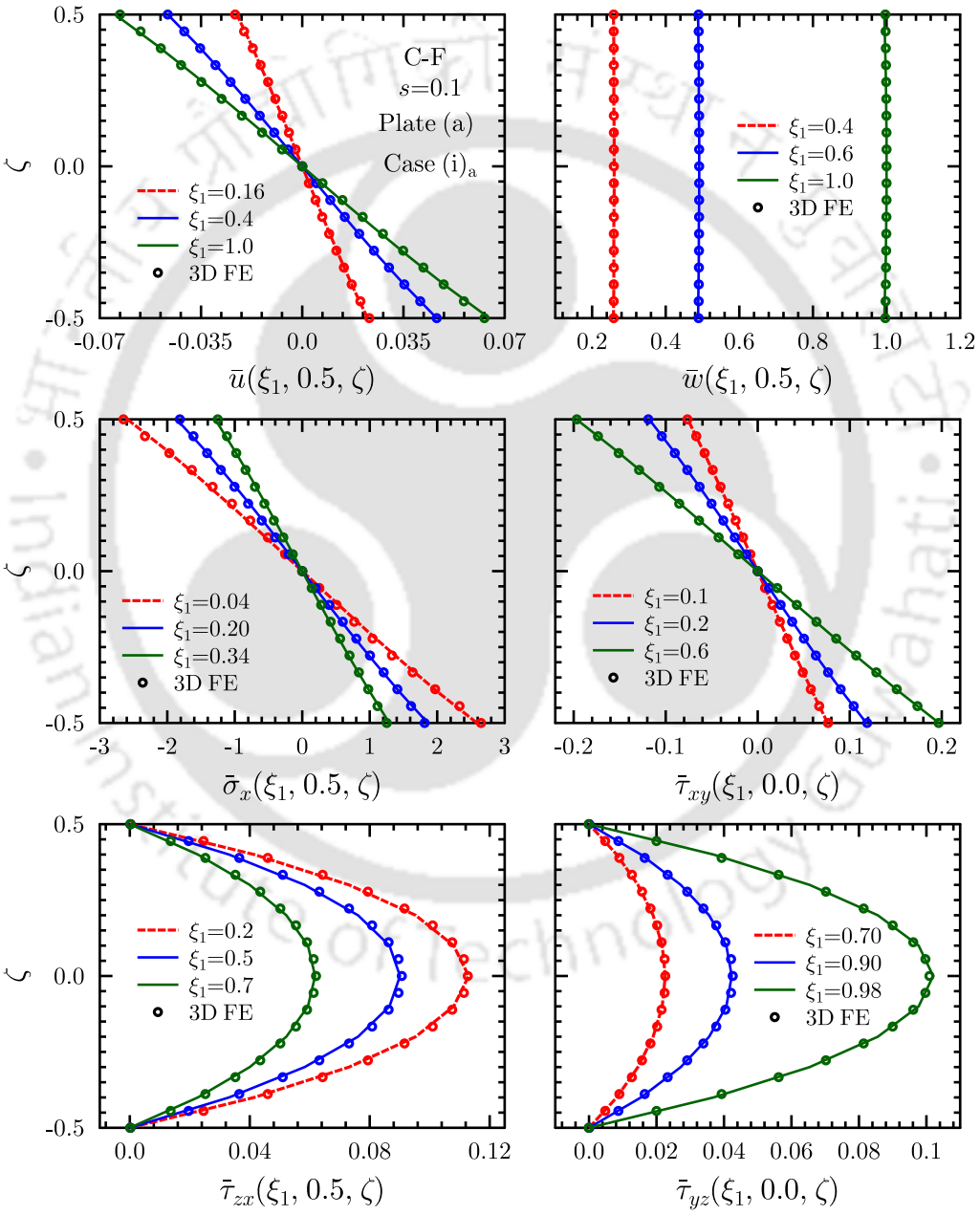

Fig. 3.25: Through-thickness distributions of displacements and stresses at different ξ_1-locations in the first flexural mode of single-layered FGM plate (a) under Case (i)$_a$ of property variation and subjected to C-F boundary condition (Case (i)$_a$, Mode-1)

3.7.3 Plate (b): Two-layered FGM Plate

A layer-wise in-plane functionally graded plate (b), as shown in Fig. 3.2, is assumed for the present study in this section. For the first time, a two-layered rectangular plate is analyzed which has functionally graded properties along in-plane (x) direction, with the different gradation indexes for the top and the bottom layers. To study the effect of in-plane varying material properties on natural frequencies of plate, first five dimensionless natural frequencies, $\omega^* = \omega h\sqrt{\rho/G_{12}}$, are tabulated for two gradation cases, Case (i)$_\mathrm{b}$: Bottom layer- $\delta_1 = \delta_2 = \delta_p = 0.0$, Top layer- $\delta_1 = \delta_2 = \delta_p = 0.5$; Case (ii)$_\mathrm{b}$: Bottom layer- $\delta_1 = \delta_2 = \delta_p = 0.5$, Top layer- $\delta_1 = \delta_2 = \delta_p = 1.0$, along with constant case, Constant: Bottom layer- $\delta_1 = \delta_2 = \delta_p = 0.0$; Top layer- $\delta_1 = \delta_2 = \delta_p = 0.0$ Numerical results for constant properties case are also tabulated along with gradation cases, Case (i)$_\mathrm{b}$ and and Case (ii)$_\mathrm{b}$. In Tables 3.15 and 3.16, benchmark results are tabulated for S–S, C–S, C–C, C–F, S–F and F–F boundary conditions, respectively. To verify the accuracy and efficacy of

Table 3.15: Effect of in-plane gradation of material properties on natural frequencies $\omega^* = \omega h\sqrt{\rho/G_{12}}$ of two-layered FGM plate (b) subjected to S–S, C–S and C–C boundary conditions (s=0.2)

B.C.	Mode→	1	2	3	4	5
S–S	Constant	0.4511425	0.6404183	0.9472923	1.0630825	1.1675824
	Case (i)$_\mathrm{b}$	0.4042117	0.5861476	0.8786149	0.9488456	1.0499511
	Case (ii)$_\mathrm{b}$	0.3333698	0.5030923	0.7700303	0.7765457	0.8730440
C–S	Constant	0.5001534	0.6680954	0.9618044	1.0816794	1.1816487
	Case (i)$_\mathrm{b}$	0.4509243	0.6113988	0.8909600	0.9693074	1.0653742
	Case (ii)$_\mathrm{b}$	0.3753078	0.5237075	0.7787079	0.7991169	0.8896464
C–C	Constant	0.5531057	0.7017077	0.9795622	1.0974620	1.1941041
	Case (i)$_\mathrm{b}$	0.4986720	0.6392149	0.9058845	0.9802574	1.0737785
	Case (ii)$_\mathrm{b}$	0.4095549	0.5429995	0.7890682	0.8047789	0.8936784

the present EKM solution approach for the multilayered plates, these results are also thoroughly verified with 3D FE results for all the cases. It is observed that the present results are in excellent agreement with 3D FE results (difference less than 2%). Significant effect of in-plane gradation is observed on the natural frequencies of the plate (b). As the variation indexes increases, the natural frequencies of the plate (b) decreases significantly for all the boundary conditions.

Table 3.16: Effect of in-plane gradation of material properties on natural frequencies $\omega^* = \omega h\sqrt{\rho/G_{12}}$ of two-layered FGM plate (b) subjected to C–F, S–F and F–F boundary conditions (s=0.2)

B.C.	Mode→	1	2	3	4	5
C–F	Constant	0.2293158	0.4821463	0.6749415	0.8353930	0.8372359
	Case (i)$_b$	0.2050632	0.4384603	0.6096201	0.7609596	0.7632273
	Case (ii)$_b$	0.1705466	0.3753864	0.5099960	0.6461618	0.6576775
S–F	Constant	0.1660161	0.4621232	0.6521498	0.8221628	0.8271057
	Case (i)$_b$	0.1496332	0.4218953	0.5854236	0.7452106	0.7571818
	Case (ii)$_b$	0.1266559	0.3637235	0.4849893	0.6306476	0.6541585
F–F	Constant	0.1265011	0.2385336	0.4274791	0.5437522	0.7989971
	Case (i)$_b$	0.1191630	0.2170881	0.4015313	0.5042046	0.7469413
	Case (ii)$_b$	0.1072086	0.1874880	0.3559698	0.4524197	0.6523559

Percentage change in natural frequencies under different boundary conditions are plotted in Figs. 3.26. For all the support conditions, nearly 6 to 10% decrement is observed in the first five natural frequencies for Case (i)$_b$ as compared to constant property cases. The percentage decrement in natural frequencies is 16 to 26% for Case (ii)$_b$. This study revealed that the in-plane gradation, even in one layer of the plate, significantly affects the natural frequencies of the plate.

The longitudinal variations of deflection ($\bar{w}$) and stresses ($\bar{\sigma}_x, \bar{\tau}_{xy}, \bar{\tau}_{zx}$), under first flexural mode, of the plate (b) are plotted in the Fig. 3.27 for S-S and F-F boundary conditions. Similarly, for C-S and C-F boundary conditions, the longitudinal variations of the deflection and stresses of the plate (b) are presented in Fig. 3.28 under the first flexural mode. To verify the accuracy of the present solution for the multilayered plate, 3D FE results for Case (i)$_b$ are also plotted, and it is observed that the present EKM solution shows excellent agreement with the FE solutions. To study the effect of gradation of material properties the longitudinal variations of deflection and stresses for the layer-wise homogeneous case (Constant properties) are also presented in these figures. Figs. 3.27 and 3.28 reveal that the in-plane gradation of material properties, even in one layer, significantly affects the mode shape of the plates. Significant effect of in-plane gradation on the stresses ($\bar{\sigma}_x$, $\bar{\tau}_{xy}$ and $\bar{\tau}_{zx}$) are observed for all the boundary conditions (S–S, S–F, F–F, C–F and C–S), whereas deflection ($\bar{w}$) are least affected under all the support conditions. Under S–S, S–F, and C–F support conditions, the stresses $\bar{\sigma}_x$, $\bar{\tau}_{xy}$ and $\bar{\tau}_{zx}$ are decreasing significantly as the variation index increases. The behavior of plate (a) under F–F support conditions are more sensitive to the gradation of material properties than other support conditions. Under F–F support conditions, the deflection (

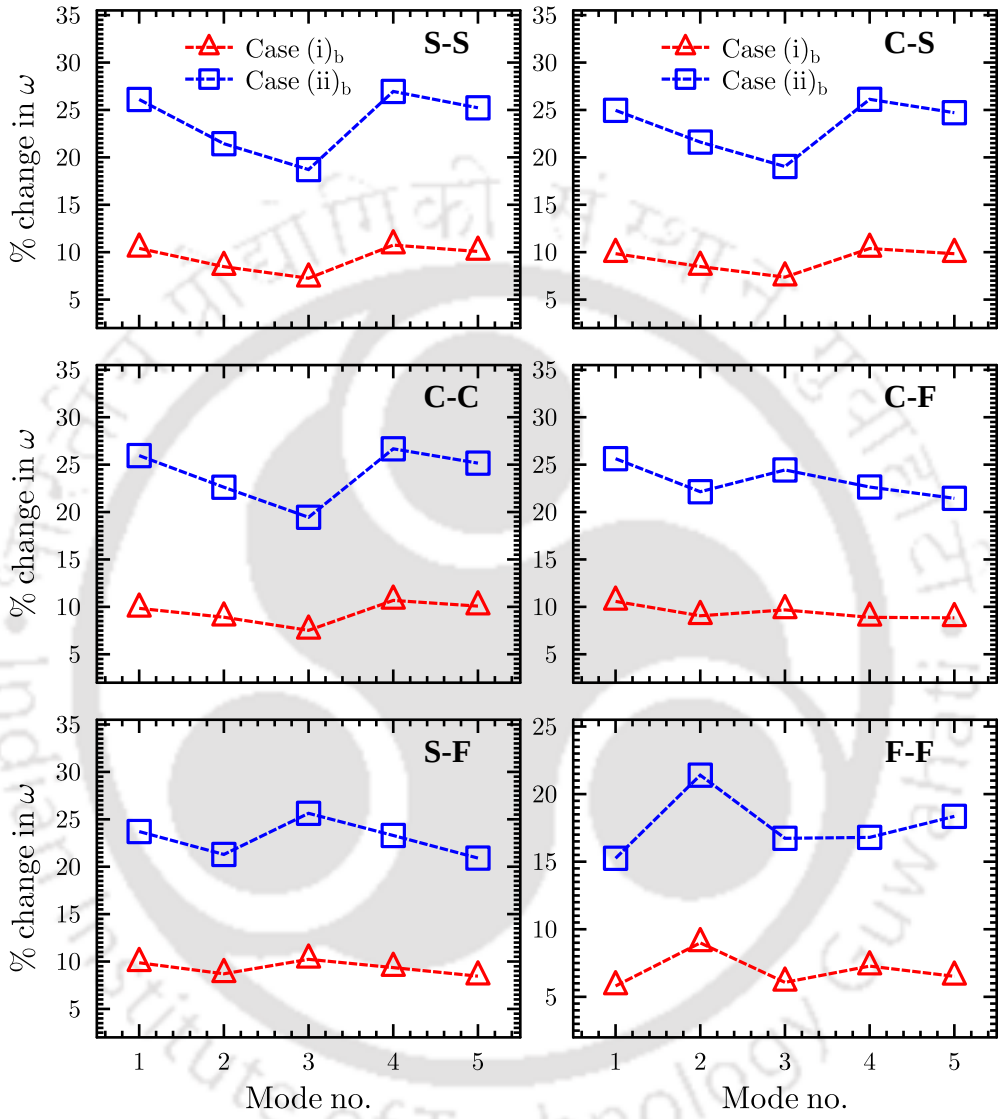

Fig. 3.26: Percentage change in first five lowest natural frequencies of plate (b), due to variation in material properties, under S–S, C–S, C–C and C–F boundary conditions (s=0.2)

$\bar{w}$) and stresses ($\bar{\sigma}_x$, $\bar{\tau}_{xy}$ and $\bar{\tau}_{zx}$) affected significantly by the in-plane gradation of properties. As the gradation indexes (δ_1, δ_2, and δ_p) increases, the nature of the longitudinal variation of stresses becomes totally different.

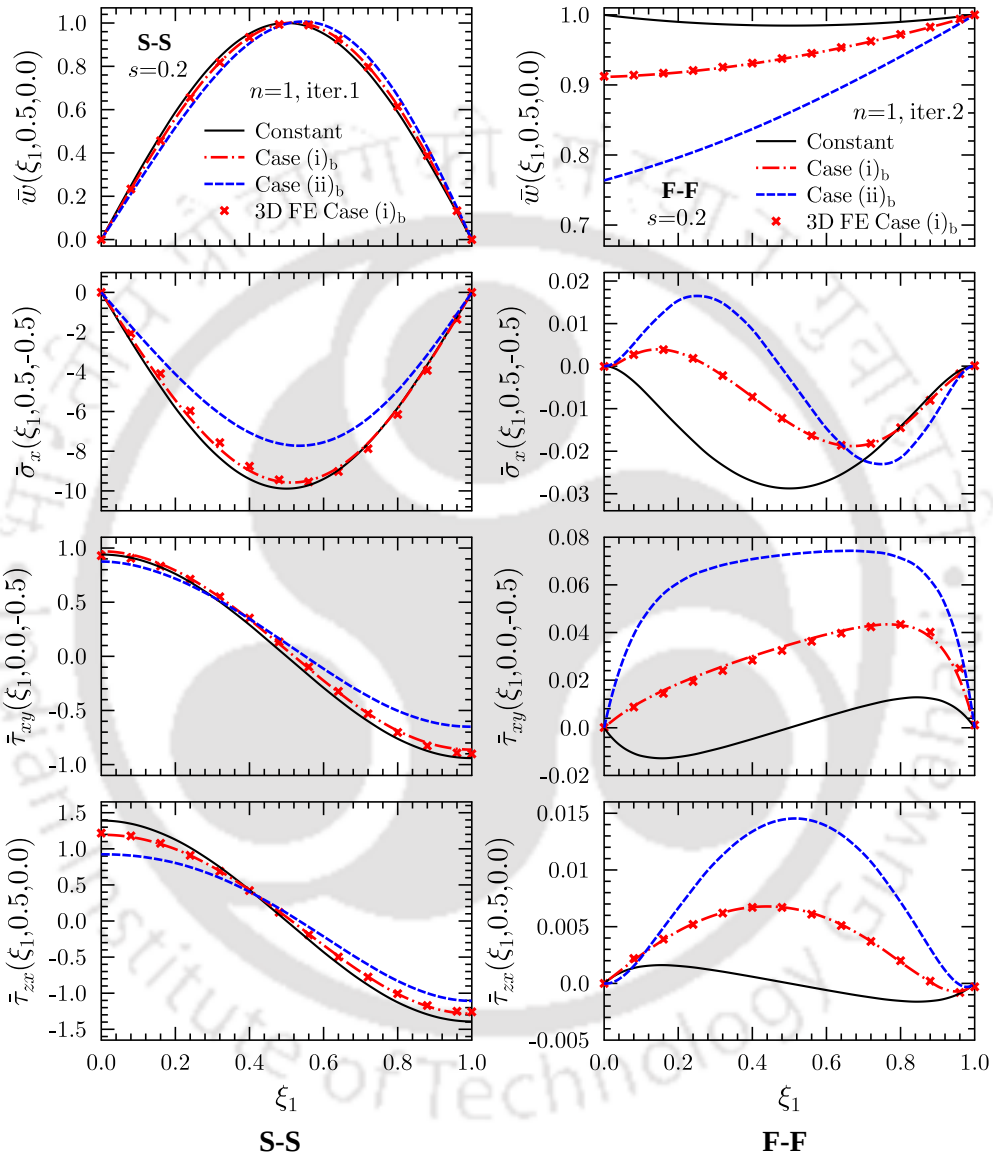

Fig. 3.27: Effect of in-plane gradation of material properties on longitudinal variations of displacements and stresses for first vibration mode of plate(b) under Mode-1 subjected to S–S and F–F boundary conditions

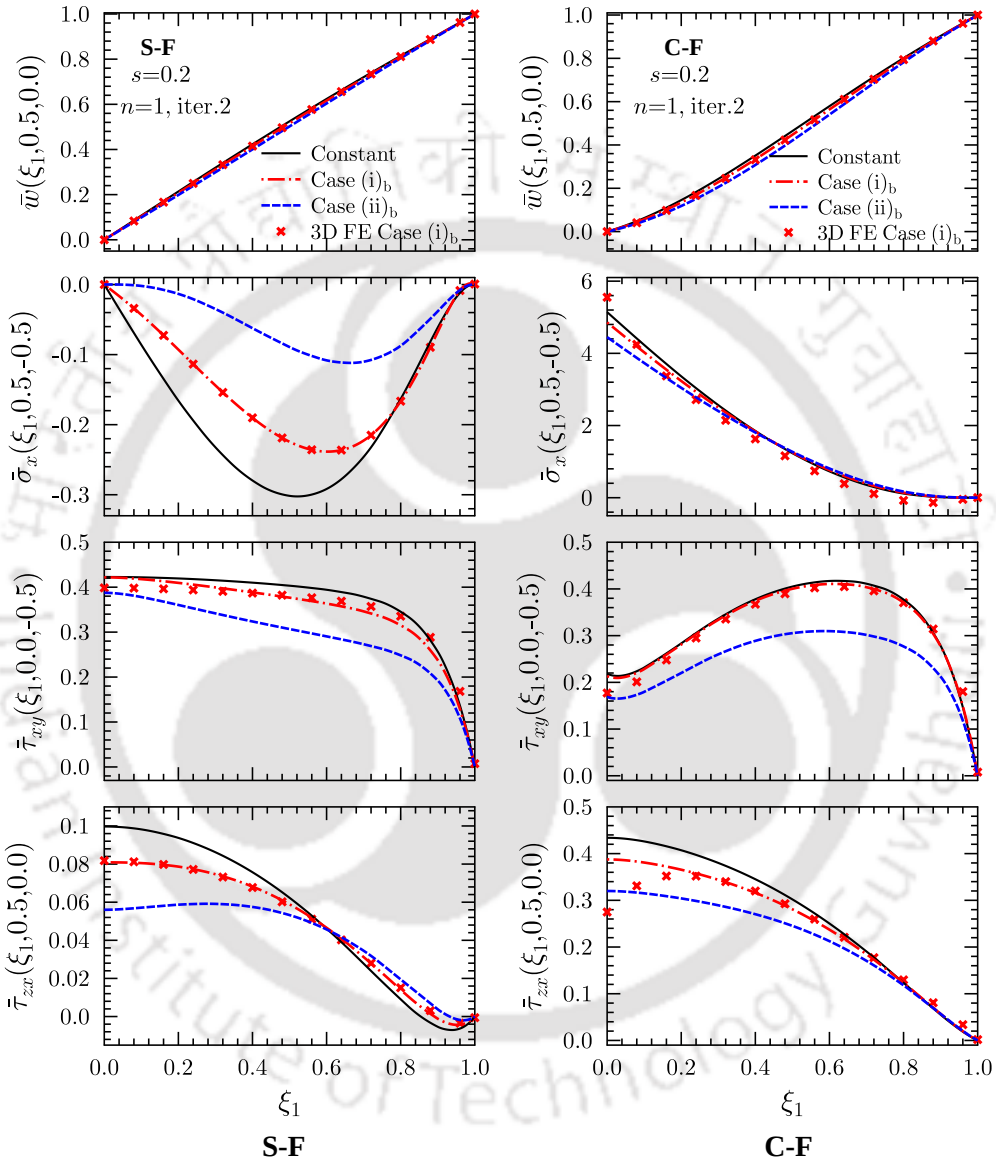

Fig. 3.28: Effect of in-plane gradation of material properties on longitudinal variations of displacements and stresses for first vibration mode of plate (b) under Mode-1 subjected to S–F and C–F boundary conditions

3.8 SUMMARY

In this chapter, an accurate 3D elasticity solution is presented for static and dynamic analysis of rectangular FGM plates with longitudinally varying material properties using the multi-term extended Kantorovich method. In this proposed solution, two opposite edges of rectangular plates, along y-direction, are assumed simply-supported, and the other two edges, along x-direction, can have any support condition, like simply-supported, free and clamped support conditions. The density and elastic properties of the layers are considered to graded linearly and continuously along the (x)-direction of the plate. The benchmark numerical results are tabulated for two types of configurations. The numerical study reveals that the EKM solution converges within just one/two terms for both single layer and two-layer FGM plates under static and dynamic case. The bending and free vibration response of plate is influenced greatly by the extent of material gradation along the in-plane direction. It is observed that as the variation indexes are doubled from 0.5 to 1, its effect on maximum deflection, stresses and natural frequencies are also nearly doubled. This development has opened the area for developing the closed form solution for FGM plates with property variation along multiple directions. Two layered square plate adhesively bonded by a functionally graded adhesive interlayer is also analysed and observed that the deflection and stresses are significantly effected by properties variation of the adhesive interlayer and boundary condition plays an important role in the behavior of adhesively bonded plates. The current research will also be beneficial to modeled adhesive structure in which adhesive interlayer properties degraded due to some environmental effect. The present analytical solution can be used as a benchmark to assessing the accuracy of the 2D plate theories for bending and free vibration analysis of rectangular plates having varying material properties along in-plane direction. This development will also assist in taking suitable kinematic assumptions, which is very helpful in the development of refined plate theories for in-plane functionally graded plates.

Chapter 4

Functionally Graded Angle-ply Flat Panels- 3D Elasticity Analysis

Many engineering structures such as turbine blades, tank bottom, floors and roof of the building often modeled as flat panels which are subjected to arbitrary boundary conditions. In this chapter, the multi-term extended Kantorovich approach, which has been developed in Chapters 2 and 3, is now extended to obtain analytical elasticity solution for laminated axially functionally graded (AFG) angle-ply flat panel subjected to arbitrary boundary condition. The analytical solution is developed for static and free vibration analysis of arbitrary supported AFG angle-ply flat panels. The linear variation of the material properties along the x-direction is assumed, similar to variation considered in Chapters 2 and 3. Mixed form of Hamilton's variation principle, which has been derived in Chapter 3 for cross-ply case, is now extended to angle-ply panels. Now, extended Kantorovich method (EKM), similar to Chapters 2 and 3, is employed to obtain the sets of first-order ordinary differential equations (ODEs), one set along the thickness (z) direction and another set along in-plane (x) direction, as explained in 4.2. The system of ODEs along the z-direction have constant coefficients which is solved in exact close-form manners. But, the system of ODEs along x-direction have variable coefficients which is solved using modified power series method. Numerical results are presented for single layer and multilayered angle-ply AFG panel in conjunction with the various type of boundary condition. The present method has been validated against the 3D FE. The influence of property variation and ply-angle on the deflection, stresses and natural frequencies are studied intensively by considering various cases and configurations. The presented static and free vibration solution can serve as a benchmark for assessing the accuracy of the two-dimensional solution or 3D numerical solutions. This is a more severe case than a homogeneous plates and cross-ply laminated plates for assessing 2-D theories.

4.1 THEORETICAL FORMULATION FOR ANGLE-PLY FGM PANELS

A flat angle-ply laminated panel of dimensions $a \times h$ along x and z-directions, as depicted in Fig. 4.1, is considered for the analysis. Panel has infinite/ very long along y-direction and two

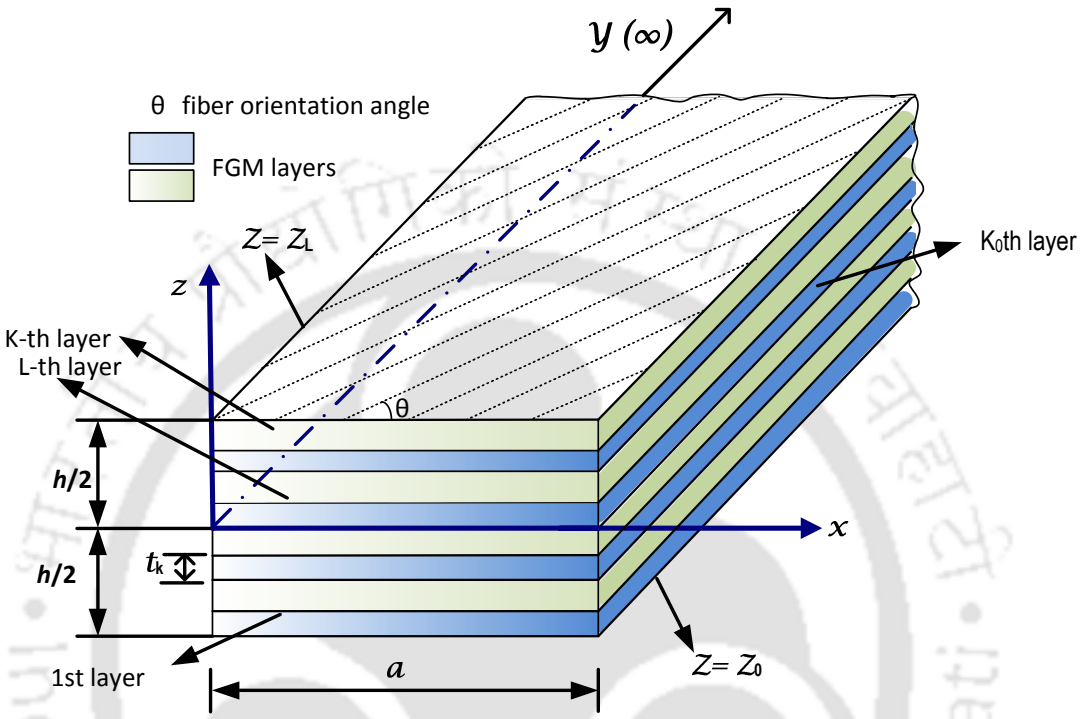

Fig. 4.1: Geometry of functionally graded angle-ply flat panel

edges corresponding to $x = 0$ and a can have any suitable combination of boundary conditions (*i.e.* clamped, free, simply-supported). Since it is a case of generalized plane strain problem of cylindrical bending, thus all variables are independent of y coordinate. Panel has L numbers of perfectly bonded layers. Each layer may have fiber orientation angle θ with respect to x-direction. Layers are numbered from bottom to top and for a typical kth layer, thickness is denoted by $t^{(k)}$ and its bottom surface is denoted as z_{k-1}

The compliances of the angle-ply layers are assumed to vary linearly along x-direction as:

$$\begin{aligned} &\bar{s}^m_{1j} = \bar{s}_{1j}(1+\delta_1\xi) \quad \text{for} \quad j = 1,2,3,6; \\ &\bar{s}^m_{45} = \bar{s}_{45}(1+\delta_2\xi) \quad \bar{s}^m_{55} = \bar{s}_{55}(1+\delta_2\xi); \quad \bar{s}^m_{66} = \bar{s}_{66}(1+\delta_2\xi) \\ &\rho^m = \rho(1+\delta_p\,\xi) \Longrightarrow \rho + \hat{\rho} \end{aligned} \tag{4.1}$$

where δ_1 and δ_2 are parameters that control the elastic properties variation, and δ_1 control the variation of density. $\xi = x/a$ are non-dimensional quantities. To represent the graded or degraded property, the variation indexes (δ_1, δ_2 and δ_p) can be positive or negative. These type of material property variation may be induced deliberately to enhance the structure strength or it may be due

to environmental factors, such as high temperature, moisture, corrosion, diffusion of chemicals like hydrogen, etc.

Then, 3D constitutive equations for the functionally graded angle-ply laminated panel written as,

$$\begin{bmatrix} \varepsilon_x \\ \varepsilon_y \\ \varepsilon_z \\ \gamma_{yz} \\ \gamma_{zx} \\ \gamma_{xy} \end{bmatrix} = \begin{bmatrix} \bar{s}_{11}^m & \bar{s}_{12}^m & \bar{s}_{13}^m & 0 & 0 & \bar{s}_{16}^m \\ \bar{s}_{12}^m & \bar{s}_{22} & \bar{s}_{23} & 0 & 0 & \bar{s}_{26}^m \\ \bar{s}_{13}^m & \bar{s}_{23} & \bar{s}_{33} & 0 & 0 & \bar{s}_{36}^m \\ 0 & 0 & 0 & \bar{s}_{44} & \bar{s}_{45}^m & 0 \\ 0 & 0 & 0 & \bar{s}_{45}^m & \bar{s}_{55}^m & 0 \\ \bar{s}_{16}^m & \bar{s}_{26}^m & \bar{s}_{36}^m & 0 & 0 & \bar{s}_{66}^m \end{bmatrix} \begin{bmatrix} \sigma_x \\ \sigma_y \\ \sigma_z \\ \tau_{yz} \\ \tau_{zx} \\ \tau_{xy} \end{bmatrix} \tag{4.2}$$

where σ_i and ε_i denote the normal stress and strains components, respectively and τ_{ij} and γ_{ij} denote the shear stress and strains components, respectively. The transformed elastic compliances are denoted by $\bar{s}_{ij}$. In this generalised plain strain problems all strains $(\epsilon_x, \epsilon_y, \epsilon_z, \gamma_{yz}, \gamma_{zx}, \gamma_{xy})$ and stresses $(\sigma_x, \sigma_y, \sigma_z, \tau_{yz}, \tau_{zx}, \tau_{xy})$ are independent of y. Therefore, the strain-displacement relations reduce to following form,

$$\varepsilon_x = u_{,x}, \quad \varepsilon_y = 0, \quad \varepsilon_z = w_{,z}, \quad \gamma_{yz} = v_{,z}, \quad \gamma_{zx} = w_{,x} + u_{,z}, \quad \gamma_{xy} = v_{,x} \tag{4.3}$$

where a subscript comma denotes differentiation. Using Eq. $(4.3)_2$ in Eqs. $(4.2)_2$, σ_y is obtained as

$$\sigma_y = -(\bar{s}_{12}/\bar{s}_{22})\sigma_x - (\hat{s}_{12}/\bar{s}_{22})\sigma_x - (\bar{s}_{26}/\bar{s}_{22})\tau_{xy} - (\bar{s}_{23}/\bar{s}_{22})\sigma_z \tag{4.4}$$

and the same is eliminated from Eq. $(4.2)_1$, Eq. $(4.2)_3$ and Eq. $(4.2)_6$ to yield

$$\begin{aligned} \varepsilon_x &= (p_{11} + \hat{p}_{11})\sigma_x + (p_{16} + \hat{p}_{16})\tau_{xy} + (p_{13} + \hat{p}_{13})\sigma_z - \delta_1\xi\bar{p}_{12} - {\delta_1}^2\xi^2\bar{p}_{12} \\ \varepsilon_z &= (p_{31} + \hat{p}_{31})\sigma_x + p_{36}\tau_{xy} + p_{33}\sigma_z \\ \gamma_{yz} &= \bar{s}_{44}\tau_{yz} + (\bar{s}_{45} + \hat{s}_{45})\tau_{zx} \\ \gamma_{zx} &= (\bar{s}_{45} + \hat{s}_{45})\tau_{yz} + (\bar{s}_{55} + \hat{s}_{55})\tau_{zx} \\ \gamma_{xy} &= (p_{16} + \hat{p}_{16})\sigma_x + (p_{66} + \hat{s}_{66})\tau_{xy} + p_{63}\sigma_z \end{aligned} \tag{4.5}$$

where $p_{ij} = \bar{s}_{ij} - \bar{s}_{i2}\bar{s}_{2j}/\bar{s}_{22}$; $\quad \hat{p}_{ij} = \delta_1\xi(\bar{s}_{ij} - \bar{s}_{i2}\bar{s}_{2j}/\bar{s}_{22})$; $\quad \hat{s}_{ij} = \delta_2\xi\bar{s}_{ij}$; $\quad \bar{p}_{12} = \bar{s}_{12}\bar{s}_{12}/\bar{s}_{22}$

The Hamilton's mixed variational principle for a angle-ply laminated panel without body force under the cylindrical bending case can be written as

$$\begin{aligned} \int_t \int_V \; & [\delta u(\sigma_{x,x} + \tau_{xz,z} - \rho^m \ddot{u}) + \delta v(\tau_{xy,x} + \tau_{yz,z} - \rho^m \ddot{v}) + \delta w(\tau_{zx,x} + \sigma_{z,z} - \rho^m \ddot{w}) \\ & + \delta\sigma_x(\varepsilon_x - u_{,x}) + \delta\sigma_z(\varepsilon_z - w_{,z}) + \delta\tau_{yz}(\gamma_{yz} - v_{,z}) \\ & + \delta\tau_{zx}(\gamma_{zx} - u_{,z} - w_{,x}) + \delta\tau_{xy}(\gamma_{xy} - v_{,x})]\mathrm{d}V\,\mathrm{d}t = 0, \quad \forall\ \delta u, \delta v, \delta w,\ \delta\sigma_i,\ \delta\tau_{ij} \end{aligned} \tag{4.6}$$

where V denotes per unit width volume of the angle-ply panel in the y-direction. Substituting the expressions of strain components ε_x, ε_z, γ_{xy}, γ_{yz} and γ_{zx} from Eq. (4.5) into Eq. (4.7) yields

$$\begin{aligned}\int_t\int_V\ & [\delta w\{\sigma_{z,z}+\tau_{zx,x}-(\rho+\hat{\rho})\ddot{u}\}+\delta v\{\tau_{yz,z}+\tau_{xy,x}-(\rho+\hat{\rho})\ddot{v}\}+\delta u\{\tau_{xz,z}+\sigma_{x,x}-(\rho+\hat{\rho})\ddot{w}\}\\ &+\delta\sigma_x\{(p_{11}+\hat{p}_{11})\sigma_x-\delta_1\xi\bar{p}_{12}-{\delta_1}^2\xi^2\bar{p}_{12}+(p_{16}+\hat{p}_{16})\tau_{xy}+(p_{13}+\hat{p}_{13})\sigma_z-u_{,x}\}\\ &+\delta\sigma_z\{(p_{31}+\hat{p}_{31})\sigma_x+p_{36}\tau_{xy}+p_{33}\sigma_z-w_{,z}\}+\delta\tau_{yz}\{\bar{s}_{44}\tau_{yz}+(\bar{s}_{45}+\hat{s}_{45})\tau_{zx}-v_{,z}\}\\ &+\delta\tau_{zx}\{(\bar{s}_{45}+\hat{s}_{45})\tau_{yz}+(\bar{s}_{55}+\hat{s}_{55})\tau_{zx}-u_{,z}-w_{,x}\}+\delta\tau_{xy}\{(p_{61}+\hat{p}_{61})\sigma_x+p_{63}\sigma_z\\ &+(p_{66}+\hat{s}_{66})\tau_{xy}-v_{,x}\}]\mathrm{d}V\,\mathrm{d}t=0,\quad \forall\ \delta u,\delta v,\delta w,\ \delta\sigma_i,\ \delta\tau_{ij}\end{aligned}\tag{4.7}$$

where ξ is dimensionless in-plane coordinate along x-direction and $\zeta^{(k)}$ is non-dimensional local thickness parameter for the kth layer ($\zeta^{(k)}=(z-z_{k-1})/t^{(k)}$) which takes value 0 to 1 for each layer. Panel is subjected to uniform distributed pressure (σ_z = -p_1, -p_2) at bottom and top surface and there is no shear stress (τ_{zx} and τ_{yz}) at bottom and top surface of panel. For perfect interlaminar bounding case, displacements (u, v ,w) and transverse stresses (σ_z, τ_{zx}, τ_{yz}) need to satisfy following condition at the kth interface:

$$[(u,\ v,\ w,\ \sigma_z,\ \tau_{yz},\ \tau_{zx})|_{\zeta=1}]^{(k)}=[(u,\ v,\ w,\ \sigma_z,\ \tau_{yz},\ \tau_{zx})|_{\zeta=0}]^{(k+1)}\tag{4.8}$$

Along x-axis AFG panel can have any type of support such as Simply supported ($\sigma_x=v=w=0$), Clamped ($u=v=w=0$), Free ($\sigma_x=\tau_{xy}=\tau_{xz}=0$).

4.2 THE GENERALIZED MULTI-TERM EKM

There are 8 primary field variables $(u,v,w,\sigma_x,\sigma_z,\tau_{xy},\tau_{yz},\tau_{zx})$ which are to be solved. Using the multi-term EKM [280], the field variables for the kth layer are expressed as,

$$X_l(\xi,\zeta)=\sum_{i=1}^{n}f_l^i(\xi)g_l^i(\zeta)\cos\omega t+\delta_{l5}[p_a+zp_d]\qquad\text{for}\qquad l=1,2,\ldots 8\tag{4.9}$$

where f and g are unknown functions of ξ and ζ, respectively, and $p_a=-(p_1+p_2)/2$ and $p_d=-(p_2-p_1)/h$. The functions $g_l^i(\zeta)$ are dependent on kth layer, while functions $f_l^i(\xi)$ are valid for all layers.

4.2.1 First Iteration Step

The initial guess functions $f_l^i(\xi)$ along ξ direction for the first iteration are assumed in trigonometric form ($\cos i\pi\xi$ or $\sin i\pi\xi$) which identically satisfy the simply supported boundary conditions. But in multi-term EKM solution, the starting guess functions need not to be assume as per the

boundary conditions. The functions $g_l^i(\xi)$ are to be solved in this step. For this purpose, first variation δX_l is obtained as,

$$\delta X_l = \sum_{i=1}^{n} f_l^i(\xi)\delta g_l^i \cos\omega t, \qquad l = 1, 2, \ldots 8. \tag{4.10}$$

Functions g_l^i are divided into two column vector $\bar{\mathbf{G}}$ and $\hat{\mathbf{G}}$. $\bar{\mathbf{G}}$ contains all the six variables that appear in the boundary and interface conditions along z-direction and $\hat{\mathbf{G}}$ contains remaining two variables:

$$\begin{aligned}\bar{\mathbf{G}} &= [\, g_1^1 \ldots g_1^n \quad g_2^1 \ldots g_2^n \quad g_3^1 \ldots g_3^n \quad g_5^1 \ldots g_5^n \quad g_7^1 \ldots g_7^n \quad g_8^1 \ldots g_8^n \,]^{\mathrm{T}} \\ \hat{\mathbf{G}} &= [\, g_4^1 \ldots g_4^n \quad g_6^1 \ldots g_6^n \,]^{\mathrm{T}}\end{aligned} \tag{4.11}$$

Equations (4.9) and (4.10) are substituted in Eq. (4.7), and perform integration along x-axis. Since variation is arbitrary, the coefficient of δg^i must vanish, yields the following set of ODEs,

$$\mathbf{M}\bar{\mathbf{G}}_{,\zeta} = \bar{\mathbf{A}}^{\mathbf{m}}(\omega)\bar{\mathbf{G}} + \hat{\mathbf{A}}^{\mathbf{m}}\hat{\mathbf{G}} + \bar{\mathbf{Q}}_{\mathbf{p}}^{\mathbf{m}} \tag{4.12}$$

$$\mathbf{K}^{\mathbf{m}}\hat{\mathbf{G}} = \tilde{\mathbf{A}}^{\mathbf{m}}\bar{\mathbf{G}} + \tilde{\mathbf{Q}}_{\mathbf{p}}^{\mathbf{m}} \tag{4.13}$$

where $\mathbf{M}$, $\bar{\mathbf{A}}^{\mathbf{m}}$, $\hat{\mathbf{A}}^{\mathbf{m}}$, $\mathbf{K}^{\mathbf{m}}$ and $\tilde{\mathbf{A}}^{\mathbf{m}}$ are $6n \times 6n$, $6n \times 6n$, $6n \times 2n$, $2n \times 2n$ and $2n \times 6n$ matrices and $\bar{\mathbf{A}}^{\mathbf{m}} = \bar{\mathbf{A}} + \bar{\mathbf{A}}^{\mathbf{v}}$; $\hat{\mathbf{A}}^{\mathbf{m}} = \hat{\mathbf{A}} + \hat{\mathbf{A}}^{\mathbf{v}}$; $\mathbf{K}^{\mathbf{m}} = \mathbf{K} + \mathbf{K}^{\mathbf{v}}$; $\tilde{\mathbf{A}}^{\mathbf{m}} = \tilde{\mathbf{A}} + \tilde{\mathbf{A}}^{\mathbf{v}}$; $\tilde{\mathbf{Q}}_{\mathbf{p}}^{\mathbf{m}} = \tilde{\mathbf{Q}}_{\mathbf{p}} + \tilde{\mathbf{Q}}_{\mathbf{p}}^{\mathbf{v}}$; $\bar{\mathbf{Q}}_{\mathbf{p}}^{\mathbf{m}} = \bar{\mathbf{Q}}_{\mathbf{p}} + \bar{\mathbf{Q}}_{\mathbf{p}}^{\mathbf{v}}$. The nonzero terms of these matrices are given as,

$$\begin{aligned}
&M_{i_1j_1} = M_{j_6i_6} = \langle f_8^i f_1^j\rangle_a, && M_{i_2j_2} = M_{j_5i_5} = \langle f_7^i f_2^j\rangle_a, && M_{i_3j_3} = M_{j_4i_4} = \langle f_5^i f_3^j\rangle_a \\
&\bar{A}_{i_1j_3} = \tfrac{-t}{a}\langle f_{3,\xi}^j f_8^i\rangle_a, && \bar{A}_{i_1j_5} = t\bar{s}_{45}\langle f_8^i f_7^j\rangle_a, && \bar{A}_{i_1j_5}^v = \delta_2 t\bar{s}_{45}\langle \xi f_8^i f_7^j\rangle_a \\
&\bar{A}_{i_1j_6} = t\bar{s}_{55}\langle f_8^i f_8^j\rangle_a, && \bar{A}_{i_1j_6}^v = \delta_2 t\bar{s}_{55}\langle \xi f_8^i f_8^j\rangle_a, && \bar{A}_{i_2j_5} = t\bar{s}_{44}\langle f_7^i f_7^j\rangle_a, \\
&\bar{A}_{i_2j_6} = t\bar{s}_{45}\langle f_7^i f_8^j\rangle_a, && \bar{A}_{i_2j_6}^v = \delta_2 t\bar{s}_{45}\langle \xi f_7^i f_8^j\rangle_a, && \bar{A}_{i_3j_4} = tp_{33}\langle f_5^i f_5^j\rangle_a \\
&\hat{A}_{i_3j_1} = tp_{31}\langle f_5^i f_4^j\rangle_a, && \hat{A}_{i_3j_1}^v = \delta_1 tp_{31}\langle \xi f_5^i f_4^j\rangle_a, && \hat{A}_{i_3j_2} = tp_{36}\langle f_5^i f_6^j\rangle_a, \\
&\bar{A}_{i_4j_6} = \tfrac{-t}{a}\langle f_3^i f_{8,\xi}^j\rangle_a && \hat{A}_{i_5j_2} = \tfrac{-t}{a}\langle f_2^i f_{6,\xi}^j\rangle_a, && \hat{A}_{i_6j_1} = \tfrac{-t}{a}\langle f_1^i f_{4,\xi}^j\rangle_a \\
&K_{i_1j_1} = p_{11}\langle f_4^i f_4^j\rangle_a, && K_{i_1j_1}^v = \delta_1(p_{11} - \bar{p}_{12})\langle \xi f_4^i f_4^j\rangle_a - \bar{k}_{11}, && K_{i_1j_2} = p_{16}\langle f_4^i f_6^j\rangle_a \\
&\bar{k}_{11} = \delta_1^2\bar{p}_{12}\langle \xi^2 f_4^i f_4^j\rangle_a, && K_{i_1j_2}^v = \delta_1 p_{16}\langle \xi f_4^i f_6^j\rangle_a, && K_{i_2j_2} = p_{66}\langle f_6^i f_6^j\rangle_a \\
&K_{i_2j_2}^v = \delta_2\bar{s}_{66}\langle \xi f_6^i f_6^j\rangle_a, && K_{i_2j_1} = K_{i_1j_2}, && K_{i_2j_1}^v = K_{i_1j_2}^v \\
&\tilde{A}_{i_1j_1} = \tfrac{1}{a}\langle f_4^i f_{1,\xi}^j\rangle_a, && \tilde{A}_{i_1j_4} = -p_{13}\langle f_4^i f_5^j\rangle_a, && \tilde{A}_{i_1j_4}^v = -\delta_1 p_{13}\langle \xi f_4^i f_5^j\rangle_a \\
&\tilde{A}_{i_2j_2} = \tfrac{1}{a}\langle f_6^i f_{2,\xi}^j\rangle_a, && \tilde{A}_{i_2j_4} = -p_{63}\langle f_6^i f_5^j\rangle_a, && \bar{A}_{i_4j_3} = -\rho\omega^2 t\langle f_3^i f_3^j\rangle_a
\end{aligned} \tag{4.14}$$

$$\bar{A}^v_{i_4j_3} = -\delta_p\omega^2 t\langle\rho\,\xi f^i_3 f^j_3\rangle_a,\ \bar{A}_{i_5j_2} = -\rho\omega^2 t\langle f^i_2 f^j_2\rangle_a, \qquad \bar{A}^v_{i_5j_2} = -\delta_p\omega^2 t\langle\rho\,\xi f^i_2 f^j_2\rangle_a$$
$$\bar{A}_{i_6j_1} = -\rho\omega^2 t\langle f^i_1 f^j_1\rangle_a, \qquad \bar{A}^v_{i_6j_1} = -\delta_p\omega^2 t\langle\rho\,\xi f^i_1 f^j_1\rangle_a$$

where $i_p = (p-1)n + i$ and $j_q = (q-1)n + j$ for $p, q = 1, 2, \ldots, 8$. $\bar{\mathbf{Q}}_\mathbf{p}$ and $\tilde{\mathbf{Q}}_\mathbf{p}$ are load vectors of size $6n$ and $2n$, respectively, whose non-zero terms are given by

$$\begin{aligned}
&\bar{Q}_{p_{i3}} = tp_{33}\langle f^i_5\rangle_a(p^k_a + \zeta t p_d), \qquad \tilde{Q}_{p_{i1}} = -p_{13}\langle f^i_4\rangle_a(p^k_a + \zeta t p_d), \qquad \bar{Q}_{p_{i4}} = -t\langle f^i_3\rangle_a p_d \\
&\tilde{Q}^v_{p_{i1}} = -\delta_1 p_{13}\langle\xi f^i_4\rangle_a(p^k_a + \zeta t p_d), \quad \tilde{Q}_{p_{i2}} = -p_{63}\langle f^i_6\rangle_a\,(p^k_a + \zeta t p_d)
\end{aligned} \tag{4.15}$$

where $\langle\ldots\rangle_a = a\int_0^1(\ldots)d\xi$, and $p^k_a = p_a + p_d z_k$. The functions f^i_l are known so the above elements of matrices are obtained in closed form.

Solving the system of algebraic equations (4.13) for $\hat{\mathbf{G}}$ and substituting back the solution into Eq. (4.12) yields

$$\bar{\mathbf{G}}_{,\zeta} = \mathbf{A}(\omega)\bar{\mathbf{G}} + \mathbf{Q}_\mathbf{p} \tag{4.16}$$

with $\mathbf{A} = \mathbf{M}^{-1}[\bar{\mathbf{A}}^m + \hat{\mathbf{A}}^m\mathbf{K}^{m-1}\tilde{\mathbf{A}}^m]$ and $\mathbf{Q}_\mathbf{p} = \mathbf{M}^{-1}[\bar{\mathbf{Q}}^m_\mathbf{p} + \hat{\mathbf{A}}^m\mathbf{K}^{m-1}\tilde{\mathbf{Q}}^m_\mathbf{p}]$. Equation (4.16) is system of first order differential equations of size $6n$.

For static case, the elements of matrices which is function of natural frequencies (ω) and time (t) now becomes zero, $\bar{A}_{i_4j_3}$=$\bar{A}_{i_5j_2}$=$\bar{A}_{i_6j_1}$=0 and $\bar{A}^v_{i_4j_3}$=$\bar{A}^v_{i_5j_2}$=$\bar{A}^v_{i_6j_1}$=0. Therefore, the coefficient of above system of first order ODEs Eq. (4.16) is not dependent on natural frequencies (ω). So the final form of ODEs along thickness direction, Eq. (4.16) now written as,

$$\bar{\mathbf{G}}_{,\zeta} = \mathbf{A}\bar{\mathbf{G}} + \mathbf{Q}_\mathbf{p} \tag{4.17}$$

This represent the set of first order non-homogenous ODEs having constant coefficient.

Similarly, for free vibration case the element corresponding to load vectors $\bar{\mathbf{Q}}_\mathbf{p}$, $\bar{\mathbf{Q}}^\mathbf{v}_\mathbf{p}$, $\tilde{\mathbf{Q}}_\mathbf{p}$ and $\tilde{\mathbf{Q}}^\mathbf{v}_\mathbf{p}$ is equals to zero due to absence of any external applied load, ($\bar{Q}_{p_{i3}}$=$\bar{Q}_{p_{i4}}$=$\tilde{Q}_{p_{i1}}$=$\tilde{Q}_{p_{i2}}$=$\tilde{Q}^v_{p_{i1}}$=0). So, final system of ODEs, Eq. (4.16) now reduced to,

$$\bar{\mathbf{G}}_{,\zeta} = \mathbf{A}(\omega)\bar{\mathbf{G}} \tag{4.18}$$

Equation (4.18) is system of first order homogenous ODEs whose coefficients are functions of natural frequencies (ω). These set of ODEs, for static case Eq. (4.17) and for dynamic case Eq. (4.18), respectively are solved in closed form manners using same the technique as discussed in Chapter 2 and 3. This completely determines $\bar{\mathbf{G}}(\zeta)$. Now, $\hat{\mathbf{G}}(\zeta)$ can be obtained by solving the algebraic equation (4.13). In this way, first iteration step is completed now.

4.2.2 Second Iteration Step

Now $g_l^i(\zeta)$ is known from the first step and arbitrary variation is considered along the x-direction therefore variation for this case is written as:

$$\delta X_l = \sum_{i=1}^{n} g_l^i(\zeta)\delta f_l^i \cos\omega t, \qquad l=1,2,\ldots,8. \tag{4.19}$$

Similarly like first step, the function $f_l^i(\xi)$ is partition into $\bar{\mathbf{F}}$ and $\hat{\mathbf{F}}$. $\bar{\mathbf{F}}$ contains all the six variables that appear in the boundary and interface conditions along x-direction and $\hat{\mathbf{F}}$ contains remaining two variables:

$$\begin{aligned}\bar{\mathbf{F}} &= [\, f_1^1 \ldots f_1^n \quad f_2^1 \ldots f_2^n \quad f_3^1 \ldots f_3^n \quad f_4^1 \ldots f_4^n \quad f_6^1 \ldots f_6^n \quad f_8^1 \ldots f_8^n \,]^{\mathrm{T}} \\ \hat{\mathbf{F}} &= [\, f_5^1 \ldots f_5^n \quad f_7^1 \ldots f_7^n \,]^{\mathrm{T}}\end{aligned} \tag{4.20}$$

Substituting Eq. (4.19) in Eq. (4.7), and perform integration along z-axis. Since variation is arbitrary, the coefficient of δf_l^i must vanish, yields the following set of governing equations:

$$\mathbf{N}\bar{\mathbf{F}}_{,\xi} = \bar{\mathbf{B}}^{\mathbf{f}}(\xi,\omega)\bar{\mathbf{F}} + \hat{\mathbf{B}}^{\mathbf{f}}(\xi)\hat{\mathbf{F}} + \bar{\mathbf{P}}^{\mathbf{f}}_{\mathbf{m}}(\xi) \tag{4.21}$$

$$\mathbf{L}\hat{\mathbf{F}} = \tilde{\mathbf{B}}^{\mathbf{f}}(\xi)\bar{\mathbf{F}} + \tilde{\mathbf{P}}_{\mathbf{m}} \tag{4.22}$$

where $\bar{\mathbf{B}}^{\mathbf{f}} = \bar{\mathbf{B}} + \xi\bar{\mathbf{B}}^{\mathbf{v}} + \xi^{\mathbf{2}}\bar{\mathbf{B}}^{\mathbf{vv}}$; $\hat{\mathbf{B}}^{\mathbf{f}} = \hat{\mathbf{B}} + \xi\hat{\mathbf{B}}^{\mathbf{v}}$; $\bar{\mathbf{P}}^{\mathbf{f}}_{\mathbf{m}} = \bar{\mathbf{P}}_{\mathbf{m}} + \xi\bar{\mathbf{P}}^{\mathbf{v}}_{\mathbf{m}}$; $\tilde{\mathbf{B}}^{\mathbf{f}} = \tilde{\mathbf{B}} + \xi\tilde{\mathbf{B}}^{\mathbf{v}}$; and $\mathbf{N}, \bar{\mathbf{B}}^{\mathbf{f}}$, $\hat{\mathbf{B}}^{\mathbf{f}}, \mathbf{L}$ and $\tilde{\mathbf{B}}^{\mathbf{f}}$ are $6n \times 6n$, $6n \times 6n$, $6n \times 2n$, $2n \times 2n$ and $2n \times 6n$ matrices, respectively and the nonzero terms of these matrices are given as,

$$\begin{aligned}
&N_{i_1j_1} = N_{j_4i_4} = \langle g_4^i g_1^j\rangle_h, && N_{i_2j_2} = N_{j_5i_5} = \langle g_6^i g_2^j\rangle_h, && N_{i_3j_3} = N_{j_6i_6} = \langle g_8^i g_3^j\rangle_h \\
&\bar{B}_{i_1j_4} = p_{11}\langle g_4^i g_4^j\rangle_h, && \bar{B}^v_{i_1j_4} = \delta_1(p_{11} - \bar{p}_{12})\langle g_4^i g_4^j\rangle_h, && \bar{B}^{vv}_{i_1j_4} = -\delta_1^2\bar{p}_{12}\langle g_4^i g_4^j\rangle_h \\
&\hat{B}_{i_1j_1} = p_{13}\langle g_4^i g_5^j\rangle_h, && \hat{B}^v_{i_1j_1} = \delta_1 p_{13}\langle g_4^i g_5^j\rangle_h, && \bar{B}_{i_1j_5} = p_{16}\langle g_4^i g_6^j\rangle_h, \\
&\bar{B}^v_{i_1j_5} = \delta_1 p_{16}\langle g_4^i g_6^j\rangle_h, && \bar{B}_{i_2j_4} = p_{61}\langle g_6^i g_4^j\rangle_h, && \bar{B}^v_{i_2j_4} = \delta_1 p_{61}\langle g_6^i g_4^j\rangle_h, \\
&\bar{B}_{i_2j_5} = p_{66}\langle g_6^i g_6^j\rangle_h, && \bar{B}^v_{i_2j_5} = \delta_2\bar{s}_{66}\langle g_6^i g_6^j\rangle_h, && \hat{B}_{i_2j_1} = p_{63}\langle g_6^i g_5^j\rangle_h \\
&\bar{B}_{i_3j_1} = -\langle g_8^i \tfrac{g_{1,\zeta}^j}{t}\rangle_h, && \hat{B}_{i_3j_2} = \bar{s}_{45}\langle g_8^i g_7^j\rangle_h, && \hat{B}^v_{i_3j_2} = \delta_2\bar{s}_{45}\langle g_8^i g_7^j\rangle_h \\
&\bar{B}_{i_3j_6} = \bar{s}_{55}\langle g_8^i g_8^j\rangle_h, && \bar{B}^v_{i_3j_6} = \delta_2\bar{s}_{55}\langle g_8^i g_8^j\rangle_h, && \bar{B}_{i_4j_6} = -\langle g_1^i \tfrac{g_{8,\zeta}^j}{t}\rangle_h \\
&\hat{B}_{i_5j_2} = -\langle g_2^i \tfrac{g_{7,\zeta}^j}{t}\rangle_h, && \hat{B}_{i_6j_1} = -\langle g_3^i \tfrac{g_{5,\zeta}^j}{t}\rangle_h, && L_{i_1j_1} = p_{33}\langle g_5^i g_5^j\rangle_h \\
&L_{i_2j_2} = \bar{s}_{44}\langle g_7^i g_7^j\rangle_h, && \tilde{B}_{i_1j_3} = \langle g_5^i \tfrac{g_{3,\zeta}^j}{t}\rangle_h, && \tilde{B}_{i_1j_4} = -p_{31}\langle g_5^i g_4^j\rangle_h \\
&\tilde{B}^v_{i_1j_4} = -\delta_1 p_{31}\langle g_5^i g_4^j\rangle_h, && \tilde{B}_{i_1j_5} = -p_{36}\langle g_5^i g_6^j\rangle_h, && \tilde{B}_{i_2j_2} = \langle g_7^i \tfrac{g_{2,\zeta}^j}{t}\rangle_h \\
&\tilde{B}_{i_2j_6} = -\bar{s}_{45}\langle g_7^i g_8^j\rangle_h, && \tilde{B}^v_{i_2j_6} = -\delta_2\bar{s}_{45}\langle g_7^i g_8^j\rangle_h, && \bar{B}_{i_4j_1} = -a\rho\omega^2\langle g_1^i g_1^j\rangle_h
\end{aligned} \tag{4.23}$$

$$\bar{B}^{v}_{i_4j_1} = -\delta_p\, a\rho\omega^2\xi\langle g^i_1 g^j_1\rangle_h,\ \bar{B}_{i_5j_2} = -a\rho\omega^2\langle g^i_2 g^j_2\rangle_h, \quad \bar{B}^{v}_{i_5j_2} = -\delta_p\, a\rho\omega^2\xi\langle g^i_2 g^j_2\rangle_h$$

$$\bar{B}_{i_6j_3} = -\rho a\omega^2\langle g^i_3 g^j_3\rangle_h, \quad \bar{B}^{v}_{i_6j_3} = -\delta_p\, a\rho\omega^2\xi\langle g^i_3 g^j_3\rangle_h$$

Similalrly, $\bar{\mathbf{P}}^{\mathbf{f}}_{\mathbf{m}}$ and $\tilde{\mathbf{P}}^{\mathbf{f}}_{\mathbf{m}}$ are $6n \times 1$ and $2n \times 1$ are load vectors and their non-zero elements are,

$$\begin{aligned}
&\bar{P}_{m_{i1}} = p_{13}\langle g^i_4(p^k_a + p_d t\zeta)\rangle_h, \quad \bar{P}_{m_{i2}} = p_{63}\langle g^i_6(p^k_a + p_d t\zeta)\rangle_h, \quad \bar{P}_{m_{i6}} = -p_d\langle g^i_3\rangle_h \\
&\bar{P}^{v}_{m_{i1}} = \delta_1 p_{13}\langle g^i_4(p^k_a + p_d t\zeta)\rangle_h, \quad \tilde{P}_{m_{i1}} = -p_{33}\langle g^i_5(p^k_a + p_d t\zeta)\rangle_h
\end{aligned} \tag{4.24}$$

where $\langle \ldots\rangle_h = \sum_{k=1}^{L} t^{(k)} \int_0^1 (\ldots)^{(k)}\, d\zeta$. Since $g^i(\zeta)$ are known in close form from previous step, so the above elements of matrices are obtained in closed form.

Rewrite the governing Eq. (4.21) and (4.22) equation as

$$\mathbf{N}\bar{\mathbf{F}}_{,\xi} = \{\bar{\mathbf{B}}(\omega) + \xi\bar{\mathbf{B}}^{\mathbf{v}}(\omega) + \xi^{\mathbf{2}}\bar{\mathbf{B}}^{\mathbf{vv}}\}\bar{\mathbf{F}} + (\hat{\mathbf{B}} + \xi\hat{\mathbf{B}}^{\mathbf{v}})\hat{\mathbf{F}} + (\bar{\mathbf{P}}_{\mathbf{m}} + \xi\bar{\mathbf{P}}^{\mathbf{v}}_{\mathbf{m}}) \tag{4.25}$$

$$\mathbf{L}\hat{\mathbf{F}} = (\tilde{\mathbf{B}} + \xi\tilde{\mathbf{B}}^{\mathbf{v}})\bar{\mathbf{F}} + \tilde{\mathbf{P}}_{\mathbf{m}} \tag{4.26}$$

Substituting $\hat{\mathbf{F}}$ from Eq. (4.26) into Eq. (4.25) yields the following set of first order ODEs with varying coefficients for $\bar{\mathbf{F}}$:

$$\bar{\mathbf{F}}_{,\xi} = \{\mathbf{B_0}(\omega) + \xi\mathbf{B_1}(\omega) + \xi^2\mathbf{B_2}\}\bar{\mathbf{F}} + \mathbf{P_0} + \xi\mathbf{P_1} \tag{4.27}$$

where $\mathbf{B_0} = \mathbf{N^{-1}}(\bar{\mathbf{B}} + \hat{\mathbf{B}}\mathbf{L^{-1}}\tilde{\mathbf{B}})$; $\mathbf{B_1} = \mathbf{N^{-1}}(\bar{\mathbf{B}}^{\mathbf{v}} + \hat{\mathbf{B}}\mathbf{L^{-1}}\tilde{\mathbf{B}}^{\mathbf{v}} + \hat{\mathbf{B}}^{\mathbf{v}}\mathbf{L^{-1}}\tilde{\mathbf{B}})$;
$\mathbf{B_2} = \mathbf{N^{-1}}(\bar{\mathbf{B}}^{\mathbf{vv}} + \hat{\mathbf{B}}^{\mathbf{v}}\mathbf{L^{-1}}\tilde{\mathbf{B}}^{\mathbf{v}})$; $\mathbf{P_0} = \mathbf{N^{-1}}(\bar{\mathbf{P}}_{\mathbf{m}} + \hat{\mathbf{B}}\mathbf{L^{-1}}\tilde{\mathbf{P}}_{\mathbf{m}})$; $\mathbf{P_1} = \mathbf{N^{-1}}(\bar{\mathbf{P}}^{\mathbf{v}}_{\mathbf{m}} + \hat{\mathbf{B}}^{\mathbf{v}}\mathbf{L^{-1}}\tilde{\mathbf{P}}_{\mathbf{m}})$

For static case, the elements of matrices which depend on natural frequencies (ω) and time (t) becomes zero, $\bar{B}_{i_4j_1}$=$\bar{B}_{i_5j_2}$=$\bar{B}_{i_6j_3}$=$\bar{B}^{v}_{i_4j_1}$=$\bar{B}^{v}_{i_5j_2}$=$\bar{B}^{v}_{i_6j_3}$=0. Therefore, the coefficients of final system of first order ODEs Eq. (4.27) is not now function of unknown natural frequencies (ω). So, final system of ODE Eq. (4.27) now expressed as,

$$\bar{\mathbf{F}}_{,\xi} = \{\mathbf{B_0} + \xi_1\mathbf{B_1} + \xi^2\mathbf{B_2}\}\bar{\mathbf{F}} + \mathbf{P_0} + \xi\mathbf{P_1} \tag{4.28}$$

Above equation represents the set of first order non-homogeneous ODEs with variable coefficient (function of ξ).

Similarly, for the dynamic case (free vibration), all the elements in the load vectors ($\bar{\mathbf{P}}^{\mathbf{f}}_{\mathbf{m}}$ and $\tilde{\mathbf{P}}^{\mathbf{f}}_{\mathbf{m}}$) becomes zero due to absence of external applied load ($\bar{P}_{m_{i1}}$=$\bar{P}^{v}_{m_{i1}}$=$\bar{P}_{m_{i2}}$=$\bar{P}_{m_{i6}}$=$\tilde{P}_{m_{i1}}$=0). Therefore, load vectors $\mathbf{P_0}$ and $\mathbf{P_1}$ in Eq. (4.27) are now equals to zero. Therefore, the Eq. (4.27) reduced to,

$$\bar{\mathbf{F}}_{,\xi_1} = \{\mathbf{B_0}(\omega) + \xi_1\mathbf{B_1}(\omega) + \xi_1^2\mathbf{B_2}\}\bar{\mathbf{F}} \tag{4.29}$$

Now, Eq. (4.29) is a system of simultaneous homogeneous first order ordinary differential equations ($6n$) with variable coefficients which is function of ξ-coordinate and also contains natural frequencies (ω).

The final approximate solution for present system of ODEs Eq. (4.28) and (4.29) are obtained by employing modified power series method as discussed in Chapter 2 and 3. Now $\bar{\mathbf{F}}$ is known functions which is substituting into Eq. (4.22) to solve the functions $\hat{\mathbf{F}}$. Now the second step is completed and further, these two steps of thickness and in-plane directions are repeated to achieve the required level of accuracy.

4.3 NUMERICAL RESULTS AND DISCUSSIONS

Four flat panels (a), (b), (c) and (d) are considered for numerical study as shown in Fig. 4.2. All

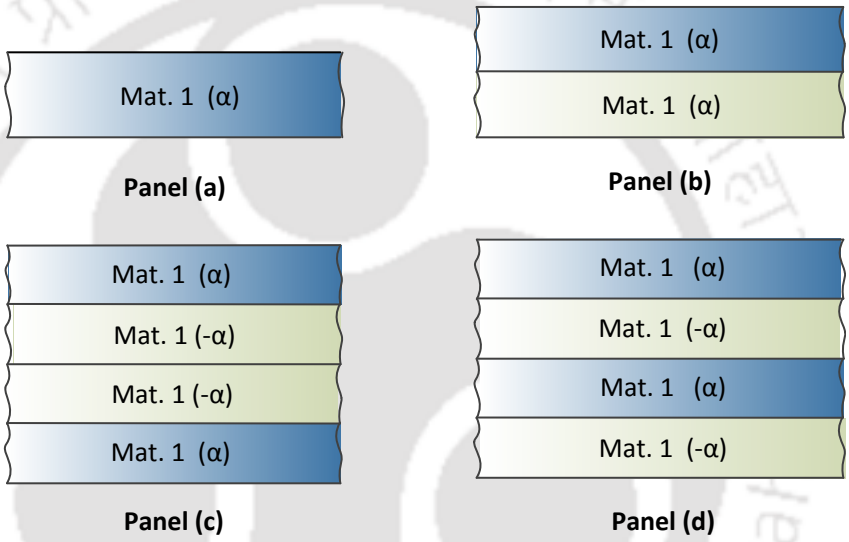

Fig. 4.2: Configuration of AFG angle-ply flat panels

the panels are made of Graphite-Epoxy material and the engineering material constant are given as: [(Y_1, Y_2, Y_3, G_{23}, G_{13}, G_{12}) , ν_{12}, ν_{13}, ν_{23}]=[(181.0, 10.3, 10.3, 2.87, 7.17, 7.17) GPa, 0.28, 0.28, 0.33]. To study the effect of varying material properties on the behaviour of flat panel, following variation indexes have been considered for panels.

Panel (a) : Case (i)$_a$ δ_1=δ_2=0.5; Case (ii)$_a$ δ_1=δ_2=1.0; Case (iii)$_a$ δ_1=1, δ_2=2

Panel (b) : Case (i)$_b$ Bottom layer δ_1=δ_2=0.0, Top layer δ_1=δ_2=0.5; Case (ii)$_b$ Bottom layer δ_1=δ_2=0.5, Top layer δ_1=δ_2=1.0; Case (iii)$_b$ Bottom layer δ_1=δ_2=1.0, Top layer δ_1=δ_2=1.0

Panel (c) and Panel (d) : variation indexes of each ply taken as - Case (i)$_{cd}$ δ_1=δ_2=0.5; Case (ii)$_{cd}$ δ_1=δ_2=1.0 The accuracy and efficiency of the present method is verified thoroughly by comparing with existing literature [279] for homogeneous case (constant material properties) and with 3D FE for varying stiffness case. Since it is a angle-ply panel, plane strain element of ABAQUS can not be used. Therefore, the rectangular plate whose length along y-direction is 20 time the width along

x-direction is modeled in ABAQUS using the element type C3D20R with mesh size of 40 (length) $\times$50 (width)$\times$16 (thickness) [279]. For present case, it is verified that these FE results do not change with a higher value of b/a. The spatially graded property distribution (at different Gauss points) is implemented by employing user material subroutine (UMAT) and the variation of mass density is implemented by dividing the panels into 20 number of equal parts along the length and each part is assigned density value according to its center point. Converged results of EKM are presented in this paper.

4.4 STATIC ANALYSIS

For static bending case, it is assumed that considered panels are subjected to uniformly distributed pressure load (p_2) is applied at top surface. The presented results are non-dimensionalized with $s = h/a$, $Y_0 = 10.3$ GPa and $p_0 = 1$ as:

$(\bar{u}, \bar{w}) = 100(u, s\ w)Y_0 s^3/(p_0 h)$; $\quad (\bar{\sigma}_x,\ \bar{\tau}_{xy},\ \bar{\tau}_{zx}) = (\sigma_x,\ 10\tau_{xy},\ \tau_{zx}/s)s^2/p_0$

4.4.1 Single Layered Panel (a)

Longitudinal variation of deflection ($\bar{w}$) and stresses ($\bar{\sigma}_x$, $\bar{\tau}_{xy}$ and $\bar{\tau}_{zx}$) for panel (a) have been presented in Figs. 4.3, 4.4 and 4.5 for simply-supported (S–S), clamped-simply supported (C–S) and clamped-free (C–F) boundary conditions, respectively. Results are plotted for different variation

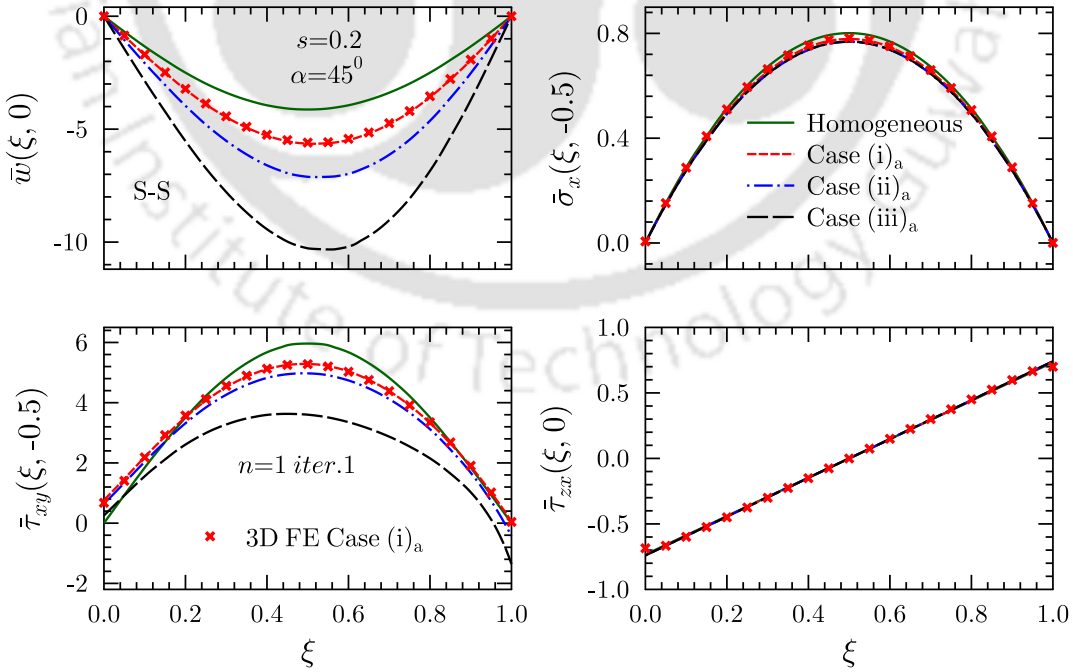

Panel (a) with α=45^0

Fig. 4.3: Effect of variation in properties on longitudinal variations of deflection and stresses for panel (a) ($\alpha = 45^o$, $s = 0.2$) subjected to S–S boundary condition

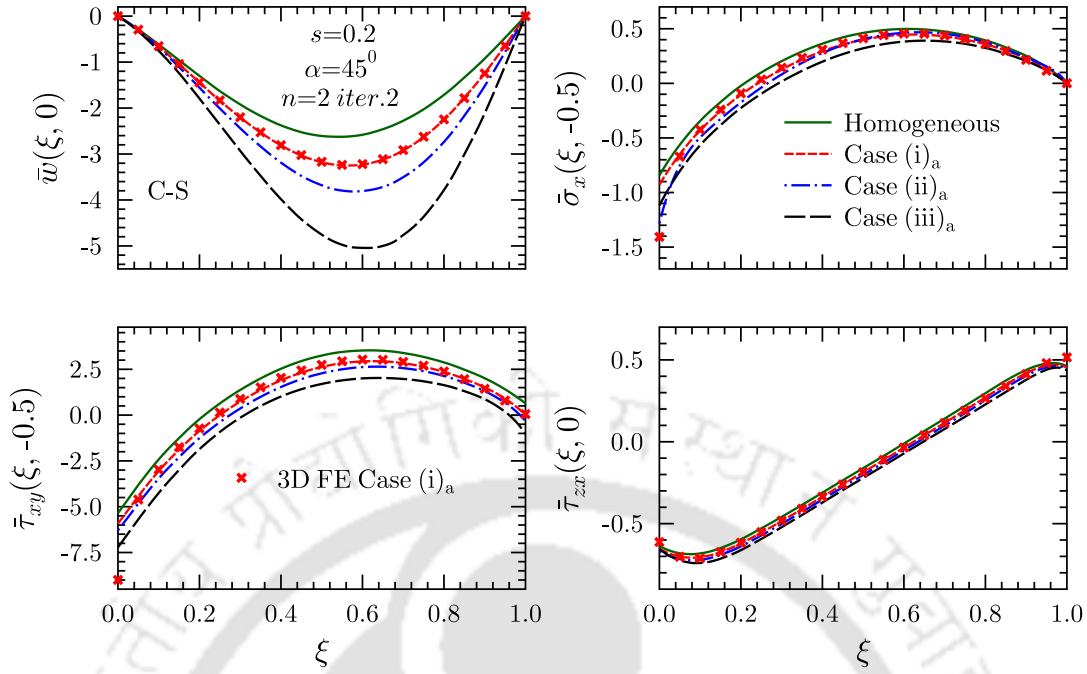

Panel (a) with α=45^0

Fig. 4.4: Effect of variation in properties on longitudinal variations of deflection and stresses for panel (a) ($\alpha = 45^o$, $s = 0.2$) subjected to C–S boundary condition

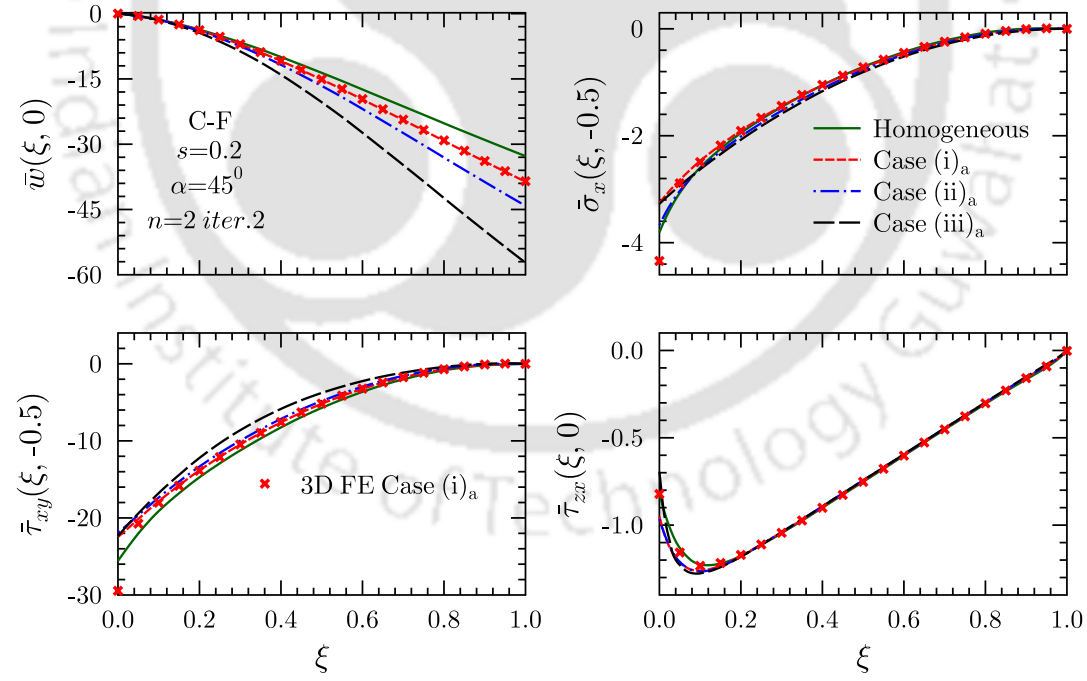

Panel (a) with α=45^0

Fig. 4.5: Effect of variation in properties on longitudinal variations of deflection and stresses for panel (a) ($\alpha = 45^o$, $s = 0.2$) subjected to C–F boundary condition

indexes ($\delta_1 = \delta_2 = 0.5$, $\delta_1 = \delta_2 = 1.0$, and $\delta_1 = 1.0$, $\delta_2 = 2.0$) along with homogeneous case to study the effect of in-plane varying material properties. 3D FE results for Case (i)$_a$ is also plotted in these

figures. It is observed that present result are in excellent agreement with 3D FE results except for stress at very clamped edges. This mismatch at very clamped edge is because the FE solution does not ensure conditions of applied normal at top and bottom surfaces of panel for transverse stresses ($\bar{\sigma}_z$ and $\bar{\tau}_{zx}$) [279] and it can be verified from Fig. 4.7. For simply-supported case, single term (n=1, *iter*.1) gives accurate prediction for all the entities whereas two-term solution (n=2, *iter*.2) is required for the other boundary conditions. It is evident that for all the boundary conditions (S–S, C–S, C–F) deflection ($\bar{w}$) is effected significantly with increase in variation index whereas $\bar{\tau}_{zx}$ is least effected. As variation indices increase, the point of maximum deflection ($\bar{w}$) for S–S and C–S boundary condition is shifted gradually toward $\xi = 1.0$. For S–S and C–S case, stress $\bar{\sigma}_x$ and $\bar{\tau}_{xy}$ decreases as the variation index increases. The decrement in $\bar{\tau}_{xy}$ is significantly high under S–S boundary conditions. It is revealed that influence of in-plane graded material properties depend significantly on boundary condition of flat panel.

Longitudinal variation of in-plane displacement ($\bar{u}$) are plotted in Fig. 4.6 for four type of support conditions (e.g. S–S, C–F, C–S, and C–C). For all the support conditions, in-plane displacement ($\bar{u}$)

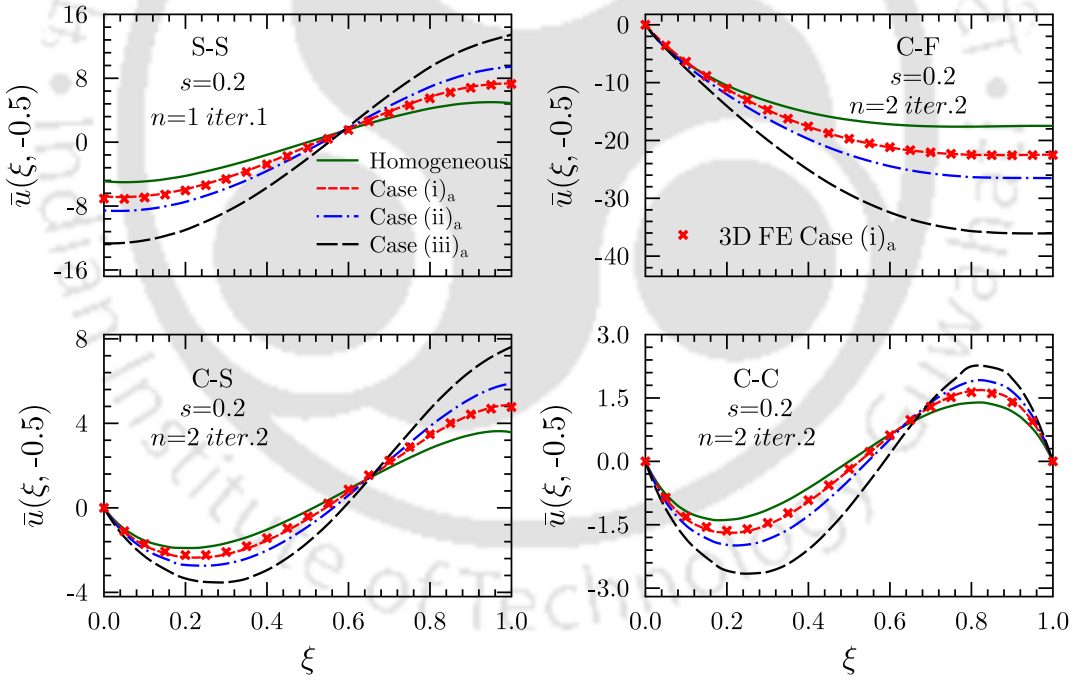

Panel (a) with α=45^0

Fig. 4.6: Effect of variation in properties on longitudinal variations of in-plane deflection ($\bar{u}$) for panel (a) ($\alpha = 45^o$, $s = 0.2$) subjected to different boundary condition (S–S, C–F, C–S, C–C)

is influenced greatly by an increase in variation index. It is observed that effect of varying material property is more pronounced near to simply-supported and free edges than the center of the flat panel. For S–S, C–S and C–C conditions, the effect is minimum, around $\xi = 0.6$, with respect to the constant case. All the lines cut the homogeneous case line at one point near to $\xi = 0.6$. For

C–C case, asymmetry is the highest for Case (iii)$_a$ and a similar trend is observed for S–S case also. For all the boundary conditions, the in-plane displacement ($\bar{u}$) increases abruptly for Case (iii)$_a$ as compared to Case (i)$_a$ and Case (ii)$_a$. The longitudinal variation of in-plane displacement for S–S and C–C boundary condition become more asymmetrical as the variation index increases.

Through-thickness variations at different ξ location have been presented in Fig. 4.7 for Case (i)$_a$ under C–F support conditions. 3D FE results for all ξ location are also plotted in the figure. It

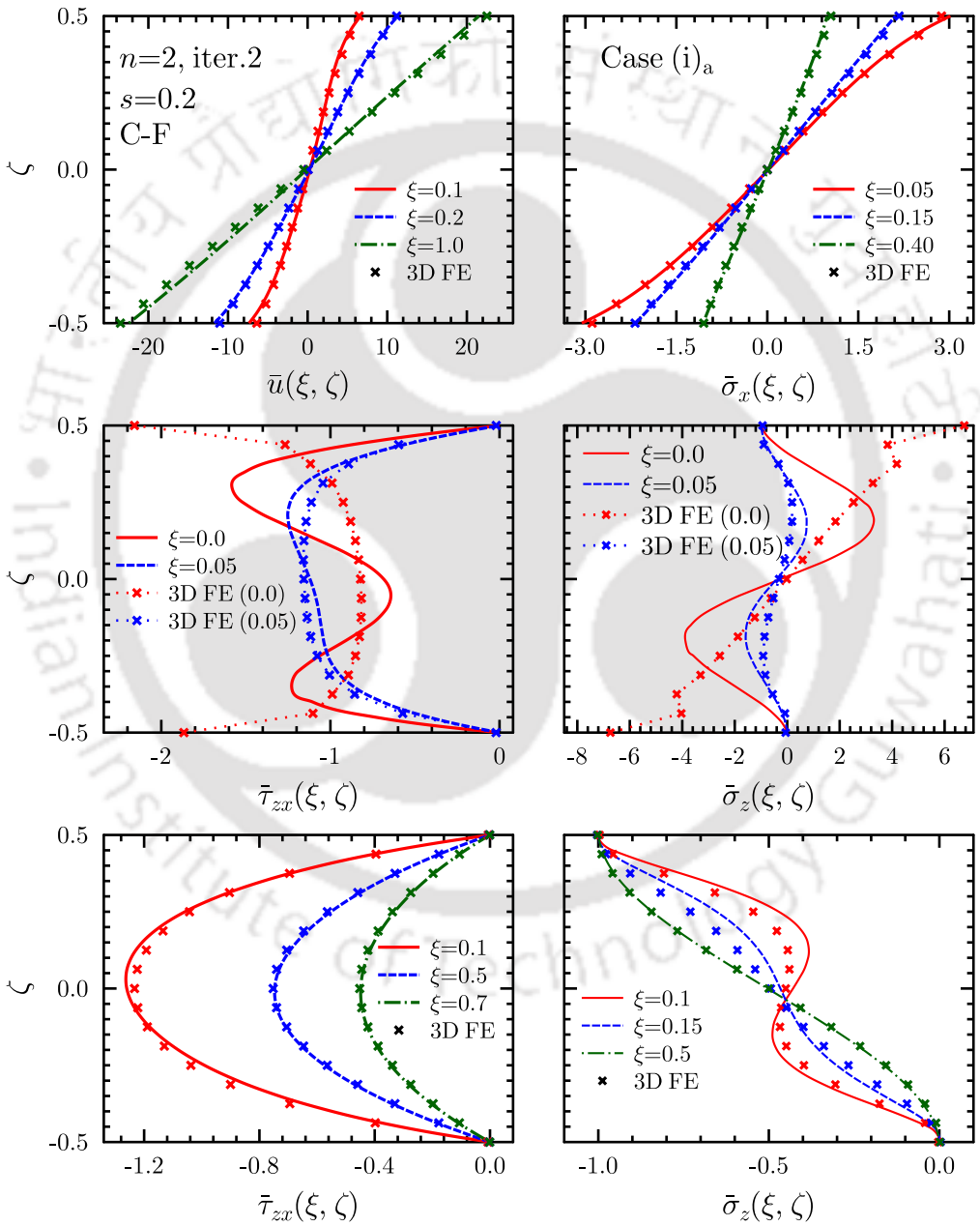

Panel (a): with α=45^o

Fig. 4.7: Comparison of in-plane deflection and stresses distributions at different ξ-locations with 3D FE solution for panel (a) ($s = 0.2$) under C–F boundary condition

is revealed that the distribution of in-plane displacement $\bar{u}$ and stress $\bar{\sigma}_x$ match well with the 3D FE solution near to clamped support, but 3D FE fails in predicting the stresses $\bar{\sigma}_x$, $\bar{\sigma}_z$ and $\bar{\tau}_{zx}$ at the clamped edge. 3D FE predicted stress distribution does not satisfy shear traction (zero) and condition of applied normal at the top and bottom surfaces of panel whereas present EKM solution satisfies these conditions exactly. The FE results for transverse stresses match well with the present solution at some distance away from the clamped edge. It is observed that in-plane displacement ($\bar{u}$) follow linear pattern near to free edges which is quadratic or cubic near the clamped support. Similar trends are observed for $\bar{\sigma}_x$ and $\bar{\sigma}_z$. Through-thickness variation of $\bar{\tau}_{zx}$ is parabolic and its magnitude decreases as we move from clamped edge to free edge.

Effect of ply-angle on longitudinal variation of deflection ($\bar{w}$) and stresses ($\bar{\sigma}_x$, $\bar{\tau}_{xy}$ and $\bar{\tau}_{zx}$) has been shown in Fig. 4.8. It is observed that, with an increase in ply-angle from 0^o to 30^o, there is a

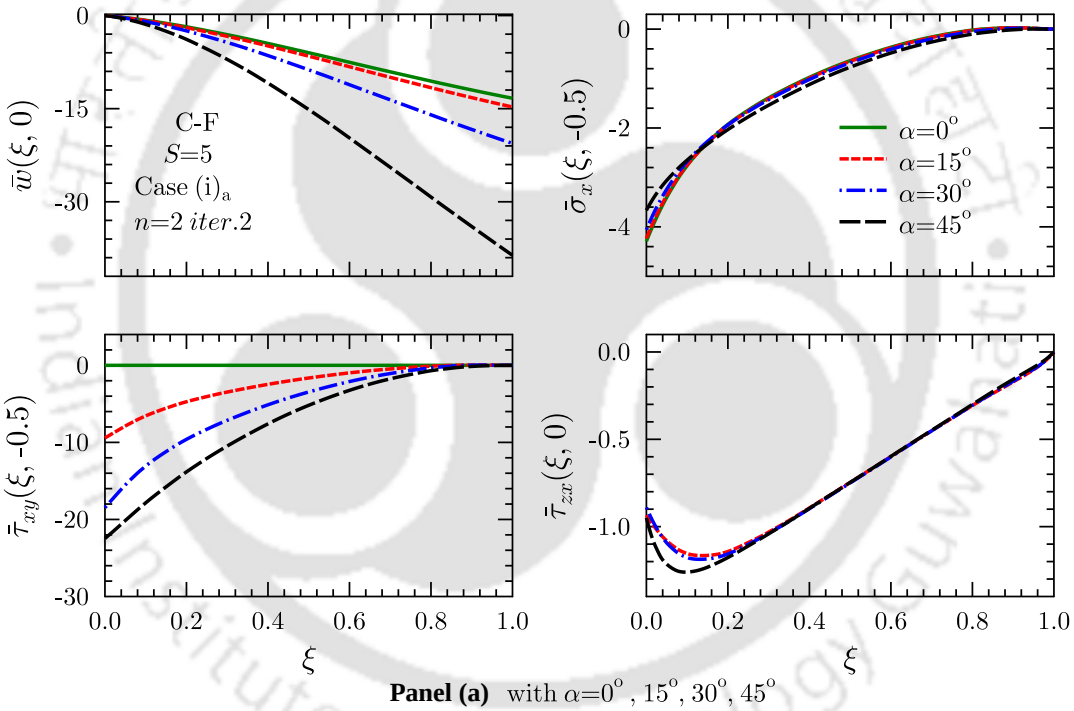

Fig. 4.8: Comparison of deflection and stresses distributions for different value of α under C–F boundary condition

gradual increase in all the entities whereas for 45^o ply-angle magnitude of all the entities increases abruptly.

Percentage increment or decrement, with respect to the homogeneous case, of various entities at the location where it is maximum, is presented in Table 4.1. It is found that in-plane displacement ($\bar{u}$) increases with increase in variation index and it is maximum for simply-supported boundary condition which is 175.65% for Case $(\text{iii})_\text{a}$. Percentage increase in deflection ($\bar{w}$) is also maximum for S–S support condition. The increment in the in-plane stress is maximum for C–S boundary

Table 4.1: Percentage(%) change in deflections and stresses with respect to homogeneous case, due to variation in material properties for panel (a) with $\alpha = 45^o$

B.C.	Entity(x, z)	Case (i)$_a$	Case (ii)$_a$	Case (iii)$_a$
S–S	$\bar{u}$ (1.0, -0.5)	50.47	93.38	175.65
	$\bar{w}$ (0.5, 0.0)	36.62	72.19	148.84
	$\bar{\sigma}_x$ (0.5, -0.5)	-2.79	-4.15	-4.07
	$\bar{\tau}_{xy}$ (0.5, -0.5)	-11.37	-16.58	-39.59
	$\bar{\tau}_{zx}$ (0.1, 0.0)	0.49	0.94	0.96
C–S	$\bar{u}$ (1.0, -0.5)	36.10	64.79	113.45
	$\bar{w}$ (0.5, 0.0)	21.87	41.10	82.28
	$\bar{\sigma}_x$ (0.5, -0.5)	-13.36	-21.72	-30.55
	$\bar{\tau}_{xy}$ (0.5, -0.5)	-19.23	-29.84	-47.71
	$\bar{\tau}_{zx}$ (0.1, 0.0)	3.34	5.72	8.71
C–F	$\bar{u}$ (1.0, -0.5)	28.36	51.64	106.17
	$\bar{w}$ (1.0, 0.0)	17.97	34.85	74.83
	$\bar{\sigma}_x$ (0.5, -0.5)	2.30	8.00	13.68
	$\bar{\tau}_{xy}$ (0.5, -0.5)	-9.28	-15.64	-33.96
	$\bar{\tau}_{zx}$ (0.1, 0.0)	2.87	3.27	4.18

condition, which is -30.55% for Case (iii)$_a$. Maximum decrement of 47.7% in $\bar{\tau}_{xy}$ is observed for Case (iii)$_a$ under C–S boundary conditions. From the Table 4.1, it is concluded that the effect of material property variation is relatively less under clamped support conditions (C–S, C–F) than simply supported condition (S–S).

4.4.2 Two Layered Panel (b)

Figures. 4.9 and 4.10 depict the effect of variation index on longitudinal variation of deflection ($\bar{w}$) and stresses ($\bar{\sigma}_x$, $\bar{\tau}_{xy}$ and $\bar{\tau}_{zx}$) for C–S and C–F support conditions, respectively. Panel (b) is a two layered flat panel in which effect of variation of material property is investigated by taking different and same variation index for the top and bottom layer. To study the effect of varying material property on the longitudinal variation of deflection and stresses for the layer-wise homogeneous case is also plotted in figures. It is observed that deflection and stresses are significantly affected even by considering the variation of material property in one layer. 3D FE results for Case (ii)$_b$ is also presented in Figs. 4.9 and 4.10. The present results are in good agreement with 3D FE except for stress at very clamped edges. Because at the support specifically clamped type, finite element solutions do not satisfy the boundary conditions and interface continuity conditions which can be verified from Figs. 4.7 and 4.14. For both C–S and C–F support conditions, deflection $\bar{w}$ is affected significantly by gradation of properties along x-direction whereas stresses $\bar{\sigma}_x$, $\bar{\tau}_{xy}$ and $\bar{\tau}_{zx}$ are least

affected. The deflection at the center of the panel for C–S support increased by 9.5% for Case $(i)_b$, 29.7% for Case $(ii)_b$ and 43.2% for Case $(iii)_b$ with respect to the homogeneous case. Similarly, for

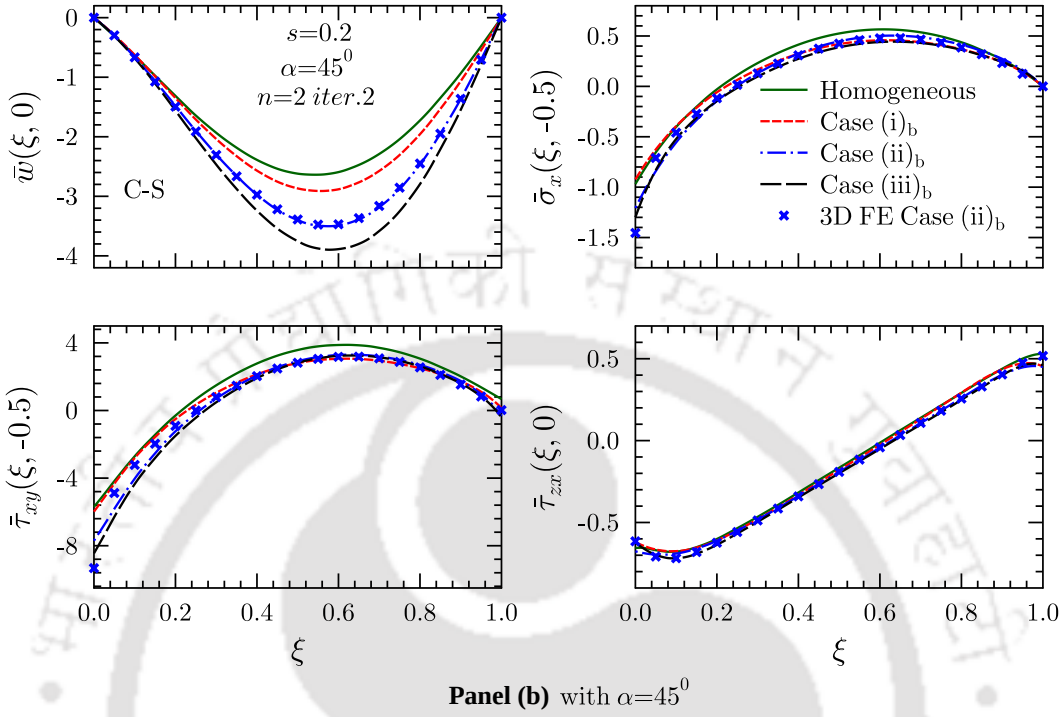

Panel (b) with α=45^0

Fig. 4.9: Effect of variation in properties on longitudinal variations of deflection and stresses for panel (b) ($\alpha = 45^o$, $s = 0.2$) under C–S boundary condition

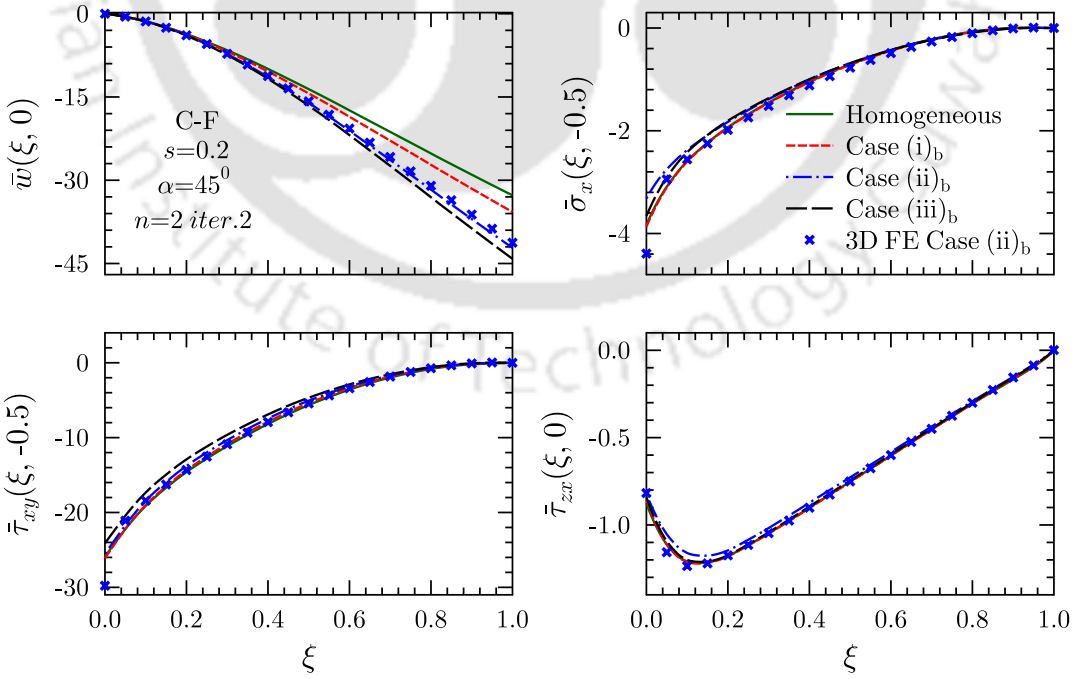

Panel (b) with α=45^0

Fig. 4.10: Effect of variation in properties on longitudinal variations of deflection and stresses for panel (b) ($\alpha = 45^o$, $s = 0.2$) under C–F boundary condition

C–F panel, the percentage change in deflection at the free edge of the panel is 9.1% for Case $(i)_b$, 29% for Case $(ii)_b$ and 35% for Case $(iii)_b$. For both C–S and C–F case, the percentage change in $\bar{\tau}_{zx}$ is less than 5%.

4.4.3 Four Layered Panels (c) and (d)

The results for panel (c) with C–C, C–S and C–F boundary condition is plotted in Figs. 4.11 and 4.12 for different cases of property variation, Case $(i)_{cd}$ and Case $(ii)_{cd}$ along with the constant property case to study the effect of gradation on behaviour of laminated panels. To verify the

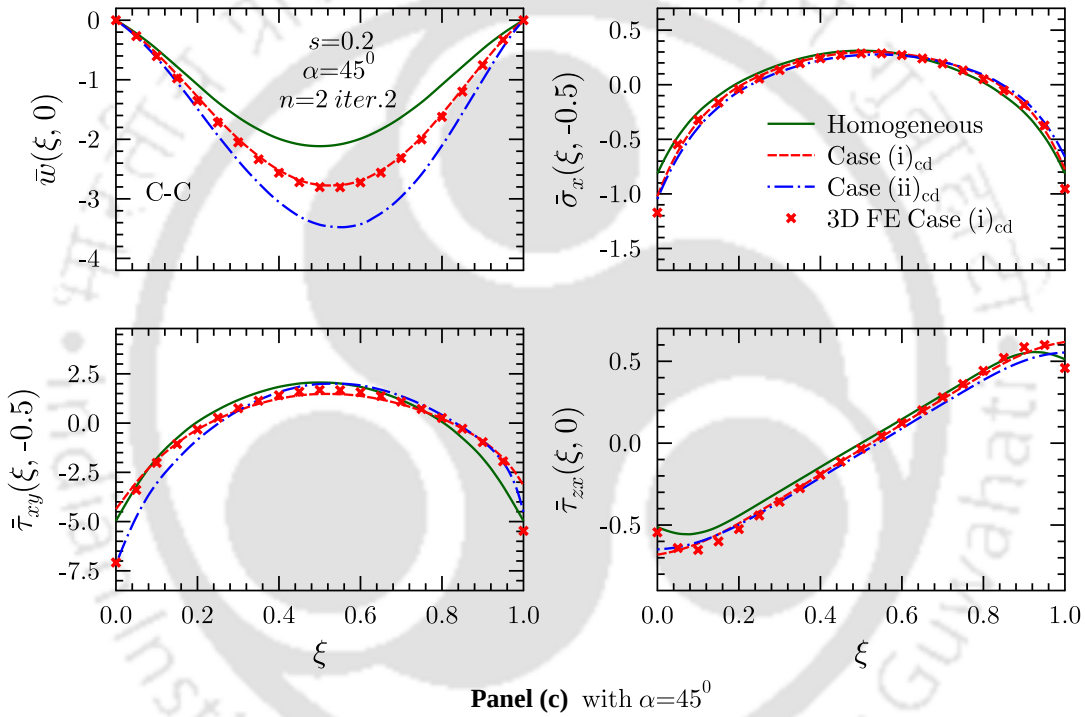

Fig. 4.11: Effect of variation in properties on longitudinal variations of deflection and stresses for panel (c) ($\alpha = 45^o$, $s = 0.2$) under C–C boundary condition

accuracy and stability of present solution for the multi-layered panel, 3D FE results for Case $(i)_{cd}$ are also plotted and thoroughly verified for all other cases. It is observed that present results are in very good agreement with 3D FE. Longitudinal variation of deflection ($\bar{w}$) and stresses ($\bar{\sigma}_x$, $\bar{\tau}_{xy}$ and $\bar{\tau}_{zx}$) for C–C support conditions are plotted in Fig. 4.11. It is observed that deflection ($\bar{w}$) affect significantly as compared to stresses $\bar{\sigma}_x$, $\bar{\tau}_{xy}$ and $\bar{\tau}_{zx}$. Similarly in Fig. 4.12 longitudinal variation of $\bar{w}$ and $\bar{\sigma}_x$ is plotted for C–S, C–F boundary conditions, respectively. For both boundary condition, the influence of varying material properties on deflection ($\bar{w}$) is significantly and more pronounced as compared to $\bar{\sigma}_x$.

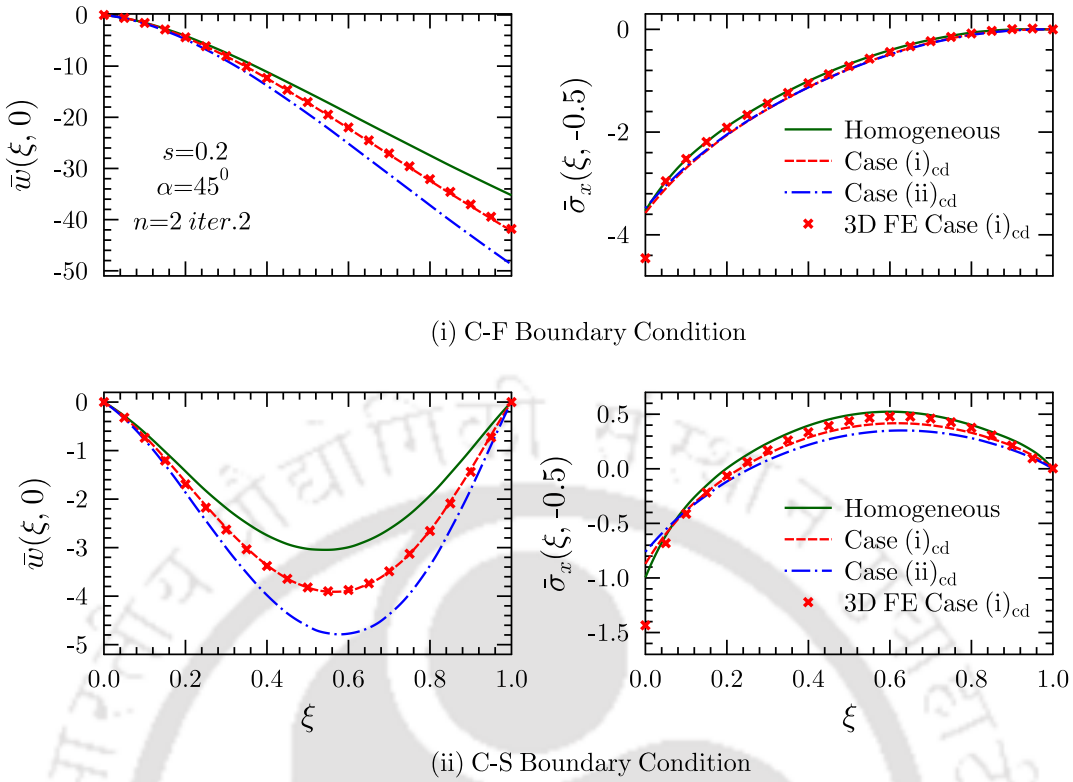

(i) C-F Boundary Condition

(ii) C-S Boundary Condition

Fig. 4.12: Effect of variation in properties on longitudinal variations of deflection and stresses for panel (c) under C–F and C–S boundary condition

Similarly in Fig. 4.13 longitudinal variation of deflections ($\bar{u}$, $\bar{w}$) and stress ($\bar{\sigma}_x$) have been presented for panel(d) under C–C and C–F boundary conditions. Here, 3D FE result for Case (i)$_{cd}$ is also plotted which is in good agreement with present results. To study the effect of gradation in material properties on deflection and stresses, the results for the layer-wise homogeneous case is also plotted in same figures. It is observed that, the effect of material properties more significant for deflections ($\bar{u}$, $\bar{w}$) as compared to stress ($\bar{\sigma}_x$) for both C–C and C–F support. For panel subjected to C–C boundary conditions, the longitudinal variation of deflections become more asymmetrical as the variation index increases.

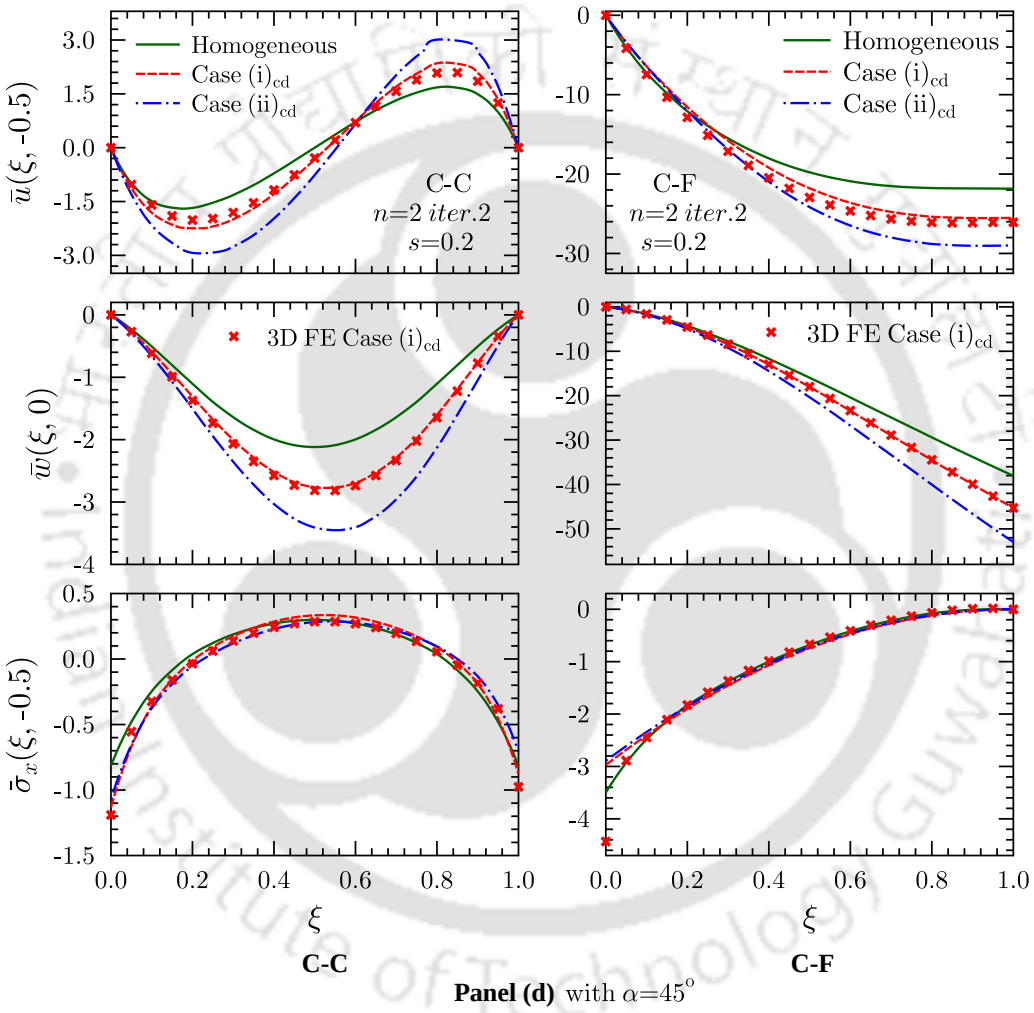

Fig. 4.13: Effect of variation in properties on longitudinal variations of deflection and stresses for panel (d) under C–C and C–F boundary condition

Through-thickness distribution of transverse stresses $\bar{\sigma}_z$ and $\bar{\tau}_{zx}$ have been presented in Fig. 4.14 for panel (d) in which material properties varying according to Case (i)$_{\text{cd}}$ and panel subjected to C–F boundary conditions. It is observed that 3D FE solution fail to predict the stress distribution

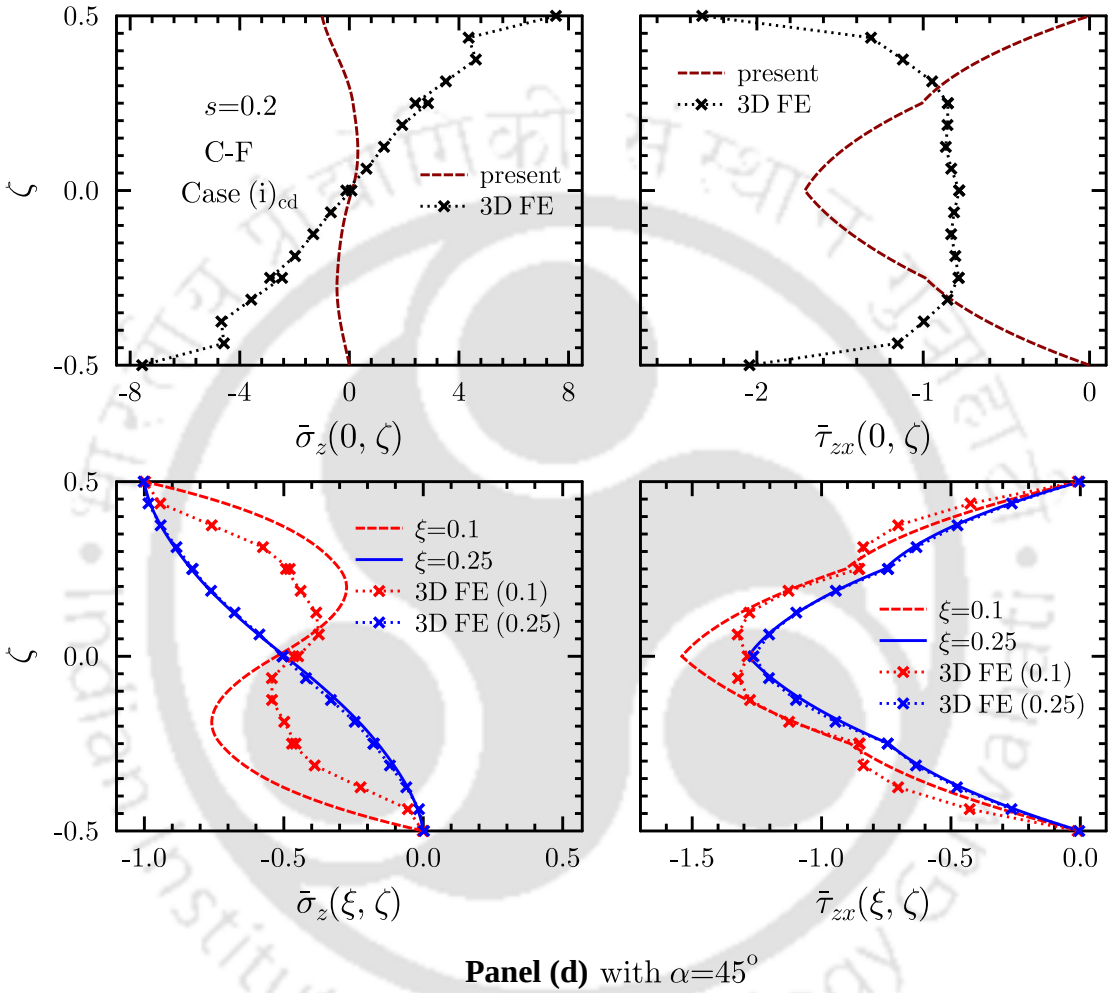

Fig. 4.14: Comparison of stresses distributions at different ξ-locations with 3D FE solution for panel (d) ($s = 0.2$) under C–F boundary condition (Case (i)$_{\text{cd}}$)

at the clamped support. At very clamped support ($\xi = 0$), stress distribution predicted by FE neither satisfy interface continuity condition nor satisfy shear traction (zero) and condition of applied normal at top and bottom surface of the panel. But present EKM solution satisfies all these conditions at the clamped support. It is observed that away from clamped support, FE results matches closely with the present EKM results.

4.5 DYNAMIC ANALYSIS

The numerical results are presented for single layer axially functionally graded panel (a), as shown in Fig. 4.2. The material properties for panels are taken as, Mat.1:[(Y_1, Y_2, Y_3, G_{23}, G_{13}, G_{12}) , ν_{12}, ν_{13}, ν_{23}]=[(181.0, 10.3, 10.3, 2.87, 7.17, 7.17) GPa, 0.28, 0.28, 0.33]. The natural frequencies ω are non-dimensionalized as $\omega^* = \omega h\sqrt{\rho/G_{12}}$. Where ρ and G_{12} are taken as 1578 Kg/m^3 and 7.17 GPa, respectively. The thickness of flat panels is consider according to thickness to span ratio ($s = h/a$). For $s = 0.2, 0.1, 0.05$ the values of h are 0.2, 0.1, 0.05, respectively. The AFG panels are designated according to their support conditions at the edges $\xi = 0, 1$. For example, the panels which is clamped (C) at $\xi = 0$ and simply-supported (S) at $\xi = 1$, is called an C–S panels. In the subsequent sections, results are obtained by taking n=1, iter.2 for simply-supported (S–S) panels and n=1, iter.3 for other panels (C–C, C–S, C–F). To examine the effects of axial gradation of material properties on natural frequencies of panels, the results are obtained for two type of gradation cases, Case(i)$_a$: $\delta_1 = \delta_2 = \delta_p = 0.5$ and Case(ii)$_a$: $\delta_1 = \delta_2 = \delta_p = 1.0$ along with constant property (homogenous panels) case (Constant: $\delta_1 = \delta_2 = \delta_p = 0.0$).

4.5.1 Effect of axial gradation on natural frequencies of panels

An single-layer angle-ply flat panel (a), as shown in Fig. 4.2, is considered for study in this section. First five lowest dimensionless flexural frequencies $\omega^* = \omega h\sqrt{\rho/G_{12}}$ are tabulated for flat panel with s=0.1 and ply-angle α=45^o. Results are presented for different variation cases, Case(i)$_a$: $\delta_1 = \delta_2 = \delta_p = 0.5$ and Case$_a$(ii): $\delta_1 = \delta_2 = \delta_p = 1.0$ along with constant properties (homogeneous) case (Constant: $\delta_1 = \delta_2 = \delta_p = 0.0$) to investigating the effect of axial gradation of material properties on natural frequencies of flat panels. In Tables 4.2 and 4.3, benchmark numerical results are tabulated for S–S, C–S, C–C and C–F support conditions, respectively.
For the axially functionally graded flat panels, the analytical elasticity solution is not available in the literature even for S–S support condition. Therefore, the accuracy and efficiency of the present 3D EKM solution for the present case are verified by comparing the present result with 3D FE. Hence, corresponding 3D FE result obtained by using commercial FE Software ABAQUS [294] is also tabulated in Tables 4.2 and 4.3 for all the support conditions and for all gradation cases. The axial gradation of material properties is implemented by employing user material subroutine (UMAT) [296]. The axial variation of density is implemented by dividing the flat panels into 20 number of equal parts along x-axis and each part are assigned density value according to its center point. It is observed that the present results are in excellent agreement with 3D FE results for all cases under all the support conditions. From these comparisons of numerical results, it is established that the single term solution is sufficient enough for obtaining accurate flexural frequencies for all

Table 4.2: Effect of axial gradation of material properties on natural frequencies $\omega^*=\omega h\sqrt{\rho/G_{12}}$ of single layered panels (a) subjected to S–S and C–S support conditions ($s = 0.1$ and $\alpha = 45^o$)

	m	Constant		Case (i)$_a$		Case (ii)$_a$	
		Present	3D FE	Present	3D FE	Present	3D FE
S–S	1	0.0753853	0.0755302	0.0562288	0.0562704	0.0453792	0.0452757
	2	0.2610064	0.2611546	0.2015759	0.2014149	0.1659895	0.1657279
	3	0.4952609	0.4953796	0.3925996	0.3923008	0.3278164	0.3269517
	4	0.7456397	0.7462234	0.6018451	0.6014650	0.5076384	0.5068165
	5	1.0021682	1.0066176	0.8172511	0.8179689	0.6941604	0.6926944
C–S	1	0.1078259	0.1080957	0.0831168	0.0832648	0.0684934	0.0684677
	2	0.2951952	0.2960605	0.2331902	0.2331963	0.1946806	0.1943170
	3	0.5212792	0.5227042	0.4189571	0.4192127	0.3532198	0.3528615
	4	0.7645385	0.7663263	0.6214966	0.6221869	0.5275237	0.5273910
	5	1.0152517	1.0175238	0.8316362	0.8327071	0.7184420	0.7177493

Table 4.3: Effect of axial gradation of material properties on natural frequencies $\omega^*=\omega h\sqrt{\rho/G_{12}}$ of single layered panels (a) subjected to C–C and C–F support conditions ($s = 0.1$ and $\alpha = 45^o$)

	m	Constant		Case (i)$_a$		Case (ii)$_a$	
		Present	3D FE	Present	3D FE	Present	3D FE
C–C	1	0.1423000	0.1430517	0.1119542	0.1116417	0.0921630	0.0924703
	2	0.3261132	0.3278950	0.2613132	0.2614671	0.2188926	0.2188973
	3	0.5451904	0.5482602	0.4414696	0.4424991	0.3727851	0.3733180
	4	0.7820662	0.7853975	0.6373188	0.6393716	0.5412903	0.5425418
	5	1.0281458	1.0219453	0.8423645	0.8430238	0.7175778	0.7190757
C–F	1	0.0276999	0.0277959	0.0215103	0.0215611	0.0177246	0.0177212
	2	0.1498461	0.1500111	0.1161567	0.1163196	0.0959182	0.0958306
	3	0.3563517	0.3571650	0.2804002	0.2822449	0.2350935	0.2354630
	4	0.5910712	0.5928579	0.4772370	0.4768390	0.3996376	0.4015859
	5	0.8390745	0.8415500	0.6849135	0.6867991	0.5729467	0.5753785

the cases and boundary conditions.

The significant effect of axial gradation is observed on the flexural frequencies of the flat panels. As the gradation indexes increases, the natural frequencies of the flat panels decreases significantly for all the boundary conditions. Percentage change in natural frequencies for Case $(i)_a$ and Case $(ii)_a$ are plotted in Fig. 4.15 under all the support conditions (S–S, C–S, C–C and C–F). For all the support conditions, it is observed the percentage decrement is maximum for first natural frequency as compared to higher mode natural frequencies. The magnitude of percentage decrement is reducing as the mode become higher. The percentage decrement in the first natural is 22-25% for Case $(i)_a$ and 35-39% for Case $(ii)_a$ under all support conditions. This percentage decrement in natural frequency is lesser for higher mode natural frequencies. For fifth flexural mode (Mode-5) natural frequency, the percentage decrement 18-19% and 29-31% for Case $(i)_a$ and Case $(ii)_a$, respectively under all support conditions.

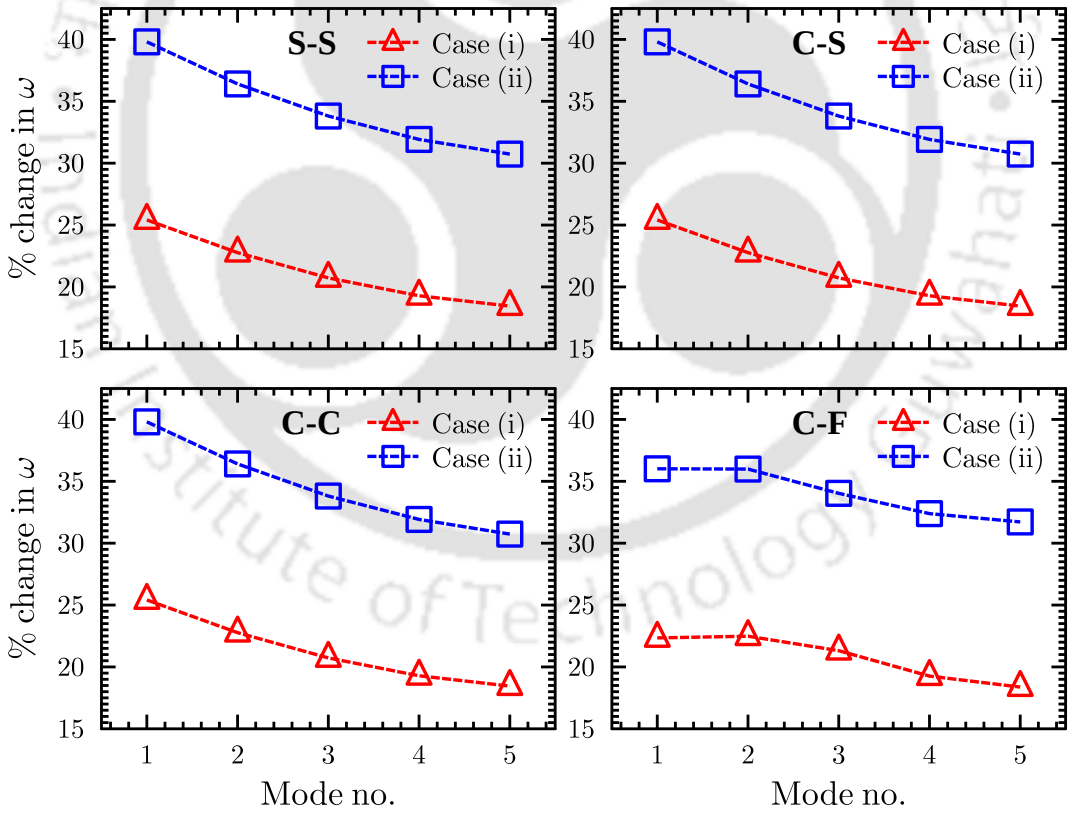

Fig. 4.15: Percentage change in first five lowest flexural frequencies of panel (a) due to axial gradation of material properties under S–S, C–S, C–C and C–F boundary conditions

Similarly, the effect of support conditions is significant on the lower mode of natural frequencies for all the variation cases. It is maximum for first vibration mode, and this effect of boundary

condition is decreasing as the mode become higher. The effect of support conditions on higher modes (Mode-4 and Mode-5) natural frequencies is negligible as compared to first mode natural frequency.

4.6 SUMMARY

An accurate analytical elasticity solution is presented for axially functionally graded angle-ply flat panel under cylindrical bending and subjected to arbitrary boundary condition. The influence of stiffness variation on bending and free vibration response of angle-ply flat panel is investigated comprehensively. Based on the present study, it is established that the variation of material properties along the axial (x) direction affects the panel deflections, stresses and natural frequencies to a great extent. The natural frequencies of panels decreases significantly with the increment of gradation indexes. It is also observed that effects of axial stiffness variation on the static and dynamic behavior of the panel depend significantly on boundary conditions. For static case, the effect of in-plane material property variation on the deflections and stresses are relatively less under clamped support conditions (C–S, C–C) as compare to simply supported case (S–S). For dynamic case, the effect of axial gradation on the flexural frequencies of the flat panels is almost similar for all the support condtions. This development has shown that, by controlling the axial gradation parameters, the desired distribution of the deflection, stress can be achieved for specific applications. The present method provided benchmark results to assess the validity and accuracy of different plate theories and computational models for analysis of axially functionally graded angle-ply flat panel under cylindrical bending. The current research will also be beneficial to modeled real life panel structures in which material properties of panel deteriorate due to some environmental effect.

Chapter 5

Smart Angle-ply Flat Panels Under Free Vibration

For the first time, an accurate analytical solution, based on coupled three-dimensional (3D) piezoelectricity equations, is presented for free vibration analysis of the angle-ply elastic and piezoelectric flat laminated panels under arbitrary boundary conditions. The present analytical solution is applicable to composite, sandwich and hybrid panels having arbitrary angle-ply lay-up, material properties and boundary conditions. The modified Hamiltons principle approach, as discussed in Chapter 4, is applied to derive the weak form of governing equations where stresses, displacements, electric potential, and electric displacement field variables has been considered as primary variables. Thereafter multi-term multi-field extended Kantorovich approach (MMEKM), as described in Chapter 4, is employed to transform the governing equation into two sets of algebraic-ordinary differential equations (ODEs), one along in-plane (x) and other along the thickness (z) direction, respectively. These ODEs are solved in closed-form manner which ensures the same order of accuracy for all the variables (stresses, displacements, and electric variables) by satisfying the boundary and continuity equations in exact manners. A robust algorithm is developed for extracting the natural frequencies and mode shapes. The numerical results are reported for various configurations such as elastic panels, sandwich panels and piezoelectric panels under different sets of boundary conditions. The effect of ply-angle and thickness to span ratio (s) on the dynamic behavior of the panels are also investigated. The presented 3D analytical solution will be helpful in the assessment of various 1D theories and numerical methods.

5.1 GOVERNING EQUATIONS FOR SMART ANGLE-PLY PANELS

A infinitely long (along y-direction) angle-ply piezoelectric laminated panel of total thickness h along the z-axis and having length a along direction of x-axis, as shown in Fig. 5.1, is considered for modeling (cylindrical bending case). The hybrid laminated panel has L number of perfectly bonded

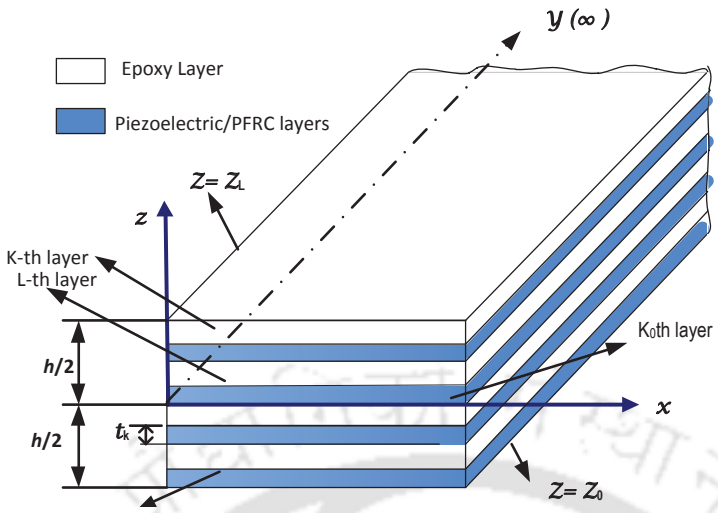

Fig. 5.1: Geometry of the Piezoelectric-laminated panel.

laminas which is generally orthotropic and a few of them can be orthotropic piezoelectric/PFRC material which could be utilized as distributed sensors and actuators, and these piezoelectric/PFRC laminas are poled along the thickness z-direction. The governing equations hold for each layer k^{th} layer having thickness $t(k)$, and its bottommost face denoted by z_{k-1}. Where the interface of k^{th} and $k+1^{th}$ ply symbolized as the k^{th} interface. For cylindrical bending case (generalized plane strain condition), strain-displacement and electric field-potential correlations reduce to [281],

$$\begin{bmatrix} \varepsilon_x \\ \varepsilon_y \\ \varepsilon_z \end{bmatrix} = \begin{bmatrix} u_{,x} \\ 0 \\ w_{,z} \end{bmatrix}, \quad \begin{bmatrix} \gamma_{xy} \\ \gamma_{zx} \\ \gamma_{yz} \end{bmatrix} = \begin{bmatrix} v_{,x} \\ w_{,x} + u_{,z} \\ v_{,z} \end{bmatrix}, \quad \begin{bmatrix} E_x \\ E_y \\ E_z \end{bmatrix} = \begin{bmatrix} -\phi_{,x} \\ 0 \\ -\phi_{,z} \end{bmatrix} \tag{5.1}$$

where u, v and w are displacements and E_x, E_y, E_z are electric field components along x, y and z-direction, respectively, which are independent of y and functions of x and z coordinates, only. ϕ denotes electric potential and a subscript comma represents partial differentiation. The coupled 3D piezoelectricity constitutive equations [281] for angle-ply are,

$$\begin{aligned}
\varepsilon_x &= \bar{s}_{11}\sigma_x + \bar{s}_{12}\sigma_y + \bar{s}_{13}\sigma_z + \bar{s}_{16}\tau_{xy} + \bar{d}_{31}E_z \\
\varepsilon_y &= \bar{s}_{12}\sigma_x + \bar{s}_{22}\sigma_y + \bar{s}_{23}\sigma_z + \bar{s}_{26}\tau_{xy} + \bar{d}_{32}E_z \\
\varepsilon_z &= \bar{s}_{13}\sigma_x + \bar{s}_{23}\sigma_y + \bar{s}_{33}\sigma_z + \bar{s}_{36}\tau_{xy} + \bar{d}_{33}E_z \\
\gamma_{yz} &= \bar{s}_{44}\tau_{yz} + \bar{s}_{45}\tau_{zx} + \bar{d}_{14}E_x + \bar{d}_{24}E_y \\
\gamma_{zx} &= \bar{s}_{54}\tau_{yz} + \bar{s}_{55}\tau_{zx} + \bar{d}_{15}E_x + \bar{d}_{25}E_y \\
\gamma_{xy} &= \bar{s}_{16}\sigma_x + \bar{s}_{26}\sigma_y + \bar{s}_{36}\sigma_z + \bar{s}_{66}\tau_{xy} + \bar{d}_{36}E_z \\
D_x &= \bar{d}_{14}\tau_{yz} + \bar{d}_{15}\tau_{zx} + \bar{\epsilon}_{11}E_x + \bar{\epsilon}_{12}E_y
\end{aligned} \tag{5.2}$$

$$D_y = \bar{d}_{24}\tau_{yz} + \bar{d}_{25}\tau_{zx} + \bar{\epsilon}_{21}E_x + \bar{\epsilon}_{22}E_y$$
$$D_z = \bar{d}_{31}\sigma_x + \bar{d}_{32}\sigma_y + \bar{d}_{33}\sigma_z + \bar{d}_{36}\tau_{xy} + \bar{\epsilon}_{33}E_z$$

where σ_i and ε_i denotes the normal stress and normal strains components, respectively. τ_{ij} and γ_{ij} denotes shear stress and shear strains, respectively. D_i denote the electric displacements and $\bar{s}_{ij}$ represent the transformed elastic compliances. Where $\bar{\epsilon}_{ij}$ and $\bar{d}_{ij}$ represent dielectric permittivity constants and piezoelectric strain constants at constant stress field, respectively. Using Eq. $(5.2)_9$, E_z can be represent in terms of D_z as [281],

$$E_z = -\bar{d}'_{31}\sigma_x - \bar{d}'_{32}\sigma_y - \bar{d}'_{33}\sigma_z - \bar{d}'_{36}\tau_{xy} + \frac{1}{\bar{\epsilon}_{33}}D_z \tag{5.3}$$

where $\bar{d}'_{ij} = \bar{d}_{ij}/\bar{\epsilon}_{33}$. Evaluate ε_y from Eq. $(5.1)_2$ and E_z from Eq. (5.3) and substituting in Eq. $(5.2)_2$, σ_y is written as [281],

$$\sigma_y = -(\bar{d}'_{32}/\bar{s}'_{22})D_z - (\bar{s}'_{23}/\bar{s}'_{22})\sigma_z - (\bar{s}'_{26}/\bar{s}'_{22})\tau_{xy} - (\bar{s}'_{12}/\bar{s}'_{22})\sigma_x \tag{5.4}$$

where $\bar{s}'_{ij} = \bar{s}_{ij} - \bar{d}_{3j}\bar{d}_{3i}/\bar{\epsilon}_{33}$. Using Eqs. (5.3) and (5.4), E_z and σ_y can be eliminated from Eqs. $(5.2)_1$, $(5.2)_3$, $(5.2)_6$ and Eq. (5.3) which yield

$$\begin{aligned}
\varepsilon_x &= p_{11}\sigma_x + p_{16}\tau_{xy} + p_{13}\sigma_z + p_{18}D_z \\
\varepsilon_z &= p_{31}\sigma_x + p_{36}\tau_{xy} + p_{33}\sigma_z + p_{38}D_z \\
\gamma_{xy} &= p_{61}\sigma_x + p_{66}\tau_{xy} + p_{63}\sigma_z + p_{68}D_z \\
E_z &= -(p_{81}\sigma_x + p_{86}\tau_{xy} + p_{83}\sigma_z + p_{88}D_z)
\end{aligned} \tag{5.5}$$

where

$$\begin{aligned}
p_{ij} &= \bar{s}'_{ij} - \bar{s}'_{2j}\bar{s}'_{2i}/\bar{s}'_{22}, \qquad & p_{88} &= -1/\bar{\epsilon}_{33} - \bar{d}'^2_{32}/\bar{s}'_{22} \\
p_{i8} &= p_{8i} = \bar{d}'_{3i} - \bar{d}'_{32}\bar{s}'_{2i}/\bar{s}'_{22}, & \text{for} \quad (i,j) &= 1, 3 \text{ and } 6
\end{aligned} \tag{5.6}$$

Again, substituting the Eq. $(5.2)_2$ in Eq. $(5.1)_2$, σ_y can be written as

$$\sigma_y = -(\bar{d}_{32}/\bar{s}_{22})E_z - (\bar{s}_{23}/\bar{s}_{22})\sigma_z - (\bar{s}_{26}/\bar{s}_{22})\tau_{xy} - (\bar{s}_{12}/\bar{s}_{22})\sigma_x \tag{5.7}$$

Again, using σ_y from Eq. (5.7) into Eqs. $(5.2)_1$, $(5.2)_3$, $(5.2)_6$ and $(5.2)_9$, ε_x, ε_z, γ_{xy} and E_z can be written in terms of σ_x, τ_{xy}, σ_z and E_z as [281],

$$\begin{aligned}
\varepsilon_x &= \bar{p}_{11}\sigma_x + \bar{p}_{16}\tau_{xy} + \bar{p}_{13}\sigma_z + \bar{p}_{18}E_z \\
\varepsilon_z &= \bar{p}_{31}\sigma_x + \bar{p}_{36}\tau_{xy} + \bar{p}_{33}\sigma_z + \bar{p}_{38}E_z \\
\gamma_{xy} &= \bar{p}_{61}\sigma_x + \bar{p}_{66}\tau_{xy} + \bar{p}_{63}\sigma_z + \bar{p}_{68}E_z \\
E_z &= -(\bar{p}_{81}\sigma_x + \bar{p}_{86}\tau_{xy} + \bar{p}_{83}\sigma_z + \bar{p}_{88}D_z)
\end{aligned} \tag{5.8}$$

where

$$\begin{aligned}
\bar{p}_{ij} &= \bar{s}_{ij} - \bar{s}_{2j}\bar{s}_{2i}/\bar{s}_{22}, \qquad & \bar{p}_{88} &= -1/[\bar{\epsilon}_{33} - (\bar{d}_{32})^2/\bar{s}_{22}], \qquad & \bar{p}_{i8} &= \bar{d}_{3i} - \bar{s}_{2i}\bar{d}_{32}/\bar{s}_{22} \\
\bar{p}_{8i} &= (\bar{d}_{3i} - \bar{s}_{2i}\bar{d}_{32}/\bar{s}_{22})/[\bar{\epsilon}_{33} - (\bar{d}_{32})^2/\bar{s}_{22}], & \text{for} \quad (i,j) &= 1, 3 \text{ and } 6
\end{aligned} \tag{5.9}$$

Utilizing Eqs. $(5.2)_4$, $(5.2)_5$ and $(5.2)_7$, γ_{yz}, γ_{zx} and E_x can also be written in terms of τ_{yz}, τ_{zx} and D_x as [281],

$$\gamma_{yz} = p_{44}\tau_{yz} + p_{45}\tau_{zx} + p_{47}D_x \tag{5.10}$$

$$\gamma_{zx} = p_{54}\tau_{yz} + p_{55}\tau_{zx} + p_{57}D_x \tag{5.11}$$

$$E_x = -p_{74}\tau_{yz} - p_{75}\tau_{zx} + p_{77}D_x \tag{5.12}$$

where

$$\begin{aligned} &p_{ij} = \bar{s}_{ij} - \bar{d}_{1i}\bar{d}_{1j}/\bar{\epsilon}_{11}, \quad p_{47} = \bar{d}_{14}/\bar{\epsilon}_{11}, \quad p_{74} = p_{47}, \\ &p_{77} = 1/\bar{\epsilon}_{11}, \quad p_{57} = p_{75} = \bar{d}_{15}/\bar{\epsilon}_{11} \qquad \text{for} \quad (i,j) = (4,5) \end{aligned} \tag{5.13}$$

Piezoelectricity based extended Hamilton principle in a mixed form, without any internal charge and body force source, for the cylindrical bending case can be expressed as, [284]:

$$\begin{aligned} \int_t \int_a \int_h [&\delta u(\sigma_{x,x} + \tau_{xz,z} - \rho\ddot{u}) + \delta v(\tau_{xy,x} + \tau_{yz,z} - \rho\ddot{v}) + \delta w(\tau_{zx,x} + \sigma_{z,z} - \rho\ddot{w}) + \delta\phi(D_{x,x} + D_{z,z}) \\ &+\delta\sigma_x(\varepsilon_x - u_{,x}) + \delta\sigma_z(\varepsilon_z - w_{,z}) + \delta\tau_{yz}(\gamma_{yz} - v_{,z}) + \delta\tau_{zx}(\gamma_{zx} - u_{,z} - w_{,x}) + \delta\tau_{xy}(\gamma_{xy} - v_{,x}) \\ &-\delta D_x(E_x + \phi_{,x}) - \delta D_z(E_z + \phi_{,z})]dz\,dx\,dt = 0 \end{aligned} \tag{5.14}$$

From Eqs. (5.5) and (5.10)-(5.12), the expressions of strain and electric field components (ε_x, ε_z, γ_{xy}, γ_{yz}, γ_{zx}, E_z and E_x) substituting into Eq. (5.14) yields

$$\begin{aligned} \int_t \int_a \int_h [&\delta u(\tau_{xz,z} + \sigma_{x,x} - \rho\ddot{u}) + \delta v(\tau_{yz,z} + \tau_{xy,x} - \rho\ddot{v}) + \delta w(\sigma_{z,z} + \tau_{zx,x} - \rho\ddot{w}) + \delta\phi(D_{x,x} + D_{z,z}) \\ &+\delta\sigma_x(p_{11}\sigma_x + p_{16}\tau_{xy} + p_{13}\sigma_z + p_{18}D_z - u_{,x}) + \delta\sigma_z(p_{31}\sigma_x + p_{36}\tau_{xy} + p_{33}\sigma_z + p_{38}D_z - w_{,z}) \\ &+\delta\tau_{yz}(p_{44}\tau_{yz} + p_{45}\tau_{zx} + p_{47}D_x - v_{,z}) + \delta\tau_{zx}(p_{54}\tau_{yz} + p_{55}\tau_{zx} + p_{57}D_x - u_{,z} - w_{,x}) \\ &+\delta\tau_{xy}(p_{61}\sigma_x + p_{66}\tau_{xy} + p_{63}\sigma_z + p_{68}D_z - v_{,x}) + D_x(p_{74}\tau_{yz} + p_{75}\tau_{zx} - p_{77}D_x - \phi_{,x}) \\ &-\delta D_z(\phi_{,z} - p_{81}\sigma_x - p_{86}\tau_{xy} - p_{83}\sigma_z - p_{88}D_z)]dz\,dx\,dt = 0 \end{aligned} \tag{5.15}$$

This form of the variational equation is used when the solution in x direction is considered as known and the ODEs are formed for the z direction. When the solution is known in z direction, and the ODEs are to be formed for the x direction, the alternative expressions for ε_x, ε_z, γ_{xy} and E_z from Eq. (5.8) are substituted in Eq. (5.14) to yield

$$\begin{aligned} \int_t \int_a \int_h [&\delta u(\tau_{xz,z} + \sigma_{x,x} - \rho\ddot{u}) + \delta v(\tau_{yz,z} + \tau_{xy,x} - \rho\ddot{v}) + \delta w(\sigma_{z,z} + \tau_{zx,x} - \rho\ddot{w}) + \delta\phi(D_{x,x} + D_{z,z}) \\ &+\delta\sigma_x(\bar{p}_{11}\sigma_x + \bar{p}_{16}\tau_{xy} + \bar{p}_{13}\sigma_z + \bar{p}_{18}E_z - u_{,x}) + \delta\sigma_z(\bar{p}_{31}\sigma_x + \bar{p}_{36}\tau_{xy} + \bar{p}_{33}\sigma_z + \bar{p}_{38}E_z - w_{,z}) \\ &+\delta\tau_{yz}(p_{44}\tau_{yz} + p_{45}\tau_{zx} + p_{47}D_x - v_{,z}) + \delta\tau_{zx}(p_{54}\tau_{yz} + p_{55}\tau_{zx} + p_{57}D_x - u_{,z} - w_{,x}) \\ &+\delta\tau_{xy}(\bar{p}_{61}\sigma_x + \bar{p}_{66}\tau_{xy} + \bar{p}_{63}\sigma_z + \bar{p}_{68}E_z - v_{,x}) + D_x(p_{74}\tau_{yz} + p_{75}\tau_{zx} - p_{77}D_x - \phi_{,x}) \\ &-\delta D_z(\phi_{,z} - \bar{p}_{81}\sigma_x - \bar{p}_{86}\tau_{xy} - \bar{p}_{83}\sigma_z - \bar{p}_{88}D_z)]dz\,dx\,dt = 0 \end{aligned} \tag{5.16}$$

It may be noted that Eqs. (5.15) and (5.16) are identical for the elastic case. Here, t is the time variable. Where a dimensionless in-plane coordinates $\xi = x/a$ along the x-direction and thickness coordinate $\zeta = (z - z_{k-1})/t^{(k)}$ for a layer along the z-direction are defined which varies from 0 to 1. The support conditions considered at the top and bottom surface are: at $z = \pm h/2$ $\sigma_z = 0, \quad \tau_{yz} = 0, \quad \tau_{zx} = 0, \quad \phi = 0$ or $D_z = 0$. For perfect bounding, the equilibrium continuity conditions at interface between k^{th} and $k+1^{th}$ laminas are given as, [281]

$$[(u,\, v,\, w,\, \sigma_z,\, \tau_{yz},\, \tau_{zx},\, \phi,\, D_z)|_{\zeta=1}]^{(k)} = [(u,\, v,\, w,\, \sigma_z,\, \tau_{yz},\, \tau_{zx},\, \phi,\, D_z)|_{\zeta=0}]^{(k+1)} \tag{5.17}$$

The interfaces of piezoelectric layers with the elastic layers are always assumed as grounded ($\phi = 0$) for effective sensing/actuation. Along x-axis, panel can have any type of mechanical support such as, Simply supported (S): $\sigma_x = 0$, $w = 0$, $\tau_{xy} = 0$; Free (F): $\tau_{xz} = 0$, $\sigma_x = 0$, $\tau_{xy} = 0$; Clamped (C): $u = 0$, $w = 0$, $v = 0$. The ends $(x = 0, a)$ can have closed circuit condition (CC) in which potential is prescribed ($\phi = 0$) or have open circuit condition with $D_x = 0$.

5.2 GENERALIZED EKM SOLUTION

These are eleven $\mathbf{X} = [\, u \quad v \quad w \quad \sigma_x \quad \sigma_z \quad \tau_{xy} \quad \tau_{yz} \quad \tau_{zx} \quad \phi \quad D_x \quad D_z \,]^{\mathrm{T}}$ primary field variables which are to be solved. Employing multi-field multi-term EKM, the field variable for the k^{th} lamina are expressed as:

$$X_l(\xi, \zeta) = \sum_{i=1}^{n} f_l^i(\xi) g_l^i(\zeta)\ \cos\omega t \qquad \text{for} \qquad l = 1, 2, \ldots 11 \tag{5.18}$$

where $g_l^i(\zeta)$ and $f_l^i(\xi)$ are the unknown functions of ζ and ξ, respectively. Here, n represents the number of terms in solution. The functions $g_l^i(\zeta)$ are dependent on the k^{th} layer, while $f_l^i(\xi)$ functions are valid for all layers. These unknown functions of ζ and ξ are to be solved in two iterative steps by satisfying all homogenous support conditions.

5.2.1 First Iterative Step - Solving Functions $g_l^i(\zeta)$

Functions $f_l^i(\xi)$, along x-direction, are assumed first for the first step and for which variation δX_i is given by

$$\delta X_l = \sum_{i=1}^{n} f_l^i(\xi) \delta g_l^i\ \cos\omega t, \qquad l = 1, 2, \ldots 11 \tag{5.19}$$

Functions $g_l^i(\zeta)$ are segregated into two column vectors $\bar{\mathbf{G}}$ and $\hat{\mathbf{G}}$. Where $\bar{\mathbf{G}}$ contains those particular eight $8n$ primary variables which are specified at the support and interface conditions along z-direction, and $\hat{\mathbf{G}}$ contains the remaining $3n$ dependent variables:

$$\begin{aligned} \bar{\mathbf{G}} &= [\, g_1^1 \ldots g_1^n \quad g_2^1 \ldots g_2^n \quad g_3^1 \ldots g_3^n \quad g_5^1 \ldots g_5^n \quad g_7^1 \ldots g_7^n \quad g_8^1 \ldots g_8^n \quad g_9^1 \ldots g_9^n \quad g_{11}^1 \ldots g_{11}^n \,]^{\mathrm{T}} \\ \hat{\mathbf{G}} &= [\, g_4^1 \ldots g_4^n \quad g_6^1 \ldots g_6^n \quad g_{10}^1 \ldots g_{10}^n \,]^{\mathrm{T}} \end{aligned} \tag{5.20}$$

Eqs. (5.18) and (5.19) are substituted into Eq. (5.15). Since the δf_l^i are known functions integration along x-direction are evaluated. Since variations for δg_l^i are arbitrary, the coefficients of δg_l^i must vanish (equal to zero) which generates following set of $8n$ first order ODEs and $3n$ linear algebraic equations for each layer:

$$\mathbf{M}\bar{\mathbf{G}}_{,\zeta} = \bar{\mathbf{A}}\bar{\mathbf{G}} + \hat{\mathbf{A}}\hat{\mathbf{G}} \tag{5.21}$$

$$\mathbf{K}\hat{\mathbf{G}} = \tilde{\mathbf{A}}\bar{\mathbf{G}} \tag{5.22}$$

Where $\mathbf{M}_{8n\times 8n}$, $\bar{\mathbf{A}}_{8n\times 8n}$, $\hat{\mathbf{A}}_{8n\times 3n}$, $\mathbf{K}_{3n\times 3n}$ and $\tilde{\mathbf{A}}_{3n\times 8n}$ are known matrices. The nonzero elements of $\mathbf{M}$, $\bar{\mathbf{A}}^{\mathbf{m}}$, $\hat{\mathbf{A}}^{\mathbf{m}}$, $\mathbf{K}^{\mathbf{m}}$, $\tilde{\mathbf{A}}^{\mathbf{m}}$ matrices of Eqs. (5.21) and (5.22) are given below

$$\begin{aligned}
&M_{i_1j_1} = M_{j_6i_6} = \langle f_8^i f_1^j\rangle_a, && M_{i_2j_2} = M_{j_5i_5} = \langle f_7^i f_2^j\rangle_a, && M_{i_3j_3} = M_{j_4i_4} = \langle f_5^i f_3^j\rangle_a\\
&M_{i_7j_7} = M_{j_8i_8} = \langle f_{11}^i f_9^j\rangle_a, && \bar{A}_{i_1j_3} = \tfrac{-t}{a}\langle f_8^i f_{3,\xi}^j\rangle_a, && \bar{A}_{i_1j_5} = tp_{45}\langle f_8^i f_7^j\rangle_a\\
&\bar{A}_{i_1j_6} = tp_{55}\langle f_8^i f_8^j\rangle_a, && \hat{A}_{i_1j_3} = tp_{57}\langle f_8^i f_{10}^j\rangle_a, && \bar{A}_{i_2j_5} = tp_{44}\langle f_7^i f_7^j\rangle_a\\
&\bar{A}_{i_2j_6} = tp_{45}\langle f_7^i f_8^j\rangle_a, && \hat{A}_{i_2j_3} = tp_{47}\langle f_7^i f_{10}^j\rangle_a, && \bar{A}_{i_3j_4} = tp_{33}\langle f_5^i f_5^j\rangle_a\\
&\bar{A}_{i_3j_8} = tp_{38}\langle f_5^i f_{11}^j\rangle_a, && \hat{A}_{i_3j_1} = tp_{31}\langle f_5^i f_4^j\rangle_a, && \hat{A}_{i_3j_2} = tp_{36}\langle f_5^i f_6^j\rangle_a\\
&\bar{A}_{i_4j_6} = \tfrac{-t}{a}\langle f_3^i f_{8,\xi}^j\rangle_a, && \hat{A}_{i_5j_2} = \tfrac{-t}{a}\langle f_2^i f_{6,\xi}^j\rangle_a, && \hat{A}_{i_6j_1} = \tfrac{-t}{a}\langle f_1^i f_{4,\xi}^j\rangle_a\\
&\bar{A}_{i_7j_4} = tp_{83}\langle f_{11}^i f_5^j\rangle_a, && \bar{A}_{i_7j_8} = tp_{88}\langle f_{11}^i f_{11}^j\rangle_a, && \hat{A}_{i_7j_1} = tp_{81}\langle f_{11}^i f_4^j\rangle_a\\
&\hat{A}_{i_7j_2} = tp_{86}\langle f_{11}^i f_6^j\rangle_a, && \hat{A}_{i_8j_3} = \tfrac{-t}{a}\langle f_9^i f_{10,\xi}^j\rangle_a, && K_{i_1j_1} = p_{11}\langle f_4^i f_4^j\rangle_a\\
&K_{i_1j_2} = p_{16}\langle f_4^i f_6^j\rangle_a, && K_{j_2i_1} = K_{i_1j_2}, && K_{i_2j_2} = p_{66}\langle f_6^i f_6^j\rangle_a\\
&K_{i_3j_3} = p_{77}\langle f_{10}^i f_{10}^j\rangle_a, && \tilde{A}_{i_1j_1} = \tfrac{1}{a}\langle f_4^i f_{1,\xi}^j\rangle_a, && \tilde{A}_{i_1j_4} = -p_{13}\langle f_4^i f_5^j\rangle_a\\
&\tilde{A}_{i_1j_8} = -p_{18}\langle f_4^i f_{11}^j\rangle_a, && \tilde{A}_{i_2j_2} = \tfrac{1}{a}\langle f_6^i f_{2,\xi}^j\rangle_a, && \tilde{A}_{i_2j_4} = -p_{63}\langle f_6^i f_5^j\rangle_a\\
&\tilde{A}_{i_2j_8} = -p_{68}\langle f_6^i f_{11}^j\rangle_a && \tilde{A}_{i_3j_5} = p_{74}\langle f_{10}^i f_7^j\rangle_a, && \tilde{A}_{i_3j_6} = p_{75}\langle f_{10}^i f_8^j\rangle_a\\
&\tilde{A}_{i_3j_7} = \tfrac{-1}{a}\langle f_{10}^i f_{9,\xi}^j\rangle_a, && \bar{A}_{i_4j_3} = -\rho\omega^2 t\langle f_3^i f_3^j\rangle_a, && \bar{A}_{i_5j_2} = -\rho\omega^2 t\langle f_2^i f_2^j\rangle_a\\
&\bar{A}_{i_6j_1} = -\rho\omega^2 t\langle f_1^i f_1^j\rangle_a
\end{aligned} \tag{5.23}$$

where the notation $\langle\ldots\rangle_a = a\int_0^1(\ldots)d\xi$ represent integration over the span length a. Since the functions f_l^i are known analytical functions, elements of the matrices defined in Eqs. (5.23) and have been evaluated in closed form.

The algebraic Eq. (5.22) are solved to obtain $\hat{\mathbf{G}}$, and put into Eq. (5.21) which yields a set of $8n$ first-order homogeneous ODEs as:

$$\bar{\mathbf{G}}_{,\zeta} = \mathbf{A}\bar{\mathbf{G}} \tag{5.24}$$

with $\mathbf{A} = \mathbf{M}^{-1}[\bar{\mathbf{A}} + \hat{\mathbf{A}}\mathbf{K}^{-1}\tilde{\mathbf{A}}]$. Above Eq. (5.24) represent a system of $8n$ homogeneous first order ODEs with constant coefficient. The general solution of Eq. (5.24) is obtained by applying the approach given in Ref.[283].

5.2.2 Second Iterative Step - Solving Functions $f_l^i(\zeta)$

Now $g_l^i(\zeta)$ is known from the first step and arbitrary variation is considered along the x-direction. Therefore, variation for this case is written as:

$$\delta X_l^i = \sum_{i=1}^{n} g_l^i(\zeta)\delta f_l^i \ \cos\omega t \quad \text{for} \quad l = 1, 2, \ldots, 11 \tag{5.25}$$

Similarly, like the first step, $f_l^i(\xi)$ are segregated into two column vectors $\bar{\mathbf{F}}$ and $\hat{\mathbf{F}}$. Where $\bar{\mathbf{F}}$ carries those particular $8n$ primary variables which come in the support conditions at edges $x = 0, 1$ and $\hat{\mathbf{F}}$ contains the remaining $3n$ variables.

$$\begin{aligned}
\bar{\mathbf{F}} &= [\, f_1^1 \ldots f_1^n \quad f_2^1 \ldots f_2^n \quad f_3^1 \ldots f_3^n \quad f_4^1 \ldots f_4^n \quad f_6^1 \ldots f_6^n \quad f_8^1 \ldots f_8^n \quad f_9^1 \ldots f_9^n \quad f_{10}^1 \ldots f_{10}^n \,]^{\mathrm{T}} \\
\hat{\mathbf{F}} &= [\, f_5^1 \ldots f_5^n \quad f_7^1 \ldots f_7^n \quad f_{11}^1 \ldots f_{11}^n \,]^{\mathrm{T}}
\end{aligned} \tag{5.26}$$

Substitute Eqs. (5.18) and Eq. (5.25) in Eq. (5.16), this time, integrations are evaluated along ζ-direction. Since variations δf_l^i are arbitrary, their coefficients equated to zero individually which generates following system of $11n$ governing differential-algebraic equations:

$$\mathbf{N}\bar{\mathbf{F}}_{,\xi} = \bar{\mathbf{B}}\bar{\mathbf{F}} + \hat{\mathbf{B}}\hat{\mathbf{F}} \tag{5.27}$$

$$\mathbf{L}\hat{\mathbf{F}} = \tilde{\mathbf{B}}\bar{\mathbf{F}} \tag{5.28}$$

Where $\mathbf{N}_{8n\times 8n}$, $\bar{\mathbf{B}}_{8n\times 8n}$, $\hat{\mathbf{B}}_{8n\times 3n}$, $\mathbf{L}_{3n\times 3n}$ and $\tilde{\mathbf{B}}_{3n\times 8n}$are known matrices. The nonzero elements of $\mathbf{N}$, $\bar{\mathbf{B}}^{\mathbf{f}}$, $\hat{\mathbf{B}}^{\mathbf{f}}$, $\mathbf{L}^{\mathbf{f}}$ and $\tilde{\mathbf{B}}^{\mathbf{f}}$ Eqs. (5.27) and (5.28) are given below

$$\begin{aligned}
&N_{i_1j_1} = N_{j_4i_4} = \langle g_4^i g_1^j\rangle_h, \quad N_{i_2j_2} = N_{j_5i_5} = \langle g_6^i g_2^j\rangle_h, \quad N_{i_3j_3} = N_{j_6i_6} = \langle g_8^i g_3^j\rangle_h \\
&N_{i_7j_7} = N_{j_8i_8} = \langle g_{10}^i g_9^j\rangle_h, \quad \bar{B}_{i_1j_4} = \langle \bar{p}_{11} g_4^i g_4^j\rangle_h, \quad \bar{B}_{i_1j_5} = \langle \bar{p}_{16} g_4^i g_6^j\rangle_h \\
&\hat{B}_{i_1j_1} = \langle \bar{p}_{13} g_4^i g_5^j\rangle_h, \quad \bar{B}_{i_1j_7} = -\langle \bar{p}_{18} g_4^i \tfrac{g_{9,\zeta}^j}{t}\rangle_h, \quad \bar{B}_{i_2j_4} = \langle \bar{p}_{61} g_6^i g_4^j\rangle_h \\
&\bar{B}_{i_2j_5} = \langle \bar{p}_{66} g_6^i g_6^j\rangle_h, \quad \hat{B}_{i_2j_1} = \langle \bar{p}_{63} g_6^i g_5^j\rangle_h, \quad \bar{B}_{i_2j_7} = -\langle \bar{p}_{68} g_6^i \tfrac{g_{9,\zeta}^j}{t}\rangle_h \\
&\bar{B}_{i_3j_1} = -\langle g_8^i \tfrac{g_{1,\zeta}^j}{t}\rangle_h, \quad \bar{B}_{i_3j_6} = \langle p_{55} g_8^i g_8^j\rangle_h, \quad \hat{B}_{i_3j_2} = \langle p_{45} g_8^i g_7^j\rangle_h \\
&\bar{B}_{i_3j_8} = \langle p_{57} g_8^i g_{10}^j\rangle_h, \quad \bar{B}_{i_4j_6} = \langle \tfrac{g_{1,\zeta}^i}{t} g_8^j\rangle_h, \quad \hat{B}_{i_5j_2} = \langle \tfrac{g_{2,\zeta}^i}{t} g_7^j\rangle_h \\
&\hat{B}_{i_6j_1} = \langle g_3^i \tfrac{g_{5,\zeta}^j}{t}\rangle_h, \quad \bar{B}_{i_7j_6} = \langle p_{75} g_{10}^i g_8^j\rangle_h, \quad \bar{B}_{i_7j_8} = -\langle p_{77} g_{10}^i g_{10}^j\rangle_h \\
&\hat{B}_{i_7j_2} = \langle p_{74} g_{10}^i g_7^j\rangle_h, \quad \hat{B}_{i_8j_3} = -\langle g_9^i \tfrac{g_{11,\zeta}^j}{t}\rangle_h, \quad L_{i_1j_1} = \langle \bar{p}_{33} g_5^i g_5^j\rangle_h \\
&L_{i_2j_2} = \langle p_{44} g_7^i g_7^j\rangle_h, \quad L_{i_3j_1} = \langle \bar{p}_{83} g_{11}^i g_5^j\rangle_h, \quad L_{i_3j_3} = \langle \bar{p}_{88} g_{11}^i g_{11}^j\rangle_h \\
&\tilde{B}_{i_1j_3} = \langle g_5^i \tfrac{g_{3,\zeta}^j}{t}\rangle_h, \quad \tilde{B}_{i_1j_4} = -\langle \bar{p}_{31} g_5^i g_4^j\rangle_h, \quad \tilde{B}_{i_1j_5} = -\langle \bar{p}_{36} g_5^i g_6^j\rangle_h \\
&\tilde{B}_{i_1j_7} = \langle \bar{p}_{38} g_5^i \tfrac{g_{9,\zeta}^j}{t}\rangle_h, \quad \tilde{B}_{i_2j_2} = \langle g_7^i \tfrac{g_{2,\zeta}^j}{t}\rangle_h, \quad \tilde{B}_{i_2j_6} = -\langle p_{45} g_7^i g_8^j\rangle_h \\
&\tilde{B}_{i_2j_8} = -\langle p_{47} g_7^i g_{10}^j\rangle_h, \quad \tilde{B}_{i_3j_4} = -\langle \bar{p}_{81} g_{11}^i g_4^j\rangle_h, \quad \tilde{B}_{i_3j_5} = -\langle \bar{p}_{86} g_{11}^i g_6^j\rangle_h \\
&\tilde{B}_{i_3j_7} = \langle g_{11}^i \tfrac{g_{9,\zeta}^j}{t}\rangle_h, \quad \bar{B}_{i_4j_1} = -a\rho\omega^2\langle g_1^i g_1^j\rangle_h, \quad \bar{B}_{i_5j_2} = -a\rho\omega^2\langle g_2^i g_2^j\rangle_h \\
&\bar{B}_{i_6j_3} = -a\rho\omega^2\langle g_3^i g_3^j\rangle_h
\end{aligned} \tag{5.29}$$

where the notation $\langle \ldots \rangle_h = \sum_{k=1}^{L} t^{(k)} \int_0^1 (\ldots)^{(k)}\, d\zeta$ represent integration across the thickness. Since $g_l^i(\zeta)$ are known in close form, all integrations in Eq. (5.29) are evaluated exactly in closed form. Equations (5.27) and (5.28) are of same type as Eqs. (5.21) and (5.22), and are solved in a similar fashion as mentioned in the previous step. These two step, one along z-direction (Sec. 5.2.1) and other along x-direction (Sec. 5.2.2) completed one iteration. These iteration steps has been continued till the desired level of accuracy achieved.

5.3 NUMERICAL RESULTS AND DISCUSSIONS

The natural frequencies are presented for three type panels such as (a) laminated elastic panels, (b) hybrid soft-core sandwich panels and (c) hybrid piezoelectric panel under different boundary conditions, and both cross-ply and angle-ply layups are considered for study. The modal displacements, stresses and electrical state variables are non-dimensionalized as:

$$(\bar{u},\, \bar{v},\, \bar{w}) = (u, v, w)/\max(u, v, w)$$

$$(\bar{\sigma}_x,\, \bar{\sigma}_y,\, \bar{\sigma}_z,\, \bar{\tau}_{zx},\, \bar{\tau}_{yz}) = (\sigma_x,\, \sigma_y,\, \sigma_z,\, \tau_{zx},\, \tau_{yz})\, h/(s\, Y_0 \max(u, v, w))$$

$$\bar{D}_x = D_x\, h/(d_0\, s\, Y_0 \max(u, v, w)) \qquad \bar{\phi} = \phi\, d_0/\max(u, v, w)$$

where $s(= h/a)$ denote the thickness-to-span ratio and $\max(u, v, w)$ denote the largest value of u, v and w along the thickness of panel for a particular vibration mode. The length of all panels are assumed equal to unity ($a = 1$) for all cases and thickness of panels are taken according to thickness to span ratio ($s = h/a$). For $s = 0.2, 0.1, 0.05$ the value of h are 0.2, 0.1, 0.05, respectively. In the subsequent sections, results are obtained by taking n=1, iter.2 for S-S boundary condition and n=1, iter.3 for other boundary conditions.

5.3.1 Laminated Elastic Panel

In this section, the notation system is followed to denote the stacking sequence from the bottom of laminate to top of laminate. Each ply has been assumed of same thickness and density. Angle (θ) denoted the orientation of the unidirectional fibers which is measured counter clockwise from the x-axis to fiber. The typical material properties [245], $E_L/E_T = 25$, $G_{LT}/E_T = 0.5$, $G_{TT}/E_T = 0.2$, $\nu_{LT} = \nu_{TT} = 0.25$. are considered. Where E represented the Young's modulus, G represented the shear modulus, ν represented the Poisson's ratio and subscripts L and T indicates in-plane and transverse directions, respectively. The natural frequency ω are non-dimensionalized as $\omega^* = \omega h\sqrt{\rho/G_{12}}$. Where ρ and G_{12} is the material property of the orthotropic ply. The density of material is considered as unity.

5.3.1.1 *Cross-ply Laminated Panels*

In Table 5.1 and 5.2, lowest dimensionless natural frequencies $\omega^* = \omega h\sqrt{\rho/G_{12}}$ for cross-ply laminated panels are compared with [245] solution, which is based on semi-analytical method known as SSDQM. In Table 5.1, results are compared for moderately thick laminate (s=0.1) with lay-up [0/90/0/90^0] and subjected to simply supported condition. Present results are in agreement with upto 6 digit. Further, Table 5.2 presented comparison of lowest dimensionless natural frequencies for thin (s=0.05), moderately thick (s=0.1) and thick panels (s=0.2) of different lay-ups and subjected to C–C and C–F boundary conditions. It is found that the present numerical results match excellently with results of [245] for all type of support conditions. Even for thick laminate (s=0.2) the present analytical model provides a excellent estimate of the lowest natural frequencies. In most of literature work, irrespective of numerical or semi-analytical approach, only first natural frequency are reported for different boundary conditions other than simply-supported. Therefore, Table 5.3 presents the first five lowest frequency parameters for thin to thick (s=0.05, 0.1, 0.2) cross-ply panels having different lay-ups and under C–F and C–C boundary conditions. Where 'm' represent the bending mode sequence. In Fig. 5.2, the longitudinal variation (along x-direction) of field variables (u, w, σ_x and τ_{zx}) are presented for the first mode of cross-ply panel (s=0.1) having lay-up [0/90/0/90^0] and subjected to simply-supported (S–S) condition. Similarly for C–F and C–C boundary conditions, the longitudinal variation of field variables (u, w and σ_x) are plotted in Fig. 5.3 for first mode of cross-ply panel (s=0.1) with configuration [0/90/0/90^0]. Converge results of single term EKM are presented for both cases which are in excellent agreement with 2D FE results for all boundary conditions.

Table 5.1: Lowest six frequency parameters $\omega^* = \omega h\sqrt{\rho/G_{12}}$ for S–S laminate of [0/90/0/90^0] ($s = 0.1$)

m	3D [245]	SSDQM [245]	Present
1	0.109461	0.109461	0.109461
2	0.316561	0.316572	0.316562
3	0.542971	0.542968	0.542970
4	0.779708	0.779632	0.779708
5	1.02465	1.02682	1.024654
6	1.27545	1.25305	1.275448

Table 5.2: Lowest frequency parameters $\omega^* = \omega h\sqrt{\rho/G_{12}}$ for C–C and C–F laminates

B.C.	s		$[0/90^0]$	$[0/90/0^0]$	$[0/90/0/90^0]$	$[(0/90)_20^0]$
	0.05	Present	0.0457601	0.0784461	0.0596918	0.0754865
		SSDQM [245]	0.0458420	0.0791464	0.0601057	0.0758616
C–C	0.1	Present	0.152817	0.202579	0.166872	0.197420
		SSDQM [245]	0.153462	0.205606	0.169593	0.200086
	0.2	Present	0.414520	0.470025	0.405018	0.449336
		SSDQM [245]	0.417144	0.474495	0.410782	0.455344
	0.05	Present	0.00771818	0.01681093	0.01154415	0.01546987
		SSDQM [245]	0.00771633	0.01682680	0.01154820	0.01547340
C–F	0.1	Present	0.0301246	0.0594961	0.0427713	0.0559596
		SSDQM [245]	0.0301118	0.0598960	0.0429367	0.0561013
	0.2	Present	0.110283	0.174933	0.136844	0.169861
		SSDQM [245]	0.110421	0.179206	0.139518	0.172043

Table 5.3: First five lowest frequency parameters $\omega^* = \omega h\sqrt{\rho/G_{12}}$ for C–C and C–F laminates

		$[0/90^0]$		$[0/90/0^0]$		$[0/90/0/90^0]$	
s	m	C–C	C–F	C–C	C–F	C–C	C–F
	1	0.0457601	0.0077182	0.0784461	0.0168109	0.0596918	0.0115442
	2	0.1162720	0.0460645	0.1725348	0.0849709	0.1375584	0.0628576
0.05	3	0.2084625	0.1207399	0.2837096	0.1940248	0.2309489	0.1504419
	4	0.3142542	0.2174756	0.4031675	0.3135859	0.3335674	0.2512594
	5	0.4300447	0.3285306	0.5283360	0.4390850	0.4418569	0.3589981
	1	0.1528171	0.0301246	0.2025790	0.0594961	0.1668715	0.0427713
	2	0.3460043	0.1602460	0.4172665	0.2347354	0.3507306	0.1867837
0.1	3	0.5731397	0.3774182	0.6680702	0.4906176	0.5673811	0.4027313
	4	0.8161667	0.6199417	0.9299897	0.7510733	0.7984438	0.6278359
	5	1.0670552	0.7586124	1.2025426	1.0236035	1.0363795	0.8817480
	1	0.4145196	0.1102826	0.4700252	0.1749326	0.4050183	0.1368444
	2	0.8415532	0.4562643	0.9460184	0.5731355	0.8179189	0.4683926
0.2	3	1.3340277	0.9615521	1.4900776	1.1378253	1.2981462	0.9509511
	4	1.8106346	1.4937885	2.0413664	1.6890179	1.7984837	1.5471892
	5	2.3185296	1.9623062	2.5410816	2.3248370	2.2403915	1.8859839

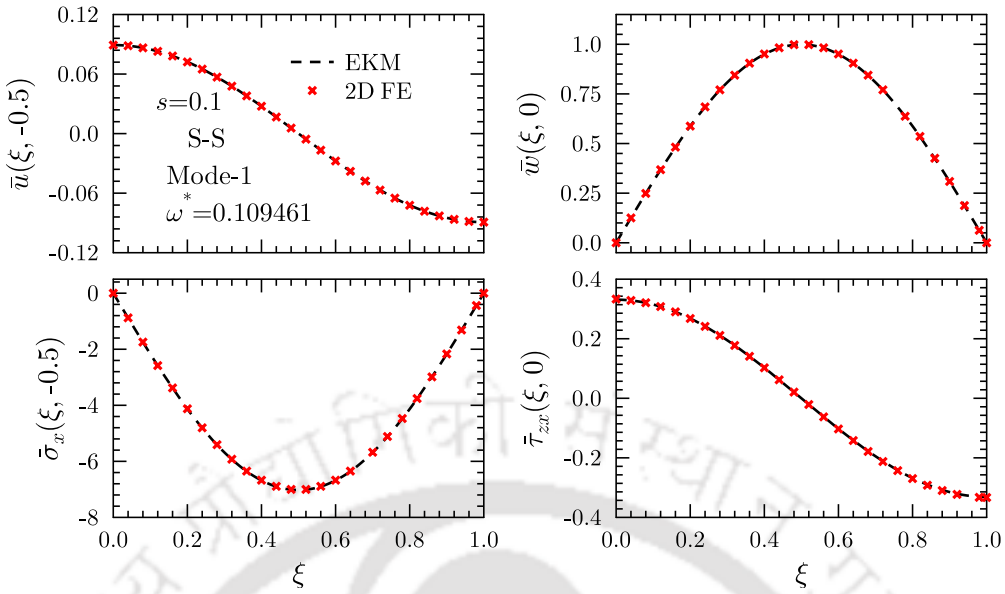

Fig. 5.2: Longitudinal variations of displacements and stresses for first mode of cross-ply panel $[0/90/0/90^0]$ under S–S boundary condition

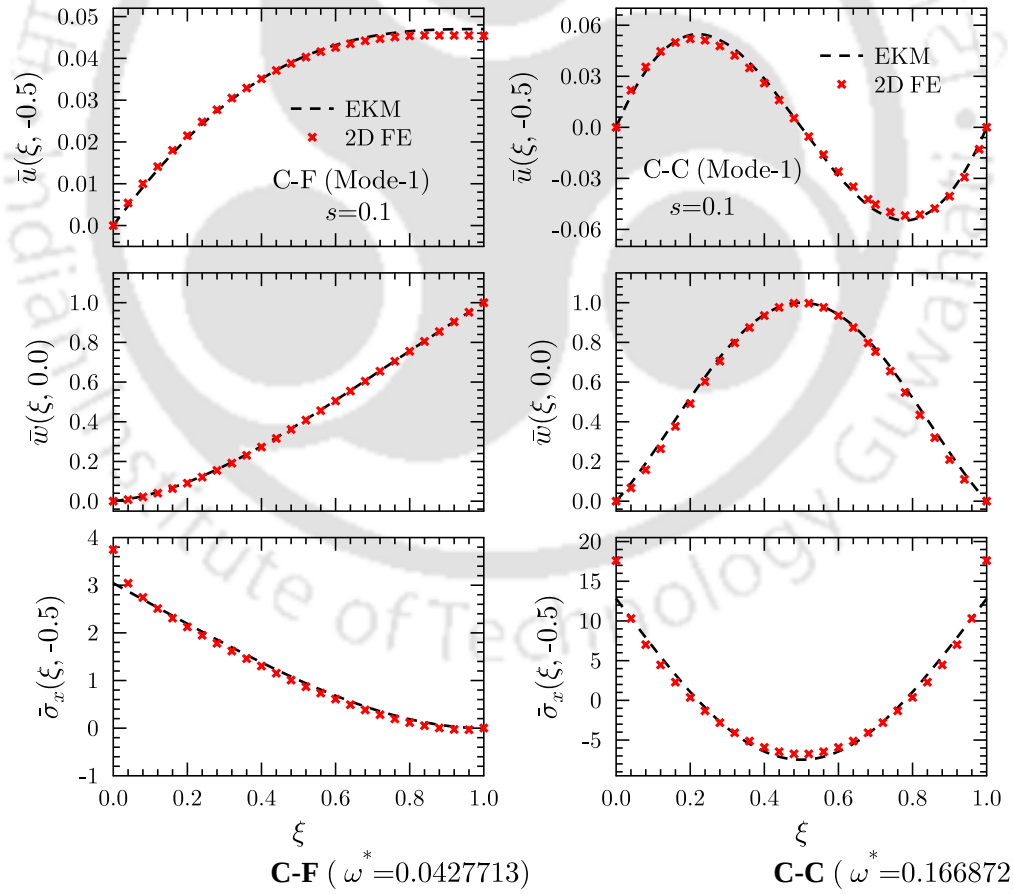

Fig. 5.3: Longitudinal variations of displacements and stresses for first mode of cross-ply panel $[0/90/0/90^0]$ subjected to C–F and C–C boundary conditions

5.3.1.2 *Angle-ply Laminated Panels*

For angle-ply laminated panels, the efficacy and accuracy of the present model has been verified by comparing the fundamental frequency parameters $\omega^* = \omega h\sqrt{\rho/G_{12}}$ for simply-supported case with [258] results which are based on parabolic shear deformable plate theory (PSDPT), as listed in Tables 5.4 and 5.5. Three dimensional (3D) exact results are also directly cited from the [258]. Table 5.4 present the comparison of fundamental frequency parameters, that correspond to bending vibrational modes, for two-layered antisymmetric $(45/-45^0)$ and three-layered symmetric $(45/-45/45^0)$ laminated panels. Similarly, Table 5.5 present the comparison of first fundamental frequency parameters for three-layered $(\theta/-\theta/\theta^0)$ laminated panel by considering different lamination angles. It is found that the present numerical results match extremely well with the results of [258]. In case of higher bending vibrational modes, it has been observed that the present analytical model is more accurate and closure to the 3D exact solution for both antisymmetric and symmetric cases. For other boundary conditions, 3D analytical or semi analytical solution does

Table 5.4: Comparison of first four lowest frequency parameters $\omega^* = \omega h\sqrt{\rho/G_{12}}$ for for S–S angle-ply laminate $(s = 0.1)$

Configuration	m	Present	3D exact [258]	PSDPT$_{ds}$ [258]
$45/-45^0$	1	0.066379	0.065634	0.065839
	2	0.23416	0.23545	0.23808
	3	0.46000	0.46217	0.47222
	4	0.71100	0.71412	0.73782
$45/-45/45^0$	1	0.092192	0.091114	0.092959
	2	0.27925	0.27537	0.28489
	3	0.49046	0.48913	0.50487
	4	0.71144	0.72074	0.73951

not exist in literature. Therefore, for other support condition the reliability and accuracy of the present analytical model has been verified by comparing the fundamental frequency parameters with 3D FE results and [256] solution which is based on classical plate theory (CLT).For angle-ply panels, FE software ABAQUS [294] is utilized to obtain 3D FE results. The generalized plane strain conditions are simulated by model a plate with length (b) to span (a) ratio of 20. A mesh size of 40 (a) × 50 (b) × 16 (h) with quadratic serendipity hexahedral element (C3D2OR) under reduced integration is used for the composite panel. Before obtaining results, It was verified that the larger value of b/a did not alter the numerical results. The comparison of present results with CLT [256] and 3D FE are present in Table 5.6 for different ply angle. It is found

Table 5.5: Comparison of first lowest frequency parameters $\omega^* = \omega h\sqrt{\rho/G_{12}}$ for different ply angle $s = 0.1$, S–S boundary conditions

	$[\theta/-\theta/\theta^0]$		
θ	Present	3D exact [258]	PSDPT$_{ds}$ [258]
0	0.164886	0.16489	0.16484
15	0.152843	0.15232	0.15330
30	0.125100	0.12396	0.12636
45	0.092192	0.091114	0.092959
60	0.060293	0.059879	0.060344
75	0.041737	0.041722	0.041754
90	0.039250	0.039250	0.039235

Table 5.6: Comparison of first lowest frequency parameters $\omega^* = \omega\frac{a^2}{h}\sqrt{\rho/E_2}$ for different ply angle $s = 0.1$

		$[\theta/-\theta^0]$		$[\theta/-\theta/\theta/-\theta^0]$	
θ		C–C	C–F	C–C	C–F
15	Present	14.4203	2.97239	15.7292	4.01342
	CLT [256]	14.2230	3.05380	16.2500	4.04350
	Abaqus [294]	14.5190	3.09189	15.8540	4.03148
30	Present	11.7070	2.29876	13.2954	3.26705
	CLT [256]	11.6720	2.28480	14.4310	3.32970
	Abaqus [294]	11.8525	2.33169	13.4583	3.30162
45	Present	9.2124	1.67596	10.6032	2.35937
	CLT [256]	9.1494	1.67770	11.5560	2.38050
	Abaqus [294]	9.2904	1.68266	10.7258	2.33436
60	Present	7.0486	1.23340	7.8612	1.50664
	CLT [256]	6.9406	1.22520	8.1679	1.49750
	Abaqus [294]	7.0909	1.23015	7.9344	1.61956
75	Present	5.9432	1.03270	6.0567	1.05995
	CLT [256]	5.9687	1.03020	6.1019	1.05600
	Abaqus [294]	5.9590	1.03222	6.0534	1.05812

that present results are in good agreement with 3D FE and CLT [256] results. The present 3D elasticity solution technique gives more accurate results as compare to CLT, which is quite obvious. Benchmark natural frequencies correspond to first five bending modes are tabulated (first

Table 5.7: Benchmarks Lowest frequency parameters $\omega^* = \omega h\sqrt{\rho/G_{12}}$ for C–C laminate

s	m	$[45/-45^0]$	$[45/-45/45^0]$	$[(45/-45^0)_2]$	$[(45/-45)_2 0^0]$
	1	0.0363552	0.0502127	0.0489102	0.0519872
	2	0.0965222	0.1188364	0.1187872	0.1246445
0.05	3	0.1770408	0.2037139	0.2054902	0.2142898
	4	0.2733247	0.2980169	0.3032272	0.3134732
	5	0.3644464	0.3984794	0.4041575	0.4184446
	1	0.1302833	0.1480611	0.1499519	0.1555493
	2	0.2989435	0.3207747	0.3257443	0.3336526
0.1	3	0.5217359	0.5278892	0.5310994	0.5414939
	4	0.7518058	0.7541789	0.7542128	0.7616162
	5	0.9844086	1.0126406	0.9656703	0.9905958
	1	0.3830465	0.3807482	0.3817375	0.3854501
	2	0.8062149	0.7853354	0.7805780	0.7806968
0.2	3	1.2891858	1.2180621	1.2340541	1.2407574
	4	1.7949425	1.6099068	1.6730938	1.6794239
	5	2.2894534	2.2575204	2.2379873	2.1996055

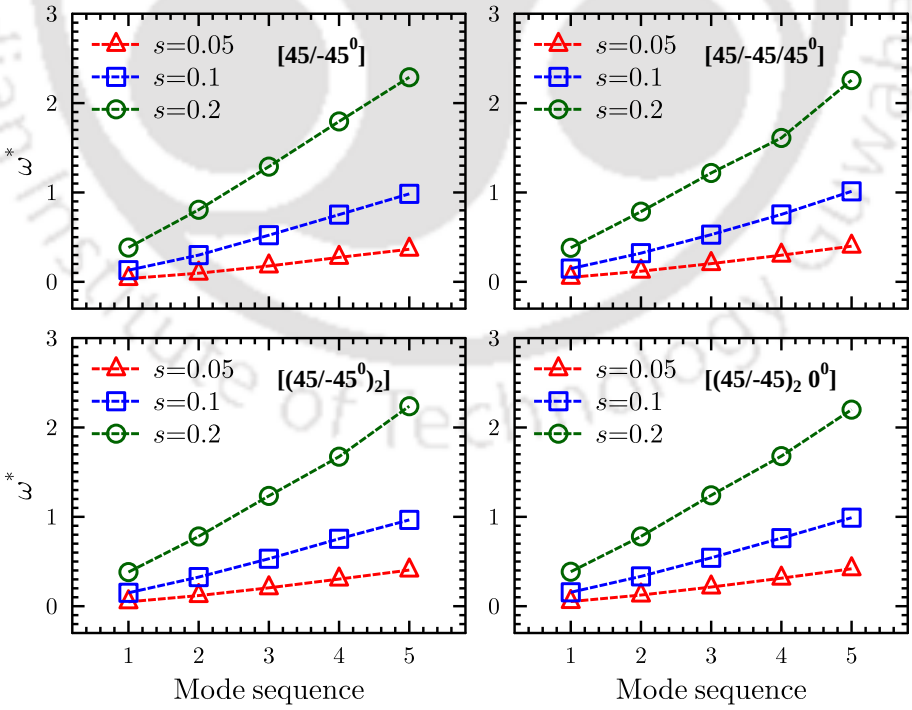

Fig. 5.4: Effect of thickness to span ratio (s) on frequency parameter for various panels subjected to C–C boundary condition

Table 5.8: Benchmarks Lowest frequency parameters $\omega^* = \omega h\sqrt{\rho/G_{12}}$ for C–F laminate

s	m	$[45/-45^0]$	$[45/-45/45^0]$	$[(45/-45^0)_2]$	$[(45/-45)_2 0^0]$
	1	0.0060335	0.0093701	0.0087129	0.0094181
	2	0.0369329	0.0522771	0.0502343	0.0536768
0.05	3	0.0985774	0.1280457	0.1263794	0.1335488
	4	0.1915312	0.2184769	0.2192084	0.2297676
	5	0.2823315	0.3171628	0.3168461	0.3350389
	1	0.0237017	0.0352313	0.0333665	0.0358267
	2	0.1358841	0.1629924	0.1631154	0.1708002
0.1	3	0.3306276	0.3614645	0.3666264	0.3793105
	4	0.5479286	0.5781347	0.5837534	0.6002771
	5	0.7970706	0.8118251	0.8152206	0.8293952
	1	0.0903066	0.1176088	0.1157008	0.1221558
	2	0.4096931	0.4344277	0.4389391	0.4509893
0.2	3	0.9045084	0.8965775	0.9090225	0.9219428
	4	1.4104348	1.3580523	1.3098672	1.3825748
	5	1.9085943	1.8777136	1.8722491	1.8579033

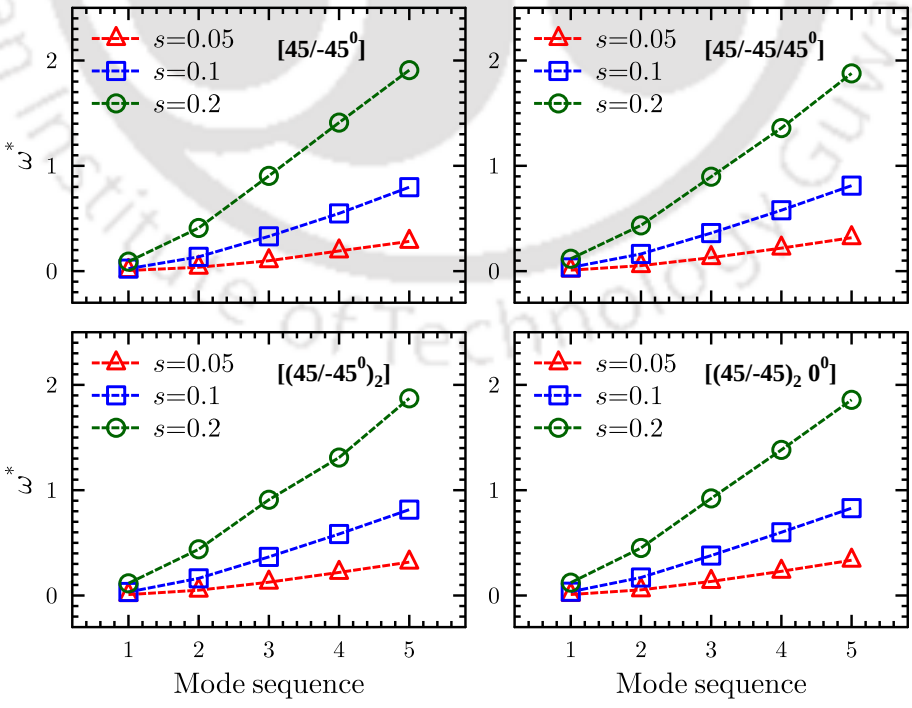

Fig. 5.5: Effect of thickness to span ratio (s) on frequency parameter for various panels subjected to C–F boundary condition

time) in Tables 5.7 and 5.8 for C–C and C–F boundary conditions, respectively. The results are presented for various symmetric and antisymmetric configurations and effect of thickness-to-span (s) ratio on the fundamental frequencies are also studied by considering three values of s=0.05, 0.1, 0.2. The similar trends in frequencies have been observed for thin (s=0.05) and moderate thick panel (s=0.1) for all configuration and boundary conditions. But for thick panel (s=0.2), the trend is slightly dissimilar for different configuration. It is also observed that an increase in laminate thickness increase the bending fundamental frequencies significantly for both the cases (C–F and C–C). It has been observed that the percentage increment in the frequency is more at the higher bending modes and it is more pronounced for the thick panel, which can also be observed from Fig. 5.4 and 5.5. Where the non-dimensionalized frequencies parameters are plotted by considering different span ratio ($s = 0.05, 0.1, 0.2$) under C–C and C–F boundary conditions, respectively. Table 5.9 presented the first fundamental frequency parameters for angle-ply panels

Table 5.9: Lowest frequency parameters $\omega^* = \omega h\sqrt{\rho/G_{12}}$ for general lay-up angle-ply panel

s	BC	$[-15/45/-15^0]$	$[-45/15/0/30/75^0]$
0.05	S–S	0.0430342	0.0216779
	C–C	0.0775099	0.0460341
	C–F	0.0159608	0.0077752
0.1	S–S	0.1440320	0.0822173
	C–C	0.2054173	0.1466186
	C–F	0.0575663	0.0303379
0.2	S–S	0.3961931	0.2788671
	C–C	0.4814271	0.4143504
	C–F	0.1749444	0.1106554

having highly heterogenous lay-up and subjected to general boundary conditions. The results are tabulated (Table 5.9) for three-layered and five-layered panels with lay-up $[-15/45/-15^0]$ and $[-45/15/0/30/75^0]$, respectively. First time, benchmark results are presented for general lay-up panels subjected to general boundary conditions. These benchmark results for angle-ply panels could be used for assessing 3D numerical solutions or two-dimensional (2D) theories.

In Fig. 5.6, the longitudinal variation of field variables (u, w, and σ_x) are presented for the first mode of angle-ply panel (s=0.1) having lay-up $[(45/-45^0)_2]$ and subjected to S–S, C–C and C–F boundary conditions. For angle-ply cases also, present EKM results matches excellently with the 3D FE results.

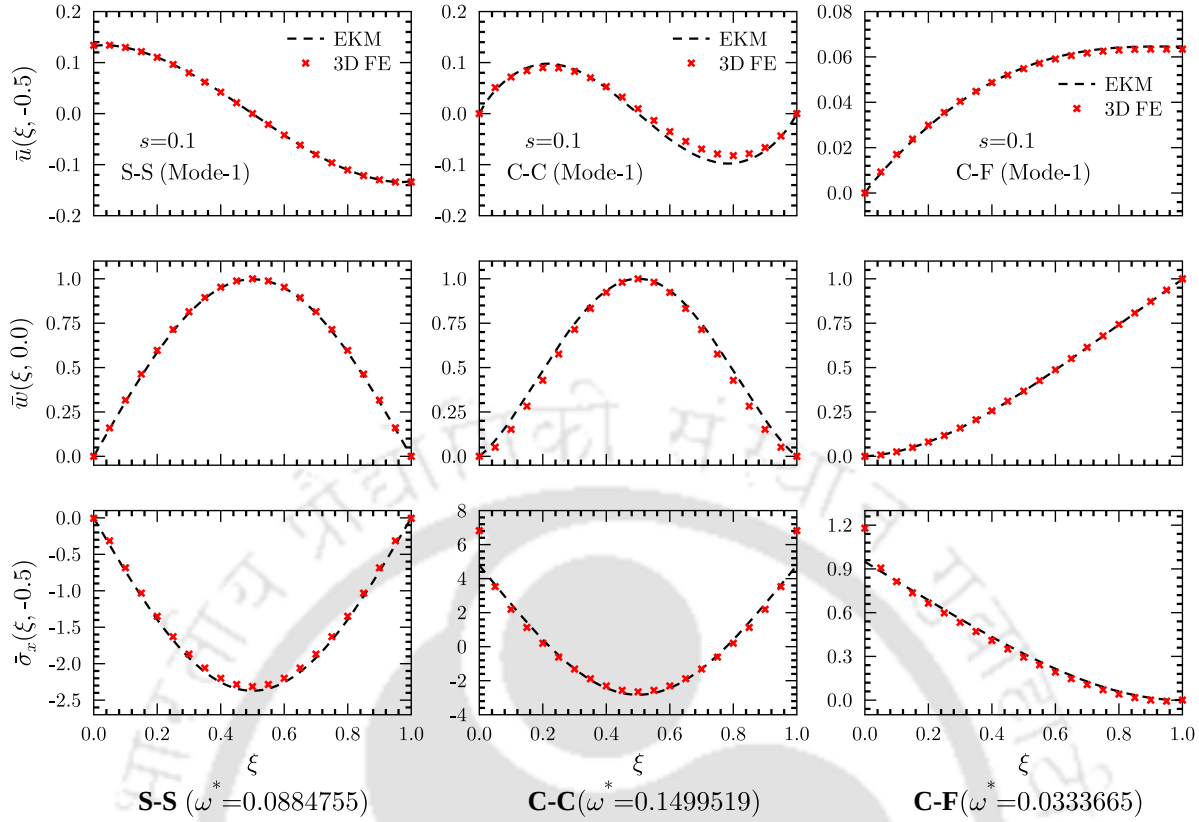

Fig. 5.6: Longitudinal variations of displacements and stresses for first mode of angle-ply panel $[45/-45/45/-45^0]$ subjected to S–S, C–C and C–F boundary conditions

5.3.2 Sandwich Panels

In this section, the present method is applied to a very challenging problem of the cross-ply and angle-ply sandwich panels. The result are presented for three-layered and five-layered sandwich panels with lay-up $[\theta/\text{Core}/\theta^0]$ and $[\theta_1/\theta_2/\text{Core}/\theta_2/\theta_1{}^0]$, respectively, as shown in Fig. 5.7. Table 5.10 contain the material properties which are used in this section. The natural frequency ω are non-dimensionalized as $\omega^* = \omega h\sqrt{\rho/G_{12}}$. Where ρ and G_{12} is the material property of the

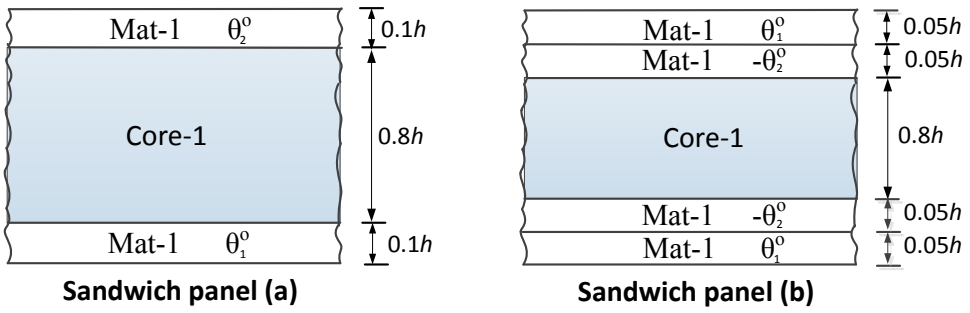

Fig. 5.7: Configurations of the sandwich panels

orthotropic ply. The density of each material is considered as unity.

Table 5.10: Material Properties for sandwich panel

Mat.1	Y_1	Y_2	Y_3	G_{23}	G_{13}	G_{12}	ν_{12}	ν_{13}	ν_{23}
Gr/Ep [261]	172.4	6.9	6.9	1.38	3.45	3.45	0.25	0.25	0.25
Core [261]	0.1	0.1	0.1	0.04	0.04	0.04	0.25	0.25	0.25

Units: Young's moduli Y_i and shear moduli G_{ij} in GPa

Table 5.11 presents the lowest natural frequency parameters ω^* of three-layered panel . The natural frequency parameters are tabulated for first five bending vibrational mode under three type of boundary conditions S–S, C–C and C–F. For simply supported case, present results are validated with existing results of [261] which are based on enhanced higher-order shear deformation theory (EHSDT). 3D exact results are also directly cited from the [261]. It has been found that present results are in excellent agreement with 3D exact and EHSDT results. In Table 5.12, benchmark lowest frequency parameters are tabulated for five layered sandwich panels (first time) of different thickness and subjected to different support conditions. The results for other boundary condition are also thoroughly verified with 3D FE results by utilizing the commercial FE software ABAQUS [294]. As the s value increases from 0.05 to 0.2 (thin to thick panel), the frequencies parameters increases significantly for all type of boundary conditions, which is clearly observed from Table 5.12.

Table 5.11: Lowest frequency parameters $\omega^* = \omega h\sqrt{\rho/G_{12}}$ for three layered sandwich panel s=0.1

Configuration	m	1	2	3	4	5
[0/Core/0^0]	S–S	0.0342692	0.0763462	0.1287443	0.1930133	0.2678181
		(0.033158)†	-	-	-	-
		(0.034068)*	-	-	-	-
	C–C	0.0394549	0.0838381	0.1418824	0.2109031	0.2878363
	C–F	0.0165047	0.0501431	0.0955755	0.1531325	0.2438995
[45/Core/-45^0]	S–S	0.0243976	0.0638127	0.1015957	0.1478207	0.2029990
		(0.024589)†	-	-	-	-
		(0.024638)*	-	-	-	-
	C–C	0.0330688	0.0671282	0.1121088	0.1630150	0.2073591
	C–F	0.0101859	0.0386711	0.0845693	0.1236272	0.1471659

†EHSDT [261] *3D exact [261]

Table 5.12: First lowest frequency parameters $\omega^* = \omega h\sqrt{\rho/G_{12}}$ for five layered sandwich panel

s	BC	[0/90/Core/90/0^0]	[30/-30/Core/-30/30^0]
	S–S	0.0148570	0.0144461
0.05	C–C	0.0172911	0.0166291
	C–F	0.0065793	0.0064328
	S–S	0.0340970	0.0328182
0.1	C–C	0.0364613	0.0351654
	C–F	0.0163220	0.0160346
	S–S	0.0721566	0.0695414
0.2	C–C	0.0795376	0.0779961
	C–F	0.0368487	0.0339653

5.3.3 Piezoelectric Panels

5.3.3.1 Validation with exact results for simply-supported (S–S) case

For Piezoelectric problems, the solution method is validated with the available exact solution given by [241] and [242] for simply-supported case. The natural frequencies compared for a single layered piezoelectric panel and a three layered cross-ply (orthotropic) hybrid panel both having $S = l/h = 4$. The material properties for piezoelectric laminated panels, taken as [242]: $[(Y_1, Y_2, Y_3, G_{23}, G_{13}, G_{12}), \nu_{12}, \nu_{13}, \nu_{23}]$, $[(e_{31}, e_{32}, e_{33}, e_{24}, e_{15}), (\varepsilon_{11}/\varepsilon_0, \varepsilon_{22}/\varepsilon_0, \varepsilon_{33}/\varepsilon_0)] =$

Material A (PZT-4): [(81.3, 81.3, 64.5, 25.6, 25.6, 30.6) GPa, 0.329, 0.432, 0.432], [(−5.20, −5.20, 15.08, 12.72, 12.72) C/m^2, (1475, 1475, 1300)],

Material C: [(132.38, 10.756, 10.756, 5.6537, 3.606, 5.6537) GPa, 0.24, 0.24, 0.49], [(0, 0, 0, 0, 0) C/m^2, (3.5, 3.5, 3)],

Material D (PVDF) : [(237.0, 23.2, 10.5, 2.15, 4.4, 6.43) GPa, 0.154, 0.178, 0.177], [(−0.13, −0.14, −0.28, −0.01, −0.01) C/m^2, (12.5, 11.98, 11.98)].

Where Y_i denotes Young's modulus, G_{ij} denotes shear modulus, ν_{ij} denotes Poisson ratios and e_{ij} denotes piezoelectric stress constants. The density of each material is considered as unity. Table 5.13 presented the first ten natural frequencies for the single layered panel of material A, having open and closed circuit conditions at the top and bottom surfaces. Similarly, Table 5.14, presented the first eight natural frequencies for the three layered hybrid panel [A(0.1h)/C(0.8h)/A(0.1h)] under closed circuit condition. Three layered panel is substrate of material C with two layers of material A (thickness 0.1h) bonded to the bottom and top of the substrate. It is observed that the present numerical results match exactly with the results of [241] and [242] for both case.

Table 5.13: Natural frequencies $\omega/100$ (rad/sec)for single layered piezoelectric panel of material A under S–S boundary conditions (L/h=4)

	Closed circuit			Open circuit		
m	Present	2D Exact [242]	2D Exact [241]	Present	2D Exact [242]	2D Exact [241]
1	52580.7492	52580.6684	52580.67	53046.7611	53046.7643	53046.76
2	234515.3381	234514.6611	234514.7	254503.0584	254503.6015	254503.6
3	560242.4709	560241.7497	560241.7	642210.6577	642210.3979	642210.4
4	969921.2367	969921.0825	969921.1	972665.6277	972665.3311	972665.4
5	1154041.3588	1154041.8570	1154042	1224773.5813	1224774.5120	1224774
6	1513041.5592	1513041.9370	1513042	1545514.4764	1545514.5710	1545515
7	2016806.6020	2016798.2430	2016798	2021618.1966	2021620.5310	2021621
8	2319010.3835	2319013.3060	2319013	2321380.5393	2321388.4520	2321388
9	2522451.7309	2522446.5400	2522449	2545885.9786	2545884.2820	2545884
10	3017992.5111	3017998.4710	3017998	3019774.5832	3019775.0540	3019775

Table 5.14: Natural frequencies ω (rad/s) for three-layer piezoelectric panel [A/C/A] subjected to S-S boundary conditions (L/h=4)

m	Present	2D Exact [242]	2D Exact [241]
1	4061328.1367	4061328.914	4061328.8
2	27900175.6980	27900191.25	27900191
3	36428990.7128	36428990.71	36428990
4	37712869.7731	37712838.66	37712838
5	55899719.6294	55899719.63	55899720
6	74614977.7303	74615081.44	74615082
7	80757918.0315	80757822.1	80757823
8	102701250.1003	102701050.5	102701050

5.3.3.2 Validation for Other Boundary Conditions

Since no 3D piezoelectricity based analytical solution is available for the other boundary conditions. Therefore, present result has been validated with [259] results which is based on an equivalent single layer accurate theory. The present results has been also compared to [246] results which are based on 2D semi-analytical method known as SS-DQM. Table 5.15 show the comparison of the natural frequencies with [259] results for three layer cross-ply hybrid panel [A($0.1h$)/C($0.8h$)/A($0.1h$)] under S–S, C–C and C–F boundary conditions. It is observed that present numerical results shows very good agreement with [259] results for all boundary conditions.

Table 5.15: Natural frequencies ω (rad/s) for three-layer piezoelectric panel [A/C/A] subjected to various boundary conditions

		L/h=4		L/h=50	
BC		Closed	Open	Closed	Open
S–S	Present	0.4061e7	0.4062e7	0.3941e5	0.3941e5
	Shu [259]	0.4043e7	0.4043e7	0.3922e5	0.3922e5
	2D Exact [241]	0.4061e7	0.4062e7	0.3941e5	0.3941e5
C–F	Present	0.1721e7	0.1703e7	0.1409e5	0.1399e5
	Shu [259]	0.1728e7	0.1727e7	0.1400e5	0.1400e5
C–S	Present	0.4725e7	0.4707e7	0.6153e5	0.6112e5
	Shu [259]	0.4682e7	0.4680e7	0.6080e5	0.6080e5
C–C	Present	0.5556e7	0.5479e7	0.8899e5	0.8813e5
	Shu [259]	0.5429e7	0.5426e7	0.8740e5	0.8739e5

In tables 5.16-5.19, natural frequencies are presented for various type of piezoelectric panels subjected to different type of mechanical and electrical boundary conditions. For such cases first time analytical results are tabulated because usually it is very difficult to derive analytical solutions based on the coupled piezoelectricity equations which is also stated by [246]. For all the cases, the present numerical results are also compared with semi-analytical results of the [246]. In this section, Z represents PZT-4 layer having ply angle $\theta = 0^o$ and V represents PVDF layer having ply angle $\theta = 90^o$. For all panels each ply is assumed to have the same thickness just as [246]. The mechanical boundary conditions at the top and bottom surfaces are always assumed to be traction-free, while the others are represents by notations such as C–S|EC–EO/EC–EO which indicates that the laminated panel has clamped boundary condition and electrically close-circuit at $x = 0$, and simply-supported boundary condition and electrically open-circuit at $x = a$, as well as electrically closed-circuit and open-circuit conditions at $z = -h/2$ and $z = h/2$, respectively.

Comparison of present results with 3D exact and SS-DQM results is carried out in Table 5.16 for a simply-supported single-layer PZT panel (S–S|EC–EC/EC–EO) with different thickness-to-span ratio (s). The present results shows excellent agreement with 3D exact and SS-DQM results of [246]. Table 5.17 gives the lowest fundamental frequency parameters for various piezolaminated panel subjected to clamped and close circuit boundary conditions at the $x = 0$ and $x = a$, as well as electrically closed-circuit conditions at $z = -h/2$ and $z = h/2$. The results show good agreement with SS-DQM results. From table 5.17 is also observed that the lowest fundamental

Table 5.16: Lowest natural frequencies prameters $\omega^* = \omega h\sqrt{\rho/G_{12}}$ for a PZT-4 panel (S–S|EC–EC/EC–EO)

	s=0.01	s=0.05	s=0.1	s=0.2
Present	0.00058417	0.01453587	0.05732267	0.217831236
3D Exact [246]	0.00058393	0.01453694	0.05740433	0.21899052
SSDQM [246]	0.00058394	0.01453706	0.05740478	0.21899218

frequency increases as the thickness-to-span ratio (s) of panels increases. The layer-up scheme also has significantly effect on the frequencies, which is quite obvious The effects electric boundary

Table 5.17: Lowest natural frequencies parameters $\omega^* = \omega h\sqrt{\rho/G_{12}}$ for piezoelectric laminated plate with different layer-up (C–C|EC–EC/EC–EC)

		[Z/V]	[Z/V/Z]	[Z/V/Z/V]	[Z/V/Z/V/Z]
s=0.01	Present	0.00084680	0.00125180	0.00098906	0.00111957
	SSDQM [246]	0.00086082	0.00131280	0.00099782	0.00122015
s=0.05	Present	0.02031843	0.02799720	0.02335348	0.02525749
	SSDQM [246]	0.02063014	0.02855171	0.02274281	0.02710401
s=0.1	Present	0.07343331	0.08581248	0.07256331	0.08103439
	SSDQM [246]	0.07453177	0.08882316	0.07527702	0.08555909
s=0.2	Present	0.23300522	0.23028151	0.20296947	0.24074441
	SSDQM [246]	0.23651852	0.23957155	0.21220645	0.22500977

Table 5.18: Lowest natural frequencies parameters $\omega^* = \omega h\sqrt{\rho/G_{12}}$ for piezoelectric laminated plate with different layer-up (C–F|EC–EC, s=0.1)

BC-z		[Z/V]	[Z/V/Z]	[Z/V/Z/V]	[Z/V/Z/V/Z]
EO–EO	Present	0.013220302	0.019210203	0.014742228	0.018085716
	SSDQM [246]	0.013192509	0.019229189	0.014949811	0.018030044
EO–EC	Present	0.013216863	0.018633168	0.014735367	0.174903612
	SSDQM [246]	0.013181205	0.01919484	0.014940033	0.018013882
EC–EO	Present	0.013103416	0.018633168	0.014328805	0.174903612
	SSDQM [246]	0.013163973	0.01919484	0.014933324	0.018013882
EC–EC	Present	0.013091886	0.018044906	0.014239077	0.016903507
	SSDQM [246]	0.013158104	0.019165257	0.014926037	0.018000255

Table 5.19: Lowest natural frequencies parameters $\omega^* = \omega h\sqrt{\rho/G_{12}}$ for piezoelectric laminated plate with different layer-up (C–C/EO–EO, s=0.1)

BC-x		[Z/V]	[Z/V/Z]	[Z/V/Z/V]	[Z/V/Z/V/Z]
EC–EC	Present	0.07373324	0.08625497	0.07325368	0.08373173
	SSDQM [246]	0.07536575	0.08978304	0.07570815	0.08615817
EO–EC	Present	0.07381218	0.08625639	0.07326633	0.08372514
	SSDQM [246]	0.07546851	0.08977754	0.07549783	0.08556069
EO–EO	Present	0.07388739	0.08625764	0.07333423	0.08372603
	SSDQM [246]	0.07542978	0.08974057	0.07538146	0.08541972
EC–EO	Present	0.07381218	0.08625639	0.07326633	0.08372514
	SSDQM [246]	0.07546857	0.08977759	0.07549792	0.08556081

conditions of the top and bottom surfaces on the natural frequencies of piezoelectric laminated panels is studied in table 5.18. The results are tabulated for various layer-up scheme of piezoelectric panels which has $s = 0.1$ and C–F and electric closed boundary condition at ends ($x = 0$ and $x = a$). Similarly, in table 5.18 the effects of electric boundary conditions at the two ends ($x = 0$ and $x = l$) on the natural frequencies of piezoelectric laminated panels is studied. The results are tabulated for various layer-up scheme of piezoelectric panels which has $s = 0.1$ and C–C and electric open boundary condition at top and bottom surfaces ($z = -h/2$ and $z = h/2$). Due to the weak coupling between the electric and elastic fields, the effect of electric boundary condition on the natural frequencies of piezoelectric laminated panels is not very significant but these small effects are very much important to detect accurately for precise control applications. For symmetric laminates the natural frequencies parameters for EO–EC-z and EC–EO-z are identical which is quite obvious.

5.3.3.3 Some New Benchmark Results

The configurations of smart composite and sandwich panels are shown in Fig. 5.8, where the properties of the materials for this section, are given in Table 5.20. In Tables 5.21 and 5.22, benchmark natural frequencies parameters, correspond to first three bending modes, are tabulated for thick (s=0.2) smart composite and sandwich piezoelectric panels subjected to various mechanical boundary conditions at ends ($x = 0$ and $x = a$), and electrically open or close boundary condition at top and bottom surfaces ($z = -h/2$ and $z = h/2$). The natural frequency ω are non-dimensionalized as $\omega^* = \omega h\sqrt{\rho/G_{12}}$. Where ρ and G_{12} is the material property of the elastic ply (Mat. 2). The natural frequencies are presented for both cross-ply and angle-ply case. First time, benchmark results are presented for angle-ply piezolaminated and piezo-sandwich panels subjected to general

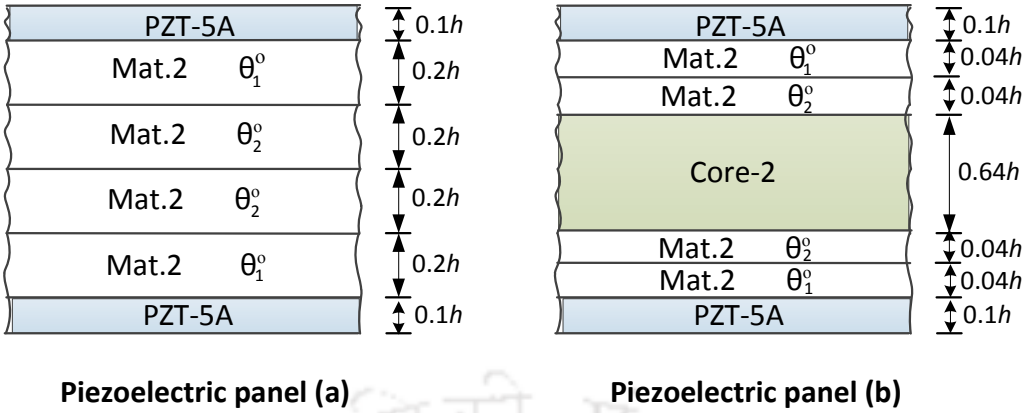

Fig. 5.8: Configurations of the piezoelectric-laminated panels

Table 5.20: Material constants.

Material	Y_1	Y_2	Y_3	G_{23}	G_{13}	G_{12}	ν_{12}	ν_{13}	ν_{23}	ρ
Mat. 2	181.0	10.3	10.3	2.87	7.17	7.17	0.28	0.28	0.33	1578
Core-2	0.276	0.276	3.45	0.1104	0.414	0.414	0.25	0.02	0.02	1000
PZT-5A	61.0	61.0	53.2	21.1	21.1	22.6	0.35	0.38	0.38	7600
Material	d_{31}	d_{32}	d_{33}	d_{24}	d_{15}	η_{11}	η_{22}	η_{33}		
PZT-5A	-171	-171	374	584	584	15.3	15.3	15.0		

Units: Young's moduli Y_i and shear moduli G_{ij} in GPa; density (ρ) in Kg/m^3; piezoelectric strain coefficients d_{ij} in pm/V; electric permittivities η_{ij} in nF/m;
*Where $d_0 = d_{33}$ pm/V; Y_0= 10.3 GPa

Table 5.21: Benchmarks results for lowest natural frequencies parameters $\omega^* = \omega h\sqrt{\rho/G_{12}}$ for piezoelectric laminated plate with different layer-up (EC–EC-x, s=0.2)

	m	[(PZT-5A/0/90)$_2$]		[(PZT-5A/30/-30)$_2$]	
		Close circuit	Open Circuit	Close circuit	Open Circuit
S–S	1	0.2262441	0.2306577	0.2273041	0.2337663
	2	0.5701732	0.5778008	0.6170847	0.6248754
	3	0.9380969	0.9502934	1.0328357	1.0504881
C–C	1	0.2961215	0.2978862	0.3254689	0.3312718
	2	0.6059094	0.6134991	0.6667578	0.6767873
	3	0.9848215	1.0024115	1.0644729	1.0774317
C–F	1	0.0952360	0.0974279	0.0916322	0.0945427
	2	0.3399906	0.3516473	0.3616073	0.3703060
	3	0.6975272	0.7073793	0.7936180	0.8036954

Table 5.22: Benchmarks results for lowest natural frequencies parameters $\omega^* = \omega h\sqrt{\rho/G_{12}}$ for sandwich piezolaminated panel with different layer-up (EC–EC-x, s=0.2)

	m	[(PZT-5A/0/90)$_2$Core]		[(PZT-5A/30/-30)$_2$Core]	
		Close circuit	Open Circuit	Close circuit	Open Circuit
S–S	1	0.1158795	0.1178767	0.115345381	0.1175675
	2	0.2649350	0.2685149	0.269836623	0.2744607
	3	0.4387201	0.4450557	0.457879817	0.4662227
C–C	1	0.1367742	0.1386386	0.140346341	0.1427526
	2	0.2806270	0.2846647	0.298404971	0.3039903
	3	0.4724557	0.4794519	0.501668413	0.5102549
C–F	1	0.0532131	0.0541403	0.052870788	0.0541787
	2	0.1674822	0.1705361	0.167115893	0.1703328
	3	0.3287606	0.3312440	0.337620828	0.3435029

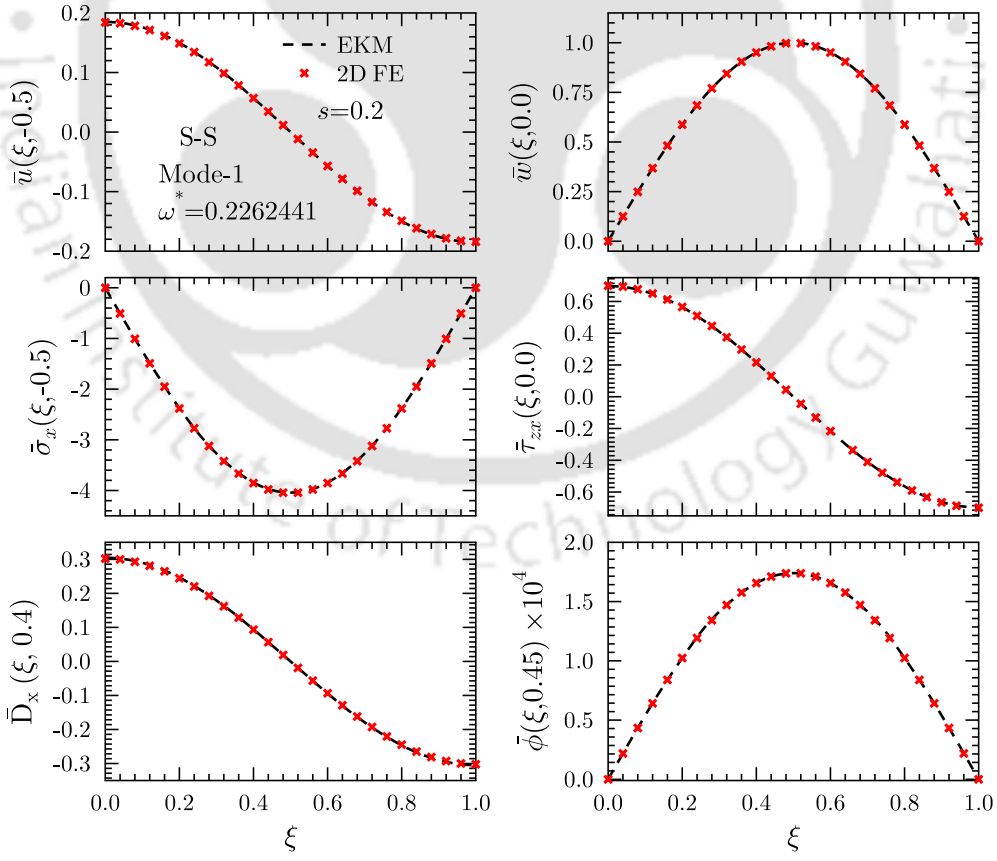

Fig. 5.9: Longitudinal variations of displacements, stresses and electrical variables for cross-ply piezoelectric panel with lay-up [(PZT-5A/0/90)$_2$] (EC–EC/EC–EC, s=0.2) and subjected to S-S boundary condition

boundary conditions. The first three frequencies of the cross-ply and angle-ply piezolaminated panel are tabulated in Table 5.21 for various type of boundary conditions i.e S–S, C–C and C–F, respectively, and with open and closed circuit conditions at the top and bottom surfaces. Similarly, first three natural frequencies of the cross-ply and angle-ply piezosandwich panel are tabulated in Table 5.22. The numerical results of this sub-section are also thoroughly verified with 3D FE results by utilizing the commercial FE software ABAQUS [294]. It is found that present results are in good agreement with 3D FE results. It is also observed that the effect of electric boundary condition at top and bottom surfaces ($z = -h/2$ and $z = h/2$) is more significant at higher bending mode as compared to first bending mode, for all the cases. The natural frequencies are higher for electrically open boundary conditions at top and bottom surfaces of panels, as compared to electrically close conditions. The effect of electric boundary conditions at the top and bottom surfaces of panels is comparatively less in piezo-sandwich panels for all three bending modes. The present method is able to detect these effects accurately which are very much important for precise control applications. In Fig. 5.9, the longitudinal variation of field variables (u, w, σ_x, τ_{zx}, ϕ, D_x)

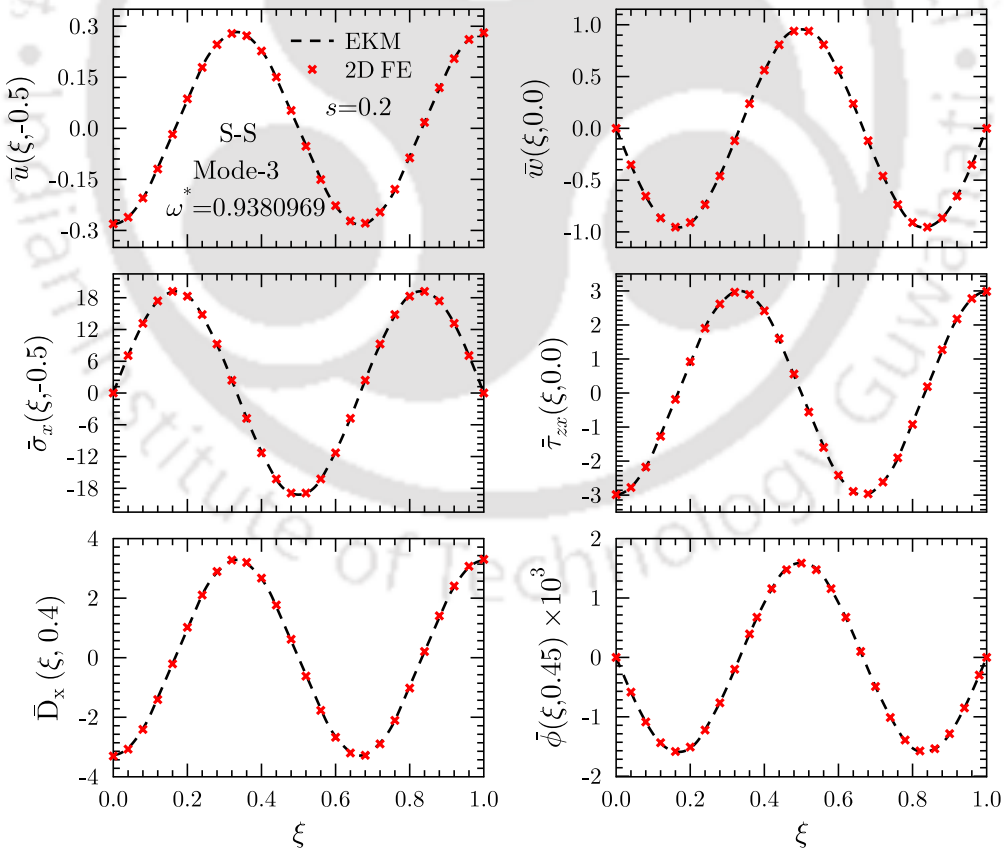

Fig. 5.10: Longitudinal variations of displacements, stresses and electrical variables for cross-ply piezoelectric panel with lay-up [(PZT-5A/0/90)$_2$] (EC–EC/EC–EC, s=0.2) and subjected to S-S boundary condition

are presented for the first mode of thick piezoelectric panel (a) (s=0.2) under to S–S boundary conditions and with close circuit condition. Similarly, the longitudinal variation of field variables (u, w, σ_x, τ_{zx}, ϕ, D_x) for third mode of thick piezoelectric panel (a) (s=0.2) are plotted in Fig. 5.10 under S–S boundary condition. Converge results of single term EKM are presented for both cases which match excellent with 2D FE results for both mode shapes.

5.4 SUMMARY

An accurate analytical solution based on coupled three-dimensional (3D) piezo-elasticity equations is presented for free vibration analysis of the angle-ply elastic and piezoelectric flat laminated panels under arbitrary boundary conditions. The present analytical solution is applicable to composite, sandwich and hybrid panels having arbitrary angle-ply lay-up, material properties and boundary conditions. A robust algorithm is developed for extracting the natural frequencies and mode shapes. The numerical results are reported for various configurations such as elastic panels, sandwich panels and piezoelectric panels under different sets of boundary conditions. First five fundamental frequencies are tabulated for various configuration and lay-ups. Free vibration behaviour of highly inhomogeneous composite panels are also investigated. The present solution is valid for thick as well as thin flat laminated composite and piezoelectric panels. The effect of ply-angle and thickness to span ratio (s) on the dynamic behavior of the panels are also investigated. The presented solution will be helpful in the assessment of various 1D theories and numerical methods.

Chapter 6

Smart Functionally Graded Beams Under Free Vibration

In recent years, axially functionally graded beams have been widely applied to many engineering fields. Moreover, structures often integrated with the piezoelectric material layers for sensing and controlling the vibration and acoustic behaviour of the structures [300–302]. Such structures are customarily known as smart structures. Thereafter, more attention is being paid to the static and dynamic analysis of axially functionally graded (AFG) beams or axially functionally graded beam integrated with piezoelectric layers. Hence, the solution of AFG beams developed in Chapter 2 is now extended to free vibration analysis of axially functionally graded beams integrated with piezoelectric layers.

A novel 2D analytical free vibration solution is developed for axially functionally graded (AFG) beams integrated with piezoelectric layers and subjected to arbitrary support boundary conditions. The material properties of the elastic layers are considered to vary linearly along the axial (x) direction of the beam. Modified Hamiltons principle, as discussed in Chapter 2, is applied to derive the weak form of coupled governing equations in which, stresses, displacements, and electric field variables acting as primary variables. Further, the extended Kantorovich method, similar to Chapter 2, is employed to reduce the governing equation into sets of ordinary differential equations (ODEs) along the axial (x) and thickness (z) directions. These sets of ODEs are solved analytically which ensures the same order of accuracy for all the variables by satisfying the boundary and continuity conditions in exact pointwise manner. New benchmark numerical results are presented for AFG beams integrated with piezoelectric layers. The influence of the axial gradation, piezoelectric layer thickness and boundary conditions on the natural frequencies of the beam are also investigated. These numerical results can be used for assessing 1D beam theories and numerical techniques.

6.1 FORMULATION FOR SMART FGM BEAMS

A multilayered axially graded hybrid beam ($x = (0, a)$, $z = -h/2$, $h/2$) as shown in Fig. 6.1, is considered for the present study.

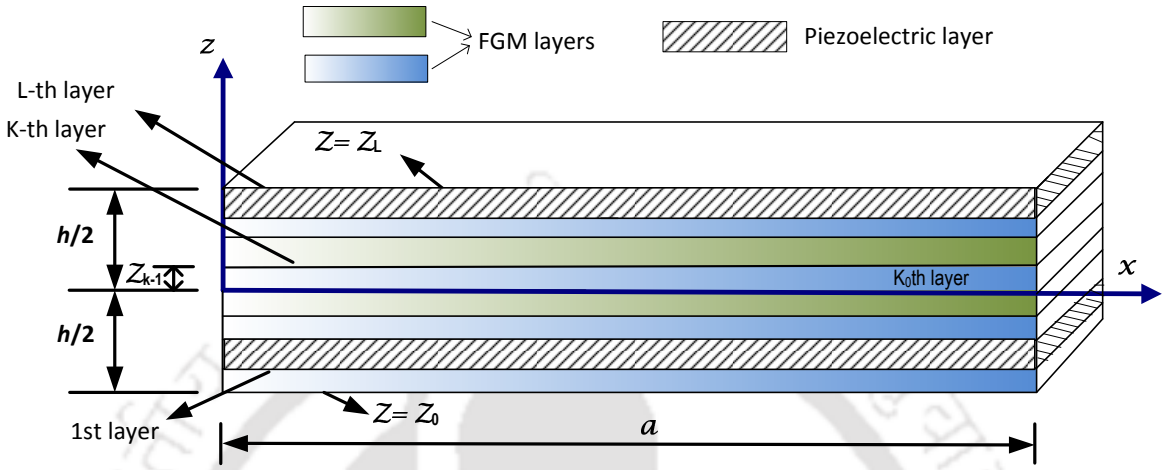

Fig. 6.1: Geometry of the AFG hybrid beam.

The material properties of the layers are assumed to vary linearly and continuously along the axis (x) of beam

$$\begin{aligned}
\bar{s}^m_{1j}(\xi) &= \bar{s}_{1j}(1+\delta_1\,\xi) \Longrightarrow \bar{s}_{1j} + \hat{s}_{1j} \quad \text{for} \quad j = 1, 3 \\
\bar{s}^m_{55}(\xi) &= \bar{s}_{55}(1+\delta_2\,\xi) \Longrightarrow \bar{s}_{55} + \hat{s}_{55} \\
\rho^m(\xi) &= \rho(1+\delta_p\,\xi) \Longrightarrow \rho + \hat{\rho}
\end{aligned} \tag{6.1}$$

where ξ non-dimensional parameter along x ($\xi = x/a$). δ_1 and δ_2 are variation indexes which control the gradation in elastic properties, and δ_p is the variation index for density. These variation indexes can have any arbitrary value. No variation is considered in the electrical properties of piezoelectric layers. The governing equations holds for each layer (kth layer) having thickness $t^{(k)}$. Since width is very small along y-direction, the displacement u and w along x-axis and z-axis, respectively are considered independent of y coordinate. Therefore, stresses $\sigma_y, \tau_{yz}, \tau_{xy}$ becomes zero. For plane stress condition following are non-zero strain-displacements and electric field-potential relations,

$$\varepsilon_x = u_{,x}; \quad \gamma_{zx} = w_{,x} + u_{,z}; \quad \varepsilon_z = w_{,z}; \quad E_x = -\phi_{,x}; \quad E_z = -\phi_{,z} \tag{6.2}$$

where differentiation denoted by a subscript comma. Two-dimensional piezoelectricity constitutive equations for AFG beams integrated with piezoelectric layer are given as,

$$\begin{aligned}
\varepsilon_x &= (\bar{s}_{11} + \hat{s}_{11})\sigma_x + (\bar{s}_{13} + \hat{s}_{13})\sigma_z + \bar{d}_{31} D_z \\
\varepsilon_z &= (\bar{s}_{31} + \hat{s}_{31})\sigma_x + \bar{s}_{33}\sigma_z + \bar{d}_{33} D_z
\end{aligned}$$

$$\gamma_{zx} = (\bar{s}_{55} + \hat{s}_{55})\tau_{zx} + \bar{d}_{15}D_z \tag{6.3}$$
$$E_x = \bar{\epsilon}_{11}D_x - \bar{d}_{15}\tau_{zx}$$
$$E_z = -(\bar{d}_{31}\sigma_x + \bar{d}_{33}\sigma_x - \bar{\epsilon}_{33}D_z)$$

where, $\bar{s}_{ij} = s_{ij} - d_{3i}\bar{d}_{3j}$, $\hat{s}_{ij} = \delta_1\bar{s}_{ij}$, $\bar{d}_{3i} = d_{3i}/\epsilon_{33}$ for i,j=1,3 and $\bar{s}_{55} = s_{55} - d_{15}\bar{d}_{15}$, $\hat{s}_{55} = \delta_2\bar{s}_{55}$ $\bar{d}_{15} = d_{15}/\epsilon_{11}$, $\bar{\epsilon}_{11} = 1/\epsilon_{11}$, $\bar{\epsilon}_{33} = 1/\epsilon_{33}$. Using equation Eq. (6.1), (6.2) and (6.3) piezoelectricity based extended Hamilton principle in a mixed form for the AFG beams integrated with piezoelectric layers, without any internal charge and body force source, case can be expressed as,

$$\begin{aligned}\int_t\int_a\int_h\ & [\delta u\{\sigma_{x,x} + \tau_{xz,z} - (\rho + \hat{\rho})\ddot{u}\} + \delta w\{\tau_{zx,x} + \sigma_{z,z} - (\rho + \hat{\rho})\ddot{w}\} \\ & +\delta\sigma_x\{(\bar{s}_{11} + \hat{s}_{11})\sigma_x + (\bar{s}_{13} + \hat{s}_{13})\sigma_z + \bar{d}_{31}D_z - u_{,x}\} \\ & +\delta\sigma_z\{(\bar{s}_{13} + \hat{s}_{13})\sigma_x + \bar{s}_{33}\sigma_z + \bar{d}_{33}D_z - w_{,z}\} \\ & +\delta\tau_{zx}\{(\bar{s}_{55} + \hat{s}_{55})\tau_{zx} + \bar{d}_{15}D_x - u_{,z} - w_{,x}\} + \delta\phi(D_{x,x} + D_{z,z}) \\ & +\delta D_x(\bar{d}_{15}\tau_{zx} - \bar{\epsilon}_{11}D_x - \phi_{,x}) + \delta D_z(\bar{d}_{31}\sigma_x + \bar{d}_{33}\sigma_z - \bar{\epsilon}_{33}D_z - \phi_{,z})]\mathrm{d}z\mathrm{d}x\mathrm{d}t = 0\end{aligned} \tag{6.4}$$

Here, t is the time variable. The bottom and top surfaces of hybrid beam are shear traction free (τ_{zx}=0). Where, ξ is a dimensionless axial coordinates considered along the x-direction and ζ is thickness coordinate for a layer along the z-direction which vary from 0 to 1. These are the support conditions considered at the top and bottom surface of hybrid beam, at z=± $h/2$: σ_z=0, τ_{zx}=0, for close circuit ϕ=0 and for open circuit D_z=0. The perfect bonding at the interface is considered. Therefore, these variable u, w, σ_z, τ_{zx}, ϕ and D_z satisfied following condition at the kth interface,

$$[(u,\ w,\ \sigma_z,\ \tau_{zx},\ \phi,\ D_z)|_{\zeta=1}]^{(k)} = [(u,\ w,\ \sigma_z,\ \tau_{zx},\ \phi,\ D_z)|_{\zeta=0}]^{(k+1)} \tag{6.5}$$

where $\zeta^{(k)}$ is non-dimensional local thickness parameter for the kth layer ($\zeta^{(k)} = (z - z_{k-1})/t^{(k)}$) which takes value 0 to 1 for each layer. Along x-axis (x=0 and 1), hybrid beam can have any mechanical support such as, Simply supported ($\sigma_x = w = 0$), Clamped ($w = u = 0$), Free ($\sigma_x = \tau_{xz} = 0$). Similary, the ends ($x = 0, a$) can have closed circuit condition (CC) in which potential is prescribed ($\phi = 0$) or have open circuit condition with $D_x = 0$.

6.2 MULTI-TERM EKM SOLUTION APPROACH

There are eight primary field variables $X_l = [\,u \quad w \quad \sigma_x \quad \sigma_z \quad \tau_{zx} \quad \phi \quad D_x \quad D_z\,]^{\mathrm{T}}$ which are to be solved. Using the multi-term EKM [296], the field variables for the k^{th} lamina are expressed as:

$$X_l = \sum_{i=1}^{n} f_l^i(\xi)g_l^i(\zeta)\ \cos\omega t, \qquad l = 1, 2, \ldots 8 \tag{6.6}$$

where $g_l^i(\zeta)$ and $f_l^i(\xi)$ are the unknown functions of ζ and ξ, respectively. Here, n represents the number of terms in solution. The functions $g_l^i(\zeta)$ are dependent on the k^{th} layer, while $f_l^i(\xi)$ functions are valid for all layers.

6.2.1 First Iterative Step for Thickness Direction

Functions $f_l^i(\xi)$, along x-direction, are assumed first for the first step and for which variation δX_i is given by

$$\delta X_l = \sum_{i=1}^{n} f_l^i(\xi)\delta g_l^i \ \cos\omega t, \qquad l = 1, 2, \ldots 8 \tag{6.7}$$

Functions $g_l^i(\zeta)$ are segregated into two column vectors $\bar{\mathbf{G}}$ and $\hat{\mathbf{G}}$. Where $\bar{\mathbf{G}}$ contains those particular $6n$ primary variables which are specified at the support and interface conditions along z-direction, and $\hat{\mathbf{G}}$ contains the remaining $2n$ dependent variables:

$$\begin{aligned}\bar{\mathbf{G}} &= [\, g_1^1 \ldots g_1^n \quad g_2^1 \ldots g_2^n \quad g_4^1 \ldots g_4^n \quad g_5^1 \ldots g_5^n \quad g_6^1 \ldots g_6^n \quad g_8^1 \ldots g_8^n \,]^{\mathrm{T}} \\ \hat{\mathbf{G}} &= [\, g_3^1 \ldots g_3^n \quad g_7^1 \ldots g_7^n \,]^{\mathrm{T}}\end{aligned} \tag{6.8}$$

Eqs. (6.6) and (6.7) are substituted into Eq. (6.4). Where, the f_l^i are known functions integration along x-direction are evaluated. Since variations for δg_l^i are arbitrary, using fundamental lemma of variational principles the coefficients of δg_l^i must vanish (equal to zero) which generates following set of $6n$ first order ODEs and $2n$ linear algebraic equations for each layer:

$$\mathbf{M}\bar{\mathbf{G}}_{,\zeta} = \bar{\mathbf{A}}(\omega)\bar{\mathbf{G}} + \hat{\mathbf{A}}\hat{\mathbf{G}} \tag{6.9}$$

$$\mathbf{K}\hat{\mathbf{G}} = \tilde{\mathbf{A}}\bar{\mathbf{G}} \tag{6.10}$$

Where $\mathbf{M}_{6n\times 6n}$, $\bar{\mathbf{A}}_{6n\times 6n}$, $\hat{\mathbf{A}}_{6n\times 2n}$, $\mathbf{K}_{2n\times 2n}$ and $\tilde{\mathbf{A}}_{2n\times 6n}$ are known matrices. Non-zero elements of the matrices are given below:

$$M_{i_1 j_1} = M_{j_4 i_4} = \langle f_5^i f_1^j \rangle_a,\ M_{i_2 j_2} = M_{j_3 i_3} = \langle f_4^i f_2^j \rangle_a$$

$$M_{i_5 j_5} = M_{j_6 i_6} = \langle f_8^i f_6^j \rangle_a,\ \bar{A}_{i_1 j_2} = \tfrac{-t}{a}\langle f_5^i f_{2,\xi}^j \rangle_a$$

$$\hat{A}_{i_1 j_2} = t\bar{d}_{15}\langle f_5^i f_7^j \rangle_a, \qquad \bar{A}_{i_1 j_4} = t\bar{s}_{55}\langle f_5^i f_5^j \rangle_a + \delta_2 t\bar{s}_{55}\langle \xi f_5^i f_5^j \rangle_a$$

$$\bar{A}_{i_2 j_3} = t\bar{s}_{33}\langle f_4^i f_4^j \rangle_a, \qquad \hat{A}_{i_2 j_1} = t\bar{s}_{13}\langle f_4^i f_3^j \rangle_a + \delta_1 t\bar{s}_{13}\langle \xi f_4^i f_3^j \rangle_a$$

$$
\begin{aligned}
&\bar{A}_{i_2j_6} = t\bar{d}_{33}\langle f_4^i f_8^j\rangle_a, && \bar{A}_{i_3j_4} = \tfrac{-t}{a}\langle f_2^i f_{5,\xi}^j\rangle_a \\
&\hat{A}_{i_4j_1} = \tfrac{-t}{a}\langle f_1^i f_{3,\xi}^j\rangle_a, && \bar{A}_{i_5j_3} = t\bar{d}_{33}\langle f_8^i f_4^j\rangle_a \\
&\hat{A}_{i_5j_1} = t\bar{d}_{31}\langle f_8^i f_3^j\rangle_a, && \bar{A}_{i_5j_6} = -t\bar{\epsilon}_{33}\langle f_8^i f_8^j\rangle_a \\
&\hat{A}_{i_6j_2} = \tfrac{-t}{a}\langle f_6^i f_{7,\xi}^j\rangle_a, && \bar{A}_{i_3j_2} = -\rho(1+\delta_p\,\xi)\omega^2 t\langle f_2^i f_2^j\rangle_a \\
&\bar{A}_{i_4j_1} = -\rho(1+\delta_p\,\xi)\omega^2 t\langle f_1^i f_1^j\rangle_a
\end{aligned}
\tag{6.11}
$$

$$
\begin{aligned}
&K_{i_1j_1} = \bar{s}_{11}\langle f_3^i f_3^j\rangle_a + \delta_1\bar{s}_{11}\langle \xi f_3^i f_3^j\rangle_a, && K_{i_2j_2} = \bar{\epsilon}_{11}\langle f_7^i f_7^j\rangle_a \\
&\tilde{A}_{i_1j_1} = \tfrac{1}{a}\langle f_3^i f_{1,\xi}^j\rangle_a, && \tilde{A}_{i_1j_3} = -\bar{s}_{13}\langle f_3^i f_4^j\rangle_a + \delta_1\bar{s}_{13}\langle \xi f_3^i f_4^j\rangle_a \\
&\tilde{A}_{i_1j_6} = -\bar{d}_{13}\langle f_3^i f_4^j\rangle_a, && \tilde{A}_{i_2j_4} = -\bar{d}_{15}\langle f_7^i f_5^j\rangle_a \\
&\tilde{A}_{i_2j_5} = -\tfrac{1}{a}\langle f_7^i f_{6,\xi}^j\rangle_a
\end{aligned}
\tag{6.12}
$$

where the notation $\langle\ldots\rangle_a = a\int_0^1(\ldots)d\xi$ represent integration over the span length a. Since the functions f_l^i are known functions, elements of the matrices defined in Eqs. (6.11) can be evaluated in closed form. The algebraic Eq. (6.10) is solved to obtain $\hat{\mathbf{G}}$, and substitute back into Eq. (6.9) which yields a set of $6n$ first-order homogeneous ODEs as,

$$\bar{\mathbf{G}}_{,\zeta} = \mathbf{A}(\omega)\bar{\mathbf{G}} \tag{6.13}$$

with $\mathbf{A} = \mathbf{M}^{-1}[\bar{\mathbf{A}} + \hat{\mathbf{A}}\mathbf{K}^{-1}\tilde{\mathbf{A}}]$. Above Eq. (6.13) represent a system of $6n$ homogeneous first order ODEs. The general solution of Eq. (6.13) to obtained natural frequency and mode shapes is obtained by applying the approach discussed in Chapter 2, Sec. 1.6.2.

6.2.2 Second Iterative Step for Axial Direction

Now variables $g_l^i(\zeta)$ (mode shapes) and frequency ω_{01} are known from the first step and arbitrary variation is considered along the x-direction. Therefore, variation for this case is written as:

$$\delta X_l^i = \sum_{i=1}^{n} g_l^i(\zeta)\delta f_l^i \;\cos\omega t \quad \text{for} \quad l = 1, 2, \ldots, 8 \tag{6.14}$$

Similarly, like the first step, $f_l^i(\xi)$ are segregated into two column vectors $\bar{\mathbf{F}}$ and $\hat{\mathbf{F}}$. Where $\bar{\mathbf{F}}$ carries those particular $6n$ primary variables which come in the support conditions at edges $x = 0, 1$ and $\hat{\mathbf{F}}$ contains the remaining $2n$ variables.

$$
\begin{aligned}
\bar{\mathbf{F}} &= [\, f_1^1 \ldots f_1^n \quad f_2^1 \ldots f_2^n \quad f_3^1 \ldots f_3^n \quad f_5^1 \ldots f_5^n \quad f_6^1 \ldots f_6^n \quad f_7^1 \ldots f_7^n \,]^{\mathrm{T}} \\
\hat{\mathbf{F}} &= [\, f_4^1 \ldots f_4^n \quad f_8^1 \ldots f_8^n \,]^{\mathrm{T}}
\end{aligned}
\tag{6.15}
$$

Substituting Eq. (6.6) and Eq. (6.14) in Eq. (6.4), performing integration over ζ direction on the known functions of ζ, applying integration by parts wherever necessary, and equating the coefficient of δf_l^i to zero individually, yields the following system of differential-algebraic equations for f_l^i:

$$\mathbf{N}\bar{\mathbf{F}}_{,\xi} = \bar{\mathbf{B}}^{\mathbf{f}}(\xi,\omega)\bar{\mathbf{F}} + \hat{\mathbf{B}}^{\mathbf{f}}(\xi)\hat{\mathbf{F}} \tag{6.16}$$

$$\mathbf{L}\hat{\mathbf{F}} = \tilde{\mathbf{B}}^{\mathbf{f}}(\xi)\bar{\mathbf{F}} \tag{6.17}$$

where $\mathbf{N}_{6n\times 6n}$, $\bar{\mathbf{B}}^f_{6n\times 6n}$, $\hat{\mathbf{B}}^f_{6n\times 2n}$, $\mathbf{L}_{2n\times 2n}$ and $\tilde{\mathbf{B}}^f_{2n\times 6n}$ are known matrices. Non-zero elements of the matrices are given below:

$$\begin{aligned}
&N_{i_1j_1} = N_{j_3i_3} = \langle g_3^i g_1^j\rangle_h, && N_{i_2j_2} = N_{j_4i_4} = \langle g_5^i g_2^j\rangle_h, && N_{i_5j_5} = N_{j_6i_6} = \langle g_7^i g_6^j\rangle_h\\
&\bar{B}^f_{i_1j_3} = (1+\delta_1\xi)\langle \bar{s}_{11} g_3^i g_3^j\rangle_h, && \hat{B}^f_{i_1j_1} = (1+\delta_1\xi)\langle \bar{s}_{13} g_3^i g_4^j\rangle_h, && \hat{B}^f_{i_1j_2} = \langle \bar{d}_{31} g_3^i g_8^j\rangle_h\\
&\bar{B}^f_{i_2j_1} = -\langle g_5^i \tfrac{g_{1,\zeta}^j}{t}\rangle_h, && \bar{B}^f_{i_2j_4} = (1+\xi\delta_2)\langle \bar{s}_{55} g_5^i g_5^j\rangle_h, && \bar{B}^f_{i_2j_6} = \langle \bar{d}_{15} g_5^i g_7^j\rangle_h\\
&\bar{B}^f_{i_3j_4} = \langle \tfrac{g_{5,\zeta}^i}{t} g_1^i\rangle_h, && \hat{B}^f_{i_4j_1} = -\langle g_2^i \tfrac{g_{4,\zeta}^j}{t}\rangle_h, && \bar{B}^f_{i_5j_4} = \langle \bar{d}_{15} g_7^i g_5^j\rangle_h\\
&\bar{B}^f_{i_5j_6} = -\langle \bar{\epsilon}_{11} g_5^i g_5^j\rangle_h, && \hat{B}^f_{i_6j_2} = -\langle g_1^i \tfrac{g_{8,\zeta}^j}{t}\rangle_h, && L_{i_1j_1} = \langle \bar{s}_{33} g_4^i g_4^j\rangle_h\\
&L_{i_1j_2} = \langle \bar{d}_{33} g_8^i g_4^j\rangle_h, && L_{i_2j_2} = -\langle \bar{\epsilon}_{33} g_8^i g_8^j\rangle_h, && L_{i_2j_1} = L_{i_1j_2}\\
&\tilde{B}^f_{i_1j_3} = -(1+\xi\delta_1)\langle \bar{s}_{13} g_4^i g_3^j\rangle_h, && \tilde{B}^f_{i_1j_2} = \langle g_4^i \tfrac{g_{2,\zeta}^j}{t}\rangle_h, && \tilde{B}^f_{i_2j_3} = -\langle \bar{d}_{31} g_8^i g_3^j\rangle_h\\
&\bar{B}^f_{i_3j_1} = -a\rho\omega^2(1+\delta_p\,\xi)\langle g_1^i g_1^j\rangle_h, && \bar{B}^f_{i_4j_2} = -a\rho\omega^2(1+\delta_p\,\xi)\langle g_2^i g_2^j\rangle_h, && \tilde{B}^f_{i_2j_5} = \langle g_8^i \tfrac{g_{6,\zeta}^j}{t}\rangle_h
\end{aligned} \tag{6.18}$$

where $\langle \ldots\rangle_h = \sum_{k=1}^{L} t^{(k)} \int_0^1 (\ldots)^{(k)}\, d\zeta$. Since $g^i(\zeta)$ are known in close form from previous step, so the above elements of matrices are obtained in closed form. Substitute algebraic equation (6.17) into Eq. (6.16) gives:

$$\bar{\mathbf{F}}_{,\xi} = \mathbf{B}(\xi,\omega)\bar{\mathbf{F}} \tag{6.19}$$

where $\mathbf{B} = \mathbf{N^{-1}}[\bar{\mathbf{B}}^{\mathbf{f}} + \hat{\mathbf{B}}^{\mathbf{f}}\mathbf{L^{-1}}\tilde{\mathbf{B}}^{\mathbf{f}}]$. Equation (6.19) is a system of simultaneous homogeneous first order differential equations ($6n$), with variable coefficients, which are solved using modified power series technique given in Chapter 2, Sec. 2.6.2. Thus, final solution for present system of equations (Eq. (6.19)) is approximated in form of power series as,

$$\bar{\mathbf{F}}^j(\xi) = \sum_{i=0}^{N_p} \mathbf{Z}_i^j \xi^i + \left(\sum_{i=0}^{N_p} \mathbf{H}_i^j \xi^i\right)\mathbf{C}_0 \tag{6.20}$$

where constants $\mathbf{Z}_i$ and $\mathbf{H}_i$ are calculated from obtained recursive relations. For free vibration case, there is no external applied load present. Therefore, $\mathbf{Z}_i = 0$. Hence, above equation is modified as,

$$\bar{\mathbf{F}}^j(\xi) = \left(\sum_{i=0}^{N_p} \mathbf{H}_i^j \xi^i\right)\mathbf{C}_0 \tag{6.21}$$

where unknown coefficient $\mathbf{C}_0$ is computed by applying x-direction support conditions. The number of terms (N_p) in power series is chosen large enough which ensure that the contribution of further succeeding terms is negligible and less than η ($= 10^{-10}$).

After applying the boundary conditions of end $\xi = 0$ and $\xi = 1$ of the beam, equation Eq. (6.21) yields

$$\sum_{i=1}^{6n} \mathbf{K_d}_i(\xi, \omega) C_i = \mathbf{0} \tag{6.22}$$

where, the coefficient matrix $\mathbf{K_d}$ now depends on $\omega = \omega_m$. Similarly, ω can be obtained by finding roots of the equation $|det(\mathbf{K_d})|$=0 using bisection method.

Now $\bar{\mathbf{F}}$ is known functions and further substituted to Eq. (6.17) to obtained the $\hat{\mathbf{F}}$ functions. Now the second step is completed. These two step, one along z-direction (Sec. 6.2.2) and next along x-direction (Sec. 6.2.2) completed one iteration. These iteration steps has been continued till the desired level of accuracy achieved.

6.3 NUMERICAL RESULTS AND DISCUSSIONS

The numerical results are presented for laminated piezoelectric beams with constant properties and axially graded beams integrated with piezoelectric layers. The material properties for elastic and piezoelectric layers are listed in Table 6.1.

Table 6.1: Material constants

Material	Y_1	Y_2	Y_3	G_{23}	G_{13}	G_{12}	ν_{12}	ν_{13}	ν_{23}	ρ
Mat. 1	181.0	10.3	10.3	2.87	7.17	7.17	0.28	0.28	0.33	1578
PZT-5A	61.0	61.0	53.2	21.1	21.1	22.6	0.35	0.38	0.38	7600
Material	d_{31}	d_{32}	d_{33}	d_{24}	d_{15}	η_{11}	η_{22}	η_{33}		
PZT-5A	-171	-171	374	584	584	15.3	15.3	15.0		

Units: Young's moduli Y_i and shear moduli G_{ij} in GPa; density (ρ) in Kg/m^3; piezoelectric strain coefficients d_{ij} in pm/V; electric permittivities η_{ij} in nF/m;
*Where $d_0 = d_{33}$ pm/V; Y_0= 10.3 GPa

The natural frequencies ω are non-dimensionalized as $\omega^* = \omega h\sqrt{\rho/G_{12}}$. Where ρ (1578 Kg/m^3) and G_{12} (7.17 GPa) is the material property of the orthotropic ply. The modal displacements and stresses are non-dimensionalized as:

$$(\bar{u},\, \bar{v},\, \bar{w}) = (u, v, w)/\max(u, v, w) \quad \bar{D}_x = D_x\, h/\{d_0\, s\, Y_0 \max(u, v, w)\} \qquad \bar{\phi} = \phi\, d_0/\max(u, v, w)$$

$$(\bar{\sigma}_x,\, \bar{\sigma}_y,\, \bar{\sigma}_z,\, \bar{\tau}_{zx},\, \bar{\tau}_{yz}) = \{\sigma_x,\, \sigma_y,\, \sigma_z,\, \tau_{zx},\, \tau_{yz}\}\, h/(s\, Y_0 \max(u, v, w))$$

Where $s(=h/a)$ denote the thickness-to-span ratio and $\max(u,w)$ denote the largest value of u and w along the thickness of beam for a particular vibration mode. The length of all beam is assumed equal to unity ($a=1$) for all cases and thickness of beams is taken according to thickness to span ratio ($s=h/a$). For $s=0.2,0.1,0.05$ the values of h are 0.2, 0.1, 0.05, respectively. The beams are designated according to their mechanical support conditions at the edges $\xi=0,1$. For example, the beam which is clamped (C) at $\xi=0$ and free (F) at $\xi=1$, is called an C–F beam. In the subsequent sections, results are obtained by taking n=1, iter.2 for S–S boundary condition and n=1, iter.3 for other boundary conditions.

6.3.1 Laminated Piezoelectric Beam

Numerical results are presented for a hybrid beam consisting of a laminate substrate and piezoelectric (PZT-5A) layer of thickness $0.1h$ (a=1) which is bonded at top of the beam, as shown in Fig. 6.2. The piezoelectric substrate is grounded at the bottom and top surfaces. The composite

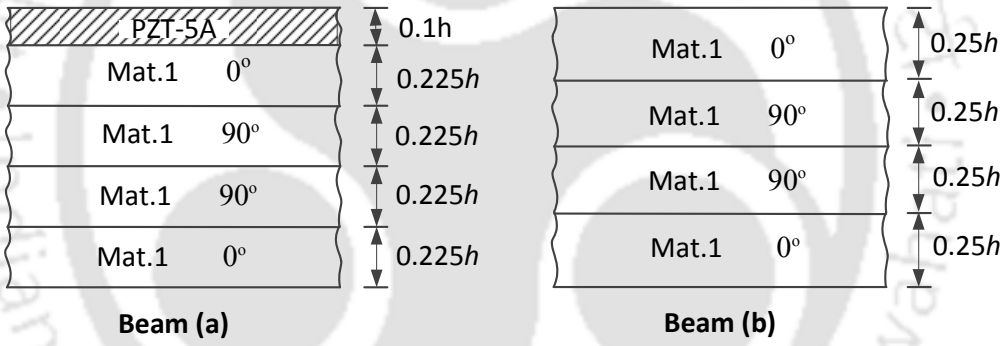

Fig. 6.2: Configuration of laminated piezoelectric and elastic beams

substrate of the beam having symmetric 4-ply laminate of Mat.1 with lay-up $[0/90/0/90^0]$ where each ply is of equal thickness $0.225h$. The dimensionless natural frequencies of first five bending modes are compared in Table 6.2 for the S–S, C–C and C–F boundary conditions. In this section, present results are validated for constant property case with the available result from literature and also with 2D FE results.

For simply–supported boundary condition present results are compared with 2D exact results of Kapuria et al. [158]. To compare the numerical results, natural frequency parameters reported by Kapuria et al. [158] further non-dimensionalized as $\omega^* = \omega h\sqrt{\rho/G_{12}}$.

Since no 2D exact or closed-form solution is available in literature for other type of support conditions. Therefore, present results are compared with 2D FE results for other combination of boundary conditions. Since it is a beam with a small width, plane stress element of ABAQUS [294] can be used. Therefore, the 2D plane beam with length a along x-direction and thickness h along

z-direction is modeled in ABAQUS using the element type CPS8R with a mesh size of 50 (length) $\times$16 (thickness). It is observed that the presented results match excellently with Ref. [158] and 2D FE results. It is observed that the present EKM results matches excellently with 2D FE results.

Table 6.2: Comparison of first five lowest natural frequency parameters $\omega^* = \omega h\sqrt{\rho/G_{12}}$ for five layered hybrid beam [(PZT-5A/0^o/90^o/0^o/90^o)] subjected to different sets of boundary conditions ($s = 0.1$)

s	B.C.	n	1	2	3	4	5
0.05	S–S	Present	0.0249623	0.0888359	0.1726535	0.2644750	0.3593576
		2D exact [158]	0.0249624	0.0888341	0.1726523	-	0.3593576
		2D FE	0.0249621	0.0888358	0.1726578	0.2644766	0.3593610
	C–S	Present	0.0363148	0.1020087	0.1833782	0.2723636	0.3651976
		2D FE	0.0363974	0.1025040	0.1846104	0.2743807	0.3678944
	C–C	Present	0.0487151	0.1142429	0.1935323	0.2800649	0.3710885
		2D FE	0.0489838	0.1153115	0.1958999	0.2838868	0.3762362
	C–F	Present	0.0091094	0.0507808	0.1238032	0.2092466	0.3009759
		2D FE	0.0091123	0.0509543	0.1245818	0.2109181	0.3039897
0.1	S–S	Present	0.0888358	0.2644750	0.4556917	0.6514738	0.8513033
		2D exact [158]	0.0888359	0.2644738	0.4556917	-	0.8512998
		2D FE	0.0888358	0.2644766	0.4557045	0.6514864	0.8513361
	C–S	Present	0.1142428	0.2800646	0.4649086	0.6581545	0.8569557
		2D FE	0.1153086	0.2838691	0.4709143	0.6658414	0.8653669
	C–C	Present	0.1387738	0.2946583	0.4751575	0.6655604	0.8633824
		2D FE	0.1420053	0.3011894	0.4865073	0.6799016	0.8794860
	C–F	Present	0.0342270	0.1554458	0.3378603	0.5265720	0.7222127
		2D FE	0.0343134	0.1577722	0.3445196	0.5390931	0.7372626
0.2	S–S	Present	0.2644752	0.6514738	1.0548077	1.4687225	1.8844207
		2D exact [158]	0.2644738	0.6514882	1.0548269	-	1.8844687
		2D FE	0.2644737	0.6514864	1.0548409	1.4687479	1.8845413
	C–S	Present	0.2946578	0.6655592	1.0656331	1.4777980	1.8918134
		2D FE	0.3012189	0.6799606	1.0826665	1.4953355	1.9098320
	C–C	Present	0.3267499	0.6816007	1.0805815	1.4878179	1.9008122
		2D FE	0.3452507	0.7063124	1.1110818	1.5204494	1.9356533
	C–F	Present	0.1127781	0.3927051	0.7975109	1.1836047	1.5917185
		2D FE	0.1143918	0.4123153	0.8257506	1.2293409	1.6369989

It is observed that for the thick beam ($s = 0.2$) the difference between the present and 2D FE results are more than moderately thick to thin beams for all modes and all boundary conditions.

Boundary conditions have a significant effect on fundamental frequencies. It can easily observe from Table 6.2 that first fundamental frequency is the highest for C–C case for all three values of s (h/a) and lowest for C–F case. For higher modes, the frequencies are near to S–S case for C–C and C–S conditions whereas, for C–F boundary condition frequencies for all modes and all s (0.05, 0.1, 0.2) are the lowest. It is observed that, as span to the thickness ratio (s) increases the non-dimensionalized natural frequencies parameters increases for all types of boundary conditions and increment is more pronounced at higher modes as compared to first mode.

In Fig. 6.3, the longitudinal variation of field variables $(u, w, \sigma_x, \tau_{zx}, \phi, D_x)$ are presented for the first mode of beam (a) $(s = 0.1)$ under to S–S boundary condition. Similarly, the longitudinal variation of field variables $(u, w, \sigma_x, \tau_{zx}, \phi, D_x)$ for third mode of beam (a) $(s = 0.1)$ under S–S boundary condition is plotted in Fig. 6.4. Converge results of single term EKM are presented for both cases which are in excellent agreement with 2D FE results for both mode shapes.

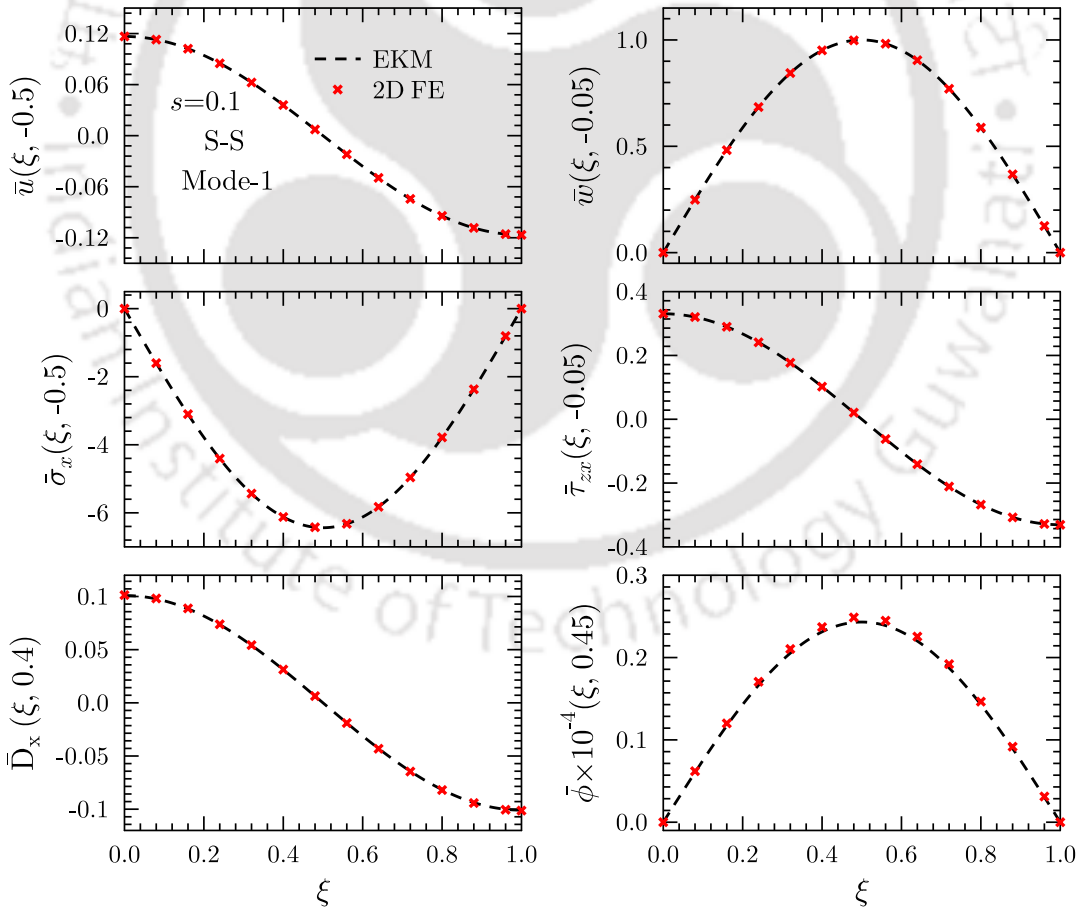

Fig. 6.3: Longitudinal variation of displacements, stresses and electrical variables for first modes of beam (a) under S–S boundary condition

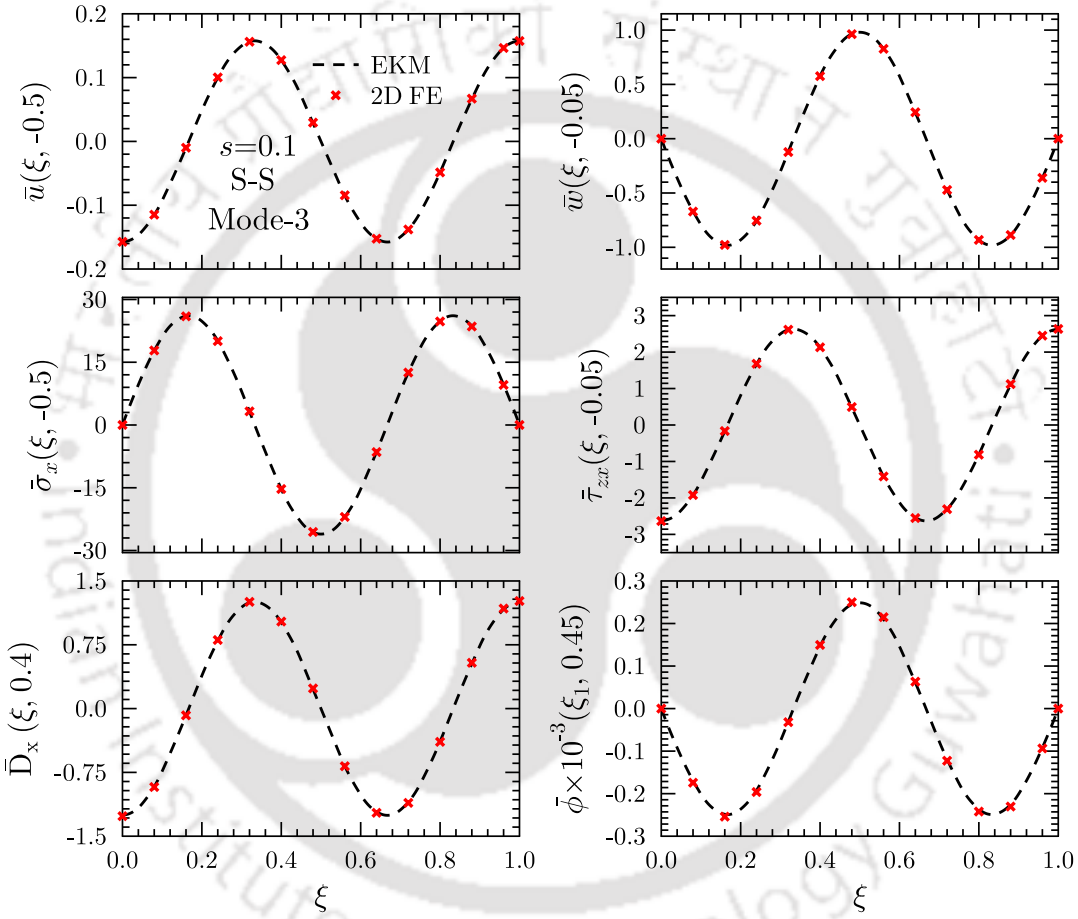

Fig. 6.4: Longitudinal variation of displacements, stresses and electrical variables for third modes of beam (a) under S–S boundary condition

Similarly, the longitudinal variation of displacements (u, w), normal stress (σ_x) and shear stress (τ_{zx}) are presented in Fig. 6.5 for piezoelectric beam (a) $(s = 0.1)$ under C–F and C–C support conditions, respectively. For these cases also, present EKM results matches excellently with the 2D FE results.

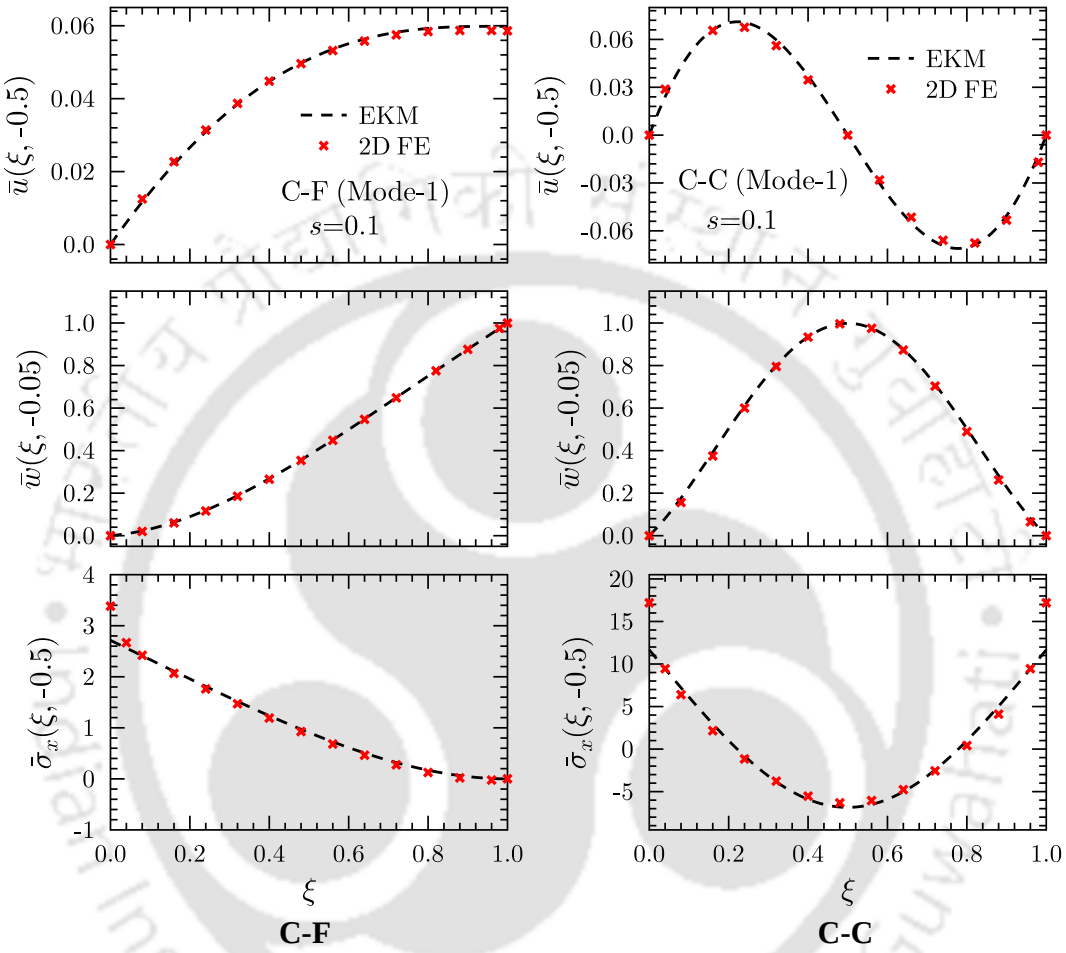

Fig. 6.5: Longitudinal variation of displacements and stresses for first modes of beam (a) under C–F and C–C boundary conditions

The through-thickness distributions of in-plane displacement (u) and stresses (σ_x, τ_{zx}) are compared in Fig. 6.6 for beam (a) and beam (b) $(s = 0.1)$ subjected to C–C, C–F boundary conditions. It is observed that the piezoelectric layer (PZT-5A) on top of the elastic beam significantly affect the behavior and natural frequency of the beam. The first mode non-dimensionalized natural frequency parameter for beam (b) (elastic beam, $s = 0.1$) is $\bar{\omega}$=0.1714813 and $\bar{\omega}$=0.0435130 for C–C and C–F support conditions, respectively. Then with inclusion of piezoelectric (PZT-5A) layer of thickness $0.1h$ on top of beam decreases the natural frequency parameter to $\bar{\omega}$=0.1387738 and $\bar{\omega}$=0.0342270 for C–C and C–F conditions, respectively.

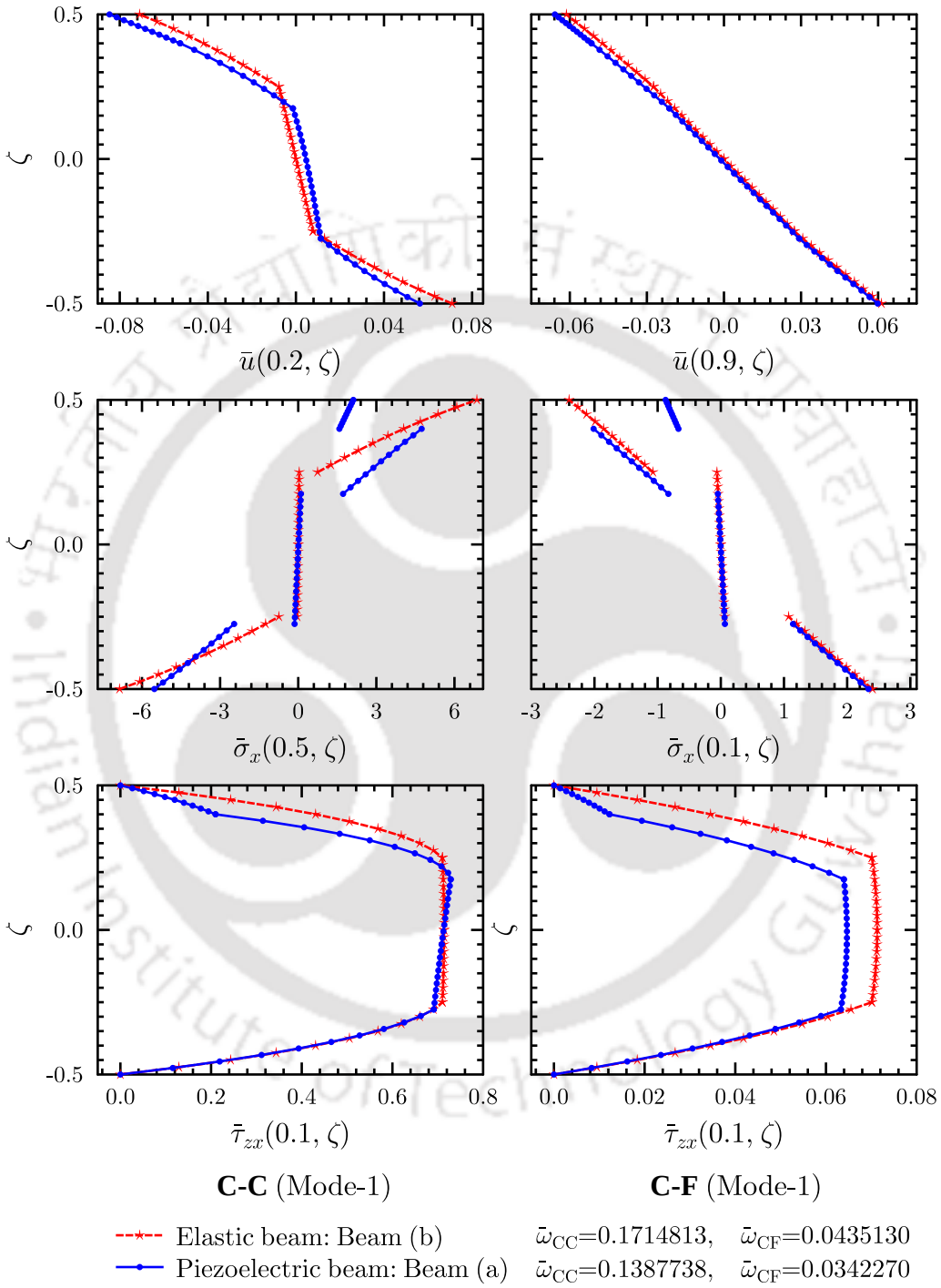

Fig. 6.6: Effect of piezoelectric layer on through-thickness distributions of in-plane displacements and stresses and electrical variables for C–C and C–F boundary conditions

6.3.2 AFG Beams Integrated with Piezoelectric Layer

The numerical results are presented for two types of beams: (a) AFG beam integrated with a single piezoelectric layer at the top, (c) AFG beam integrated with a piezoelectric layer at top and bottom, as shown in Fig. 6.7. Numerical results are presented for constant property (homogeneous)

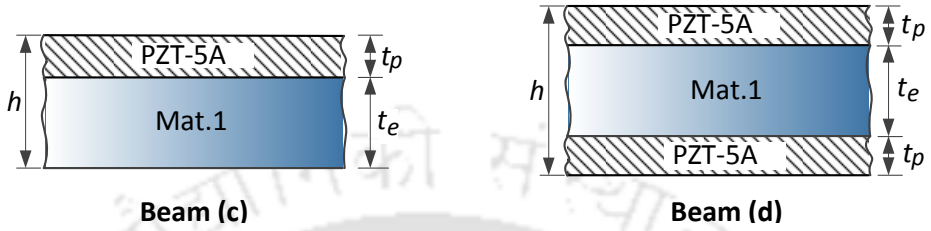

Fig. 6.7: Configuration of AFG beams

beam as well as axially graded beams subjected to different support conditions. To study the effect of axially gradation of material properties on dynamic behaviour of beam, the results are obtained for three type of material properties variation cases, Case (i): $\delta_1 = \delta_2 = \delta_p = 0.5$; Case (ii): $\delta_1 = \delta_2 = \delta_p = 1.0$; and Case (iii): $\delta_1 = 2.0$, $\delta_2 = 1.0$, $\delta_p = 1.5$ along with constant property (homogenous beam) case (Constant: $\delta_1 = \delta_2 = \delta_p = 0.0$). Table 6.3 shows the comparison of the

Table 6.3: Comparison of first five lowest natural frequency parameters $\omega^* = \omega h\sqrt{\rho/G_{12}}$ for single layered axially graded beam (c) subjected to different sets of boundary conditions ($s = 0.1$)

Variation	B.C.	n	1	2	3	4	5
Constant	S–S	Present	0.1278214	0.4048405	0.7183917	1.0363056	1.3532438
		2D FE	0.1278213	0.4048283	0.7183977	1.0363002	1.3532595
	C–S	Present	0.1718361	0.4370542	0.7365858	1.0469044	1.3599797
		2D FE	0.1722569	0.4384903	0.7390017	1.0498594	1.3631341
	C–C	Present	0.2161815	0.4652442	0.7544107	1.0573630	1.3668714
		2D FE	0.2170197	0.4676719	0.7587804	1.0628584	1.3729497
	C–F	Present	0.0481663	0.2360164	0.5285832	0.8391847	1.1571825
		2D FE	0.0481879	0.2366745	0.5308692	0.8426406	1.1614863
Case (i)	S–S	Present	0.1020078	0.3237784	0.5745036	0.8287549	1.0823242
		2D FE	0.1020088	0.3237978	0.5745826	0.8289341	1.0826371
	C–S	Present	0.1388961	0.3538251	0.5938627	0.8413565	1.0910437
		2D FE	0.1391431	0.3546300	0.5952455	0.8431122	1.0930422
	C–C	Present	0.1728368	0.3725154	0.6044040	0.8469430	1.0945339
		2D FE	0.1735509	0.3744971	0.6079204	0.8513066	1.0993502
	C–F	Present	0.0387337	0.1922727	0.4302224	0.6792120	0.9329132
		2D FE	0.0387703	0.1928608	0.4317697	0.6815228	0.9358743

natural frequencies with 2D FE results for single layered beam (a) subjected to S–S, C–s, C–C and C–F boundary conditions. Similarly, no 2D elasticity based analytical solution is available in the literature for the axially graded beams. Therefore, the accuracy and efficiency of the present EKM solution for the axially graded beams are verified by comparing the present result with 2D FE. For AFG beams, the spatial gradation of elastic property (at different Gauss points) is implemented by employing user material subroutine (UMAT) [296]. The variation of mass density is implemented by dividing the beam into 20 number of equal parts along the length and each part is assigned density value according to its center point. The results are compared for homogenous (constant property) case and gradation Case (i). The present results are in excellent agreement with 2D FE results for both cases and for all the boundary conditions. In the succeeding subsections, all the results are also thoroughly verified with 2D FE results and found an excellent agreement for all the cases.

6.3.2.1 Beam (c): AFG beam integrated with piezoelectric layer at top

An axially functionally graded beam (c) integrated with piezoelectric layer at top, as shown in Fig. 6.7, is considered for study in this section. The material properties of elastic layer (composite layer) are varying along the axial direction where the material properties of piezoelectric layers remains constant. No material property variation is considered in the piezoelectric layers. Side edges and top/bottom surface of piezoelectric layer is subjected to closed circuit condition. First five lowest dimensionless natural frequencies $\omega^* = \omega h\sqrt{\rho/G_{12}}$ are tabulated for AFG beam (s=0.1) by considering three thickness of piezoelectric layers (t_p=0.05h, 0.1h, 0.2h). Results are presented for different variation cases Case (i), Case (ii), and Case (iii) along with constant properties case to study the effect of axially varying material properties on natural frequencies of hybrid beam. In Tables 6.4, 6.5, 6.6 and 6.7, benchmark results are tabulated for S–S, C–S, C–C and C–F boundary conditions, respectively.

Significant effect of axial gradation is observed on the natural frequencies of the hybrid beam. As the variation indexes increase the natural frequencies of the hybrid beam decreases significantly for all the boundary conditions. For piezoelectric layers thickness t_p=0.05, nearly 16 to 18% decrement is observed in the first five natural frequencies for Case (i) as compared to constant property case under all the support conditions. Where the percentage decrement in natural frequencies is 27 to 29% for Case (ii) and 35 to 40% for Case (iii), respectively. Similarly, when the piezoelectric layers thickness t_p=0.1, nearly 14 to 16% decrement is observed in the first five natural frequencies for Case (i) as compared to constant property case under all the support conditions. Where the percentage decrement in natural frequencies is 25 to 27% for Case (ii) and 31 to 36% for Case (iii), respectively. Similarly, when the piezoelectric layers are very thick (t_p=0.2), nearly 11 to 13% decrement is

Table 6.4: Effect of axial gradation and piezoelectric layer thickness on first five lowest dimensionless natural frequencies $\omega^* = \omega h\sqrt{\rho/G_{12}}$ of two-layered AFG hybrid beam (c) subjected to S–S boundary condition (s=0.1)

	n	Constant	Case (i)	Case (ii)	Case (iii)
t_p=0.05h	1	0.1122119	0.0920205	0.0780062	0.0652428
	2	0.3583820	0.2941753	0.2496956	0.2180177
	3	0.6386995	0.5242888	0.4447429	0.3983407
	4	0.9220159	0.7576013	0.6427255	0.5840693
	5	1.2019259	0.9893856	0.8399398	0.7698601
t_p=0.1h	1	0.1000638	0.0839295	0.0724157	0.0617911
	2	0.3224564	0.2704378	0.2333880	0.2069083
	3	0.5775371	0.4844943	0.4177250	0.3792777
	4	0.8348076	0.7018228	0.6053676	0.5573762
	5	1.0869662	0.9172180	0.7923535	0.7357600
t_p=0.2h	1	0.0826207	0.0719042	0.0639678	0.0564143
	2	0.2718413	0.2360380	0.2094624	0.1904652
	3	0.4943920	0.4291029	0.3800747	0.3527092
	4	0.7218040	0.6280480	0.5565156	0.5227618
	5	0.9465264	0.8274077	0.7346669	0.6951936

Table 6.5: Effect of axial gradation and piezoelectric layer thickness on first five lowest dimensionless natural frequencies $\omega^* = \omega h\sqrt{\rho/G_{12}}$ of two-layered AFG hybrid beam (c) subjected to C–S boundary condition (s=0.1)

	n	Constant	Case (i)	Case (ii)	Case (iii)
t_p=0.05h	1	0.1519352	0.1261434	0.1079209	0.0925679
	2	0.3884418	0.3226350	0.2761717	0.2447383
	3	0.6557982	0.5428113	0.4635315	0.4182224
	4	0.9316750	0.7695929	0.6560247	0.5984148
	5	1.2075951	0.9975082	0.8497620	0.7805477
t_p=0.1h	1	0.1364798	0.1158063	0.1007473	0.0887865
	2	0.3511199	0.2978524	0.2591246	0.2329877
	3	0.5942019	0.5027591	0.4364249	0.3991510
	4	0.8441911	0.7138515	0.6189245	0.5721185
	5	1.0922459	0.9254701	0.8026443	0.7470875
t_p=0.2h	1	0.1144491	0.1005337	0.0899330	0.0791734
	2	0.2994585	0.2626843	0.2347304	0.2160293
	3	0.5120144	0.4483182	0.3997466	0.3733939
	4	0.7327420	0.6418601	0.5719339	0.5391593
	5	0.9536698	0.8379934	0.7474998	0.7087876

Table 6.6: Effect of axial gradation and piezoelectric layer thickness on first five lowest dimensionless natural frequencies $\omega^* = \omega h\sqrt{\rho/G_{12}}$ of two-layered AFG hybrid beam (c) subjected to C–C boundary condition (s=0.1)

	n	Constant	Case (i)	Case (ii)	Case (iii)
t_p=0.05h	1	0.1918424	0.1571945	0.1332041	0.1172127
	2	0.4147502	0.3406170	0.2894733	0.2603639
	3	0.6724521	0.5529715	0.4704999	0.4270666
	4	0.9410514	0.7747610	0.6593531	0.6029849
	5	1.2133601	1.0005238	0.8516677	0.7831593
t_p=0.1h	1	0.1732911	0.1447606	0.1244451	0.1106288
	2	0.3763088	0.3155264	0.2723783	0.2482945
	3	0.6104112	0.5129349	0.4434844	0.4079424
	4	0.8532294	0.7190209	0.6223129	0.5766814
	5	1.0976370	0.9284365	0.8045800	0.7497076
t_p=0.2h	1	0.1471146	0.1267247	0.1115694	0.1009626
	2	0.3242075	0.2808904	0.2488134	0.2317328
	3	0.5293515	0.4598304	0.4080107	0.3831202
	4	0.7437004	0.6485996	0.5765651	0.5448033
	5	0.9612674	0.8425083	0.7505993	0.7124792

Table 6.7: Effect of axial gradation and piezoelectric layer thickness on first five lowest dimensionless natural frequencies $\omega^* = \omega h\sqrt{\rho/G_{12}}$ of two-layered AFG hybrid beam (c) subjected to C–F boundary condition (s=0.1)

	n	Constant	Case (i)	Case (ii)	Case (iii)
t_p=0.05h	1	0.0421665	0.0350297	0.0300990	0.0258127
	2	0.2083501	0.1742763	0.1501901	0.1296468
	3	0.4682251	0.3913555	0.3364676	0.2976715
	4	0.7434751	0.6187819	0.5302241	0.4777452
	5	1.0227978	0.8496338	0.7266066	0.6622009
t_p=0.1h	1	0.0374919	0.0319572	0.0279404	0.0243225
	2	0.1870781	0.1600806	0.1394798	0.1226832
	3	0.4220926	0.3605945	0.4434844	0.2832180
	4	0.6707718	0.5715587	0.4983808	0.4557744
	5	0.9205812	0.7850770	0.6840230	0.6323184
t_p=0.2h	1	0.0307713	0.0272709	0.0245413	0.0219446
	2	0.1570542	0.1390495	0.1246464	0.1121017
	3	0.3590005	0.3173626	0.2851465	0.2624614
	4	0.5757800	0.5083743	0.4557900	0.4261029
	5	0.7960330	0.7040953	0.6311318	0.5956246

observed in the first five natural frequencies for Case (i) as compared to constant property case under all the support conditions. Where the percentage decrement in natural frequencies is 20 to 23% for Case (ii) and 16 to 31% for Case (iii), respectively. It is observed that the percentage effect of gradation in material properties very much depends on the piezoelectric layer thickness.

For all the variation cases, the effect of boundary conditions are significant on the lower mode natural frequencies of the hybrid beam and it is maximum for the first vibration mode. But for higher mode frequencies the effect of boundary conditions is negligible. For all the variation cases, a significant effect of piezoelectric layers thickness (t_p) is also observed on natural frequencies of the beams. As the thickness to expect ratio (t_p) increases the natural frequencies of all the vibration modes decreases significantly. The effect of piezoelectric layers thickness (t_p) is more on lower mode frequencies as compared to higher mode frequencies.

6.3.2.2 Beam (d): AFG beam integrated with piezoelectric layer at top and bottom

An axially functionally graded beam (d) integrated with a piezoelectric layer at top and bottom, as shown in Fig. 6.7 is considered for study in this section. The material properties of the elastic layer are varying linearly along the axial direction of the beam. No material property variation is considered in the piezoelectric layers. First five lowest dimensionless natural frequencies $\omega^* = \omega h\sqrt{\rho/G_{12}}$ are tabulated for hybrid AFG beam for various type of boundary conditions i.e S–S, C–S, C–C and C–F, respectively.

In Table 6.8, the dimensionless natural frequencies are presented for a hybrid beam with closed circuit conditions at the top and bottom surfaces. Similarly in Table 6.9, dimensionless natural frequencies is tabulated for hybrid beam subjected to open circuit condition at the top and closed circuit condition at the bottom surface. The effect of electric boundary conditions at the top and bottom surfaces of the hybrid beam is comparatively less for all five vibration modes. The present method is able to detect these small effects accurately which are very much important for precise control applications. The numerical results of this sub-section are also thoroughly verified with 2D FE results. It is found that present results are in excellent agreement with 2D FE results for all type of support conditions. As the gradation indexes increases, the free vibration frequencies of the hybrid beam decreases significantly for all the boundary conditions. For all the mechanical and electrical boundary conditions, nearly 11 to 13% decrement is observed in the first five natural frequencies for Case (i) as compared to constant property case. The percentage decrement in natural frequencies is 20 to 23% for Case (ii) and 26 to 31% for Case (iii), respectively. For all the gradation cases, the effect of mechanical support conditions are very significant on the lower mode natural frequencies of the hybrid beam and it is maximum for the first vibration mode. But for higher mode frequencies the effect of mechanical support conditions is nominal.

Table 6.8: Effect of axial gradation on first five lowest dimensionless natural frequencies $\omega^* = \omega h\sqrt{\rho/G_{12}}$ of three-layered AFG hybrid beam (d) with close circuit at top and bottom surface (s=0.1, t_p=0.1h)

B.C.	n	Constant	Case (i)	Case (ii)	Case (iii)
S–S	1	0.0811143	0.0705573	0.0628038	0.0556017
	2	0.2668505	0.2313253	0.2051895	0.1870889
	3	0.4857815	0.4200826	0.3714259	0.3454424
	4	0.7107772	0.6143772	0.5424901	0.5105054
	5	0.9350406	0.8089883	0.7142782	0.6768532
C–S	1	0.1122780	0.0985355	0.0881668	0.0775414
	2	0.2936143	0.2571099	0.2296425	0.2119614
	3	0.5024714	0.4382251	0.3900479	0.3653816
	4	0.7206869	0.6268578	0.5565468	0.5259764
	5	0.9409687	0.8179103	0.7253553	0.6892164
C–C	1	0.1442620	0.1241550	0.1092277	0.1005733
	2	0.3173482	0.2743152	0.2427475	0.2266461
	3	0.5186352	0.4486202	0.3972704	0.3739153
	4	0.7303329	0.6324119	0.5601317	0.5304182
	5	0.9470729	0.8212159	0.7274492	0.6917801
C–F	1	0.0302295	0.0267734	0.0240891	0.0215471
	2	0.1541417	0.1363420	0.1226305	0.1098623
	3	0.3526349	0.3109167	0.2791178	0.2573532
	4	0.5667813	0.4968550	0.4450150	0.4171485
	5	0.7860119	0.6887645	0.6145798	0.5811956

Table 6.9: Effect of axial gradation on first five lowest dimensionless natural frequencies $\omega^* = \omega h\sqrt{\rho/G_{12}}$ of three-layered AFG hybrid beam (d) with open circuit condition at top and close circuit condition at bottom surface (s=0.1, t_p=0.1h)

B.C.	n	Constant	Case (i)	Case (ii)	Case (iii)
S–S	1	0.0814750	0.0709253	0.0631737	0.0560067
	2	0.2677782	0.2322578	0.2061064	0.1881197
	3	0.4871227	0.4214190	0.3727216	0.3469166
	4	0.7124121	0.6159977	0.5440518	0.5122661
	5	0.9369008	0.8108304	0.7160437	0.6788129
C–S	1	0.1126673	0.0989722	0.0886075	0.0779500
	2	0.2945073	0.2580160	0.2305151	0.2129706
	3	0.5037623	0.4395124	0.3912968	0.3667947
	4	0.7222930	0.6284423	0.5580642	0.5276711
	5	0.9428276	0.8197285	0.7270836	0.6911125
C–C	1	0.1447247	0.1245985	0.1100096	0.1009496
	2	0.3182147	0.2751637	0.2435626	0.2275570
	3	0.5198805	0.4498404	0.3984450	0.3752146
	4	0.7319294	0.6339664	0.5616155	0.5320435
	5	0.9489259	0.8230114	0.7291499	0.6936259
C–F	1	0.0303637	0.0269076	0.0242175	0.0216760
	2	0.1547662	0.1369988	0.1233100	0.1116025
	3	0.3537172	0.3120266	0.2802264	0.2587603
	4	0.5682998	0.4984179	0.4464928	0.4188109
	5	0.7879476	0.6905084	0.6163488	0.5831476

Similarly, effect of axial gradation of material property on the longitudinal variation of displacements $(\bar{u}, \bar{w})$, stresses $(\bar{\sigma}_x, \bar{\tau}_{zx})$ and electrical field variables $(\bar{D}_x, \bar{\phi})$ are presented in Fig. 6.8 for the first vibration mode of AFG beam (d) (s=0.1) subjected to S–S and closed-circuit boundary conditions. Further, the longitudinal variation of displacements (u, w), stresses $(\bar{\sigma}_x, \bar{\tau}_{zx})$ and electrical variables $(\bar{D}_x, \bar{\phi})$ for third vibration mode of AFG beam (d) (s=0.1), under S–S and closed-circuit boundary condition, are plotted in Fig. 6.9 for all the properties variation cases. Results for the

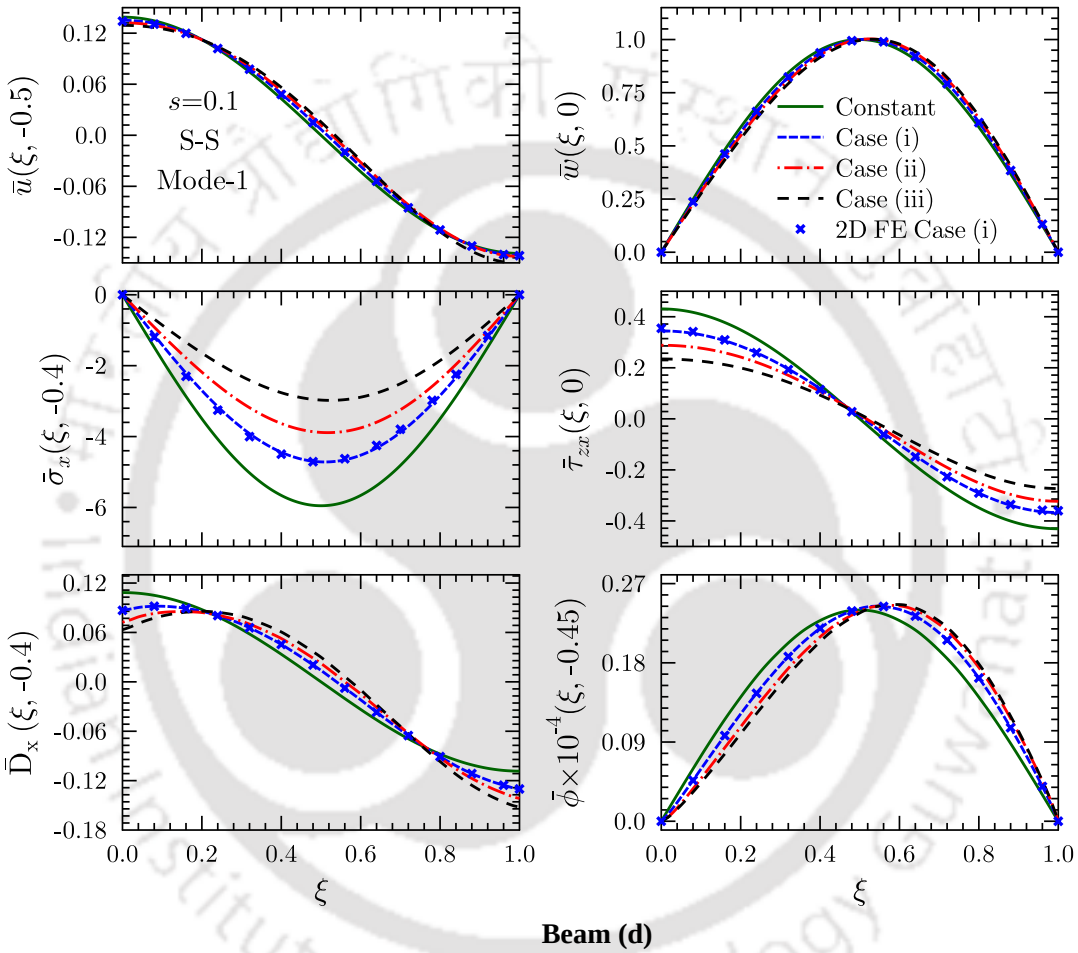

Fig. 6.8: Effect of axial gradation on longitudinal variations of displacements, stresses and electrical field variables for first vibration mode (Mode-1) of beam (d) under S–S and closed-circuit boundary conditions

constant properties case (homogeneous beam) are also potted in Figs. 6.8 and 6.9 to study the effect of gradation on longitudinal variation of entities. The 2D FE results for gradation Case (i) are also plotted in these figures. The present results are in excellent agreement with 2D FE results. For both mode (Mode 1 and 3), the stresses $(\bar{\sigma}_x, \bar{\tau}_{zx})$ are affected significantly due to the gradation of material properties whereas deflections $(\bar{u}, \bar{w})$ and electrical field variables $(\bar{D}_x, \bar{\phi})$ are least affected. The stresses $(\bar{\sigma}_x, \bar{\tau}_{zx})$ are decreasing significantly as the variation index increases. It is observed that the influence of material gradient much more on the first mode shape as compared to higher

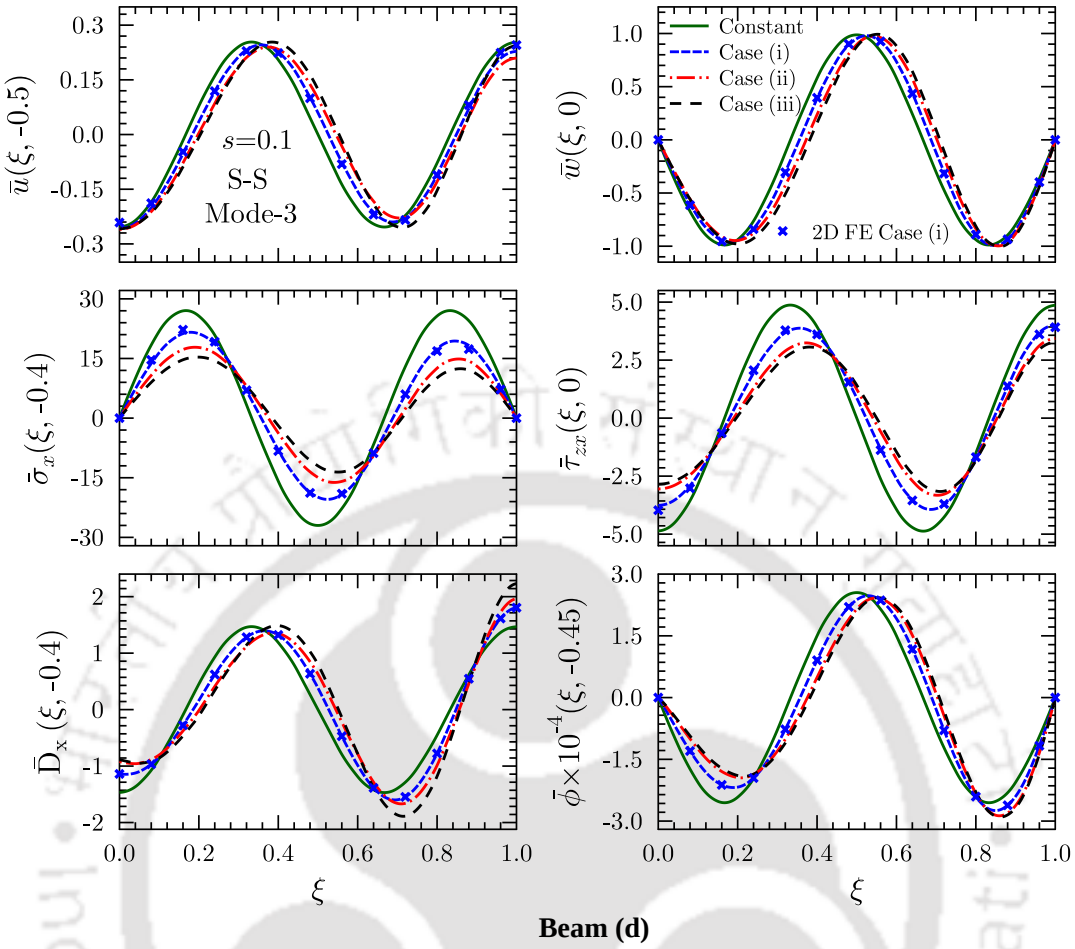

Fig. 6.9: Effect of axial gradation on longitudinal variations of displacements, stresses and electrical field variables for first vibration mode (Mode-3) of beam (d) under S–S and closed-circuit boundary conditions

vibration modes. It shows that the effect of material gradation on stresses become nominal as the mode number increasing.

Further, through-thickness distributions of displacements $(\bar{u}, \bar{w})$, stresses $(\bar{\sigma}_x, \bar{\tau}_{zx})$ and electrical variables $(\bar{D}_x, \bar{\phi})$ at different ξ-locations in the first flexural mode of simply-supported closed-circuit beam (d) are plotted Figs. 6.10 and 6.11 under constant case (homogenous) and gradation Case (i), respectively. It is observed that the nature of through-thickness distribution not affected much due to the axial gradation of material properties weather the magnitude of stresses are affected significantly. It is observed that the distribution of stress $(\bar{\tau}_{zx})$ and electric potential $(\bar{\phi})$ across the thickness are highly non-linear. Therefore, elasticity based solution must be required to predict such distribution of entities across the thickness.

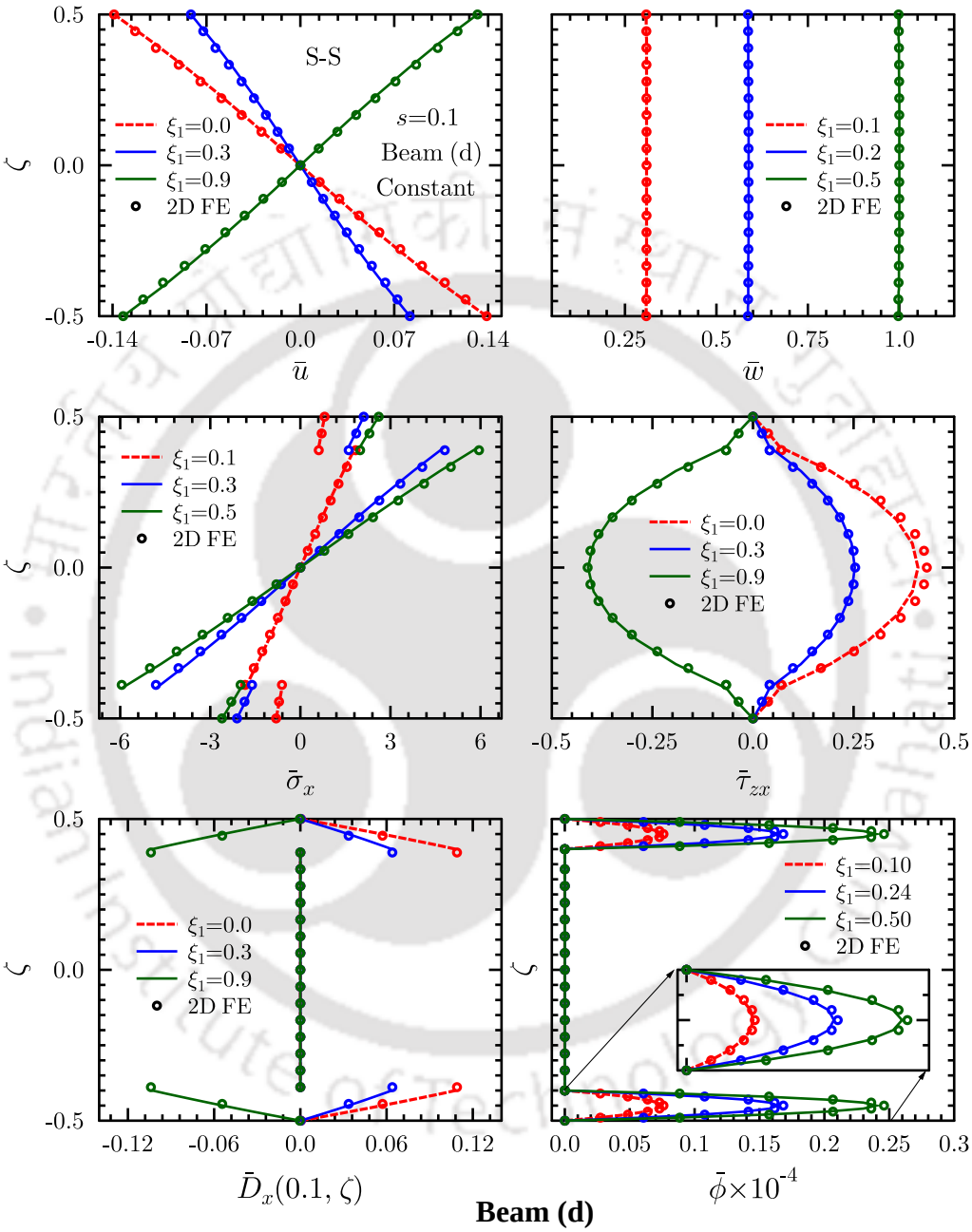

Fig. 6.10: Through-thickness distributions of displacements, stresses and electrical field variables at different ξ-locations in the first flexural mode of beam (d) under constant case of property variation and subjected to S–S and closed-circuit boundary conditions

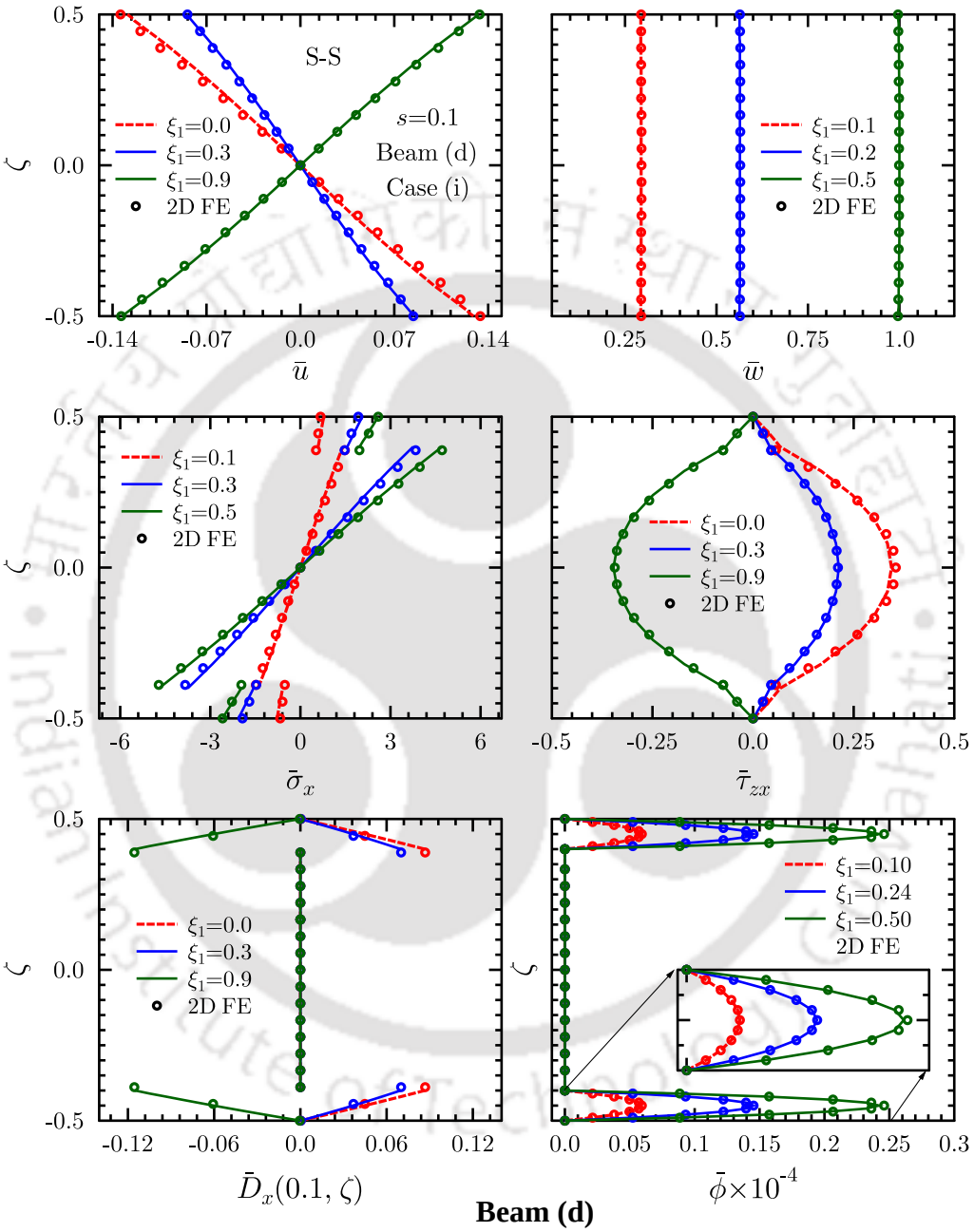

Fig. 6.11: Effect of axial gradation on through-thickness distributions of displacements, stresses and electrical field variables at different ξ-locations in the first flexural mode of beam (d) under Case (i) of property variation and subjected to S–S and closed-circuit boundary conditions

Similarly, the longitudinal variation of deflection and stresses for C–F and C–C boundary conditions are plotted in Fig. 6.12 for first vibration mode of AFG beam (d) (s=0.1) under all the gradation cases. The present results for C–C and C–F support conditions are also in excellent agreement with 2D FE results. For C–F and C–C support conditions also, the influence of axial gradation are significant on stresses whereas the effect of gradation on deflections ($\bar{u}$, $\bar{w}$) are nominal.

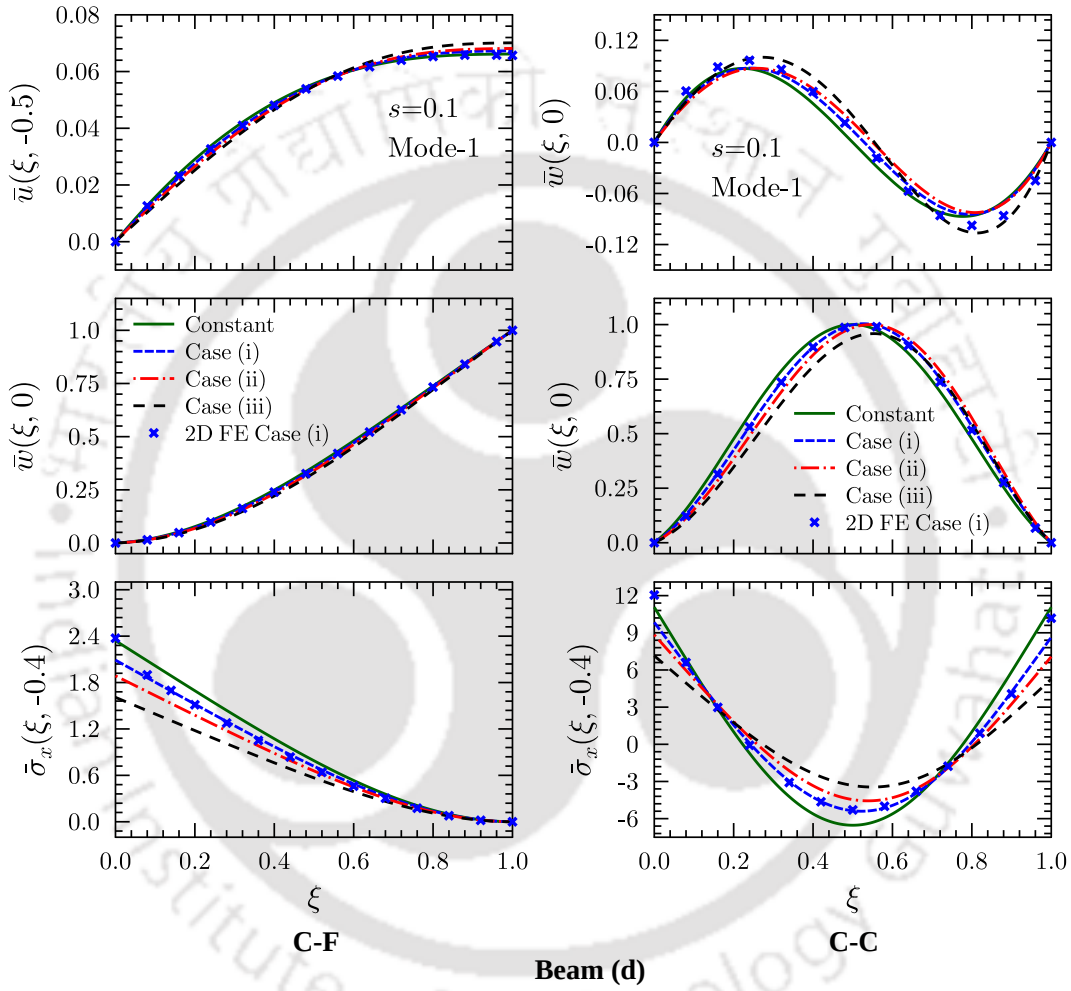

Fig. 6.12: Longitudinal variations of displacements and stresses for first vibration mode of beam (d) under C–C and C–F, and closed-circuit boundary conditions

6.4 SUMMARY

First time, a coupled 2D piezoelectricity based analytical solution is presented for the free vibration analysis of arbitrary supported axially functionally graded beams integrated with piezoelectric layers. Further, the free vibration solution for the arbitrary supported piezoelectric beams having constant properties is also obtained as a special case of the present study. The fundamental frequencies and corresponding mode shapes are presented for the laminated piezoelectric beams under different combinations of support conditions. The influence of the longitudinal variation of material properties on natural frequency and mode shape of piezoelectric beams is studied in conjunction with different boundary conditions. Significant effect of axial gradation on the natural frequencies of the piezoelectric beams is observed. As the gradation indexes increase the natural frequencies of beam decrease significantly. For all the cases, the influence of boundary conditions are significant on the lower mode natural frequencies and it is maximum for the first vibration mode. But for higher mode frequencies the effect of boundary conditions is negligible. The present numerical study reveals that the desired free vibration response is obtained by control the behaviour of beam with help of piezoelectric layers. The present analytical solution provided benchmark results which can be utilized for assessing 1D beam theories and other numerical models for free vibration analysis of piezoelectric laminated beams and axially functionally graded beams integrated with piezoelectric layers.

Chapter 7

Conclusions

First time, the elasticity based accurate analytical solutions are presented for static and free vibration analysis of in-plane functionally graded composite and piezoelectric structures. Modified Hamiltons principle is applied to derive the weak form of coupled governing equations in which, stresses and displacements variables acting as primary variables. Interface continuity and boundary conditions are satisfied in exact pointwise manners, which ensures the same order of accuracy for all the variables (stresses, displacements, and electric variables). Further multi-term extended Kantorovich method, recently developed powerful iterative technique, is employed to reduce the governing equation into sets of ordinary differential equations (ODEs). These sets of ODEs are solved analytically, which is key in the accurate prediction of free edge stresses. A novel power series based algorithm is developed and proposed to extract the static response, flexural frequencies and mode shape from a set of non-homogeneous ODEs having variable coefficients. A detailed numerical study established excellent agreement of the present iterative series solution with existing literature results and 3D FE results. Further, the influence of the in-plane graded material properties on the static and dynamic response of structures are studied extensively for different support conditions and thickness ratios. The present solution is valid for thick as well as thin FGM structures (beams, plates and panels). Benchmark results are presented for both homogeneous and in-plane graded rectangular plates for various configurations and different combinations of boundary conditions. The significant effect of in-plane gradation of material properties is observed on the static and free vibration response of the functionally graded structures. The present analytical solution for in-plane functionally graded structures serves as benchmarks in the assessment of the accuracy of the numerical models and 1D/2D theories. This development will also assist in taking suitable kinematic assumption which is very helpful in the development of refined beam and plate theories for in-plane functionally graded structures. Further, the following novel and significant conclusions are drawn based on the present numerical study.

7.1 CHAPTERWISE SYNOPTIC CONCLUSIONS FROM THE PRESENT WORK

1. An accurate two-dimensional elasticity based analytical solution is presented for static and free vibration analysis of axially functionally graded beam subjected to the arbitrary boundary condition using extended Kantorovich method. Further, static and free vibration results for the arbitrary supported homogeneous beam are also obtained as a special case of present development. New benchmark results are presented for the axially functionally graded beams as well as a homogeneous beam subjected to arbitrary support conditions. The influence of material properties variation on the static and dynamic response of axially FG beam, as compared to the homogeneous beam is investigated comprehensively by considering various material property variation cases. The numerical study reveal that:

   (i) The static and free vibration response of beam affected significantly by the axial gradation of material properties. For static case, the axial variation of material properties affected displacements of beams significantly as compare to stresses. But for free vibration case, the stresses affected significantly by axial gradation in properties as compared to deflections. The effects of axial gradation on the static and dynamic behavior of the beam depend significantly on boundary conditions of the beams.

   (ii) For accurate prediction of deflections and stresses under simply-supported (S–S) conditions, single term (n=1, *iter*.1) is sufficient enough. Whereas, two-term solution (n=2, *iter*.2) is required for the other boundary conditions.

   (iii) The single term solution is adequate to obtaining the accurate flexural frequencies for all the gradation cases under all boundary conditions.

   (iv) It is observed that the natural frequencies of the beam significant affected by axial gradation of material properties. As the gradation indexes increase the natural frequencies of beam decrease significantly. The percentage effect is almost increased by 1.5 times as the gradation indexes are doubled from 0.5 to 1. The percentage decrement in natural frequency due to gradation in material properties does not affect much with boundary conditions of beam.

   (v) The effect of axial gradation of density on natural frequencies of beams is also studied which revealed that the percentage decrement in natural frequencies become double as the value of density variation index (δ_p) make double from δ_p=0.5 to δ_p=1.0.

   (vi) For all the cases, the influence of boundary conditions are significant on the lower mode natural frequencies and it is maximum for the first vibration mode. But for higher mode

frequencies the effect of boundary conditions is nominal.

(vii) For S-S and C-C boundary condition, the longitudinal variation of in-plane displacement ($\bar{u}$) become asymmetrical as the variation indices increases.

(viii) For both axially graded and homogeneous beams, in-plane displacement ($\bar{u}$) and stress $\bar{\sigma}_x$ vary nonlinearly through the thickness near the edges. In most of the 1D theories, like Euler-Bernoulli and Timoshenko beam theory, in-plane displacement ($\bar{u}$) approximated linearly through the thickness. Therefore, two-dimensional elasticity solution is required to predict the bending and free vibration behavior of beams accurately.

(ix) The axial gradation of material property even in one layer significantly affected the static and free vibration behaviour for all boundary condition.

(x) For both axially graded and homogeneous beams, $\bar{\sigma}_z$ and $\bar{\tau}_{zx}$ are highly non-linear near to clamped support and 2D FE fail to predict it because finite element solution does not satisfy the boundary conditions and interface continuity conditions at very clamped edge.

(xi) The present numerical study reveals that the desired static and free vibration response of beam for specific applications can be achieved by controlling the axial variation of material properties.

(xii) The present analytical solution provided benchmark results for assess the accuracy of the 1D beam theories and numerical models for free vibration analysis of axially graded beams.

2. A three-dimensional elasticity solution has been presented for static and dynamic analysis of rectangular FGM plates with longitudinally varying material properties using the multi-term extended Kantorovich method. The influence of the gradation of material properties on the static bending and free vibration behavior is studied for different boundary conditions. The detailed numerical study reveals that:

   (i) The EKM solution converges within just one/two terms for both single-layer and two-layer FGM plates for all the variation cases under the static and dynamic case.

   (ii) For simply-supported (S–S)conditions, single term (n=1, *iter*.1) gives accurate prediction for deflections and stresses under both static and dynamic case. Whereas, two-term solution (n=2, *iter*.2) is required for the other boundary conditions. To obtaining the accurate flexural frequencies the single term solution is sufficient enough for all the property variation cases and boundary conditions.

(iii) The bending and free vibration response of rectangular plate is influenced greatly by the extent of material gradation along the in-plane direction for all the boundary conditions.

(iv) It has been observed that as the gradation indexes are doubled from 0.5 to 1, its effect on maximum deflection, stresses and natural frequencies are also nearly doubled. The in-plane gradation of material property even in one layer significantly affected the stresses and deflection of the plate for all boundary condition.

(v) For static case, the deflections of plates increased as the gradation index increases. The effect on deflection of plate is more significant and notable as compared to in-plane stresses in plate. Where for dyanaimic case the effect of gradation on behavior of plate is entirely different than static case. Under free vibration, the in-plane stresses affected significantly by in-plane gradation of material properties but the effect of gradation on deflection is negligible.

(vi) The natural frequencies of the rectangular plate decreases significantly for all the boundary conditions as the variation indexes increases.

(vii) The effects of in-plane gradation of material properties on the bending and free vibration behavior of the rectangular plate depend significantly on boundary conditions of the plate. The plate subjected to simply-supported or clamped boundary condition shows similar trends. But the behavior of a plate subjected to free boundary conditions is entirely different than simply-supported or clamped plates for both static and free vibration case. For plate subjected to S–F and F–F support conditions, the effect of in-plane gradation on the flexural frequencies of plate are comparatively less. But, longitudinal variation of deflections and stresses (mode shapes) affected significantly for S–F and F–F plates.

(viii) For all the cases, the effect of boundary conditions are significant on the lower mode flexural frequencies and it is maximum for the first vibration mode (m=1). But for higher mode frequencies the effect of boundary conditions comparatively less.

(ix) From the analysis of two-layered square plate adhesively bonded by a functionally graded adhesive interlayer, it is observed that the deflection and stresses are effected significantly by in-plane gradation of the adhesive interlayer material properties and moreover, boundary condition plays an important role in the behavior of adhesively bonded plates. It is observed that the shear stress $\bar{\tau}_{zx}$ in adhesive layer decreases as the variation index of the adhesive layer increases. Therefore, the bonding strength of joint can be increased by using functionally graded adhesive interlayer

(x) The present analytical elasticity solution can be used as a benchmark for assessing the accuracy of the 2D plate theories in bending and free vibration analysis of composite FGM rectangular plates having in-plane heterogeneity. This is a more severe case than a homogeneous plate for assessing 2-D theories.

(xi) This development has opened the area for developing the closed form solution for FGM plates with property variation along multiple directions

3. An accurate analytical elasticity solution is presented for axially functionally graded angle-ply flat panel under cylindrical bending and subjected to arbitrary boundary condition. The influence of stiffness variation on bending and free vibration response of angle-ply flat panel is investigated comprehensively. The detailed numerical study has led to following inferences:

(i) For static case, single term (n=1, *iter*.1) gives accurate prediction for deflections and stresses for simply-supported case whereas two-term solution (n=2, *iter*.2) is required for the other boundary conditions.

(ii) For free vibration case, the single term solution is sufficient enough to obtaining the accurate flexural frequencies for all the cases and boundary conditions.

(iii) Based on the present study, it is established that the variation of material properties along the axial (x) direction affects the panel deflections, stresses and natural frequencies to a great extent.

(iv) It is also observed that effects of axial stiffness variation on the static and dynamic behavior of the panel depend significantly on boundary conditions. For static case, the effect of in-plane material property variation on the deflections and stresses are relatively less under clamped support conditions (C–S, C–C) as compare to simply supported case (S–S). For dynamic case, the effect of axial gradation on the flexural frequencies of the flat panels is almost similar for all the support conditions.

(v) The natural frequencies of panels decreases significantly with the increment of gradation indexes. For all the support conditions, it is observed the percentage decrement is maximum for first natural frequency as compared to higher mode natural frequencies. This percentage decrement in natural frequency is lesser for higher mode natural frequencies.

(vi) Similarly, the effect of support conditions is significant on the lower mode of natural frequencies for all the variation cases. It is maximum for first vibration mode, and this effect of boundary condition is decreasing as the mode become higher. The effect of support conditions on higher modes (Mode-4 and Mode-5) natural frequencies is negligible as compared to first mode natural frequency.

(vii) This development has shown that by controlling the axial gradation parameters the desired distribution of the deflection, stress can be achieved for specific applications.

(viii) The present method provided benchmark results to assess the validity and accuracy of different plate theories and computational models for analysis of axially functionally graded angle-ply plate under cylindrical bending. This is a more critical case than a cross-ply functionally graded plate for assessing 2-D theories and numerical solution techniques.

(ix) The current research will also be beneficial to modeled real life panel structures in which material properties of panel deteriorate due to some environmental effect.

4. An accurate analytical solution based on coupled three-dimensional (3D) piezo-elasticity equations is presented for free vibration analysis of the angle-ply elastic and piezoelectric flat laminated plates in cylindrical bending. These are some novel and significant contributions of the present work:

   (i) An 3D piezoelectricity based analytical solution for free vibration analysis of arbitrary supported (S–S, C–C, C–F, and C–S) angle-ply elastic and piezolaminated panel is presented for the first time.

   (ii) The present analytical solution is applicable to thick as well as thin laminates of general configurations with arbitrary angle-ply layup or materials properties.

   (iii) First time, multi-term multi-field extended Kantorovich approach in conjunction with modified Hamiltons principle is applied to derive the dynamic solution for an angle-ply smart laminated plate under cylindrical bending.

   (iv) For extracting the natural frequencies and mode shapes of elastic and piezolaminated panels a robust algorithm is developed, which is very challenging [241] even for simple case and configurations even when ODEs are solved in one direction, only.

   (v) The numerical results are reported for various type panels such as cross-ply/angle-ply elastic panels, sandwich panels and piezoelectric panels under different combination of boundary conditions and lay-up scheme. It is found that the single-term solution is sufficient enough for obtaining the natural frequencies.

   (vi) Accuracy and efficacy of the present method is confirmed by comparing the present result with the existent solutions in literature or with the finite element.

   (vii) The presented 3D analytical solution able to predict the effect of electric boundary condition on the natural frequencies of piezoelectric laminated panels. Thought the

effect is not very significant due to the weak coupling between the electric and elastic fields. But these small effects are very much important to detect accurately for precise control applications.

(viii) The presented 3D analytical solution will fill up the gap in the literature and further help in the assessment of various 1D theories and numerical methods.

(ix) In future, this method can also be extended to the dynamic analysis of imperfect angle-ply elastic/piezoelectric laminated panels subjected to arbitrary boundary conditions.

5. A coupled 2D piezoelectricity based analytical solution is presented for the free vibration analysis of arbitrary supported axially functionally graded beams integrated with piezoelectric layers. Further, the free vibration solution for the arbitrary supported piezoelectric beams, having constant properties, is also obtained as a special case of the present study. The fundamental frequencies and corresponding mode shapes are presented for the laminated piezoelectric beams under different combinations of support conditions. These are some novel contributions and significant observations of the present work:

   (i) The influence of the longitudinal variation of material properties on natural frequency and mode shape of piezoelectric beams is studied in conjunction with different boundary conditions.

   (ii) Significant effect of axial gradation on the natural frequencies of the piezoelectric beams is observed. As the gradation indexes increase the natural frequencies of beam decrease significantly.

   (iii) It is determined that as the thickness-to-span ratio increases the non-dimensionalized natural frequency parameters increases and the increment is more pronounced for the beam subjected to clamped-clamped (C–C) boundary condition

   (iv) It is observed that inclusion of piezoelectric layers significantly affect the behavior and natural frequency of the beams. The piezoelectric (PZT-5A) layer on top of the elastic beams significantly decrease the natural frequencies of beams.

   (v) For all the cases, the influence of boundary conditions are significant on the lower mode natural frequencies and it is maximum for the first vibration mode. But for higher mode frequencies the effect of boundary conditions is negligible.

   (vi) The present numerical study reveals that the desired free vibration response is obtained by control the behaviour of beam with help of piezoelectric layers

   (vii) The present analytical solution can be utilized for assessing 1D beam theories and other

numerical models for free vibration analysis of piezoelectric composite beams and axially functionally graded beams integrated with piezoelectric layers.

7.2 SOME GUIDELINES FOR THE PRACTICAL DESIGN OF FGM ENGINEERING STRUCTURES

These are some interesting outcomes of present work which can serve as guidelines in the practical design of functionally graded engineering structures:

1. The localized sharp stress distribution is observed at very near to edges in a functionally graded structure. The through-thickness stress distributions are truly three-dimensional (3D) in nature and decay rapidly away from the edges. Therefore, the designer should take care of such stresses very carefully, and to tackle this sharp distribution of stresses very near to supports some more reinforcement should be used and the factor of safety also should be higher.

2. The distribution of stresses in FGM structures significantly affected by the variation of material properties. The selection of appropriate gradation profiles can reduce the stresses and stress intensity factors efficiently. Therefore, stresses can be minimized by selecting the gradation parameters properly in such FGM structures.

3. The through-thickness distributions of elastic variables in the functionally graded layer appear to be higher-order polynomial function variations, which totally differ from the basic kinematical and kinetic assumptions of the existing 2D equivalent single-layered beam/plate theories. The traditional 1D/2D theories might not be suitable for the analysis of in-plane FGM structures. Mosty these theories underestimate the variation of stresses in such structures. If the designer used such theories for the analysis of FGM structure then the factor of safety should be taken higher.

4. The behavior of FGM structure significant depends upon the boundary conditions of the structure. The FGM structures subjected to clamped support has been found to be more stable than structure under other support conditions. Therefore to clamped support can neutralizing the instability in such structures.

5. The natural frequencies of the structure affected significantly by the in-plane gradation of material properties, and under the unit amplitude, the point of maximum deflection also shifted significantly. Therefore, the designer should take care of such effects very carefully to obtain a stable structural design.

6. The effect of in-plane gradation is independent of the thickness of the structure. But, the extent of effect due to in-plane gradation largely depends upon the boundary conditions of the FGM structure, which should be taken care of to obtain optimum design of such structures.

7.3 CONTRIBUTION OF PRESENT THESIS TO ALLEVIATE THE HINDERING ISSUES RELATED TO THE APPLICATION OF FGMs

These are novel and significant contributions which directly assists the engineers in the designing of functionally graded engineering structures:

1. In the practical design, it is difficult to produce the FGM with a continuous gradient. Therefore, mostly the gradation is achieved in a stepwise manner. In this method, stepwise staking, of the premixed powder according to a predesigned spatial distribution of the composition, is used to obtain the desired gradation along the span. By this method, the FGM fabricated usually has the stepwise structure in which stresses are discontinued, and stress concentrations also occur at the interface of two-steps. During this research work, it is observed that these stress discontinuity and localized stress concentrations can be minimized by increasing the number of stacks. If the number of stacks is higher then the similar variation of material properties can be achieved, as observed in the continuously graded structures.

2. The biggest challenge in functionally graded material is to optimized the material properties according to the requirements of engineering structures. However, future optimization studies of functionally graded structure depend on a more accurate static and dynamic analysis of such structures. This thesis provides benchmark results for in-plane functionally graded structures under static and dynamic conditions, which contribute to further optimization studies in this field.

3. The numerical results presented in this thesis can be helpful in the development and assessment of the finite element packages, which assist the designer in the analysis of practical engineering FGM structures of complicated shape and configurations.

7.4 FUTURE SCOPE OF WORK

The future studies based on this work can be in following aspects:

1. The present elasticity solutions can be extended to the thermomechanical analysis of laminated composite and functionally graded structures.

2. The above elasticity solutions can be extended to the static and modal analysis of multidirectional functionally graded structures.

3. The present elasticity solution can be further extended to develop accurate 3D elasticity solution for static and dynamic analysis laminated structures (rectangular plates and flat panels) with interlaminar bonding imperfection.

4. Buckling and transient vibration analysis of functionally graded structures can be developed based on the 3D EKM.

5. The present approach and solution method can further be used to develop elasticity solutions for static and dynamic analysis of stepped plates with cutouts.

6. Using present approach, non-linear elasticity based analytical solutions for static and dynamic (free vibration) analysis of laminated composite, piezoelectric laminates and functionally graded structures like beams, panels, and rectangular plates can be developed.

7. The present study can form the basis of developing 2D theories for functionally graded plate which are able to predict the stresses near the supports more accurately.

Bibliography

[1] Gehman Jr, H. W., Barry, J. L., Deal, D. W., Hallock, J. N., Hess, K. W., Hubbard, G. S., Logsdon, J. M., Osheroff, D. D., Ride, S. K., and Tetrault, R. E., 2003. "Columbia accident investigation board report. volume 1". *NASA,* **1**, pp. 1–248.

[2] Columbia Accident Investigation Board, 2006. "In-flight options assessment". *NASA,* **12**(30), pp. 1–2003.

[3] Cooley, W. G., 2005. Application of functionally graded materials in aircraft structures. Tech. rep., Air Force Institute of Technology, Ohio, U.S.A.

[4] Koizumi, M., 1997. "FGM activities in Japan ". *Composites Part B: Engineering,* **28**(12), pp. 1 – 4.

[5] El-Wazery, M., and El-Desouky, A., 2015. "A review on functionally graded ceramic-metal materials". *Journal of Materials and Environmental Science,* **6**(5), pp. 1369–1376.

[6] Udupa, G., Rao, S. S., and Gangadharan, K., 2014. "Functionally graded composite materials: an overview". *Procedia Materials Science,* **5**, pp. 1291–1299.

[7] Mahamood, R. M., Akinlabi, E. T., Shukla, M., and Pityana, S., 2012. "Functionally graded material:an overview". In Proceedings of the World Congress on Engineering WCE 2012, Vol. 3, pp. 1593–1597.

[8] Kieback, B., Neubrand, A., and Riedel, H., 2003. "Processing techniques for functionally graded materials". *Materials Science and Engineering: A,* **362**(12), pp. 81 – 106.

[9] Suresh, S., and Mortensen, A., 1998. *Fundamentals of Functionally Graded Materials: Processing and Thermomechanical Behaviour of Graded Metals and Metal-ceramic Composites.* IOM Communications Limited.

[10] Birman, V., and Byrd, L. W., 2007. "Modeling and analysis of functionally graded materials and structures". *Applied mechanics reviews,* **60**(5), pp. 195–216.

[11] Jha, D., Kant, T., and Singh, R., 2013. "A critical review of recent research on functionally graded plates". *Composite Structures,* **96**, pp. 833–849.

[12] Thai, H.-T., and Kim, S.-E., 2015. "A review of theories for the modeling and analysis of functionally graded plates and shells". *Composite Structures,* **128**, pp. 70–86.

[13] Swaminathan, K., Naveenkumar, D., Zenkour, A., and Carrera, E., 2015. "Stress, vibration and buckling analyses of fgm plates a state-of-the-art review". *Composite Structures,* **120**, pp. 10–31.

[14] Liew, K., Lei, Z., and Zhang, L., 2015. "Mechanical analysis of functionally graded carbon nanotube reinforced composites: a review". *Composite Structures,* **120**, pp. 90–97.

[15] Wu, C.-P., Chiu, K.-H., Wang, Y.-M., et al., 2008. "A review on the three-dimensional analytical approaches of multilayered and functionally graded piezoelectric plates and shells". *Comput Mater Continua,* **8**(2), pp. 93–132.

[16] Wu, C.-P., and Liu, Y.-C., 2016. "A review of semi-analytical numerical methods for laminated composite and multilayered functionally graded elastic/piezoelectric plates and shells". *Composite Structures,* **147**, pp. 1–15.

[17] Noor, A. K., 1973. "Free vibrations of multilayered composite plates.". *AIAA journal,* **11**(7), pp. 1038–1039.

[18] Noor, A. K., 1975. "Stability of multilayered composite plates". *Fibre Science and Technology,* **8**(2), pp. 81–89.

[19] Noor, A. K., and Burton, W. S., 1989. "Stress and free vibration analyses of multilayered composite plates". *Composite Structures,* **11**(3), pp. 183–204.

[20] Heyliger, P., and Reddy, J., 1988. "A higher order beam finite element for bending and vibration problems". *Journal of sound and vibration,* **126**(2), pp. 309–326.

[21] Heyliger, P., and Saravanos, D., 1995. "Exact free-vibration analysis of laminated plates with embedded piezoelectric layers". *The Journal of the Acoustical Society of America,* **98**(3), pp. 1547–1557.

[22] Saravanos, D. A., and Heyliger, P. R., 1995. "Coupled layerwise analysis of composite beams with embedded piezoelectric sensors and actuators". *Journal of Intelligent Material Systems and Structures,* **6**(3), pp. 350–363.

[23] Saravanos, D. A., Heyliger, P. R., and Hopkins, D. A., 1997. "Layerwise mechanics and finite element for the dynamic analysis of piezoelectric composite plates". *International Journal of Solids and Structures,* **34**(3), pp. 359–378.

[24] Heyliger, P., 1997. "Exact solutions for simply supported laminated piezoelectric plates". *Journal of Applied Mechanics,* **64**(2), pp. 299–306.

[25] Pan, E., and Heyliger, P., 2002. "Free vibrations of simply supported and multilayered magneto-electro-elastic plates". *Journal of Sound and Vibration,* **252**(3), pp. 429–442.

[26] Ramirez, F., Heyliger, P. R., and Pan, E., 2006. "Free vibration response of two-dimensional magneto-electro-elastic laminated plates". *Journal of Sound and Vibration,* **292**(3-5), pp. 626–644.

[27] Reddy, J. N., 1984. "A simple higher-order theory for laminated composite plates". *Journal of applied mechanics,* **51**(4), pp. 745–752.

[28] Praveen, G., and Reddy, J., 1998. "Nonlinear transient thermoelastic analysis of functionally graded ceramic-metal plates". *International journal of solids and structures,* **35**(33), pp. 4457–4476.

[29] Reddy, J., 2000. "Analysis of functionally graded plates". *International Journal for numerical methods in engineering,* **47**(1-3), pp. 663–684.

[30] Reddy, J. N., 2004. *Mechanics of laminated composite plates and shells: theory and analysis*. CRC press.

[31] Reddy, J. N., 2006. *Theory and analysis of elastic plates and shells*. CRC press.

[32] Reddy, J., 2007. "Nonlocal theories for bending, buckling and vibration of beams". *International Journal of Engineering Science,* **45**(2-8), pp. 288–307.

[33] Kapania, R. K., and Yang, T., 1987. "Buckling, postbuckling, and nonlinear vibrations of imperfect plates". *AIAA journal,* **25**(10), pp. 1338–1346.

[34] Kapania, R. K., and Raciti, S., 1989. "Nonlinear vibrations of unsymmetrically laminated beams". *AIAA journal,* **27**(2), pp. 201–210.

[35] Nosier, A., Kapania, R. K., and Reddy, J., 1993. "Free vibration analysis of laminated plates using a layerwise theory". *AIAA journal,* **31**(12), pp. 2335–2346.

[36] Kapania, R. K., and Liu, Y., 2000. "Static and vibration analyses of general wing structures using equivalent-plate models". *AIAA journal,* **38**(7), pp. 1269–1277.

[37] Vel, S. S., and Batra, R., 2002. "Exact solution for thermoelastic deformations of functionally graded thick rectangular plates". *AIAA journal,* **40**(7), pp. 1421–1433.

[38] Vel, S. S., and Batra, R., 2003. "Three-dimensional analysis of transient thermal stresses in functionally graded plates". *International Journal of Solids and Structures,* **40**(25), pp. 7181–7196.

[39] Vel, S. S., and Batra, R., 2004. "Three-dimensional exact solution for the vibration of functionally graded rectangular plates". *Journal of Sound and Vibration,* **272**(3), pp. 703–730.

[40] Qian, L.-F., and Ching, H.-K., 2004. "Static and dynamic analysis of 2-D functionally graded elasticity by using meshless local petrov-galerkin method". *Journal of the Chinese Institute of Engineers,* **27**(4), pp. 491–503.

[41] Kant, T., and Swaminathan, K., 2001. "Analytical solutions for free vibration of laminated composite and sandwich plates based on a higher-order refined theory". *Composite structures,* **53**(1), pp. 73–85.

[42] Kant, T., and Swaminathan, K., 2002. "Analytical solutions for the static analysis of laminated composite and sandwich plates based on a higher order refined theory". *Composite structures,* **56**(4), pp. 329–344.

[43] Khare, R. K., Kant, T., and Garg, A. K., 2004. "Free vibration of composite and sandwich laminates with a higher-order facet shell element". *Composite Structures,* **65**(3-4), pp. 405–418.

[44] Garg, A. K., Khare, R. K., and Kant, T., 2006. "Higher-order closed-form solutions for free vibration of laminated composite and sandwich shells". *Journal of Sandwich Structures & Materials,* **8**(3), pp. 205–235.

[45] Jha, D., Kant, T., and Singh, R., 2013. "Free vibration response of functionally graded thick plates with shear and normal deformations effects". *Composite Structures,* **96**, pp. 799–823.

[46] Dube, G., Kapuria, S., and Dumir, P., 1996. "Exact piezothermoelastic solution of simply-supported orthotropic flat panel in cylindrical bending". *International Journal of Mechanical Sciences,* **38**(11), pp. 1161–1177.

[47] Dumir, P., Dube, G., and Kapuria, S., 1997. "Exact piezoelastic solution of simply-supported orthotropic circular cylindrical panel in cylindrical bending". *International Journal of Solids and Structures,* **34**(6), pp. 685–702.

[48] Kapuria, S., Sengupta, S., and Dumir, P., 1997. "Three-dimensional solution for simply-supported piezoelectric cylindrical shell for axisymmetric load". *Computer Methods in Applied Mechanics and Engineering,* **140**(1-2), pp. 139–155.

[49] Kapuria, S., Sengupta, S., and Dumir, P., 1997. "Three-dimensional piezothermoelastic solution for shape control of cylindrical panel". *Journal of thermal stresses,* **20**(1), pp. 67–85.

[50] Kapuria, S., Dumir, P., and Ahmed, A., 2003. "An efficient coupled layerwise theory for dynamic analysis of piezoelectric composite beams". *Journal of Sound and Vibration,* **261**(5), pp. 927–944.

[51] Wu, C.-P., and Syu, Y.-S., 2007. "Exact solutions of functionally graded piezoelectric shells under cylindrical bending". *International Journal of Solids and Structures,* **44**(20), pp. 6450–6472.

[52] Wu, C.-P., and Lu, Y.-C., 2009. "A modified pagano method for the 3d dynamic responses of functionally graded magneto-electro-elastic plates". *Composite structures,* **90**(3), pp. 363–372.

[53] Wu, C.-P., Chen, S.-J., and Chiu, K.-H., 2010. "Three-dimensional static behavior of functionally graded magneto-electro-elastic plates using the modified pagano method". *Mechanics Research Communications,* **37**(1), pp. 54–60.

[54] Wu, C.-P., and Li, H.-Y., 2010. "The rmvt-and pvd-based finite layer methods for the three-dimensional analysis of multilayered composite and fgm plates". *Composite Structures,* **92**(10), pp. 2476–2496.

[55] Carrera, E., and Giunta, G., 2010. "Refined beam theories based on a unified formulation". *International Journal of Applied Mechanics,* **2**(01), pp. 117–143.

[56] Carrera, E., Giunta, G., and Petrolo, M., 2011. *Beam structures: classical and advanced theories.* John Wiley & Sons.

[57] Carrera, E., Filippi, M., and Zappino, E., 2013. "Free vibration analysis of rotating composite blades via carrera unified formulation". *Composite Structures,* **106**, pp. 317–325.

[58] Pagani, A., and Carrera, E., 2017. "Large-deflection and post-buckling analyses of laminated composite beams by carrera unified formulation". *Composite Structures,* **170**, pp. 40–52.

[59] Haojiang, D., Yimu, G., Qingda, Y., and Weiqiu, C., 1997. "Free vibration of piezoelectric cylindrical shells". *Acta mechanica solida sinica,* **10**(1), pp. 48–55.

[60] Weiqiu, C., and Haojiang, D., 1998. "Exact static analysis of a rotating piezoelectric spherical shell". *Acta Mechanica Sinica,* **14**(3), pp. 257–265.

[61] Lü, C., Chen, W., and Zhong, Z., 2006. "Two-dimensional thermoelasticity solution for functionally graded thick beams". *Science in China Series G: Physics, Mechanics and Astronomy,* **49**(4), pp. 451–460.

[62] Yan, W., Ying, J., and Chen, W., 2006. "A three-dimensional solution for laminated orthotropic rectangular plates with viscoelastic interfaces". *Acta Mechanica Solida Sinica,* **19**(2), pp. 181–188.

[63] Chen, J., Ding, H., and Chen, W., 2007. "Three-dimensional analytical solution for a rotating disc of functionally graded materials with transverse isotropy". *Archive of Applied Mechanics,* **77**(4), pp. 241–251.

[64] Li, Q., Iu, V., and Kou, K., 2008. "Three-dimensional vibration analysis of functionally graded material sandwich plates". *Journal of Sound and Vibration,* **311**(1), pp. 498–515.

[65] Huang, D., Ding, H., and Chen, W., 2009. "Analytical solution and semi-analytical solution for anisotropic functionally graded beam subject to arbitrary loading". *Science in China Series G: Physics, Mechanics and Astronomy,* **52**(8), pp. 1244–1256.

[66] Zhang, C., Zhu, J., Chen, W., and Zhang, C., 2014. "Two-dimensional theory of piezoelectric shells considering surface effect". *European Journal of Mechanics-A/Solids,* **43**, pp. 109–117.

[67] Yuan, J., Pao, Y.-H., and Chen, W., 2016. "Exact solutions for free vibrations of axially inhomogeneous timoshenko beams with variable cross section". *Acta Mechanica,* **227**(9), pp. 2625–2643.

[68] Ferreira, A., Batra, R., Roque, C., Qian, L., and Martins, P., 2005. "Static analysis of functionally graded plates using third-order shear deformation theory and a meshless method". *Composite Structures,* **69**(4), pp. 449–457.

[69] Ferreira, A., Batra, R., Roque, C., Qian, L., and Jorge, R., 2006. "Natural frequencies of functionally graded plates by a meshless method". *Composite Structures,* **75**(1-4), pp. 593–600.

[70] Neves, A., Ferreira, A., Carrera, E., Roque, C., Cinefra, M., Jorge, R., and Soares, C., 2012. "A quasi-3d sinusoidal shear deformation theory for the static and free vibration analysis of functionally graded plates". *Composites Part B: Engineering,* **43**(2), pp. 711–725.

[71] Neves, A., Ferreira, A., Carrera, E., Cinefra, M., Roque, C., Jorge, R., and Soares, C. M., 2013. "Static, free vibration and buckling analysis of isotropic and sandwich functionally graded plates using a quasi-3d higher-order shear deformation theory and a meshless technique". *Composites Part B: Engineering,* **44**(1), pp. 657–674.

[72] Thakkar, D., and Ganguli, R., 2004. "Dynamic response of rotating beams with piezoceramic actuation". *Journal of Sound and Vibration,* **270**(4-5), pp. 729–753.

[73] Umesh, K., and Ganguli, R., 2008. "Shape and vibration control of a smart composite plate with matrix cracks". *Smart Materials and Structures,* **18**(2), p. 025002.

[74] Murugan, S., Harursampath, D., and Ganguli, R., 2008. "Material uncertainty propagation in helicopter nonlinear aeroelastic response and vibratory analysis". *AIAA journal,* **46**(9), pp. 2332–2344.

[75] Sarkar, K., and Ganguli, R., 2014. "Modal tailoring and closed-form solutions for rotating non-uniform euler–bernoulli beams". *International Journal of Mechanical Sciences,* **88**, pp. 208–220.

[76] Sarkar, K., Ganguli, R., Ghosh, D., and Elishakoff, I., 2016. "Closed-form solutions and uncertainty quantification for gravity-loaded beams". *Meccanica,* **51**(6), pp. 1465–1479.

[77] Sarkar, K., Ganguli, R., and Elishakoff, I., 2016. "Closed-form solutions for non-uniform axially loaded rayleigh cantilever beams". *Struct. Eng. Mech,* **60**(3), pp. 455–470.

[78] Mohan, K., Hon, Y. T., Idapalapati, S., and Seow, H. P., 2005. "Failure of sandwich beams consisting of alumina face sheet and aluminum foam core in bending". *Materials Science and Engineering: A,* **409**(1-2), pp. 292–301.

[79] Kumar, S., Sivashanker, S., Bag, A., and Sridhar, I., 2005. "Failure of aerospace composite scarf-joints subjected to uniaxial compression". *Materials Science and Engineering: A,* **412**(1-2), pp. 117–122.

[80] Kumar, S., Sridhar, I., Sivashanker, S., Osiyemi, S., and Bag, A., 2006. "Tensile failure of adhesively bonded cfrp composite scarf joints". *Materials Science and Engineering: B,* **132**(1-2), pp. 113–120.

[81] Tang, J., Sridhar, I., and Srikanth, N., 2013. "Static and fatigue failure analysis of adhesively bonded thick composite single lap joints". *Composites Science and Technology,* **86**, pp. 18–25.

[82] Rao, M. K., Desai, Y., and Chitnis, M., 2001. "Free vibrations of laminated beams using mixed theory". *Composite Structures,* **52**(2), pp. 149–160.

[83] Dafedar, J., Desai, Y., and Mufti, A., 2003. "Stability of sandwich plates by mixed, higher-order analytical formulation". *International journal of solids and structures,* **40**(17), pp. 4501–4517.

[84] Desai, Y., Ramtekkar, G., and Shah, A., 2003. "Dynamic analysis of laminated composite plates using a layer-wise mixed finite element model". *Composite structures,* **59**(2), pp. 237–249.

[85] Rao, M., and Desai, Y., 2004. "Analytical solutions for vibrations of laminated and sandwich plates using mixed theory". *Composite Structures,* **63**(3-4), pp. 361–373.

[86] Gupta, U., Lal, R., and Verma, C., 1986. "Buckling and vibrations of polar orthotropic annular plates on elastic foundation subjected to hydrostatic peripheral loading". *Journal of sound and vibration,* **109**(3), pp. 423–434.

[87] Gupta, U., Lal, R., and Jain, S., 1990. "Effect of elastic foundation on axisymmetric vibrations of polar orthotropic circular plates of variable thickness". *Journal of Sound and Vibration,* **139**(3), pp. 503–513.

[88] Lal, R., and Sharma, S., 2004. "Axisymmetric vibrations of non-homogeneous polar orthotropic annular plates of variable thickness". *Journal of sound and vibration,* **272**(1-2), pp. 245–265.

[89] Gupta, U., Lal, R., and Sharma, S., 2006. "Vibration analysis of non-homogeneous circular plate of nonlinear thickness variation by differential quadrature method". *Journal of Sound and Vibration,* **298**(4), pp. 892–906.

[90] Lal, R., et al., 2007. "Transverse vibrations of non-homogeneous orthotropic rectangular plates of variable thickness: A spline technique". *Journal of sound and vibration,* **306**(1), pp. 203–214.

[91] Patel, B., Ganapathi, M., and Touratier, M., 1999. "Nonlinear free flexural vibrations/post-buckling analysis of laminated orthotropic beams/columns on a two parameter elastic foundation". *Composite structures,* **46**(2), pp. 189–196.

[92] Makhecha, D., Ganapathi, M., and Patel, B., 2001. "Dynamic analysis of laminated composite plates subjected to thermal/mechanical loads using an accurate theory". *Composite Structures,* **51**(3), pp. 221–236.

[93] Ganapathi, M., Patel, B., and Makhecha, D., 2004. "Nonlinear dynamic analysis of thick composite/sandwich laminates using an accurate higher-order theory". *Composites Part B: Engineering,* **35**(4), pp. 345–355.

[94] Patel, B., Gupta, S., Loknath, M., and Kadu, C., 2005. "Free vibration analysis of functionally graded elliptical cylindrical shells using higher-order theory". *Composite structures,* **69**(3), pp. 259–270.

[95] Kapuria, S., Dube, G., and Dumir, P., 1997. "Exact piezothermoelastic solution for simply supported laminated flat panel in cylindrical bending". *ZAMM-Journal of Applied Mathematics and Mechanics/Zeitschrift für Angewandte Mathematik und Mechanik,* **77**(4), pp. 281–293.

[96] Dhanesh, N., Kapuria, S., and Achary, G., 2017. "Accurate prediction of three-dimensional free edge stress field in composite laminates using mixed-field multiterm extended kantorovich method". *Acta Mechanica,* **228**(8), pp. 2895–2919.

[97] Kapuria, S., and Dhanesh, N., 2014. "Three-dimensional extended kantorovich solution for accurate prediction of interlaminar stresses in composite laminated panels with interfacial imperfections". *Journal of Engineering Mechanics,* **141**(4), p. 04014140.

[98] Kapuria, S., and Dhanesh, N., 2017. "Free edge stress field in smart piezoelectric composite structures and its control: An accurate multiphysics solution". *International Journal of Solids and Structures,* **126**, pp. 196–207.

[99] Somireddy, M., and Rajagopal, A., 2014. "Meshless natural neighbor galerkin method for the bending and vibration analysis of composite plates". *Composite Structures,* **111**, pp. 138–146.

[100] Raghu, P., Preethi, K., Rajagopal, A., and Reddy, J. N., 2016. "Nonlocal third-order shear deformation theory for analysis of laminated plates considering surface stress effects". *Composite Structures,* **139**, pp. 13–29.

[101] Srividhya, S., Raghu, P., Rajagopal, A., and Reddy, J., 2018. "Nonlocal nonlinear analysis of functionally graded plates using third-order shear deformation theory". *International Journal of Engineering Science,* **125**, pp. 1–22.

[102] Raghu, P., Rajagopal, A., and Reddy, J., 2018. "Nonlocal nonlinear finite element analysis of composite plates using tsdt". *Composite Structures,* **185**, pp. 38–50.

[103] Elishakoff, I., and Candan, S., 2001. "Apparently first closed-form solution for vibrating: inhomogeneous beams". *International Journal of Solids and Structures,* **38**(19), pp. 3411–3441.

[104] Huang, Y., and Li, X.-F., 2010. "A new approach for free vibration of axially functionally graded beams with non-uniform cross-section". *Journal of sound and vibration,* **329**(11), pp. 2291–2303.

[105] Giunta, G., Belouettar, S., and Carrera, E., 2010. "Analysis of fgm beams by means of classical and advanced theories". *Mechanics of Advanced Materials and Structures,* **17**(8), pp. 622–635.

[106] Wang, C., and Wang, C., 2012. "Exact vibration solutions for a class of nonuniform beams". *Journal of Engineering Mechanics,* **139**(7), pp. 928–931.

[107] Sarkar, K., and Ganguli, R., 2013. "Closed-form solutions for non-uniform euler–bernoulli free–free beams". *Journal of Sound and Vibration,* **332**(23), pp. 6078–6092.

[108] Sarkar, K., and Ganguli, R., 2014. "Closed-form solutions for axially functionally graded timoshenko beams having uniform cross-section and fixed–fixed boundary condition". *Composites Part B: Engineering,* **58**, pp. 361–370.

[109] Li, X.-F., Kang, Y.-A., and Wu, J.-X., 2013. "Exact frequency equations of free vibration of exponentially functionally graded beams". *Applied Acoustics,* **74**(3), pp. 413–420.

[110] Tang, A.-Y., Wu, J.-X., Li, X.-F., and Lee, K., 2014. "Exact frequency equations of free vibration of exponentially non-uniform functionally graded timoshenko beams". *International Journal of Mechanical Sciences,* **89**, pp. 1–11.

[111] Nguyen, N., Kim, N., Cho, I., Phung, Q., and Lee, J., 2014. "Static analysis of transversely or axially functionally graded tapered beams". *Materials Research Innovations,* **18**(sup2), pp. S2–260.

[112] Rezaiee-Pajand, M., and Hozhabrossadati, S. M., 2016. "Analytical and numerical method for free vibration of double-axially functionally graded beams". *Composite Structures,* **152**, pp. 488–498.

[113] Wang, Z.-h., Wang, X.-h., Xu, G.-d., Cheng, S., and Zeng, T., 2016. "Free vibration of two-directional functionally graded beams". *Composite structures,* **135**, pp. 191–198.

[114] Huang, Y., and Rong, H.-W., 2017. "Free vibration of axially inhomogeneous beams that are made of functionally graded materials". *International Journal of Acoustics and Vibration,* **22**(1), pp. 68–74.

[115] Cao, D., Gao, Y., Yao, M., and Zhang, W., 2018. "Free vibration of axially functionally graded beams using the asymptotic development method". *Engineering Structures,* **173**, pp. 442–448.

[116] Cao, D., and Gao, Y., 2019. "Free vibration of non-uniform axially functionally graded beams using the asymptotic development method". *Applied Mathematics and Mechanics,* **40**(1), pp. 85–96.

[117] Hein, H., and Feklistova, L., 2011. "Free vibrations of non-uniform and axially functionally graded beams using haar wavelets". *Engineering Structures,* **33**(12), pp. 3696–3701.

[118] Shahba, A., and Rajasekaran, S., 2012. "Free vibration and stability of tapered euler–bernoulli beams made of axially functionally graded materials". *Applied Mathematical Modelling,* **36**(7), pp. 3094–3111.

[119] Li, S., Hu, J., Zhai, C., and Xie, L., 2013. "A unified method for modeling of axially and/or transversally functionally graded beams with variable cross-section profile". *Mechanics Based Design of Structures and Machines,* **41**(2), pp. 168–188.

[120] Fang, J., and Zhou, D., 2015. "Free vibration analysis of rotating axially functionally graded-tapered beams using chebyshev–ritz method". *Materials Research Innovations,* **19**(sup5), pp. S5–1255.

[121] Giunta, G., Belouettar, S., and Ferreira, A., 2016. "A static analysis of three-dimensional functionally graded beams by hierarchical modelling and a collocation meshless solution method". *Acta Mechanica,* **227**(4), pp. 969–991.

[122] Nikolić, A., 2017. "Free vibration analysis of a non-uniform axially functionally graded cantilever beam with a tip body". *Archive of Applied Mechanics,* **87**(7), pp. 1227–1241.

[123] Zhao, Y., Huang, Y., and Guo, M., 2017. "A novel approach for free vibration of axially functionally graded beams with non-uniform cross-section based on chebyshev polynomials theory". *Composite Structures,* **168**, pp. 277–284.

[124] Ghazaryan, D., Burlayenko, V. N., Avetisyan, A., and Bhaskar, A., 2018. "Free vibration analysis of functionally graded beams with non-uniform cross-section using the differential transform method". *Journal of Engineering Mathematics*, pp. 1–25.

[125] Ghayesh, M. H., and Farokhi, H., 2018. "Bending and vibration analyses of coupled axially functionally graded tapered beams". *Nonlinear Dynamics,* **91**(1), pp. 17–28.

[126] Šalinić, S., Obradović, A., and Tomović, A., 2018. "Free vibration analysis of axially functionally graded tapered, stepped, and continuously segmented rods and beams". *Composites Part B: Engineering,* **150**, pp. 135–143.

[127] Sınır, S., Çevik, M., and Sınır, B. G., 2018. "Nonlinear free and forced vibration analyses of axially functionally graded euler-bernoulli beams with non-uniform cross-section". *Composites Part B: Engineering,* **148**, pp. 123–131.

[128] Zhou, Y., and Zhang, X., 2019. "Natural frequency analysis of functionally graded material beams with axially varying stochastic properties". *Applied Mathematical Modelling,* **67**, pp. 85–100.

[129] Tang, Y., Lv, X., and Yang, T., 2019. "Bi-directional functionally graded beams: asymmetric modes and nonlinear free vibration". *Composites Part B: Engineering,* **156**, pp. 319–331.

[130] Shahba, A., Attarnejad, R., Marvi, M. T., and Hajilar, S., 2011. "Free vibration and stability analysis of axially functionally graded tapered timoshenko beams with classical and non-classical boundary conditions". *Composites Part B: Engineering,* **42**(4), pp. 801–808.

[131] Rajasekaran, S., 2013. "Free vibration of centrifugally stiffened axially functionally graded tapered timoshenko beams using differential transformation and quadrature methods". *Applied Mathematical Modelling,* **37**(6), pp. 4440–4463.

[132] Rajasekaran, S., and Tochaei, E. N., 2014. "Free vibration analysis of axially functionally graded tapered timoshenko beams using differential transformation element method and differential quadrature element method of lowest-order". *Meccanica,* **49**(4), pp. 995–1009.

[133] Bambill, D., Rossit, C., and Felix, D., 2015. "Free vibrations of stepped axially functionally graded timoshenko beams". *Meccanica,* **50**(4), pp. 1073–1087.

[134] Calim, F. F., 2016. "Free and forced vibration analysis of axially functionally graded timoshenko beams on two-parameter viscoelastic foundation". *Composites Part B: Engineering,* **103**, pp. 98–112.

[135] Ghayesh, M. H., 2018. "Nonlinear vibrations of axially functionally graded timoshenko tapered beams". *Journal of Computational and Nonlinear Dynamics,* **13**(4), p. 041002.

[136] Sun, D.-L., and Li, X.-F., 2019. "Initial value method for free vibration of axially loaded functionally graded timoshenko beams with nonuniform cross section". *Mechanics Based Design of Structures and Machines,* **47**(1), pp. 102–120.

[137] Xie, K., Wang, Y., and Fu, T., 2019. "Dynamic response of axially functionally graded beam with longitudinal–transverse coupling effect". *Aerospace Science and Technology,* **85**, pp. 85–95.

[138] Ghayesh, M. H., 2019. "Resonant dynamics of axially functionally graded imperfect tapered timoshenko beams". *Journal of Vibration and Control*, p. 1077546318777591.

[139] Shahba, A., Attarnejad, R., and Hajilar, S., 2013. "A mechanical-based solution for axially functionally graded tapered euler-bernoulli beams". *Mechanics of Advanced Materials and Structures,* **20**(8), pp. 696–707.

[140] Kumar, S., Mitra, A., and Roy, H., 2015. "Geometrically nonlinear free vibration analysis of axially functionally graded taper beams". *Engineering Science and Technology, an International Journal,* **18**(4), pp. 579–593.

[141] Karamanlı, A., 2018. "Free vibration analysis of two directional functionally graded beams using a third order shear deformation theory". *Composite Structures,* **189**, pp. 127–136.

[142] Mukherjee, S., Sekhar, B. R., Gopalakrishnan, S., and Ganguli, R., 2018. "Static and dynamic analysis of sandwich panel with spatially varying non-gaussian properties". *Journal of Sandwich Structures & Materials*, p. 1099636218793979.

[143] Ghayesh, M. H., 2018. "Nonlinear vibration analysis of axially functionally graded shear-deformable tapered beams". *Applied Mathematical Modelling,* **59**, pp. 583–596.

[144] Mahmoud, M., 2019. "Natural frequency of axially functionally graded, tapered cantilever beams with tip masses". *Engineering Structures,* **187**, pp. 34–42.

[145] Chen, M., Jin, G., Zhang, Y., Niu, F., and Liu, Z., 2019. "Three-dimensional vibration analysis of beams with axial functionally graded materials and variable thickness". *Composite Structures,* **207**, pp. 304–322.

[146] Sayyad, A. S., and Ghugal, Y. M., 2017. "Bending, buckling and free vibration of laminated composite and sandwich beams: A critical review of literature". *Composite Structures,* **171**, pp. 486–504.

[147] Sayyad, A. S., and Ghugal, Y. M., 2018. "Modeling and analysis of functionally graded sandwich beams: A review". *Mechanics of Advanced Materials and Structures*, pp. 1–20.

[148] Zhang, N., Khan, T., Guo, H., Shi, S., Zhong, W., and Zhang, W., 2019. "Functionally graded materials: An overview of stability, buckling, and free vibration analysis". *Advances in Materials Science and Engineering,* **2019**.

[149] Chopra, I., 2002. "Review of state of art of smart structures and integrated systems". *AIAA journal,* **40**(11), pp. 2145–2187.

[150] Bailey, T., and Hubbard, J. E., 1985. "Distributed piezoelectric-polymer active vibration control of a cantilever beam". *Journal of Guidance, Control, and Dynamics,* **8**(5), pp. 605–611.

[151] Crawley, E. F., and De Luis, J., 1987. "Use of piezoelectric actuators as elements of intelligent structures". *AIAA journal,* **25**(10), pp. 1373–1385.

[152] Crawley, E. F., and Anderson, E. H., 1990. "Detailed models of piezoceramic actuation of beams". *Journal of Intelligent Material Systems and Structures,* **1**(1), pp. 4–25.

[153] Yang, S.-M., and Lee, Y., 1994. "Modal analysis of stepped beams with piezoelectric materials". *Journal of Sound and Vibration,* **176**(3), pp. 289–300.

[154] Low, T., and Guo, W., 1995. "Modeling of a three-layer piezoelectric bimorph beam with hysteresis". *Journal of Microelectromechanical Systems,* **4**(4), pp. 230–237.

[155] Sunar, M., and Rao, S. S., 1999. "Recent advances in sensing and control of flexible structures via piezoelectric materials technology". *Applied Mechanics Reviews,* **52**(1), pp. 1–16.

[156] Saravanos, D. A., and Heyliger, P. R., 1999. "Mechanics and computational models for laminated piezoelectric beams, plates, and shells". *Applied Mechanics Reviews,* **52**(10), pp. 305–320.

[157] Gopinathan, S. V., Varadan, V. V., and Varadan, V. K., 2000. "A review and critique of theories for piezoelectric laminates". *Smart Materials and Structures,* **9**(1), p. 24.

[158] Kapuria, S., Dumir, P., and Ahmed, A., 2005. "Coupled consistent third-order theory for hybrid piezoelectric composite and sandwich beams". *Journal of reinforced plastics and composites,* **24**(2), pp. 173–194.

[159] Kekana, M., 2006. "Calculation of eigenvalues of a piezoelastic beam using the pseudospectral method". *Smart materials and structures,* **15**(4), p. 1079.

[160] Della, C. N., and Shu, D., 2006. "Vibration of beams with embedded piezoelectric sensors and actuators". *Smart materials and structures,* **15**(2), p. 529.

[161] Della, C. N., and Shu, D., 2007. "Vibration of beams with piezoelectric inclusions". *International journal of solids and structures,* **44**(7-8), pp. 2509–2522.

[162] Wang, R.-T., 2010. "Structural responses of surface-mounted piezoelectric beams". *Journal of Mechanics,* **26**(1), pp. 47–59.

[163] Khdeir, A., Darraj, E., and Aldraihem, O., 2012. "Free vibration of cross ply laminated beams with multiple distributed piezoelectric actuators". *Journal of Mechanics,* **28**(1), pp. 217–227.

[164] Khdeir, A., and Aldraihem, O., 2016. "Free vibration of sandwich beams with soft core". *Composite Structures,* **154**, pp. 179–189.

[165] Muthalif, A. G., and Nordin, N. D., 2015. "Optimal piezoelectric beam shape for single and broadband vibration energy harvesting: Modeling, simulation and experimental results". *Mechanical Systems and Signal Processing,* **54**, pp. 417–426.

[166] Fu, Y., Wang, J., and Mao, Y., 2011. "Nonlinear vibration and active control of functionally graded beams with piezoelectric sensors and actuators". *Journal of Intelligent Material Systems and Structures,* **22**(18), pp. 2093–2102.

[167] Li, Y., Feng, W., and Cai, Z., 2014. "Bending and free vibration of functionally graded piezoelectric beam based on modified strain gradient theory". *Composite Structures,* **115**, pp. 41–50.

[168] Chattaraj, N., and Ganguli, R., 2016. "Electromechanical analysis of piezoelectric bimorph actuator in static state considering the nonlinearity at high electric field". *Mechanics of Advanced Materials and Structures,* **23**(7), pp. 802–810.

[169] Chattaraj, N., and Ganguli, R., 2017. "Effect of self-induced electric displacement field on the response of a piezo-bimorph actuator at high electric field". *International Journal of Mechanical Sciences,* **120**, pp. 341–348.

[170] Chattaraj, N., and Ganguli, R., 2018. "Multi-objective optimization of a triple layer piezoelectric bender with a flexible extension using genetic algorithm". *Mechanics of Advanced Materials and Structures,* **25**(9), pp. 785–793.

[171] Kapuria, S., Dumir, P., and Ahmed, A., 2004. "Exact 2d piezoelasticity solution of hybrid beam with damping under harmonic electromechanical load". *ZAMM-Journal of Applied Mathematics and Mechanics/Zeitschrift für Angewandte Mathematik und Mechanik: Applied Mathematics and Mechanics,* **84**(6), pp. 391–402.

[172] Gupta, V., Sharma, M., and Thakur, N., 2011. "Mathematical modeling of actively controlled piezo smart structures: A review". *Smart Structures and Systems,* **8**(3), pp. 275–302.

[173] Hajianmaleki, M., and Qatu, M. S., 2013. "Vibrations of straight and curved composite beams: A review". *Composite Structures,* **100**, pp. 218–232.

[174] Kumar, Y., 2018. "The rayleigh–ritz method for linear dynamic, static and buckling behavior of beams, shells and plates: A literature review". *Journal of Vibration and Control,* **24**(7), pp. 1205–1227.

[175] Cao, D., Gao, Y., Wang, J., Yao, M., and Zhang, W., 2019. "Analytical analysis of free vibration of non-uniform and non-homogenous beams: Asymptotic perturbation approach". *Applied Mathematical Modelling,* **65**, pp. 526–534.

[176] Kulikov, G., Plotnikova, S., Kulikov, M., and Monastyrev, P., 2016. "Three-dimensional vibration analysis of layered and functionally graded plates through sampling surfaces formulation". *Composite Structures,* **152**, pp. 349–361.

[177] Reddy, J., and Cheng, Z.-Q., 2001. "Three-dimensional solutions of smart functionally graded plates". *Journal of Applied Mechanics,* **68**(2), pp. 234–241.

[178] Reddy, J., and Cheng, Z.-Q., 2001. "Three-dimensional thermomechanical deformations of functionally graded rectangular plates". *European Journal of Mechanics-A/Solids,* **20**(5), pp. 841–855.

[179] Pan, E., 2003. "Exact solution for functionally graded anisotropic elastic composite laminates". *Journal of Composite materials,* **37**(21), pp. 1903–1920.

[180] Kashtalyan, M., 2004. "Three-dimensional elasticity solution for bending of functionally graded rectangular plates". *European Journal of Mechanics-A/Solids,* **23**(5), pp. 853–864.

[181] Zhong, Z., and Shang, E., 2008. "Closed-form solutions of three-dimensional functionally graded plates". *Mechanics of Advanced Materials and Structures,* **15**(5), pp. 355–363.

[182] Zenkour, A., 2007. "Benchmark trigonometric and 3-D elasticity solutions for an exponentially graded thick rectangular plate". *Archive of Applied Mechanics,* **77**(4), pp. 197–214.

[183] Woodward, B., and Kashtalyan, M., 2010. "Bending response of sandwich panels with graded core: 3d elasticity analysis". *Mechanics of Advanced Materials and Structures,* **17**(8), pp. 586–594.

[184] Ootao, Y., and Tanigawa, Y., 2007. "Three-dimensional solution for transient thermal stresses of an orthotropic functionally graded rectangular plate". *Composite structures,* **80**(1), pp. 10–20.

[185] Liu, W., and Zhong, Z., 2011. "Three-dimensional thermoelastic analysis of functionally graded plate". *Acta Mechanica Solida Sinica,* **24**(3), pp. 241–249.

[186] Zhong, Z., and Shang, E., 2003. "Three-dimensional exact analysis of a simply supported functionally gradient piezoelectric plate". *International Journal of Solids and Structures,* **40**(20), pp. 5335–5352.

[187] Alibeigloo, A., 2010. "Exact solution for thermo-elastic response of functionally graded rectangular plates". *Composite Structures,* **92**(1), pp. 113–121.

[188] Chen, W., and Ding, H., 2002. "On free vibration of a functionally graded piezoelectric rectangular plate". *Acta Mechanica,* **153**(3-4), pp. 207–216.

[189] Chen, W., and Lee, K. Y., 2003. "Alternative state space formulations for magnetoelectric thermoelasticity with transverse isotropy and the application to bending analysis of nonhomogeneous plates". *International Journal of Solids and Structures,* **40**(21), pp. 5689–5705.

[190] Huang, Z., Lü, C., and Chen, W., 2008. "Benchmark solutions for functionally graded thick plates resting on Winkler–Pasternak elastic foundations". *Composite Structures,* **85**(2), pp. 95–104.

[191] Yang, B., Ding, H.-j., and Chen, W.-q., 2008. "Elasticity solutions for functionally graded plates in cylindrical bending". *Applied Mathematics and Mechanics,* **29**(8), pp. 999–1004.

[192] Lü, C., Lim, C. W., and Chen, W., 2009. "Exact solutions for free vibrations of functionally graded thick plates on elastic foundations". *Mechanics of Advanced Materials and Structures,* **16**(8), pp. 576–584.

[193] LomtePatil, Y. T., Kant, T., and Desai, Y. M., 2018. "Comparison of three dimensional elasticity solutions for functionally graded plates". *Composite Structures,* **202**, pp. 424–435.

[194] Vafakhah, Z., and Neya, B. N., 2019. "An exact three dimensional solution for bending of thick rectangular fgm plate". *Composites Part B: Engineering,* **156**, pp. 72–87.

[195] Aragh, B. S., Hedayati, H., Farahani, E. B., and Hedayati, M., 2011. "A novel 2-D six-parameter power-law distribution for free vibration and vibrational displacements of two-dimensional functionally graded fiber-reinforced curved panels". *European Journal of Mechanics-A/Solids,* **30**(6), pp. 865–883.

[196] Asemi, K., Salehi, M., and Akhlaghi, M., 2013. "Three dimensional static analysis of two dimensional functionally graded plates". *IJMECH,* **2**(2), pp. 21–32.

[197] Tahouneh, V., and Naei, M., 2014. "A novel 2-D six-parameter power-law distribution for three-dimensional dynamic analysis of thick multi-directional functionally graded rectangular plates resting on a two-parameter elastic foundation". *Meccanica,* **49**(1), pp. 91–109.

[198] Xiang, T., Natarajan, S., Man, H., Song, C., and Gao, W., 2014. "Free vibration and mechanical buckling of plates with in-plane material inhomogeneity– A three dimensional consistent approach". *Composite Structures,* **118**, pp. 634–642.

[199] Lü, C., Lim, C. W., and Chen, W., 2009. "Semi-analytical analysis for multi-directional functionally graded plates: 3-D elasticity solutions". *International Journal for Numerical Methods in Engineering,* **79**(1), pp. 25–44.

[200] Adineh, M., and Kadkhodayan, M., 2017. "Three-dimensional thermo-elastic analysis of multi-directional functionally graded rectangular plates on elastic foundation". *Acta Mechanica,* **228**(3), pp. 881–899.

[201] Ravindran, A., and Bhaskar, K., 2019. "Three-dimensional analysis of composite fgm rectangular plates with in-plane heterogeneity". *International Journal of Mechanical Sciences,* **160**, pp. 386–396.

[202] Tomar, J., Gupta, D., and Jain, N., 1982. "Axisymmetric vibrations of an isotropic elastic non-homogeneous circular plate of linearly varying thickness". *Journal of Sound and Vibration,* **85**(3), pp. 365–370.

[203] Tomar, J., Gupta, D., and Jain, N., 1984. "Free vibrations of an isotropic non-homogeneous infinite plate of parabolically varying thickness". *Indian J. pure appl. Math,* **15**(2), pp. 211–220.

[204] Aboudi, J., Pindera, M.-J., and Arnold, S. M., 1996. "Thermoelastic theory for the response of materials functionally graded in two directions". *International Journal of Solids and Structures,* **33**(7), pp. 931–966.

[205] Aboudi, J., Pindera, M.-J., and Arnold, S. M., 1999. "Higher-order theory for functionally graded materials". *Composites Part B: Engineering,* **30**(8), pp. 777–832.

[206] Fares, M., and Zenkour, A., 1999. "Buckling and free vibration of non-homogeneous composite cross-ply laminated plates with various plate theories". *Composite structures,* **44**(4), pp. 279–287.

[207] Liu, D., Wang, C., and Chen, W., 2010. "Free vibration of FGM plates with in-plane material inhomogeneity". *Composite Structures,* **92**(5), pp. 1047–1051.

[208] Yu, T.-C., Nie, G.-J., Zhong, Z., and Chu, F.-y., 2013. "Analytical solution of rectangular plate with in-plane variable stiffness". *Applied Mathematics and Mechanics,* **34**, pp. 395–404.

[209] Boreyri, S., Ketabdari, M. J., Mohtat, P., and A, M., 2016. "Transverse vibration analysis of fgm plates with in-plane exponentially non-homogeneous material". *International Journal of Physical Research,* **4**(2), pp. 43–47.

[210] Amirpour, M., Das, R., and Flores, E. S., 2016. "Analytical solutions for elastic deformation of functionally graded thick plates with in-plane stiffness variation using higher order shear deformation theory". *Composites Part B: Engineering,* **94**, pp. 109–121.

[211] Amirpour, M., Das, R., and Flores, E. I. S., 2017. "Bending analysis of thin functionally graded plate under in-plane stiffness variations". *Applied Mathematical Modelling,* **44**, pp. 481–496.

[212] Chakraverty, S., and Petyt, M., 1999. "Vibration of non-homogeneous plates using two-dimensional orthogonal polynomials as shape functions in the Rayleigh-Ritz method". *Proceedings of the Institution of Mechanical Engineers, Part C: Journal of Mechanical Engineering Science,* **213**(7), pp. 707–714.

[213] Lal, R., and Kumar, Y., 2013. "Transverse vibrations of nonhomogeneous rectangular plates with variable thickness". *Mechanics of Advanced Materials and Structures,* **20**(4), pp. 264–275.

[214] Lal, R., and Saini, R., 2013. "Buckling and vibration of non-homogeneous rectangular plates subjected to linearly varying in-plane force". *Shock and Vibration,* **20**(5), pp. 879–894.

[215] Chu, F., Wang, L., Zhong, Z., and He, J., 2014. "Hermite radial basis collocation method for vibration of functionally graded plates with in-plane material inhomogeneity". *Computers & Structures,* **142**, pp. 79–89.

[216] Lal, R., and Saini, R., 2015. "Transverse vibrations of nonhomogeneous rectangular kirchhoff plates of variable thickness". In *Mathematical Analysis and its Applications*. Springer, pp. 609–618.

[217] Lal, R., and Saini, R., 2015. "Buckling and vibration analysis of non-homogeneous rectangular kirchhoff plates resting on two-parameter foundation". *Meccanica,* **50**(4), pp. 893–913.

[218] Malekzadeh, P., and Alibeygi Beni, A., 2015. "Nonlinear free vibration of in-plane functionally graded rectangular plates". *Mechanics of Advanced Materials and Structures,* **22**(8), pp. 633–640.

[219] Chu, F., He, J., Wang, L., and Zhong, Z., 2016. "Buckling analysis of functionally graded thin plate with in-plane material inhomogeneity". *Engineering Analysis with Boundary Elements,* **65**, pp. 112–125.

[220] Yin, S., Yu, T., Bui, T. Q., Zheng, X., and Yi, G., 2017. "Rotation-free isogeometric analysis of functionally graded thin plates considering in-plane material inhomogeneity". *Thin-Walled Structures,* **119**, pp. 385–395.

[221] Lal, R., and Saini, R., 2017. "Mode shapes and frequencies of thin rectangular plates with arbitrarily varying non-homogeneity along two concurrent edges". *Journal of Vibration and Control,* **23**(17), pp. 2841–2865.

[222] Kumar, S., Mitra, A., and Roy, H., 2018. "Large amplitude free vibration study of non-uniform plates with in-plane material inhomogeneity". *Proceedings of the Institution of Mechanical Engineers, Part L: Journal of Materials: Design and Applications,* **232**(5), pp. 371–387.

[223] Leissa, A., and Martin, A., 1990. "Vibration and buckling of rectangular composite plates with variable fiber spacing". *Composite Structures,* **14**(4), pp. 339–357.

[224] Pandey, M. D., and Sherbourne, A. N., 1993. "Stability analysis of inhomogeneous, fibrous composite plates". *International journal of solids and structures,* **30**(1), pp. 37–60.

[225] Lal, R., et al., 2009. "Effect of nonhomogeneity on vibration of orthotropic rectangular plates of varying thickness resting on pasternak foundation". *Journal of Vibration and Acoustics,* **131**(1), p. 011007.

[226] Hwan, C.-L., 2008. "Thermal-stress analysis of plates with variable fiber spacing". *Journal of Engineering Mathematics,* **62**(3), pp. 223–232.

[227] Kuo, S.-Y., and Shiau, L.-C., 2009. "Buckling and vibration of composite laminated plates with variable fiber spacing". *Composite Structures,* **90**(2), pp. 196–200.

[228] Gupta, A., Johri, T., and Vats, R., 2010. "Study of thermal gradient effect on vibrations of a non-homogeneous orthotropic rectangular plate having bi-direction linearly thickness variations". *Meccanica,* **45**(3), pp. 393–400.

[229] Kumar, Y., and Lal, R., 2011. "Buckling and vibration of orthotropic nonhomogeneous rectangular plates with bilinear thickness variation". *Journal of Applied Mechanics,* **78**(6), p. 061012.

[230] Kumar, Y., and Lal, R., 2012. "Vibrations of nonhomogeneous orthotropic rectangular plates with bilinear thickness variation resting on Winkler foundation". *Meccanica,* **47**(4), pp. 893–915.

[231] Lal, R., and Saini, R., 2015. "On the use of GDQ for vibration characteristic of non-homogeneous orthotropic rectangular plates of bilinearly varying thickness". *Acta Mechanica,* **226**(5), pp. 1605–1620.

[232] Haciyev, V., Sofiyev, A., and Kuruoglu, N., 2018. "Free bending vibration analysis of thin bidirectionally exponentially graded orthotropic rectangular plates resting on two-parameter elastic foundations". *Composite Structures,* **184**, pp. 372–377.

[233] Uymaz, B., Aydogdu, M., and Filiz, S., 2012. "Vibration analyses of FGM plates with in-plane material inhomogeneity by Ritz method". *Composite Structures,* **94**(4), pp. 1398–1405.

[234] Alinaghizadeh, F., and Shariati, M., 2016. "Geometrically non-linear bending analysis of thick two-directional functionally graded annular sector and rectangular plates with variable thickness resting on non-linear elastic foundation". *Composites Part B: Engineering,* **86**, pp. 61–83.

[235] Yin, S., Yu, T., Bui, T. Q., Zheng, X., and Tanaka, S., 2016. "In-plane material inhomogeneity of functionally graded plates: A higher-order shear deformation plate isogeometric analysis". *Composites Part B: Engineering,* **106**, pp. 273–284.

[236] Van Do, T., Nguyen, D. K., Duc, N. D., Doan, D. H., and Bui, T. Q., 2017. "Analysis of bi-directional functionally graded plates by fem and a new third-order shear deformation plate theory". *Thin-Walled Structures,* **119**, pp. 687–699.

[237] Xue, Y., Jin, G., Ding, H., and Chen, M., 2018. "Free vibration analysis of in-plane functionally graded plates using a refined plate theory and isogeometric approach". *Composite Structures,* **192**, pp. 193–205.

[238] Shariati, M., Sadeghi, H., Ghannadi, M., and Gharooni, H., 2015. "Semi analytical analysis of fgm thick-walled cylindrical pressure vessel with longitudinal variation of elastic modulus under internal pressure". *Journal of Solid Mechanics,* **7**(2), pp. 131–145.

[239] Jones, A. T., 1970. "Exact natural frequencies for cross-ply laminates". *Journal of Composite materials,* **4**(4), pp. 476–491.

[240] Jones, A. T., 1971. "Exact natural frequencies and modal functions for a thick off-axis lamina". *Journal of Composite Materials,* **5**(4), pp. 504–520.

[241] Heyliger, P., and Brooks, S., 1995. "Free vibration of piezoelectric laminates in cylindrical bending". *International Journal of Solids and Structures,* **32**(20), pp. 2945–2960.

[242] Kumari, P., Nath, J., Dumir, P., and Kapuria, S., 2007. "2d exact solutions for flat hybrid piezoelectric and magnetoelastic angle-ply panels under harmonic load". *Smart Materials and Structures,* **16**(5), p. 1651.

[243] Yang, J., Batra, R., and Liang, X., 1994. "The cylindrical bending vibration of a laminated elastic plate due to piezoelectric actuators". *Smart Materials and Structures,* **3**(4), p. 485.

[244] Vel, S. S., Mewer, R., and Batra, R., 2004. "Analytical solution for the cylindrical bending vibration of piezoelectric composite plates". *International Journal of Solids and Structures,* **41**(5-6), pp. 1625–1643.

[245] Chen, W., and Lee, K. Y., 2004. "On free vibration of cross-ply laminates in cylindrical bending". *Journal of sound and vibration,* **3**(273), pp. 667–676.

[246] Zhou, Y., Chen, W., Lü, C., and Wang, J., 2009. "Free vibration of cross-ply piezoelectric laminates in cylindrical bending with arbitrary edges". *Composite Structures,* **87**(1), pp. 93–100.

[247] Zhou, Y., Chen, W., and Lü, C., 2010. "Semi-analytical solution for orthotropic piezoelectric laminates in cylindrical bending with interfacial imperfections". *Composite Structures,* **92**(4), pp. 1009–1018.

[248] Udayakumar, B., and Gopal, K. N., 2017. "A modified state space differential quadrature method for free vibration analysis of soft-core sandwich panels". *Journal of Sandwich Structures & Materials*, p. 1099636217727801.

[249] Ebrahimi, F., and Barati, M. R., 2016. "Size-dependent thermal stability analysis of graded piezomagnetic nanoplates on elastic medium subjected to various thermal environments". *Applied Physics A,* **122**(10), p. 910.

[250] Ebrahimi, F., and Barati, M. R., 2017. "Damping vibration analysis of smart piezoelectric polymeric nanoplates on viscoelastic substrate based on nonlocal strain gradient theory". *Smart Materials and Structures,* **26**(6), p. 065018.

[251] Ebrahimi, F., and Barati, M. R., 2017. "Magnetic field effects on dynamic behavior of inhomogeneous thermo-piezo-electrically actuated nanoplates". *Journal of the Brazilian Society of Mechanical Sciences and Engineering,* **39**(6), pp. 2203–2223.

[252] Barati, M. R., and Zenkour, A. M., 2018. "Electro-thermoelastic vibration of plates made of porous functionally graded piezoelectric materials under various boundary conditions". *Journal of Vibration and Control,* **24**(10), pp. 1910–1926.

[253] Abad, F., and Rouzegar, J., 2019. "Exact wave propagation analysis of moderately thick levy-type plate with piezoelectric layers using spectral element method". *Thin-Walled Structures,* **141**, pp. 319–331.

[254] Sayyad, A. S., and Ghugal, Y. M., 2015. "On the free vibration analysis of laminated composite and sandwich plates: A review of recent literature with some numerical results". *Composite Structures,* **129**, pp. 177–201.

[255] Yan, W., Lv, T., Lei, T., and Zhi, J., 2019. "Exact analysis of imperfect angle-ply laminated panels with surface-bonded piezoelectric layers". *Archive of Applied Mechanics*, pp. 1–12.

[256] Khdeir, A., 2001. "Free and forced vibration of antisymmetric angle-ply laminated plate strips in cylindrical bending". *Journal of Vibration and Control,* **7**(6), pp. 781–801.

[257] Messina, A., 2001. "Two generalized higher order theories in free vibration studies of multi-layered plates". *Journal of Sound and Vibration,* **242**(1), pp. 125–150.

[258] Messina, A., and Soldatos, K. P., 2002. "A general vibration model of angle-ply laminated plates that accounts for the continuity of interlaminar stresses". *International journal of solids and structures,* **39**(3), pp. 617–635.

[259] Shu, X., 2005. "Free vibration of laminated piezoelectric composite plates based on an accurate theory". *Composite Structures,* **67**(4), pp. 375–382.

[260] Shu, X., 2005. "Modelling of cross-ply piezoelectric composite laminates in cylindrical bending with interfacial shear slip". *International Journal of Mechanical Sciences,* **47**(11), pp. 1673–1692.

[261] Kim, J.-S., 2007. "Free vibration of laminated and sandwich plates using enhanced plate theories". *Journal of Sound and Vibration,* **308**(1-2), pp. 268–286.

[262] Behera, S., and Kumari, P., 2018. "Free vibration of levy-type rectangular laminated plates using efficient zig-zag theory". *Advances in Computational Design,* **3**(3), pp. 213–232.

[263] Sinai, Y., 2003. "Leonid vitalyevich kantorovich". In *Russian Mathematicians In The 20th Century*. World Scientific, pp. 549–557.

[264] Kantorovich, L. V., 1958. "Approximate methods of higher analysis". *Interscience*.

[265] Kerr, A. D., 1968. "An extension of the kantorovich method". *Quarterly of Applied Mathematics,* **26**(2), pp. 219–229.

[266] Kerr, A. D., 1969. "An extended kantorovich method for the solution of eigenvalue problems". *International Journal of solids and structures,* **5**(6), pp. 559–572.

[267] Dalaei, M., and Kerr, A., 1996. "Natural vibration analysis of clamped rectangular orthotropic plates". *Journal of Sound and Vibration,* **189**(3), pp. 399–406.

[268] Naumenko, K., Altenbach, J., Altenbach, H., and Naumenko, V., 2001. "Closed and approximate analytical solutions for rectangular mindlin plates". *Acta Mechanica,* **147**(1-4), pp. 153–172.

[269] Ungbhakorn, V., and Wattanasakulpong, N., 2006. "Bending analysis of symmetrically laminated rectangular plates with arbitrary edge supports by the extended kantorovich method". *Science & Technology Asia*, pp. 33–44.

[270] Shufrin, I., Rabinovitch, O., and Eisenberger, M., 2008. "A semi-analytical approach for the non-linear large deflection analysis of laminated rectangular plates under general out-of-plane loading". *International Journal of Non-Linear Mechanics,* **43**(4), pp. 328–340.

[271] Aghdam, M., and Mohammadi, M., 2009. "Bending analysis of thick orthotropic sector plates with various loading and boundary conditions". *Composite structures,* **88**(2), pp. 212–218.

[272] Nik, A. M. N., and Tahani, M., 2009. "Analytical solutions for bending analysis of rectangular laminated plates with arbitrary lamination and boundary conditions". *Journal of mechanical science and technology,* **23**(8), pp. 2253–2267.

[273] Alijani, F., and Aghdam, M., 2009. "A semi-analytical solution for stress analysis of moderately thick laminated cylindrical panels with various boundary conditions". *Composite Structures,* **89**(4), pp. 543–550.

[274] Fereidoon, A., Mohyeddin, A., Sheikhi, M., and Rahmani, H., 2012. "Bending analysis of functionally graded annular sector plates by extended Kantorovich method". *Composites Part B: Engineering,* **43**(5), pp. 2172–2179.

[275] Bigdeli, K., and Aghdam, M., 2011. "A semianalytical solution for the bending of clamped laminated doubly curved or spherical panels". *Journal of Mechanics of Materials and Structures,* **5**(6), pp. 855–873.

[276] Ranji, A. R., and Hoseynabadi, H. R., 2012. "A semi-analytical technique for bending analysis of cylindrical panels with general loading and boundary conditions". *Journal of mechanical science and technology,* **26**(6), pp. 1711–1718.

[277] Singhatanadgid, P., and Singhanart, T., 2019. "The kantorovich method applied to bending, buckling, vibration, and 3d stress analyses of plates: A literature review". *Mechanics of advanced materials and structures,* **26**(2), pp. 170–188.

[278] Kapuria, S., and Kumari, P., 2011. "Extended kantorovich method for three-dimensional elasticity solution of laminated composite structures in cylindrical bending". *Journal of applied mechanics,* **78**(6), p. 061004.

[279] Kapuria, S., and Kumari, P., 2012. "Multiterm extended kantorovich method for three-dimensional elasticity solution of laminated plates". *Journal of Applied Mechanics,* **79**(6), p. 061018.

[280] Kumari, P., Kapuria, S., and Rajapakse, R., 2014. "Three-dimensional extended kantorovich solution for levy-type rectangular laminated plates with edge effects". *Composite Structures,* **107**, pp. 167–176.

[281] Kapuria, S., and Kumari, P., 2013. "Extended kantorovich method for coupled piezoelasticity solution of piezolaminated plates showing edge effects". In Proc. R. Soc. A, Vol. 469, The Royal Society, p. 20120565.

[282] Kumari, P., Behera, S., and Kapuria, S., 2016. "Coupled three-dimensional piezoelasticity solution for edge effects in levy-type rectangular piezolaminated plates using mixed field extended kantorovich method". *Composite Structures,* **140**, pp. 491–505.

[283] Kumari, P., and Behera, S., 2017. "Three-dimensional free vibration analysis of levy-type laminated plates using multi-term extended kantorovich method". *Composites Part B: Engineering,* **116**, pp. 224–238.

[284] Behera, S., and Kumari, P., 2019. "Analytical piezoelasticity solution for natural frequencies of levy-type piezolaminated plates". *International Journal of Applied Mechanics,* **11**(03), p. 1950023.

[285] Moeenfard, H., and Maleki, S., 2017. "Characterization of the static behavior of electrically actuated micro-plates using extended kantorovich method". *Proceedings of the Institution of Mechanical Engineers, Part C: Journal of Mechanical Engineering Science,* **231**(12), pp. 2327–2339.

[286] Kumari, P., and Kar, S., 2019. "Static behavior of arbitrarily supported composite laminated cylindrical shell panels: An analytical 3d elasticity approach". *Composite Structures,* **207**, pp. 949–965.

[287] Andakhshideh, A., Rafiee, R., and Maleki, S., 2019. "3d stress analysis of generally laminated piezoelectric plates with electromechanical coupling effects". *Applied Mathematical Modelling,* **74**, pp. 258–279.

[288] Nakamura, T., Singh, R., and Vaddadi, P., 2006. "Effects of environmental degradation on flexural failure strength of fiber reinforced composites". *Experimental mechanics,* **46**(2), pp. 257–268.

[289] Barbero, E., Cosso, F., and Campo, F., 2013. "Benchmark solution for degradation of elastic properties due to transverse matrix cracking in laminated composites". *Composite Structures,* **98**, pp. 242–252.

[290] Adda-Bedia, E., Bouazza, M., Tounsi, A., Benzair, A., and Maachou, M., 2008. "Prediction of stiffness degradation in hygrothermal aged $[\theta_m/90_n]_s$ composite laminates with transverse cracking". *journal of materials processing technology,* **199**(1), pp. 199–205.

[291] Kapuria, S., and Achary, G., 2005. "Exact 3d piezoelasticity solution of hybrid cross–ply plates with damping under harmonic electro-mechanical loads". *Journal of sound and vibration,* **282**(3-5), pp. 617–634.

[292] Kukla, S., and Zamorska, I., 2014. "Power series solution of first order matrix differential equations". *Journal of Applied Mathematics and Computational Mechanics,* **13**(3).

[293] Kumari, P., 2012. "Analytical solutions for micro and macro mechanics of smart structures integrated with piezoelectric composites". PhD thesis, Indian Institute of Technology Delhi.

[294] Simulia, D. S., 2013. "Abaqus 6.13 users manual". *Dassault Systems, Providence, RI.*

[295] Kapuria, S., Dumir, P., and Jain, N., 2004. "Assessment of zigzag theory for static loading, buckling, free and forced response of composite and sandwich beams". *Composite structures,* **64**(3-4), pp. 317–327.

[296] Kumari, P., Singh, A., Rajapakse, R., and Kapuria, S., 2017. "Three-dimensional static analysis of levy-type functionally graded plate with in-plane stiffness variation". *Composite Structures,* **168**, pp. 780–791.

[297] da Silva, L. F., das Neves, P. J., Adams, R., and Spelt, J., 2009. "Analytical models of adhesively bonded jointspart i: Literature survey". *International Journal of Adhesion and Adhesives,* **29**(3), pp. 319–330.

[298] Costa, M., Viana, G., Da Silva, L., and Campilho, R., 2017. "Environmental effect on the fatigue degradation of adhesive joints: a review". *The Journal of Adhesion,* **93**(1-2), pp. 127–146.

[299] Durodola, J., 2017. "Functionally graded adhesive joints–a review and prospects". *International Journal of Adhesion and Adhesives,* **76**, pp. 83–89.

[300] Ray, M., and Sachade, H., 2006. "Exact solutions for the functionally graded plates integrated with a layer of piezoelectric fiber-reinforced composite". *Journal of applied mechanics,* **73**(4), pp. 622–632.

[301] Selim, B., Zhang, L., and Liew, K., 2016. "Active vibration control of fgm plates with piezoelectric layers based on reddys higher-order shear deformation theory". *Composite Structures,* **155**, pp. 118–134.

[302] Bendine, K., Boukhoulda, F., Nouari, M., and Satla, Z., 2016. "Active vibration control of functionally graded beams with piezoelectric layers based on higher order shear deformation theory". *Earthquake Engineering and Engineering Vibration,* **15**(4), pp. 611–620.

[303] Swaminathan, K., and Sangeetha, D., 2017. "Thermal analysis of fgm plates–a critical review of various modeling techniques and solution methods". *Composite Structures,* **160**, pp. 43–60.

[304] Carrera, E., Fazzolari, F. A., and Cinefra, M., 2016. *Thermal Stress Analysis of Composite Beams, Plates and Shells: Computational Modelling and Applications.* Academic Press.

Appendix A

A.1 COMPARISON OF PRESENT GRADATION WITH OTHER PROBABILISTIC MICROMECHANICAL/GRADATION MODELS

In literature, the most commonly used models to express the variation of material properties in FGMs are the power-law distribution of the volume fraction, and exponential function variation of material properties [303]. In this section, a comparison between the present variation of material properties with other micromechanical models is carried out. It is found that these types of variation can also be achieved in the present case by selecting the proper parameter of gradation (δ_1, δ_2 and δ_p). For comparison of models, the following material properties are assumed as,

Silicon-Steel FGM [304]:

Silicon Nitride: E_c= 348.43 GPa, ν_c=0.24, ρ_c=2370 Kg/m^3,

Steel: E_m= 201.04 GPa, ν_m=0.3262, ρ_m=8166 Kg/m^3,

A.1.1 Power law variation

Generally, in the FGMs material properties variation is achieved by gradually changing the volume fraction of constituent phases which followed a Power law.

Power law variation of volume fraction [303]:

$$V_m = (x/a)^p, \qquad V_c = 1 - V_m \tag{A.1}$$

Where V_m subscript represents the volume fraction of the metal phase, V_c represents the volume fraction of the ceramic phase, and p is a power-law index of material property gradient index. For present case, it is taken as a unit. Then, the effective material properties across the plate length are calculated by following rules.

(i) ***Rule of Mixture-*** This method of estimation is based on the linear rule of the mixture (ROM) and has been extensively used in the literature to investigate the response of FGM structures. This is one of the simplest and well-established models, in which the material properties are graded across the length (x) of the FGM plate, from the ceramic rich surface at x=0 to metal-rich surface at x=1, by changing the volume fraction of the constituents. The position-dependent variation of material property across the longitudinal direction is given by [303],

$$E = V_m E_m + V_c E_c;$$

$$\nu = V_m\nu_m + V_c\nu_c; \qquad G = \frac{E}{2(1+\nu)} \tag{A.2}$$
$$\rho = V_m\rho_m + V_c\rho_c;$$

where E, G, ν, and ρ are the modulus of elasticity, modulus of rigidity, Poisson's ratio, and density respectively. The subscripts 'c' and 'm' represent the constituents of ceramic and metal respectively. The comparison of properties calculated by the rule of the mixture and present variation case is given in Fig. A.1. It is observed that the present variation is very much similar as obtained by the rule of mixture.

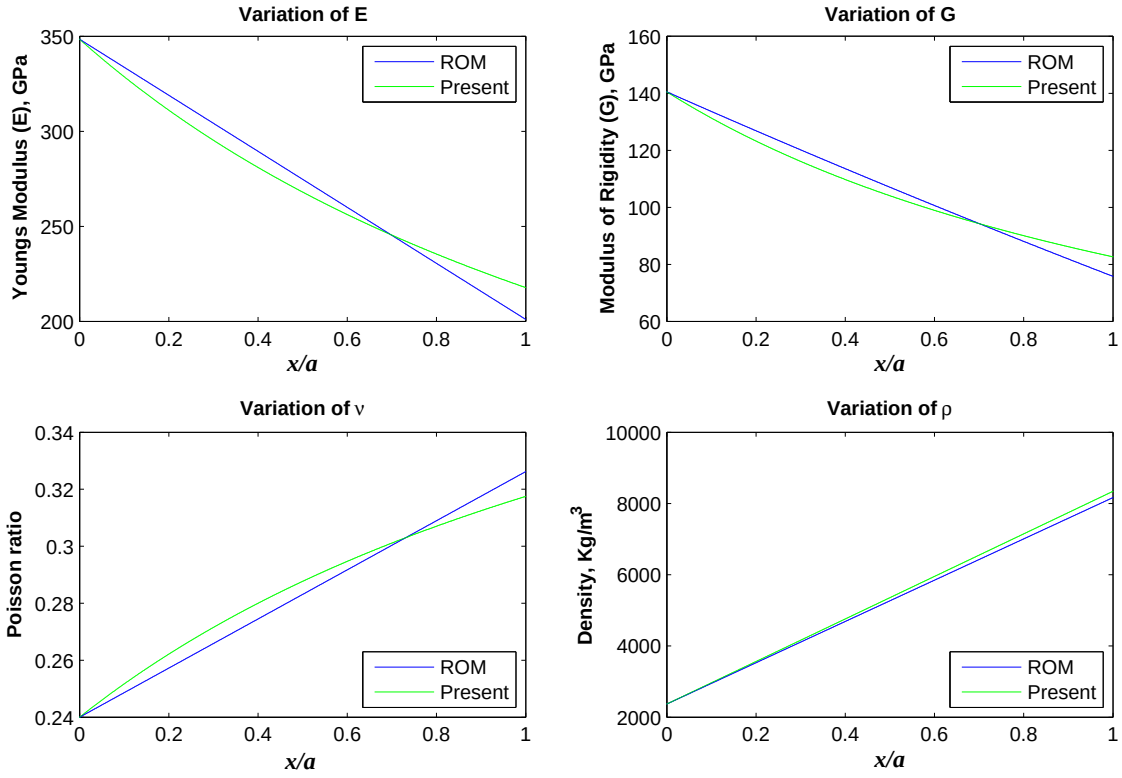

Fig. A.1: Comparison of present variation of material properties with the Rule of Mixture. For present case, the gradation parameter are taken as, δ_1=0.6; δ_2=0.7; δ_p=2.52

(ii) ***Mori-Tanaka scheme-*** Mori-Tanaka method [303] of estimation is most applicable for regions with graded microstructure, which have well defined continuous matrix phase and randomly distributed spherical particulate phase. This method accounts the effect of elastic fields among neighboring inclusions and their interactions with the constituents. The effective bulk modulus K_e, and shear modulus G_e are evaluated using the relations given by [303],

$$\frac{K_e - K_m}{K_c - K_m} = \frac{V_c}{1 + V_m\left(\frac{K_c - K_m}{K_m + \frac{4}{3}G_m}\right)};$$
$$\frac{G_e - G_m}{G_c - G_m} = \frac{V_c}{1 + V_m\left(\frac{G_c - G_m}{G_m + f_1}\right)}, \qquad f_1 = \frac{G_m\left(9K_m + 8G_m\right)}{6\left(K_m + 2G_m\right)} \tag{A.3}$$

Then the effective values of Young's Modulus of elasticity (E), Poissons ratio (ν), and modulus of rigidity (G) are calculated as,

$$E = \frac{9K_eG_e}{3K_e + G_e}; \qquad \nu = \frac{3K_e - 2G_e}{2\,(3K_e + G_e)}; \qquad G = \frac{E}{2(1+\nu)} \tag{A.4}$$

The comparison of properties calculated by the Mori-Tanaka scheme and present variation case is given in Fig. A.2. It is observed that the present variation is very much similar as obtained by the Mori-Tanaka scheme.

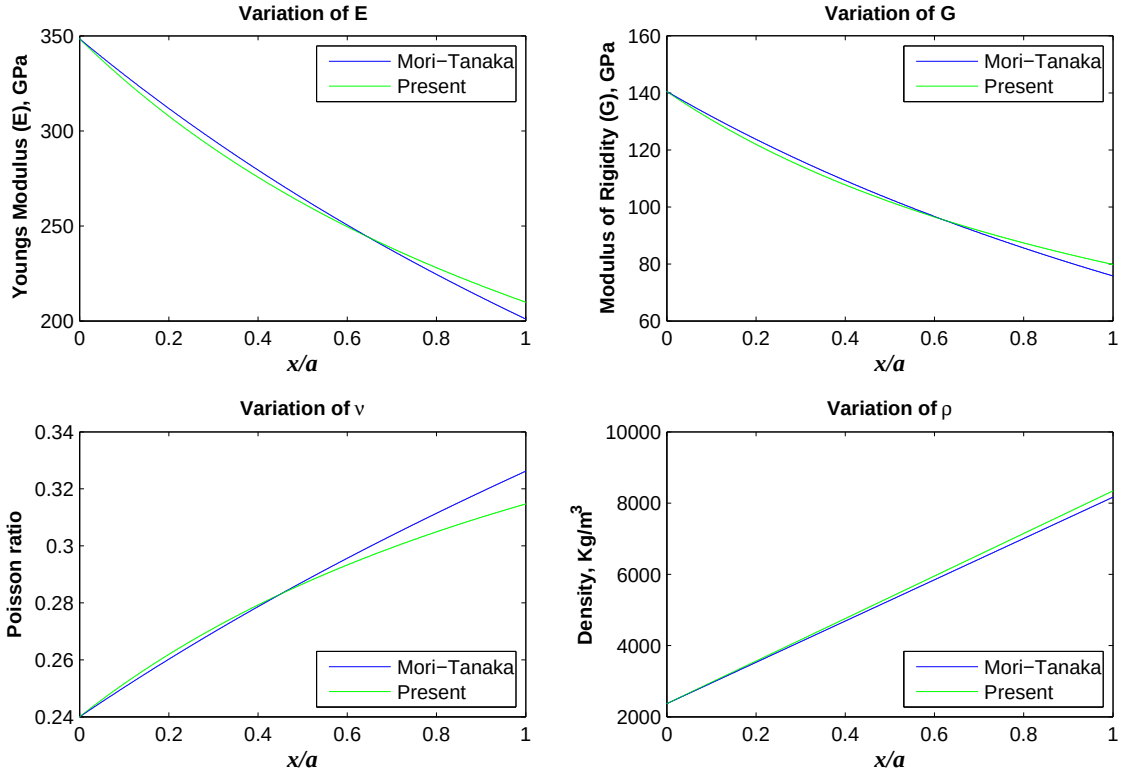

Fig. A.2: Comparison of present variation of material properties with the Mori-Tanaka scheme. For present case, the gradation parameter are taken as, δ_1=0.66; δ_2=0.76; δ_p=2.52

A.1.2 Exponential function

This idealization method for FGM is most common in studies related to fracture mechanics. Several investigators adopted the exponential gradation of materials for the analysis of FGM plates and sandwich plates. The variation of material properties are represented as [303],

$$\begin{aligned} E &= E_c\; e^{p\;x\ln(\frac{E_m}{E_c})}; \\ \nu &= \nu_c\; e^{p\;x\ln(\frac{\nu_m}{\nu_c})}; \qquad G = \frac{E}{2(1+\nu)} \\ \rho &= \rho_c\; e^{p\;x\ln(\frac{\rho_m}{\rho_c})}; \end{aligned} \tag{A.5}$$

The comparison of properties calculated by the Exponential function scheme and present variation case is given in Fig. A.3. It is observed that the present variation is very much similar as obtained by the Exponential function scheme.

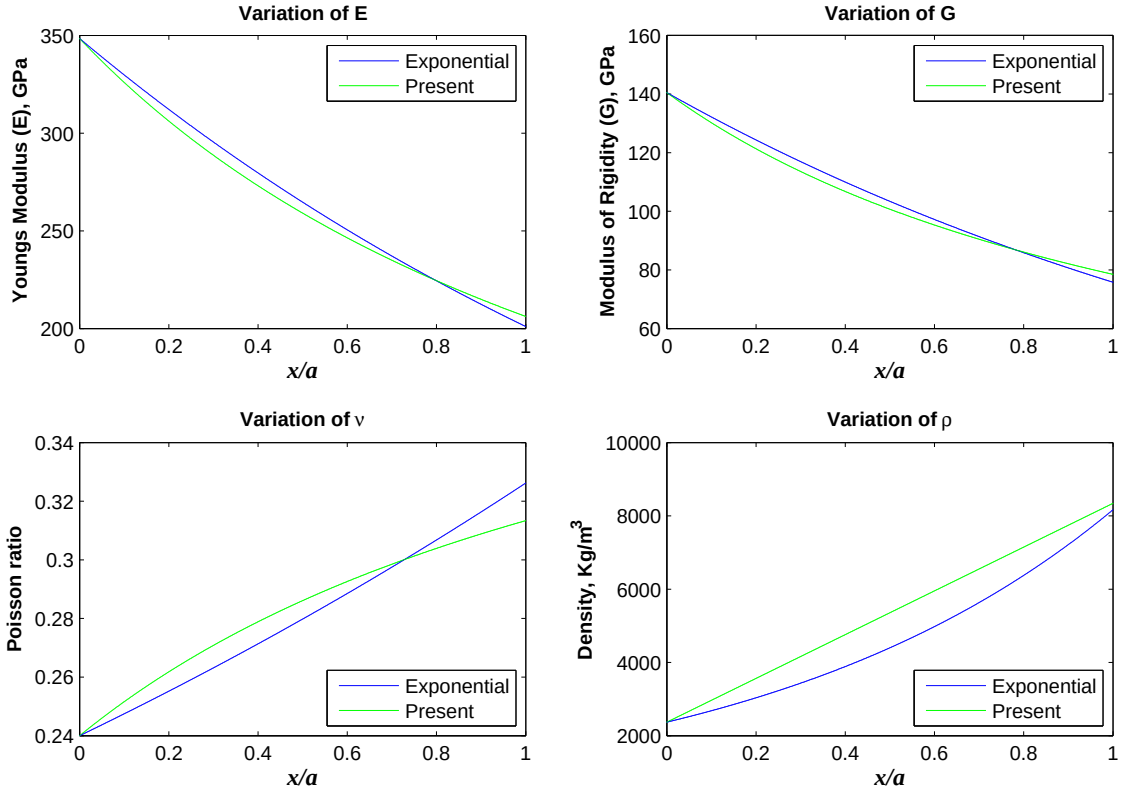

Fig. A.3: Comparison of present variation of material properties with the Exponential function scheme ($p = 1$). For present case, the gradation parameter are taken as, δ_1=0.69; δ_2=0.79; δ_p=2.52

Brief Biodata of the Author

The author, Agyapal Singh, was born in the year 1987 in the town Jaito situated in Faridkot District of Punjab State. He graduated in Mechanical Engineering in the year 2010 from Giani Zail Singh College of Engineering and Technology, Bathinda, Punjab. Then, he joined Guru Kashi University (Punjab) in the same year to work as a lecturer in the Department of Mechanical Engineering. He scored 1037th All India Rank (AIR) in GATE (All India Graduate Aptitude Test in Engineering) 2013 with 99.37 percentile (2013), and also scored 4168th All India Rank (AIR) in GATE 2014 with 97.75 percentile (2014). In July 2014, he joined the Ph.D. program at IIT Guwahati in the Department of Mechanical Engineering and this research work is carried out during this period

List of Publications from the Thesis

List of Publications in International Journals

1. Kumari, P., **Singh, A.**, Rajapakse, R. K. N. D., and Kapuria, S. (2017). Three-dimensional static analysis of Levy-type functionally graded plate with in-plane stiffness variation. *Composite Structures* 168:780-791.

2. Singh, A., and Kumari, P. (2018). Two-Dimensional Elasticity Solution for Arbitrarily Supported Axially Functionally Graded Beams. *Journal of Solid Mechanics* 10(4):719-733.

3. Singh, A., Kumari, P., and Hazarika, R. (2018). Analytical Solution for Bending Analysis of Axially Functionally Graded Angle-Ply Flat Panels. *Mathematical Problems in Engineering* (2597484):1-17.

4. Singh, A., and Kumari, P. (2018). Analytical Solution of Functionally Graded Beam Having Longitudinal Stiffness Variation. *International Journal for Computational Methods in Engineering Science and Mechanics* 19(6):390-395..

5. Singh, A., Kumari, P. and Bind P.(2019). 2D free vibration solution of the hybrid piezoelectric laminated beams using extended Kantorovich method. *Journal of The Institution of Engineers (India): Series C - Springer*. https://doi.org/10.1007/s40032-019-00518-w

6. Singh, A., and Kumari, P. (*Accepted*). Accurate estimation of natural frequencies for arbitrarily supported angle-ply piezoelectric laminated panels: An analytical piezoelectricity approach. *Advances in Computational Design, An International Journal.*

7. Singh, A., and Kumari, P. (*Under review*). Free vibration analysis of axially functionally graded beams integrated with piezoelectric layers: An analytical elasticity solution. *International Journal of Applied Mechanics.*

8. Singh, A., and Kumari, P. (*Under review*). Three-Dimensional analytical elasticity free vibration solution for in-plane functionally graded plates. *International Journal of Mechanical Sciences.*

9. Singh, A., and Kumari, P. (*Under preparation*). Effect of in-plane material properties gradation on natural frequency of arbitrarily supported angle-ply flat panels

Book Chapters

1. Kumari, P., and **Singh, A.** (2019). Three-Dimensional Analytical Solution for FGM Plate with Varying Material Properties in In-plane Directions Using Extended Kantorovich Method. *Recent Advances in Structural Engineering* 1:611-621. Springer, Singapore. ISBN 978-981-13-0362-3, ISSN 2366-2557

Conference Publications

1. Kumari, P., and **Singh, A.** (2016). Three-dimensional analytical solutions for FGM plate with varying material properties in in-plane directions using extended Kantorovich method. *Proceedings of Structural Engineering convention (SEC)*:548-553.

2. Singh, A., and Kumari, P. (2017). Accurate stress solution for laminated rectangular plates bonded with functionally graded adhesive interlayer and subjected to transverse loading. *3rd Indian Conference on Applied Mechanics (INCAM-2017)*, MNNIT Allahabad (U.P.), India

3. Singh, A., Hazarika, R., and Kumari, P. (2017). Three-dimensional analytical solution of FGM panel with varying material properties along in-plane directions using Extended Kantorovich Method. *25th Annual International Conference on Composites/ Nanoengineering (ICCE-25)*, Rome, Italy.

4. Singh, A., and Kumari, P. (2017). Analytical solution of functionally graded beam having longitudinal stiffness variation. *International Conference on Composite Materials and Structures (ICCMS) 2017*, Hyderabad, India.

5. Singh, A., and Kumari, P. (2019). Analytical free vibration solution of functionally graded beam having longitudinal stiffness variation. *10th International Conference on Materials for Advanced Technologies 2019*, Singapore.

6. Yadav, R. K., **Singh, A.**, and Kumari, P. (2019). Three-dimensional analytical free vibration solution of cross-ply panel subjected to arbitrary boundary conditions. *4th Indian Conference on Applied Mechanics*, July 3-5, 2019, IISc Bangalore

7. Hussain, E., **Singh, A.**, and Kumari, P. (2019). Analytical free vibration solution of axially functionally graded beam subjected to arbitrary boundary conditions. *4th Indian Conference on Applied Mechanics*,July 3-5, 2019, IISc Bangalore